POZNAN UNIVERSITY OF TECHNOLOGY

FACULTY OF COMPUTING AND TELECOMMUNICATION
Institute of Radiocommunications

Doctor of Philosophy Dissertation

UTILIZATION OF CONTEXT INFORMATION FOR SPECTRAL-EFFICIENCY ENHANCEMENT IN FUTURE RADIO COMMUNICATION SYSTEMS

mgr inż. Łukasz Kułacz

Supervisor
dr hab. inż. Adrian Kliks

POZNAŃ 2022

To my wife Klaudia

Contents

List of Figures **III**

List of Tables **VI**

Acronyms **VII**

Symbols **XI**

1 Introduction **1**
1.1 Dissertation overview . . . 2

2 Context information processing and storage **5**
2.1 Spectrum utilization issues . . . 5
2.1.1 Demand on wireless services . . . 5
2.1.2 Spectrum tenders and white spaces . . . 7
2.1.3 The need of context information . . . 8
2.2 Radio environment database . . . 10
2.2.1 Database overview . . . 10
2.2.2 Radio environment and radio service maps . . . 14
2.2.3 Edge intelligence . . . 17
2.3 Standardization and regulation activities . . . 19
2.4 Radio environment maps for TVWS — experimental implementation . . . 27
2.4.1 TVWS-based dynamic spectrum access . . . 27
2.4.2 Measurements in terrestrial television band . . . 27
2.4.3 Radio environment maps . . . 31

3 Theoretical approach to context information utilization in DSA systems **37**
3.1 Research topic 1a: Algorithm for dynamic spectrum access . . . 38
3.2 Research topic 1b: Experiment of DSA system utilization . . . 43
3.2.1 Experiment setup . . . 43
3.2.2 Experiment results . . . 45
3.3 Research topic 2: Joint spectrum and power allocation in CBRS-based DSA . . . 49
3.3.1 System model and problem formulation . . . 49
3.3.2 Joint spectrum and power allocation - problem statement . . . 51
3.3.3 Heuristic analysis . . . 52
3.3.4 Optimized power allocation and proposed multi-choice algorithm . . . 56
3.3.5 Performance evaluation . . . 61
3.4 Research topic 3: Waveform flexibility in context-aware network . . . 70
3.4.1 Database-supported waveform adaptation . . . 70

3.4.2 Proposed algorithm for database-oriented waveform adaptation 71
3.4.3 Simulation results 73

4 Practical approach to context information utilization in DSA systems 77
4.1 Research topic 1: Experiment of CBRS-based system utilization - field trials 78
4.1.1 Considered spectrum sharing scheme 78
4.1.2 Experiment results 82
4.2 Research topic 2: RSM in wireless network simulator 88
4.2.1 Simulation results 89
4.3 Research topic 3: RSM in M-MIMO LTE-A network simulator 97
4.3.1 Radio service maps for CRE adaptation 99
4.3.2 Simulation results 100

5 Context information utilization in ultra-dense wireless networks 103
5.1 Research topic 1: Reliability and availability analysis in ultra dense network 104
5.1.1 Inspirations from the nervous system 105
5.1.2 Proposed application of HNS elements for high network reliability 107
5.1.3 Reliability block diagrams - an example 108
5.1.4 Simulation results 109
5.2 Research topic 2: Brain-inspired data transmission in dense wireless network . . . 114
5.2.1 Network reliability assessment through the percolation theory 116

6 Spectrum virtualization - spectrum management application 127
6.1 Research topic 1: SMA as a flexible and efficient resource utilization 128
6.1.1 SMA design and implementation 130
6.1.2 SMA use cases 135
6.2 Research topic 2: Freemium spectrum sharing and pricing 139
6.2.1 Freemium spectrum sharing concept 139
6.2.2 Simulation results 143
6.3 Research topic 3: Open radio network access 148
6.3.1 Open RAN concept 149
6.3.2 Traffic steering use case analysis 152
6.3.3 Simulation results 155

7 Conclusions 159

Bibliography 165

A Author's publications 181

List of Figures

1.1 Graphical summary of the thesis content 2

2.1 Examples of the considered map grid structures 12
2.2 Structure of the database system in the application domain 16
2.3 Spectrum management and access system based on REM databases 19
2.4 Management system based on a set of rules proposed by the project FARAMIR 20
2.5 Information flow graph in a database-driven spectrum management system (Ofcom) . 20
2.6 General architecture of a DSA based on the IEEE Policy Set 1900.5 22
2.7 Basic architecture of Licensed Shared Access 24
2.8 Three tiers of spectrum access in CBRS 24
2.9 Location of DVB-T transmitters with regards to the PUT premises 28
2.10 Floor plans and photos of the PUT premises 29
2.11 Measurement setup applied in Poznan 30
2.12 Measurement points identified for PUT premises 30
2.13 Coverage map for the channel 27 at the ground floor 32
2.14 Coverage map — concatenation of indoor and outdoor samples 33
2.15 Coverage map — considering transmitter location (Srem) 34
2.16 Coverage map — considering transmitter location (Piatkowo) 34
2.17 Coverage map — impact of the walls not considered 34
2.18 Coverage map — considered impact of the walls in the kriging algorithm 34

3.1 Spectrum emission mask of secondary user 39
3.2 Simplified algorithm of Dynamic Spectrum Access 39
3.3 Map of interference margin [dB] 41
3.4 Map of Signal-to-Interference-plus-Noise Ratio [dB] for secondary users 41
3.5 Block diagram of the experiment setup. 43
3.6 Receiver schema of secondary user 44
3.7 Photograph of first white-space transceiver and remote database 44
3.8 Photograph of second white-space transceiver 45
3.9 Power spectral density observed during white-space transmission 46
3.10 Spatial distribution of the observed SINR [dB] when one white-space device is active . 47
3.11 Example of interference graph 54
3.12 Interference graph after executing "add-edge" procedure 55
3.13 Distance between CBSD and point on the border of another CBSD scheme 58
3.14 Multi-choice algorithm 59
3.15 CBSDs position (Scenario I) 62
3.16 CBSDs position (Scenario II) 62
3.17 Solution space (Scenario I) 63

3.18 Solution space (Scenario II) . . . 63
3.19 Performance comparison (first scenario) . . . 64
3.20 Performance comparison (second scenario) . . . 65
3.21 Clustering algorithm (5 clusters) . . . 66
3.22 Clustering algorithm (3 clusters) . . . 66
3.23 Clustering algorithm (1 cluster) . . . 66
3.24 Transmit power and bandwidth of CBSDs . . . 67
3.25 Bitrate per km^2 of CBSDs . . . 67
3.26 Clustering algorithm on grid (4 clusters) . . . 67
3.27 Clustering algorithm on grid (2 clusters) . . . 68
3.28 Bitrate per km^2 for regular grid of CBSDs . . . 68
3.29 Comparison proportional and equal assignment . . . 68
3.30 Bitrate per km^2 (comparison proportional and equal assignment) . . . 69
3.31 Bitrate per km^2 (comparison proportional and equal assignment) for limited power . . . 69
3.32 Simplified block diagram of waveform selection algorithm . . . 73
3.33 Transmit power and spectrum allocation in the third scenario . . . 74
3.34 Allowed transmission mode for 2 and 18 MHz bandwidth request . . . 75
3.35 Allowed transmission power for 2 MHz bandwidth FBMC request . . . 75

4.1 Network schema in considered experiment scenario . . . 79
4.2 Diagram of interfaces in the analyzed system . . . 80
4.3 First area of field trials — map of measurement points . . . 83
4.4 Second area of field trials — map of measurement points . . . 83
4.5 Field trials — exemplary measurement point at the countryside . . . 84
4.6 Maximum allowed transmit power in dBm — interpolation result . . . 85
4.7 Photograph of SC receiver location at the countryside bus-stop . . . 86
4.8 Photograph of SC transmitter inside the car . . . 86
4.9 Example scenario of the analyzed network (3D and top view) . . . 88
4.10 Average bitrates for UEs as the function of time in the advanced LSA . . . 90
4.11 Mean UEs bitrates versus time (one outdoor UE) . . . 91
4.12 Traffic map — the standard deviation of the MCS index . . . 92
4.13 Sumaric bitrate achieved by UEs using RSMs with traffic prediction . . . 93
4.14 Illustration of the considered scenario (buildings and BSs locations) . . . 98
4.15 Illustration of the calculation of CRE values based on RSMs . . . 99
4.16 Illustration of the time evolution of RSRP-based UEs allocation to BSs . . . 101
4.17 Illustration of the time evolution of RSM-based UEs allocation to BSs . . . 101
4.18 UEs data rates without and with RSM-aided CRE adaptation . . . 101
4.19 Comparison of handover count for RSRP-based and RSM-aided association . . . 102

5.1 The neuron cell schema . . . 105
5.2 Reliability Block Diagram of the exemplary network . . . 108
5.3 Simulated network topology . . . 109
5.4 Simulated network mean time to failure . . . 111
5.5 Use case A — reliability of devices . . . 111
5.6 Use case A — reliability of the analyzed network . . . 112
5.7 Use case B — mean availability of proposed network . . . 112
5.8 Use case B — simulation results . . . 113

5.9 Considered dense wireless network . . . 116
5.10 Example of the analyzed topology . . . 119
5.11 Cluster size as function of node operation probability — 30 neuron-nodes . . . 120
5.12 Cluster size as function of node operation probability — 100 neuron-nodes . . . 120
5.13 Cluster size as function of node operation probability — various number of nodes . . . 121
5.14 Cluster size as function of node operation probability — various duty cycle . . . 121
5.15 Distribution of delivery confirmation delay . . . 123
5.16 Distribution of energy consumed during transmission . . . 123

6.1 High-level architecture of SMA . . . 129
6.2 Processing flow of SMA . . . 130
6.3 Input and output of SMA . . . 132
6.4 SMA band selection based on policy rule . . . 134
6.5 Normalized spectrum costs based on dynamic rules . . . 134
6.6 Reconfiguration time-line . . . 135
6.7 Indicative UE-related delay for different COTS UEs . . . 136
6.8 Benefits of phantom cell via applying SMA . . . 136
6.9 Cell zooming impacts on different UE distances . . . 137
6.10 Freemium spectrum sharing model . . . 139
6.11 Example of the network topology with medium user density . . . 141
6.12 Considered frequency bands . . . 142
6.13 Distribution of user rate for low user density . . . 144
6.14 Distribution of user rate for medium user density . . . 144
6.15 Distribution of user rate for high user density . . . 145
6.16 Distribution of user rate (second scenario) . . . 145
6.17 Distribution of user rate for low user density . . . 146
6.18 Distribution of user rate for high user density . . . 146
6.19 O-RAN architecture . . . 150
6.20 RAN Intelligent Controller: non-RT RIC and near-RT RIC . . . 151
6.21 Mapping of xApps installations to RICs . . . 153
6.22 Achieved results for three considered experimentation schemes . . . 156

List of Tables

2.1 Summary of the challenges for developing clear context dataset 17
2.2 Currently available DVB-T channels at PUT premises 28

3.1 Summary of work presented in chapter 3.1 42
3.2 Summary of work presented in chapter 3.2 48
3.3 Summary of work presented in chapter 3.3 69
3.4 Summary of work presented in chapter 3.4 76

4.1 Measurement results — in both locations 85
4.2 Summary of work presented in chapter 4.1 87
4.3 Simulation parameters used in experiments 89
4.4 Selected aspects of the RSM subsystem design 94
4.5 Storage and AI tools analysis (worst case scenario) 95
4.6 Summary of work presented in chapter 4.2 96
4.7 Summary of work presented in chapter 4.3 102

5.1 Summary of work presented in chapter 5.1 113
5.2 Simulation parameters used in the first phase of the study 119
5.3 Simulation parameters used in the second phase of the work 122
5.4 Summary of work presented in chapter 5.2 125

6.1 Summary of work presented in chapter 6.1 138
6.2 Package Scores 145
6.3 Summary of work presented in chapter 6.2 147
6.4 Summary of work presented in chapter 6.3 158

7.1 Summary of context information influence on the wireless system 160
7.2 Summary of system aspects modified with context information utilization in author's publications 161

Acronyms

3GPP	3rd Generation Partnership Project
ACIR	Adjacent Channel Interference Ratio
ACLR	Adjacent Channel Leakage Ratio
ACS	Adjacent Channel Selectivity
AI	Artificial Intelligence
API	Application Platform Interfaces
ASA	Authorized Shared Access
ATSC	Advanced Television Systems Committee
AWGN	Additive White Gaussian Noise
BBB	Blood-Brain Barrier
BPSK	Binary Phase Shift Keying
BS	Base Station
CAP	Consistency, Availability, Partition tolerance
CBRS	Citizen Broadband Radio System
CBSD	Citizens Broadband Radio Service Device
CDF	Cumulative Density Functions
CI	Context Information
CINR	Carrier-to-Interference-and-Noise Ratio
COTS	Commercial Off-The-Shelf
CPE	Customer-Premises Equipment
CRE	Cell Range Extension
CRN	Cognitive Radio Networks
CU	Centralized Unit
CxM	Coexistence Manager
DB	Database
DCF	Distributed Coordination Function
DL	DownLink
DSA	Dynamic Spectrum Access
DSM	Dynamic Spectrum Management
DSS	Dynamic Spectrum Sharing
DU	Distributed Unit
DVB-T	Digital Video Broadcasting - Terrestrial
DVB-T2	Digital Video Broadcasting - Second Generation Terrestrial

DySPAN	Dynamic SPectrum Access Networks
EC	European Commission
ECC	Electronic Communications Committee
ECDF	Empirical Cumulative Density Functions
EESM	Effective Exponential SNR Mapping
EIRP	Effective Isotropical Radiated Power
ESC	Environmental Sensing Capability
ETSI	European Telecommunications Standards Institute
FBMC	Filter Bank MultiCarrier
FCC	Federal Communications Commission
FCT	Faculty of Computing and Telecommunications
FDD	Frequency Division Duplex
FEC	Forward Error Correction
FSPL	Free-Space Path Loss
FSS	Freemium Spectrum Sharing
GAA	General Authorized Access
GB	Guard Band
GIS	Geographic Information System
GMSK	Gaussian Minimum Shift Keying
HNS	Human Nervous System
IAP	Iterative Allocation Process
IDW	Inverse Distance Weighting
IEEE	Institute of Electrical and Electronics Engineers
IM	Interference Management
IoT	Internet of Things
ISM	Industrial, Scientific, Medical
ITU	International Telecommunication Union
JSON	JavaScript Object Notation
LOAD	Lightweight On-Demand Ad-hoc Distance Vector Routing Protocol
LOADng	LOAD - next generation
LSA	Licensed Shared Access
LTE	Long Term Evolution
LTE-A	LTE-Advanced
M-MIMO	Massive Multiple Input, Multiple Output
MAC	Medium Access Control
MBB	Mobile BroadBand
MCD	Measurement Capable Devices
MCS	Modulation and Coding Scheme

MIB	Management Information Base
MIMO	Multiple Input, Multiple Output
ML	Machine Learning
MNO	Mobile Network Operator
MRT	Maximum Ratio Transmission
MTC	Machine-Type Communication
MTTF	Mean Time To Failure
MVNO	Mobile Virtual Network Operator
MW	MicroWave
NC-FBMC	Non-Contiguous Filter Bank MultiCarrier
NC-OFDM	Non-Contiguous Orthogonal Frequency-Division Multiplexing
NRA	National Regulatory Authority
O-RAN	Open Radio Access Network
OAI	OpenAirInterface
Ofcom	Office of Communication
OFDM	Orthogonal Frequency-Division Multiplexing
OID	Object IDentifier
OOB	Out-Of-Band
OSP	O-RAN Service Provider
PAL	Priority Access License
PF	Proportional Fairness
PMSE	Programme Making and Special Events
PSD	Power Spectral Density
PU	Primary User
PUT	Poznan University of Technology
QAM	Quadrature Amplitude Modulation
QoE	Quality of Experience
QoS	Quality of Service
RAN	Radio Access Network
RB	Resource Block
RBD	Reliability Block Diagram
REM	Radio Environment Map
REM SA	REM Storage and Acquisition
RH	Remote Head
RIC	RAN Intelligent Controller
RRM	Radio Resource Management
RSM	Radio Service Map
RSRP	Reference Signal Received Power
RSSI	Received Signal Strength Indication
RT	Real-Time
RTC	Real-Time Controller

RU	Remote Unit
SAS	Spectrum Access System
SC	Small-Cell
SDK	Software Development Kit
SDN	Software Defined Network
SDR	Software Defined Radio
SEM	Spectrum Emission Mask
SFN	Single Frequency Network
SIB	System Information Block
SINR	Signal-to-Interference-plus-Noise Ratio
SIR	Signal-to-Interference Ratio
SMA	Spectrum Management Application
SMO	Service Management and Orchestration
SNMP	Simple Network Management Protocol
SNR	Signal-to-Noise Ratio
SON	Self-Organizing Network
SP	Service Provider
SQL	Structured Query Language
SRS	Sounding Reference Signal
SU	Secondary User
TDD	Time Division Duplex
TS	Traffic Steering
TVWS	TV Whitespace
U-NII	Unlicensed National Information Infrastructure
UDP	User Datagram Protocol
UE	User Equipment
UHF	Ultra High Frequency
UL	UpLink
UPS	Uninterruptible Power Supply
USRP	Universal Software Radio Peripheral
VLC	VideoLAN Client
VPN	Virtual Private Network
WiMAX	Worldwide Interoperability for Microwave Access
WInnForum	Wireless Innovation Forum
WLAN	Wireless Local Area Network
WRAN	Wireless Regional Area Network
XML	eXtensible Markup Language

Symbols

B_{CH}	Bandwidth of a single channel
B_i	Bandwidth used by i-th device
B	Bandwidth of the system
$CH_{\max}$	Maximum channel index
$CH_{\min}$	Minimum channel index
D	Considered area size
E_b	Signal energy
G_R	Receiver antenna gain
G_T	Transmitter antenna gain
$I(x, y, ch)$	Interference margin at position (x, y) in the ch-th channel
$L(x, y, ch)$	Attenuation at position (x, y) in the ch-th channel
L_E	Euclidean distance between points
$L_{fs}(x - x_u, y - y_u)$	Free space attenuation between (x, y) and user's position (x_u, y_u)
L_{fs}	Free space attenuation
$M_{\max}$	Number of solutions
N_m	Number of measurement points
N_u	Number of points with unknown value
N_w	Number of walls
N_C	Number of CBSDs
N_K	Number of options of channel usage
N_M	Number of protection points
N_Q	Number of square subregions
N_{ch}	Number of channels
$P(x, y, ch)$	Measured power at position (x, y) in the ch-th channel
P_{TX}	Allowed transmit power
P_{INT}	Predefined interference level – porownac z Pmin, Preq, itp.
P_{REG}	Maximal transmit power limited by regulatory authority
$P_{\text{SAS}i,n}$	Maximal transmit power of i-th device and n-th channel provided by SAS
P_{SEN}	Receiver sensitivity
$P_{\text{WC}i}$	Worst-case transmit power of i-th device (among all channels)
$P_{\min}$	Minimum power needed for proper digital TV signal reception
P_{noise}	Noise power
P_{req}	Minimal transmit power for user's service
P_i	Transmit power of i-th device
R_i	Transmission range of i-th device
R_E	Earth radius
R	Transmission range

SG	Second greatest cluster size
$SINR(x, y, ch)$	SINR at position (x, y) in the ch-th channel
T	Throughput
V_m	Set of measurement points
V_u	Set of points with unknown value
W_l	Attenuation of l-th wall
W	Vector of entities weights
X	Chromatic number
Ψ	Vector of spatial correlation between known and unknown points
Υ	Matrix of entities weights
η	Free space attenuation coefficient
γ_{nugget}	The value at which the semi-variogram (almost) intercepts the y-value
γ_{range}	The distance at which the semi-variogram model first flattens out
γ_{sill}	The value at which the semi-variogram model first flattens out
γ	Function of spatial correlation between points (semi-variogram)
κ	Lagrange multiplier
λ	Wavelength
$\mathbf{A}$	Adjacency matrix of interference graph
$\mathbf{W}^{a,b}$	Matrix of interference attenuation between colors a and b
$\mathbf{\Gamma}$	Binary matrix of spectrum utilization scheme
β	Binary matrix of spectrum allocation
ρ	Scale parameter of 2P exponential distribution
θ^*	SINR threshold
θ	Latitude
$\tilde{N}_I$	Number of CBSDs (subset of total number of CBSDs)
$\tilde{P}_{TX}$	Final value of allowed transmit power
φ	Longitude
ϱ	Location parameter of 2P exponential distribution
$\xi_{j,i}$	Path loss observed between j-th transmitter and i-th receiver
ζ_{ij}	Reliability of the link between i-th and j-th device
ζ_i	Reliability of i-th device
ζ_s	System reliability
ζ	Reliability
ch_u	Channel index, where u-th user transmits
ch	Channel index
$d_{i,j}$	Distance between the i-th and j-th entity on a two-dimensional surface
f_c	Carrier frequency
f	Frequency
$g_{i,j,m}$	Distance between j-th device and m-th point on the border of i-th device
p_T	Percolation threshold
u	Point with unknown value
w_i	Weight of the i-th entity
x_i, y_i	Position of the i-th entity on a two-dimensional surface
z_i	Value of investigated metric of the i-th entity
z_u	Unknown value of investigated metric of the u-th entity

Chapter 1

Introduction

Currently, observed trends in wireless telecommunications, especially the huge need for wireless services, induce many scientists to make various attempts to meet these requirements. Wireless telecommunications is no longer just a means of communication between people, but a more (maybe even above all) convenient way to content and media delivery regardless of where you are (whether in a city, village or while traveling). Adding to this the significant development of the quality of screens (especially their size and resolution), the problem of the demand for the amount of data transferred is enormous. One of the most straightforward solutions to this problem is allocating and using more bandwidth for transmission. However, static allocation of spectrum resources to various services/systems causes it to be impossible to use them freely, mainly due to contracts, agreements, and licensing restrictions. This method of radio resources split is not the best and, in many situations, entails insufficient allocation of resources to one service and excess resources to another service. The use of subsequent (and so far unused) frequency ranges is associated with a more demanding propagation environment and often with the need to design and manufacture new radio devices. However, one may look at currently reserved bands and their usage; in many cases, one would notice geographic areas and specific time intervals in which some band fragments are not used. In light of the enormous demand for radio spectrum, this situation requires a conceptual redesign. The demand for wireless services in most cases is dynamic and depends on various factors. Such factors are time (time of day, day of the week, season of the year) and location (a place close to shopping facilities, factories, highways); therefore, the radio resources split should also be dynamic.

Spectrum efficiency is a metric that evaluates the utilization of radio resources and their efficiency. By spectral efficiency, one can mean the number of transmitted bits per unit time using a given bandwidth. Therefore, the goal is to maximize this value, transmitting as many bits as possible while maintaining the same bandwidth. This value can be improved in many ways, e.g., by issuing advanced radio resource allocation methods, control of transmit power of devices, multi-antenna systems, etc. However, the best results often require much additional information (contextual information), such as the position of users, historical statistics on the presence of users, the quality of their service, etc. This metric is beneficial for assessing the operation of a radio access system, the primary assumption of which is to improve the spectral efficiency concerning the method of static spectrum allocation.

With the ever-growing demand for wireless services, improving spectrum efficiency is necessary and inevitable. Consequently, contextual information becomes very important or even crucial data needed to achieve this goal. This fact, in turn, creates the need to develop algorithms and systems that collect, store, process, update, and, most importantly, use contextual information.

At the same time, a crucial aspect is to determine what exact contextual information a given algorithm or system requires for operation. Additionally, most of the time, the type of contextual information alone is not sufficient. The format of the recorded information should also be specified, its accuracy, frequency of updates, etc. In light of these facts, it is necessary to look at the contextual information itself and how these data are managed and represented. At this point, we should look at, for example, radio environment databases that can be successfully used in the radio resource allocation process. Databases of this type not only store contextual information but also enable inference based on these data. It is also impossible to mention a significant current trend where radio access is virtualized. Virtualization allows the entire spectrum management algorithm to be transferred to spectrum management applications without designing the entire system.

When all the data presented above are combined, the use of dynamic spectrum division using contextual information seems to be a promising solution to the problem of insufficient radio resources and often inefficient use of them. In this dissertation, an extensive justification of the thesis will be presented: *With the use of contextual information, it is possible to design a spectrum management algorithm, as a result of which the spectral efficiency of the system is increased.* The justification will be presented in the form of a theoretical analysis of the spectrum access system itself through several simulations and experiments using actual equipment.

1.1 Dissertation overview

A conceptual breakdown of the document structure is shown in Fig. 1.1. The main topic of the work is conceptually divided into five parts, each devoted to separate chapters. Each chapter contains several subsections in which the research or experiments carried out are described.

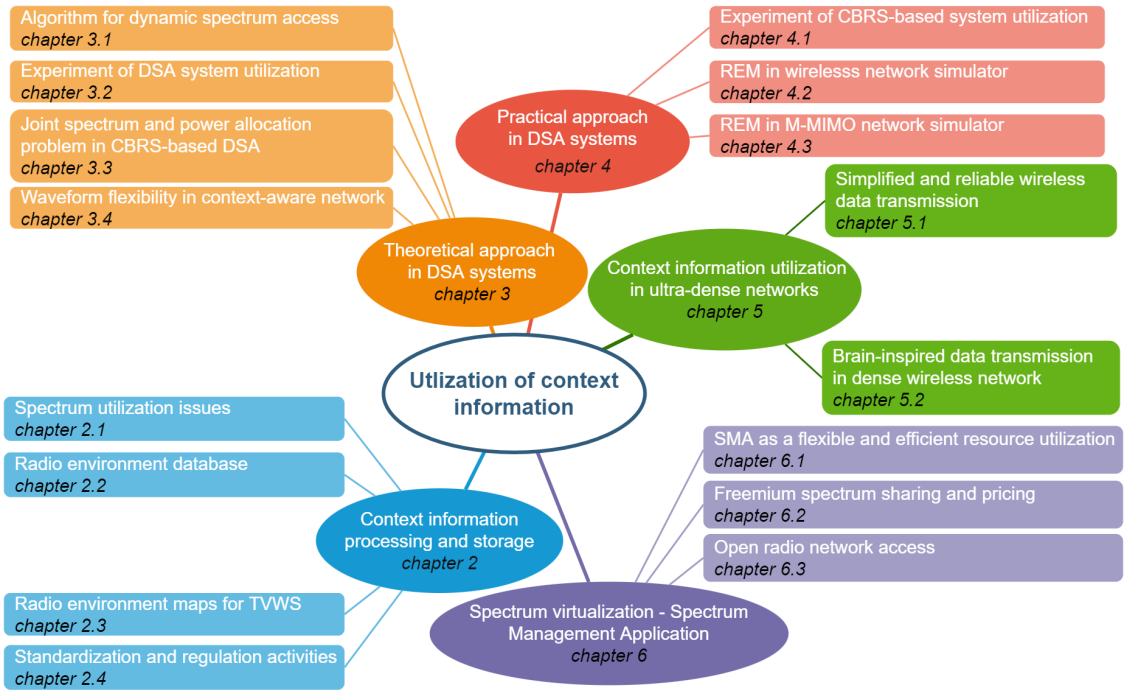

Figure 1.1: Graphical summary of the thesis content

Context Information (CI) itself is a fairly broad topic; therefore, to introduce the reader, the Chap. 2 is devoted to, first of all, a description of contextual information and aspects related to it, including an example of obtaining, storing, and using such information. In particular, the concept of Radio Environment Map (REM) and Radio Service Map (RSM) is presented there.

They are is served as the basis for the operation of the Dynamic Spectrum Access (DSA) system considered at the beginning of Chap. 3. As an example, in this case, such radio environment maps can be built based on information about the power received in the TV band in the analyzed area. The measurement set made filling the discussed map with actual data. Then, using interpolation, the missing places (i.e., the points with no associated measurements) in the analyzed area can be supplemented, creating a complete map of the received signal power. This procedure allows one to propose, design, and test a system of dynamic access to the spectrum, which enables the band's use in question for other purposes (transmission of unlicensed users) while maintaining the original transmission. It, in turn, is a practical example of the use of contextual information to improve spectral efficiency in the area served.

Chap. 3 is devoted to theoretical considerations on how to use various types of contextual information to design or improve the performance of a dynamic spectrum assignment system. The word "theoretical" has been used here to indicate research (simulations and experiments) that does not restrict the user from using a particular transmission technology, network standard, etc. The worst-case for spectral efficiency is when no one uses a band fragment - provided that someone is willing to access the spectrum. In this case, spectrum-sharing methods are often considered based on the detection of primary users' transmissions. Such detection allows to keep the current (original) purpose of a given part of the band, but in the case of a temporary lack of primary users - it allows the use of the same part of the band for other purposes. Among other things, such a solution is presented in Chap. 3, where an experiment with the use of a REM database with information about the power received in the TV band allows unlicensed users to transmit with the simultaneous protection of licensed users. Another problem is the spectrum division between users in such a way as to meet their needs and at the same time achieve the highest spectral efficiency. With the simultaneous possibility of controlling the transmitting power of users, this problem becomes very complex. Chap. 3 describes an attempt to solve this problem, where two-stage suboptimal algorithms are proposed for the simultaneous allocation of resources and power control. In addition, this chapter describes an algorithm that optimizes spectral efficiency by appropriate modulation selection for users. Selecting waveform with less power leakage to adjacent channels allows for a different (often more advantageous) way of allocating channels between users.

Chap. 4 presents a practical approach to the use of contextual information in a dynamic spectrum access system. The aforementioned "practical" aspect concerns, first of all, additional challenges imposed by an already operating network, where we cannot modify it, and limitations introduced by the applied standard, protocol, or transmission system. Compared to Chap. 3, the experiments described here are closer to the actual implementation in already functioning networks. The first described experiment is the field testing of the proposed dynamic spectrum access system that allows new unlicensed users to access the spectrum while protecting primary users. In this case, the primary users are access points to the radio network implemented with Worldwide Interoperability for Microwave Access (WiMAX) technology in several villages. The second described experiment is a computer simulation of the Long Term Evolution (LTE) network operating in the building - the resources of which are shared with users outside the building. The main limitation is the LTE transmission system used. The third experiment described is again the simulation of a wireless network; however, in this case a dense radio environment and Massive Multiple Input, Multiple Output (M-MIMO) with a very accurate channel model based on the ray-tracing method are considered.The method of assigning users to cells is modified on the basis of the historical information on the assignment of users to optimize spectral efficiency. The main limitation of this approach is the use of the LTE-Advanced (LTE-A) network, which significantly reduces the freedom of choice of assigning users to cells.

In terms of spectral efficiency in radio networks, it is impossible not to mention the trend observed for some time (especially in the context of the 5G network), which assumes increasing the density of network nodes and reducing the size of cells (increasing their number). Chap. 5 presents considerations on the use of context information in very dense radio networks. The main inspiration for the described works is the observation of the human nervous system (especially the brain), where a very simple method of transmission is used. However, the density of nerve connections is enormous. Of course, neural connections are much more similar to a wired transmission system, but many observations from the nervous system can still be used in wireless transmission systems. In particular, two additional cell types in the human nervous system, i.e., astrocytes and microglia, have been highlighted. The astrocyte acts as a kind of link between two independent systems (circulatory system and nervous system) and adds the influence of one system to the other. On the other hand, microglia is an essential cell of the immune system, which initially rests. However, when a nervous system malfunction is detected, it turns into an active form and "fixes" the abnormality. The inspiration coming from the described cells allows, above all, to improve the reliability of the wireless network. In the case of this thesis, the contextual information is twofold. The microglia-inspired node detects transmission problems (e.g., loss of transmission of a neighboring node). In contrast, for the astrocyte-inspired node, external information (from outside the network) may come from, for example, sensors. Spectral efficiency, in this case, is closely related to transmission reliability. It is worth noting that the spectrum is effectively used when much information is sent with its use. However, the transmission of these data must be correct.

A significant trend in telecommunications is currently (observed for some time) radio access virtualization, where software performs individual functions. In the last but equally important Chap. 6, several approaches to spectrum management are described, but in the form of a spectrum management application. First, Spectrum Management Application (SMA) used in conjunction with OpenAirInterface (OAI) is described, which, based on a selected set of rules and policies, selects an optimal (according to operator-defined criteria) set of transmission parameters for each user in particular, a frequency range. The author's decision-making algorithm is described along with the implementation using real devices (mobile phones). In this case, we do not consider the contextual information directly - however, let us emphasize that the selected policy set has an essential impact on how the analyzed system works, i.e., its spectral efficiency. In turn, even in the simplest scenario, the sets of rules are selected based on some contextual information, in the most automated form, based on the collected contact information, and machine learning algorithms select the appropriate sets of rules. This is an example of indirect use of contextual information at a higher level of spectrum management. Next, a new approach to spectrum sharing is presented, where some spectrum bands are available for free to all users, and the rest of the spectrum is available for a fee. Such an approach has been described from the perspective of the user and owner of such a network ("owner" of the spectrum). Similar to the previously described situation, we do not consider directly contextual information but sets of rules. This, in turn, implies a change in the spectral efficiency of the analyzed system. The final work described in this chapter is the application of contextual information to Open Radio Access Network (O-RAN). It is an excellent example where the entire system is virtualized, and it is possible to attach applications to such a system (the so-called xApp) that implement certain functionalities. An example of an application that controls users' traffic by changing their connection to the cells, allocating resources, and simultaneously selecting the band in the cell is described here.

A summary table has been added to each described work to improve readability and define how to use contextual information. It collects the type of contextual information, the way it is used, its impact on the system, particularly spectral efficiency, and any additional comments.

Chapter 2

Context information processing and storage

One of the promising solutions to the problems of spectral resource efficiency is the use of contextual information stored in the form of a radio environment database. Such a base for TVWS has been created and described in this chapter. Standardization and regulatory work on this topic were also described.

2.1 Spectrum utilization issues

2.1.1 Demand on wireless services

The idea of simultaneous use of the spectrum by incumbents, also known as Primary User (PU), and Secondary User (SU) has attracted the research community for many years. This trend has been intensified by key findings in the area of spectrum sharing, which was the invention of cognitive radio technology, proposed for the first time by Mitola and Maguire [1]. The idea of introducing some artificial intelligence into the wireless communication ecosystem has paved the way for the development of new paradigms for better spectrum utilization. It appeared to be a good solution to the well-known problem of highly underutilized spectrum resources. Numerous measurements have shown that at certain times and locations, the spectrum is occupied even only at the level of 20 % [2–8]. Moreover, various research activities associated with these campaigns have been conducted. In [9], the focus was on the extended spectral analysis of the Ultra High Frequency (UHF) TV band, which was carried out to achieve realistic values of the selected merit figures: occupancy threshold, sensing bandwidth, noise, and hidden node margin. The authors of [10] concentrated on the discussion of co-channel and adjacent channel interference and protection aspects with regard to the Digital Video Broadcasting - Second Generation Terrestrial (DVB-T2) and Institute of Electrical and Electronics Engineers (IEEE) 802.22 Wireless Regional Area Network (WRAN) systems. Other interesting results from measurement campaigns or field tests can be found, e.g., in [11, 12]. As a consequence, various bodies, including academia, regulators, and mobile network operators, have proposed and discussed new spectrum-sharing policies among various stakeholders. The application of the cognitive radio idea has been particularly analyzed in the context of TV bands, where large portions of the spectrum have been released due to digital switch off in many countries, e.g., [13]. However, various decisions have been made which envisage the flexible usage of certain frequency bands and the application of the so-called white space devices, e.g. [14–20]. At the same time, communications regulators such as Office of Communication (Ofcom) open up a fragment of TV spectrum for opportunistic use.

Also, other approaches for flexible spectrum sharing are investigated and gain an interest (e.g. Licensed Shared Access (LSA) or Citizen Broadband Radio System (CBRS) with Spectrum Access System (SAS)) [21, 22].

The demands in capacity and latency for the fifth generation (5G) mobile networks can be summarized as 1000x more capacity of the fourth generation (4G) technologies and latency over the radio link occasionally lower than 1 ms. According to the requirements International Telecommunication Union (ITU) IMT-2020 [23], maximum bitrate speeds of up to 20 Gbps are expected for 5G. At the same time, in 4G, at frequencies in the sub-6 GHz domain, the average download bitrates are below 20 Mbps. Verizon, in its millimeter-wave 5G trial fields at 28 GHz in the United States, has achieved throughput speeds of 1.8 Gbps, but with a rather low latency of 1.5 ms [24]. 5G systems open high frequencies (up to 30 GHz) to practical application, but these mm-wave frequencies are short in travel distance, requiring many radio-heads and antennas to be deployed. Knowing this, one may observe that in 6G, the possible operating frequencies may be shifted up to 100 GHz or even to 1 THz to utilize wider potentially available bandwidths. Moreover, more stringent requirements on latency (i.e., even below 1 ms, down to microsecond level) and rates (i.e., even up to 100 Gbps or 1 Tbps in peak) may be defined. Such Key Performance Indicators have been discussed in [25]. Although base stations operating in the terahertz band will operate with less power while providing more capacity (enabling thousands of simultaneous wireless connections), they will require extreme densification of the network. As a result, Massive Multiple Input, Multiple Output (M-MIMO) with spatial multiplexing could be subject to further research, so the bandwidth is spatially reused simultaneously.

In this context, we suppose that even more extreme requirements will be defined for the next sixth-generation (6G) networks than is currently the case for the 5G network [26]. These requirements will cover various network domains and features, such as higher rate (1 Tbps peak rate), lower latency (e.g., real tactile Internet), high reliability, security, programmability, and device density (e.g., 10^7 devices per km^2), etc. To meet the above, prospective demands, Mobile Network Operator (MNO) have to utilize the available spectrum more efficiently or assign new frequency bands for communication purposes. The latter approach is associated with a high cost of obtaining long-term transmission licenses. Recent studies have shown that improvements in spectral efficiency can be achieved by further densification of Radio Access Network (RAN), application of M-MIMO and millimeter-wave solutions, and by more flexible spectrum sharing approaches to Dynamic Spectrum Management (DSM) [27, 28]. Various sharing schemes have been investigated so far, mentioning light licensing, pluralistic licensing, co-primary sharing, or microlicensing, among others [29]. Two of them are of particular importance nowadays: LSA and CBRS. However, we foresee that for 6G networks, even more advanced but mature solutions will be defined, which may benefit from access to rich context information, such as [30, 31].

Therefore, efficient and adaptive spectrum sharing and usage become a matter of dynamic network planning and interference coordination between the access nodes of the operators. This fact poses demands on the availability of a tremendous amount of information (also called big data) that determines the intra- and inter-RAN dependencies. It is often not enough to utilize only data which is related stricktly to radio environment. Therefore, more types of information are used, e.g., related to the user, the quality of its service, etc., and stored in Radio Service Maps (RSMs). These maps are populated with data related to radio aspects, as in the well-known Radio Environment Map (REM), such as coverage maps or interference maps. On top of that, RSM contain various types of network and service-related data, such as traffic maps (distribution of requested or served traffic, traffic patterns) or trajectory databases (user mobility patterns) [32]. In [33], the authors considered the usage of REM, a RSM, to reduce the number of handovers by

predicting the trajectory of the users. Knowing the characteristics of the channel (stored in REM) and the prospective route of the user, the handover system procedure may not be initiated if the so-called ping pong effect is expected. However, the more data required by the DSM operation, the higher the operational costs and the load on the backhaul part of a system. For this reason, current technologies restrict RSM to statistical databases that have been shown to be suitable mainly for long-term system optimization [32, 33]. In particular, in [34] the authors discussed ways in which artificial intelligence-oriented algorithms could, in general, improve 5G radio access networks.

Future 6G wireless networks may benefit significantly from access to rich and accurate context information, but this requires highly efficient processing and management of these large data sets. Our considerations in this paper are also motivated by the fact that various types of context information are typically available in wireless systems. Therefore, the performance of numerous algorithms for signal processing and communication can be improved. Many algorithms use feedback information about the communication channel or user preferences to better adapt to the ongoing scenario.

2.1.2 Spectrum tenders and white spaces

In that context, the increasing traffic demand in wireless networks and the problems of getting exclusive spectrum will lead future wireless networks to face a severe spectrum shortage, especially in urban areas. This problem can be particularly critical when considering highly dense deployments of small cells intended to meet the demands of future systems. Again, technological solutions that enable spectrum sharing, such as Cognitive Radio Networks (CRN), will bring light to this spectrum scarcity problem. At least two questions arise when thinking about the deployment of these solutions: *What bands can be considered to share?* and *How to manage this spectrum sharing?* A popular answer to the first question is the television band due to the presence of several channels not used, called TV Whitespace (TVWS), and due to the nearby static assignment of the TV channels. In contrast, the answer to the second question is more complex and requires a deeper analysis and discussion of advanced and flexible spectrum management systems. However, it has appeared that the practical implementation of the concept of pure cognitive radio with all phases of the cognitive cycle is very challenging. It is mainly due to the insufficient precision or efficiency of spectrum detection methods [35,36]. Single-node spectrum sensing seems to be unable to guarantee the expected protection level of incumbents, as the reliability of sensing procedures is not high enough to meet the requirements defined by various regulators. For example, in [37, 38] Federal Communications Commission (FCC) identified many criteria for white space devices, such as the detection threshold at the level of -114 dBm averaged of 6 MHz channel for Advanced Television Systems Committee (ATSC) signals[1]. Analogously, Electronic Communications Committee (ECC) discussed the detection thresholds at the level of around -120, or even -140 dBm [39–41].

One of the possible solutions to the problem of unreliability of single node spectrum detection or the problem of hidden nodes is to apply either separately or jointly: (a) cooperative sensing algorithms [40, 42, 43] and (b) the so-called Radio Environment Map (REM) [32, 44–47]. The former is not investigated in this work; the latter instead is an advanced form of database with some learning capabilities, the ability to enforce optimized solutions, and interactive decision making. A REM, originally introduced by the Virginia Tech team [48], is a database consulted by intelligent devices that contains information on the radio environment. Thus, a REM could be able to estimate the state of certain locations where no measurement data are available using its cognitive engine.

[1] Please note that this value is below the thermal noise power observed within such band at the temperature of 20° C, what equals approximately -106 dBm

Particular attention should be paid to some EU-founded projects, that is, FARAMIR[2], ARAGORN[3] and COGEU[4], where some technical considerations on such databases have been discussed. The use of shared spectrum, such as TVWS to extend capacity in LTE-A and LTE networks has been found to be particularly relevant in different works [49–52] for small cell scenarios. It raises practical considerations on the deployment of REM. It aims to support theoretical activities by analyzing, in particular, the characteristics of the TVWS band (e.g., stability, etc.) so that a REM database can be built as a support for the deployment of small cells using TVWS. Furthermore, the design of the REM structure is also addressed, including the relevant parameters to be stored. The characterization is done based on measurements in both indoor and outdoor locations. A proper characterization of indoor behavior can be relevant for deploying local REMs that include detailed radio environmental information of a reduced area. It could be, e.g., at the level of a building and its surrounding buildings, usually corresponding to the coverage area of a few small cells. Instead, the characterization of outdoor locations will be relevant from the perspective of global REMs that encompass larger areas. In a nutshell, much work has been done to identify the best way to utilize the spectrum flexibly and how to make devices more spectrum agile. At this stage, it is apparent that REM can be considered a key technology enabler for the practical implementation of the cognitive radio concept. Furthermore, the hierarchical structure mentioned above, composed of local and global REMs, has been identified as appropriate for better management of local resources [46].

This hierarchical approach is advantageous when the secondary system will be deployed in a small geographical area. An exemplary case is the mass deployment of cognitive small-cells outside building (e.g., along the streets on road infrastructure) for better broadband service delivery to mobile users. Another interesting case would be to utilize the licensed spectrum inside the building that benefits from the high wall attenuation. In other words, the spectrum occupied outside the building will be treated as vacant inside the building because of the attenuation of the signal after passing the walls. One may foresee that the application of local REM databases for these transmission schemes would increase the utilization of the spectrum and provide new services to the users while protecting the PUs, e.g., TV broadcasters.

2.1.3 The need of context information

The spectrum usage problems mentioned so far are most often the case where the spectrum is reserved for specific users (who are not currently active), or the spectrum is fully used; however, it would be possible to utilize additional data to increase the users' bitrate. In many cases, it would be possible in a simple way to improve this situation, i.e., to increase energy efficiency. However, additional knowledge is required in the form of contextual information. When the spectrum is reserved for not present or not active users, it would be sufficient to use a spectrum access system that at least has information about the presence of primary users. Moreover, this information depends on the type of network and its purpose, i.e., it can be simple information (achieved through sensing) about the current status of spectrum occupancy. It can also be a particular pattern of occupation (e.g., spectrum is busy at specific times) or more complicated dependencies (e.g., the spectrum is occupied depending on a specific schedule, but it is not precisely defined - like in a bus ride). In the second case, we will use more advanced algorithms to allocate resources and algorithms for assigning users to cells. For example, these algorithms may separate resource blocks depending on the type of users' traffic, their approximate or exact location, or other metrics.

[2]https://cordis.europa.eu/project/id/248351
[3]https://cordis.europa.eu/project/id/216856
[4]https://cordis.europa.eu/project/id/248560

Similarly, one can use the information about the change of the user's location, especially if it is similar in time, or detect places with more user activity. The analysis of contextual data is not always obvious, and the use of machine learning algorithms can be considered with great success to, for example, detect user traffic patterns, their position, or simply presence.

The definition of context information is extensive, and, in general, context information can be any type of information. The context of such information is any information that characterizes some entities (devices, places, persons, etc.), relations between users, or relations between users and different entities. The common context is the location of the entity, but it can also be some state of the entity or a group of entities [53]. As can be seen, contextual information is needed in many cases because it can be used in many different ways to improve the spectral efficiency of the network. There are more possibilities for contextual information use. The collected data can be used to plan the modernization of an existing network (e.g., to designate where an additional cell should be located). It can also be used to optimize energy efficiency (e.g., switching off some devices) based on historical data, leading to energy savings). In this thesis, we want to show various possibilities of CI utilization to improve spectrum efficiency.

2.2 Radio environment database

2.2.1 Database overview

Databases are widely used and generally refer to data sets with a specific structure. Databases provide a standardized way to record, store, filter, update, and access information. The structure of a database strictly depends on the type of information stored in it. In the simplest case, a database is each table with data, an independent entity that does not cooperate with any other documents. This type of database is usually used for a single specific purpose, such as telephone directories, lists of books, CDs, etc. Such simplest databases are not very useful in the context of this work. More extensive types of databases are much more useful for contextual information. The utility mentioned above comes mainly from the fact that, apart from storage, they enable one to determine the relationship between information and performing operations on the stored data. Therefore, it is worth looking at two types of databases: relational and non-relational databases. The first is made up of multiple arrays of data that can work together using an internal programming language Structured Query Language (SQL). The basis of relational database operation is a suitable data type for all values, collecting data in the form of two-dimensional arrays, the ability to bind and merge data from different arrays and perform relatively complex operations on them. Non-relational databases, on the other hand, do not define a specific format of stored data (such as a two-dimensional array) and do not use an internal programming language called SQL. They are often called NoSQL databases. There are several non-relational databases, i.e., key-value store, graph store, column store, and document store. The most popular types of non-relational databases are those based on the document store data model (e.g., MongoDB). They assume the possibility of saving the fundamental element in the database, that is, a whole document based on some standard formats (i.e., eXtensible Markup Language (XML), JavaScript Object Notation (JSON)). In addition to accessing a document via its identifier (key-value), the database also offers a query interface or language that retrieves documents based on their content. This type of database is often used for Big Data processing.

From the point of view of this work, that is, storing contextual information, there is no indication whatsoever as to which database type will be the best. The selection process of the most appropriate database type for the specific type of contextual information should consider the representations of that information, its format, quantity, and any relationships associated with it. However, it is worth discussing the issue of database systems, which connect many databases into a distributed system, because this is an inevitable situation in extensive radio networks (due to the often large network coverage area). Thus, we consider a whole network of interconnected databases that make up one database system. Inextricably linked with this term is the Consistency, Availability, Partition tolerance (CAP) theorem, which says that only two of the three desirable features of distributed system logic can be achieved at any one time. These features are consistency, availability, and partitioning resistance. Consistency means that simultaneous access to identical data is possible, regardless of the access node (immediately after updating the data in one node, other nodes' updates are required). Availability means that data access is possible even when some nodes are temporarily down (each node always returns the correct answer). Partitioning immunity, in turn, means that, regardless of the number of interruptions in communication between nodes, the entire distributed database system must continue to operate.

There is no single best solution when choosing a distributed database system as with choosing the database itself. One should consider the available options, taking into account the requirements of the network in which these databases will be used.

Dynamic spectrum management - beyond 5G

As mentioned, databases of various types (relative, graph, etc.) are widely used nowadays. On the one hand, one may consider the registers for storing user-specific data (such as a Unified Data Management entity in the NR architecture [54]) and, on the other, advanced technologies designed for processing and computing at the edge, in the fog, or cloud. However, envisaged for 6G is the presence of a dedicated map-oriented subsystem created and managed for collecting, storing, and processing massive information about the communication context. In other words, it includes all the information about the context that might be useful for improving the network's performance. Such information can be geographical data, architectural maps, telecommunication data, electromagnetic data, user behavior in different time scales, habits, user profiles, social data, data from other systems, such as public transportation, weather forecasts, etc. Information has to be gathered using the crowd-sourcing approach to populate the database and keep it up-to-date. Databases may be shared between operators or in the sole possession of one stakeholder; however, standardized interfaces must be defined in the former case. The volume and variety of prospective information entail the need for custom processing typical for big data schemes.

One may consider the following analogy: what we foresee for 6G in terms of massive context information processing for 5G solutions is similar to the technological and conceptual change between the conventional MIMO scheme in LTE and its massive version in NR. In what follows, we focus our analysis on radio-specific aspects of the proposed solution, that is, on the application of a subsystem based on RSM for context-aware communications.

Dynamic spectrum management - context-aware communication

Initially, the term "context-aware communication and computing" referred to a software engineering solution that allows the automatic customization of devices, systems, and applications according to the changing context of the radio environment, e.g., [55]. The context refers to the information that characterizes the operational state of each entity in MNO RAN. It comprises a set of parameters that define the state of RAN in detail. Typically, location information (a map) is associated with a set of context parameters that define certain aspects of RAN states. Numerous types of maps can be identified at different hierarchy levels, ranging from the level of base stations (BSs) to the level of RAN, backhaul, and core network. Different contexts can characterize the corresponding operational states at each hierarchy level, i.e., a higher-level description can utilize less specific, generalized metrics/parameters. The hierarchical approach addresses the problem of complexity and computational cost, which in dense heterogonous networks are expected to be considerably high. This is mainly due to an increasing amount of prospective context information that requires big data processing with high geographical granularity. Moreover, artificial intelligence algorithms are envisaged for proper inference and reasoning based on rich context information. Please note that when referring to big data processing, we refer to the definitions and approaches presented in [56] where the datasets are described by four or five "Vs", that is, volume, velocity, variety, veracity, and value.

Geographic Information System (GIS)

It is impossible not to mention spatial databases to present various types of databases and distributed database systems. It is a database optimized for storing and querying data related to objects in space, such as points, lines, or polygons. Traditional databases operate on numeric and character data by default, while they need additional functionality to handle spatial data types.

In addition to typical operations possible in each database, it is possible to perform many spatial operations, such as spatial measurements (distance between points, polygon area, etc.) or modification of existing spatial objects (such as translation, rotation, etc.). A popular and willingly used example of a database that can be used as a spatial database is PostgreSQL, which, based on the PostGIS extension, includes all the necessary data types and functions to handle spatial data. Moving further into the spatial database topic, more complex systems are built. From the point of view of this work, the most important is Geographic Information System - that is, a system for entering, collecting, processing, and visualizing geographic data. Each of the GIS systems consists of a geographic (spatial) database, computer hardware, software, and the creators and users of GIS. A broad group of GIS records includes all types of records (land, buildings, and resources in general) used by, for example, surveyors. Other applications are the location of various phenomena (e.g., weather) or the analysis and imaging of statistical data (e.g., the occurrence of diseases). Databases of this type constitute the basis of the radio environment databases. The previously mentioned data are stored data closely related to the radio environment (e.g., signal strength in a specific location).

Data collection and maintenance

As previously described the various database systems that can be used to store contact data, let us now discuss contextual information itself and the process of creating the data structure in which the information is placed. Additionally, we raise the issue of updating the stored value and, more importantly, accessing the stored information itself.

The general observation regarding the contextual information database is the need to adjust many parameters and the database structure itself depending on the type of contextual information we intend to store. Moreover, the same contextual information may require different parameters and structures for different geographic areas (urban environment, large environment, etc.) and applications. The selection process should be carefully analyzed for a specific application each time. The main parameters and structures whose selection should be analyzed are:

- type of data grid (mainly whether it is a regular grid)
- the process of adding a new value
- value storage algorithm (in particular, information aging)
- the exact way of data interpolation

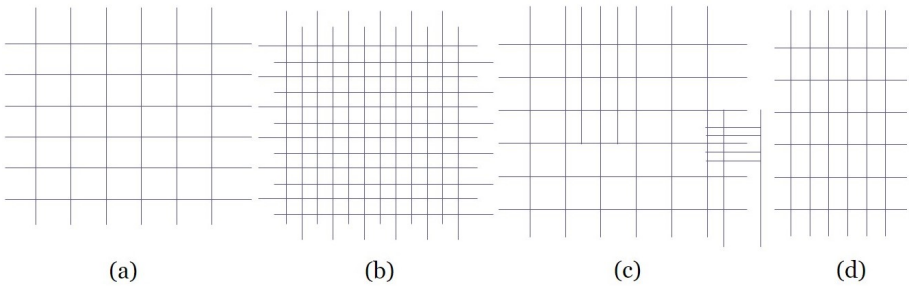

FIGURE 2.1: Examples of the considered map grid structures

The first considered aspect is the structure of the map (data). Examples of the various grid structures can be seen in Fig. 2.1. In the conceptually most uncomplicated case, a regular grid of points (positions) can be considered, which is static; therefore, at an early stage, the same set

of positions considered on the map is determined (see Fig. 2.1 (a)). The most crucial parameter, in this case, is the distance between the closest points on the map because this directly affects the accuracy of the map, but also its size, and thus the memory and calculation time related to these data. It should be noted that in some cases, it would be wise to use different distances between adjacent points in both planes (see Fig. 2.1 (d)). However, there are no contraindications to considering a grid with a low density of points and, in some places, using a higher density of points (e.g., low density in a rural area and dense in an urban area) (see Fig. 2.1 (b-c)). This hybrid approach is a trade-off between accuracy and size, and complexity. When this problem is examined differently, a regular (rectangular) mesh is not always the best structure. In some cases, it is worth considering the use of meshes based on a Voronoi diagram [57]. Additionally, other structures such as a structured, unstructured, or weighted Voronoi mesh can be considered.

Another important aspect is the addition of new data to an existing database. For simplicity, we temporarily assume a map with a regular grid of points. When considering one point on the map, we have a single value at a particular position. As long as the new information (regardless of the source of this information) is located at the same point on the map, it can be assumed that we are simply updating the map value. However, when a new value is found near a point on the map or when there is more than one piece of new information, one should manage this sufficiently. One of the possible options is to map it to the nearest point. Another is to apply weighted mapping (where the new value affects the map value with the weight based on the distance to the point on the map). In the second case, the closest point on the map is the greater influence of the value of a point on the map. A single value on the map does not have to be represented by one value in the database - we can store many values (and their weights) and calculate the final value of a map point based on them. Going one step further, consider, for example, a structure based on a Voronoi diagram, and each new piece of information can create a new division of the sieve. That is, it can be treated independently of the previous one. All these observations should be taken into account. When planning the database structure for contextual information, depending on the application and requirements, the solution will be completely different.

Another important aspect is the way (or algorithm) of storing information. In particular, it is about aging information and how long it is valid and should be stored. Some contextual information may be hours or even days/months, and for others, it may only be seconds or milliseconds. In addition, attention should be paid to the fact that the length of information storage is one thing, but one needs to answer whether the new one should replace the old information; if not, it should be of the same importance, or maybe more, or maybe less. On the largest scale, all typical behaviors and values can be found (e.g., channel-type map, loss map, etc.). Apart from exceptional situations, these maps should be the same (or similar), e.g., every day. On the medium-time scale (hours or minutes), it is possible to present changes in the long-term observations that modify the typical values considerably. In a short time scale of observations, one presents the latest (real-time) events, e.g., the impact of the radio network load and user traffic.

A very interesting approach to creating a radio environment database structure is the use of Machine Learning (ML) algorithms. These could be useful for a clustering process where adaptive decision making on the map "points" would be possible with a Voronoi grid. However, ML algorithms can also help with the time scale of creating such a database and determine the validity of historical information by adapting to a particular type of contextual information and situation.

The last but not least aspect is an effective reading of the values from the database at a specific point. This topic is closely related to the map structure (e.g., a regular mesh) and the information aging. However, it is worth discussing reading a value from the map which is unknown, i.e., a point exists on the map but has no information, or the point is close to another point (distance at the

level of the distance between the nearest points). Here, one needs to decide on the value returned by the database. One of the most straightforward approaches is to read the value at the closest known point. Alternatively, the use of spatial interpolation can be considered. In many cases, basic (simple) spatial interpolation methods are sufficient, such as Inverse Distance Weighting (IDW) [58], that is, when determining a value in a place where the value is unknown, the nearest few points with a known value are taken into account. The weights of individual values are calculated based on the inverse of the distance value to a power. Create a simple dependence were the more significant the weight, the smaller the distance between the points. The main advantage of the IDW method is its simplicity and straightforward algorithm. However, this method gives good results only for some data types because the weights of individual measuring points are independent of the tested value.

Kriging [59] is a much more accurate and complex method of spatial interpolation. The principle of operation is the same as in the case of IDW, i.e., the calculated value at a given point is influenced by a number of the closest measurements, and the weight of each of them is based on the distance. However, the function used to determine the weight of individual values is created by carefully examining all samples of the quantity under study. It is based on a semivariogram, where the variance between each pair of samples is determined, and a graph is created in tandem with the distance between the points. It shows the relationship between the difference in values at individual points and the distance between them. For some values (such as the value of the received signal), samples located almost in the same place (distance close to zero) should not have the maximum possible weight. It should be noted that the value of the received power fluctuates (it is not a constant value, such as height above sea level). In this case, creating a semivariogram allows for building a model of the dependence of the sample weight on its distance and better adapting to the characteristics of the tested value.

2.2.2 Radio environment and radio service maps

Radio Environment Map (REM) are radio data (such as the strength of a received signal) presented and recorded in the form of a geographic map [60–63]. A straightforward example of an environmental map in geography is the elevation map of the terrain above sea level. In the case of radio environment maps, one can imagine replacing the value of altitude above sea level with the value of the received power at a given point. As in most areas, we cannot perform precise and accurate measurements at every possible point in the analyzed area. For this reason, a very popular solution is the use of spatial interpolation to complete the map fragments (places) where the measurement has not taken place (as introduced above). Measurement that was not carried out at a given point may be different, such as the lack of physical possibility to place the measuring equipment at a certain location, or simply the assumed density of the measurements entails the lack of no measurement at some points. The REM itself most often represents a physical (measurable) quantity, such as received power, interference, user density, etc. Taking this type of information into account and adding logical inference to it, we can create a different type of map, that is, a Radio Service Map (RSM) [64]. RSM is a more general term and REM is a subset of it. RSM may present parameters that are not measurable but still related to radio networks, e.g. the Sounding Reference Signal (SRS) delay, a Modulation and Coding Scheme (MCS) distribution.

The data stored by REMs or RSMs can be of very different types. The most interesting suggestions of map types that can be useful for improving the spectral efficiency of the network are discussed below:

- maps contain data on the radio environment; this type of map contains parameters specific to the physics phenomena of wireless signals. In such a situation, several subtypes can be distinguished:
  - capacity maps describe parameters directly related to system or cell capacity, such as spatial distribution of traffic volume, spectral efficiency, percentage of users served, type of network traffic, probability of user failure, etc.
  - like the previous ones, coverage maps show the parameters of coverage of a given area with the signal. They may include information such as: Signal-to-Noise Ratio (SNR) spatial distribution, Received Signal Strength Indication (RSSI) or Reference Signal Received Power (RSRP), interference level, shading data, etc.
  - performance maps, which have data on performance and level of service provided, such as Quality of Service (QoS), Quality of Experience (QoE), latency and transmission time, throughput, etc.
  - mobility maps showing data related to cellular networks, e.g., switching regions and pilot coverage. Such maps can be beneficial in advanced spectrum allocation systems
- traffic density maps store various information specific to the characteristics of network traffic. For example, they allow one to determine in which areas the traffic is very high and where it is almost nonexistent
- trajectory and traffic maps contain data on the typical or exact physical traffic of users of a given network, e.g., in cities, the typical trajectory of traffic for cars and people is the path along the streets
- history maps have very different information gathered from long observations of the network. This type of map can be especially useful for dynamic resource allocation systems as it enables optimal decisions based on previous decisions

We should also remember that the very initial concept of an REM is a single map that represents certain information. However, it is necessary to use many such maps simultaneously in more complex systems, which brings us to the term radio environment database. It comprises a plurality of radio environment maps or radio service maps and information about the radio environment that is not necessarily represented in map form. When designing and presenting radio systems using REM or RSM, we most often mean this database of the radio environment.

Note that the idea of databases applied to improve system performance has been considered in numerous contexts, particularly regarding dynamic spectrum access and spectrum sharing, where radio service data are of particular importance. In essence, RSM can contain all the maps listed above to optimize the performance of the radio service in a given area. The RSM-based subsystem for DSM consists of three main functional blocks:

- databases (repositories), which contain various types of data: private or public, understandable by a human and by a machine

- RSM manager, playing the role of a cognitive engine, responsible for database management and data processing, general reasoning and decision making, conformance verification, coordination, and control, as well as communication with other RSM managers and corresponding operators' legacy entities
- data acquisition function responsible for collecting data from the environment covered by RSM, either periodically or in an event-driven way (here, the application of sensing or monitoring modules can be considered)

It is worth noting that the word map is not (or is not always) the best representation of contextual information on a radio network. Most often, the context for the information, in this case, is the network user himself. Although the user has a geographical location, it is not always the best way to represent it. Instead of referring to a specific user's location, it may be the user himself or some relationship between him and someone or something else, e.g., other users. As an example of a different approach, it is possible to indicate a situation where it is not essential where the user is, but only whether there are many or few other users in his immediate vicinity. This type of information can be used in the resource allocation process, especially in Multiple Input, Multiple Output (MIMO) systems, to reduce interference.

Architecture of RSM-based subsystem

The architecture of a generic subsystem based on RSM containing the above elements is shown in Fig. 2.2. Assume that each operator has its RSM-based spectrum management system. Each operator will have user data that cannot be shared but can be processed for service delivery (e.g., some sensitive user data). The set of repositories is split into two parts: the private (including sensitive information) and the shared one. Furthermore, each RSM-based spectrum management system needs dedicated interfaces between the RSM and network domains. Operators' RSM subsystems can exchange data directly; however, the publicly available data can also be managed by a third-party RSM subsystem.

The generic structure of the RSM-subsystem can be further adjusted for specific applications.

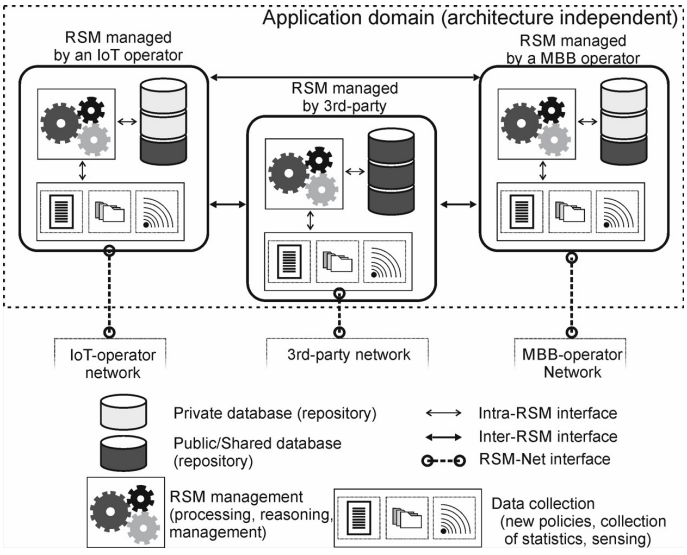

FIGURE 2.2: Structure of the database system in the application domain

The RSM subsystem can be implemented in a distributed or centralized manner, and this implementation depends on the deployment of BS in the covered area. If the BS density is low,

it should be beneficial to use a centralized RSM for BSs coordination. The physical location of the elements of the RSM subsystem depends on the application time scale for which the database is designed. Therefore, a layered (hierarchical) architecture seems to be the most appropriate for practical deployment, where long-term data are stored in centralized RSMs. In contrast, short-term information is stored in distributed, local RSMs.

Defining the context

Rich content and possibly massive data sets that define the surrounding environment (that is, the widely understood communication context) can improve the performance of the future network. Such improvement will be possible when the quality and veracity of the data are preserved and when access and data processing are manageable. In Table 2.1 we compare selected aspects of context maintenance.

Table 2.1: Summary of the challenges for developing clear context dataset

Parameter	**Challenge**	**Supporting technology/solution**
Data collection and their veracity	Massive datasets have to be updated, this requires permanent (periodic or continuous) data gathering	Crowdsourcing achieved by the deployment of dedicated sensors and/or utilization of measurements conducted by UEs
Variety of data	In terms of dynamic spectrum access, numerous maps can be defined; depending on the application use case, some maps will be of higher importance	Although the types of created and stored maps have to be decided in the design phase, the role of each map may vary in time, so adaptive algorithms could be applicable
Storage and processing	Due to the "five Vs" concept [56], massive datasets require specific approaches for their storage and processing	Currently developed technologies like fog/edge/cloud computing are the basis for the development of new frameworks for big data processing for DSM
Ownership	Management of a dedicated RSM-based subsystem is costly	Various databases may be shared between the operators reducing OPEX; also, the establishment of dedicated context-information datacentres (as it is now the case for cloud-computing) could be a valuable option

2.2.3 Edge intelligence

A recently popular concept is edge intelligence, which introduces more and more adaptive algorithms to the very edge of the network, e.g., base stations. To accurately present the concepts of edge intelligence, some words about edge computing should be said [65]. In a nutshell, it is an approach that involves collecting, storing, processing, and analyzing data closer to the location where these data are needed. This approach aims to reduce data transfer delays and the amount of data sent across the entire network (saving bandwidth and time). The primary rationale behind this approach is that the data is generated at the network's edge. The amount of information generated is currently huge and is expected to be even more significant (big data). Note that this approach does not move all tasks to the network edge. A combined approach between edge computing and cloud computing can be used. Depending on the desired effect, it is possible, first, to relieve the backbone network (increase its efficiency) by reducing the amount of data transferred,

second, to reduce delay in applications located at the edge of the network, and third, the cloud has huge reserves (backup) for calculations and storage. Due to the presence of huge amounts of data generated in the network and various types of data, the promising tools for effective analysis of these data are artificial intelligence algorithms. These algorithms are essential in the decision-making process. Combining the concepts of edge computing and artificial intelligence leads to the idea of edge intelligence. In this approach, the resources available at the network's edge are used to meet artificial intelligence needs. In addition to the advantages mentioned above of this approach, there is one more thing, namely privacy. The use of AI near the edge significantly improves user data privacy, as it is no longer necessary to send it to the cloud. In many cases, contextual information does not need to be collected by thousands of nodes and then passed to the central node, but it is sufficient for the end node collecting the data to take advantage of it. This reduces the delay in making decisions and the amount of information sent over the network. A prime example is a base station that allocates resources to users based on traffic class or traffic history.

Summary

The concepts presented in the above sections were used in the investigations described in subsequent chapters, where a specific set of contextual information was used to improve the spectral efficiency of the system. Moreover, each of the works uses REM or RSM with a different level of complexity. In Sec. 2.4, an exact set of measurements of the power received in the TV band has been stored in the form of REM. In subsequent works, presented in Sec. 3.1, the previously created REM was used in the spectrum access algorithm. The next work described in Sec. 4.1 uses a dynamically created RSM to monitor, among others, the information about the observed quality of services by primary users. In Sec. 4.3, the contextual information was collected and saved in the form of RSM, with the help of which an algorithm for assigning users to base stations were developed. In each case, the proposed algorithms were placed close to the end-user (in a single base station or a small group of base stations), which is in line with the edge intelligence approach.

2.3 Standardization and regulation activities

In many projects, there are examples of contextual data to make better use of the spectrum. However, it is currently not clear what data should be collected in REM databases and how it should be used to use their potential fully. There are many ideas for solving this issue, and the chosen ones are presented below. First, research projects were mentioned, and then standards in which the issues of implementing the entire system architecture were discussed and descriptions of the concept itself and how it should work.

Project FARAMIR

FARAMIR [66] was an EU-funded project focused on designing and managing maps of the radio environment in the context of frequency sharing and dynamic spectrum access. Some crucial discoveries were made as the project consortium discussed several issues related to creating, populating, and managing databases. The main flow of information on spectrum access and management, implemented using REM databases, is shown in Fig. 2.3.

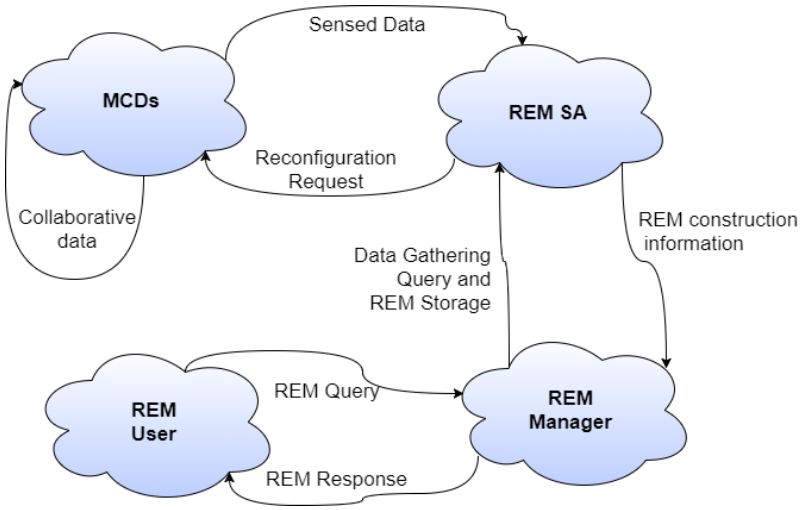

FIGURE 2.3: Information flow graph for a spectrum management and access system based on REM databases [66]

One can observe the presence of measuring devices Measurement Capable Devices (MCD) that can independently or jointly send data about the radio environment (also after calling them) to the REM data storage and acquisition unit REM Storage and Acquisition (REM SA). MCDs are also able to exchange various types of information with each other, which is generally referred to in the figure as "Collaborative Data". Finally, these devices are subject to the reconfiguration request provided by REM SA. Additionally, the REM data storage and acquisition unit sends design information to the REM manager based on the data collected from the MCDs. REM SA can also accept queries from the manager (so-called *Data Gathering Query and REM Storage*) that may trigger a reconfiguration request to the MCDs. The main role in the system is played by the REM manager, who is responsible for information and system management, is able to ask REM SA for new data, and can also provide final answers to REM inquiries initiated by users. An interesting approach is shown in Fig. 2.4. It can be seen that the entire system is logically divided into a network and a terminal domain, and it is assumed that the terminal will have its logic implemented. The cognitive device supporting the policy comprises a functional block (rules engine) consisting of the selected rules and a policy set database. The rule requesting system is responsible for analyzing the consistency of the rules and the full rule requesting process.

The EP communicates with the *Policy Enforcing Point* (PEP), which is responsible for controlling and enforcing the correct implementation of the current rules. A *policy capable Cognitive Device* (PCD) communicates with a policy server (*Policy Server*) through a dedicated control channel for exchanging policy-related data, including notifications and registration. On the network side, the policy manager controls the policy server, which in turn collects data from the radio environment.

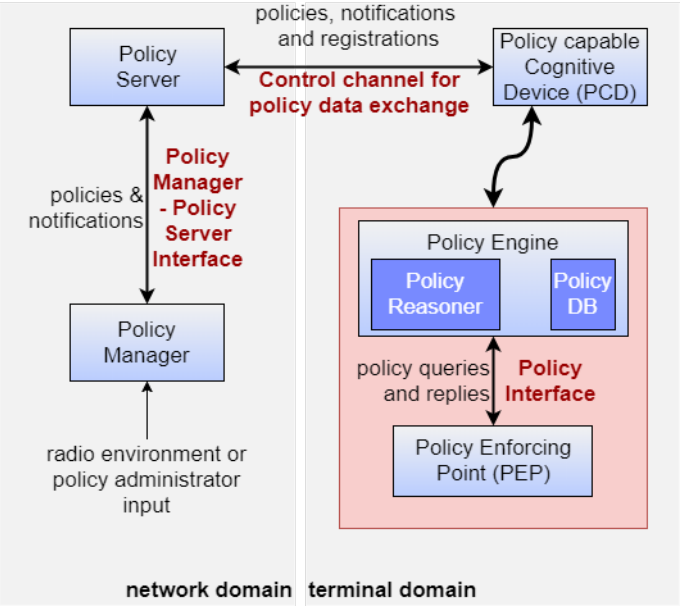

FIGURE 2.4: Management system based on a set of rules proposed by the project FARAMIR

Ofcom Activities

In the European context, it is worth mentioning the activities initiated and managed by the British state body controlling and supervising the media and telecommunications market Office of Communication (Ofcom). In the UK, it was decided to open up a fragment of the TV spectrum for opportunistic use (characterized by no fixed rules) based on databases. The structure defined in the official guidelines is shown in Fig. 2.5. It can be seen that the *Master-Slave* relationship is considered here (as opposed to some solutions presented earlier).

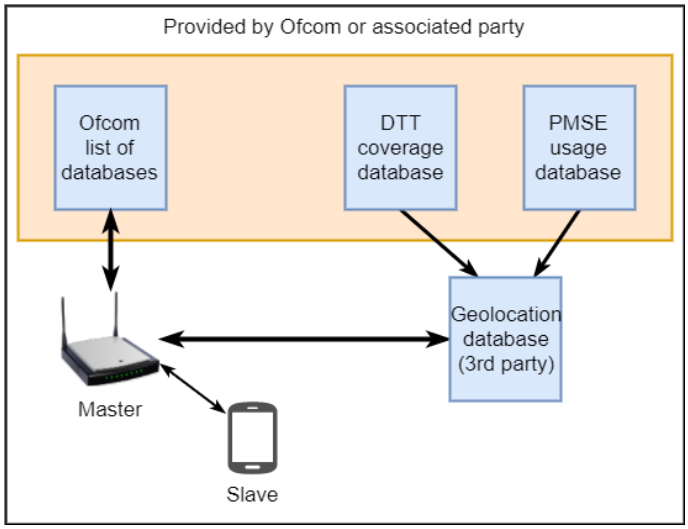

FIGURE 2.5: Information flow graph in a database-driven spectrum management system (Ofcom)

The mobile device communicates with a base station (or another access point) responsible for negotiating with a database-based spectrum sharing system. In the first step, the master device requests a list of available and active databases and then communicates with the appropriate geolocation database. This, in turn, consists of two essential parts, one dedicated to Programme Making and Special Events (PMSE) devices, and the other to store information related to digital terrestrial television.

Standard family IEEE 1900.X

As part of developing a cognitive radio technology that uses contextual information as the basis for its operation, various standardization groups are developing system solutions for communication systems. The most interesting is the IEEE 1900 family of standards. The IEEE family of standards is being developed by the IEEE Dynamic SPectrum Access Networks (DySPAN) Standard Committee. This committee works closely with the Telecommunications Society IEEE Com. Soc. (IEEE Communications Sociatety) and the CSSB (Com. Soc. Standards Bard). The aim of IEEE DySPAN is to develop:

- rules of dynamic access to spectrum in new systems increasing resource efficiency
- spectrum management methods and new generation wireless networks management
- principles of Coordination of the exchange of information between them

As part of the work of these organizations, the family of IEEE 1900.x solutions was developed:

- IEEE 1900.1 *Definitions and Concepts for Dynamic Spectrum Access: Terminology Relating to Emerging Wireless Networks, System Functionality and Spectrum Management.* This standard provides the basis for developing other standards in terms of their definition and terminology used in dynamic spectrum management. This standard was adopted in 2008 and extended in 2011 by the updated addendum 1900.1a (the current one from 2013) defines terms used in dynamic spectrum management and their use. It allows unifying the dictionary of terms used around the world by engineers and researchers dealing with cognitive radio [67]
- IEEE 1900.2 *Recommended Practice for the Analysis of In-band and Adjacent Band Interference and Coexistence Between Radio Systems.* This standard was adopted in 2008 and is subject to further development. It contains guidelines for the analysis of interference between systems and the rules of their coexistence [68]
- IEEE 1900.3 *Recommended Practice for Conformance Evaluation of Software Defined Radio (SDR) Software Modules.* This standard provides guidelines in the form of mathematical rules for the evaluation of SDR platforms in terms of their compliance with the requirements for dynamic spectrum management
- IEEE 1900.4 *Architectural Building Blocks Enabling Network-Device Distributed Decision Making for Optimized Radio Resource Usage in Heterogeneous Wireless Access Networks.* This standard was extended by the development in P1900.4a *Architecture and Interfaces for Dynamic Spectrum Access Networks in White Space Frequency Bands* and P1900.4.1 *Standard for Interfaces and Protocols Enabling Distributed Decision Making for Optimized Radio Resource Usage in Heterogeneous Wireless Networks* defines the architecture and provides a detailed description of the interfaces and protocols for intelligent spectrum management by the CRS (Cognitive Radio System). It should be noted that the extension of the P1900.4a

standard adopted in 2011 enables the provision of mobile wireless access services in free frequency bands (White Space Frequency Band) [69]

- IEEE 1900.5 *Policy Language and Architectures for Managing Cognitive Radio for Dynamic Spectrum Access Applications.* This standard defines a vendor-independent set of architecture control policies and language requirements for networks with dynamic spectrum access. The language of requirements is usually the rules that define the rules in force in a given area regarding the operation of cognitive radio. The standard was published in 2012, and the working group is planning to work on 1900.5a project, which includes the definition of interfaces between elements of architecture and policies. For a schematic of the components and interfaces of the IEEE 1900.5 DSA policy set architecture, see Fig. 2.6. As can be seen, five separate ones have been identified as components (i.e., one optional and four compulsory). These are SSRC, Policy Enforcer (PE), PCR, Policy Management Point (PMP), and optional policy repository. Currently, the standard has two extensions marked with the symbols 1900.5.1 and 1900.5.2 [70]

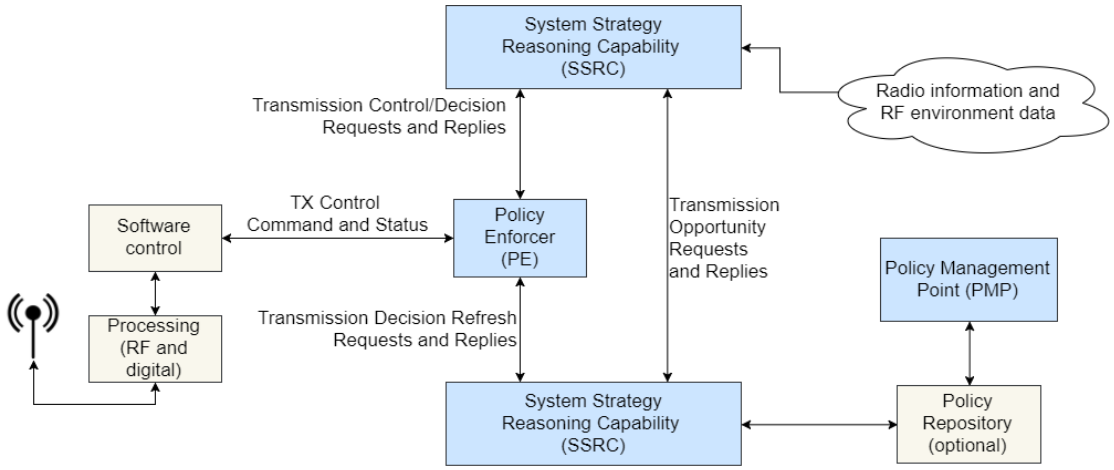

Figure 2.6: General architecture of a DSA based on the IEEE Policy Set 1900.5

- IEEE 1900.6 *Spectrum Sensing Interfaces and Data structures for Dynamic Spectrum Access and the Advanced Radio Communication Systems.* This standard defines the interfaces and data formats to exchange spectrum detection information between sensors and clients. In 2014, the standard was supplemented with the extension 1900.6a concerning procedures, protocols, and interfaces for storing and acquiring data. The supplement includes the definitions of protocols, procedures, and formats for transferring information, control, and configuration data between sensors and clients. Work is currently underway in 1900.6b extending the standard with interface definitions for databases containing information about spectrum occupancy, including REM databases [71]

- IEEE 1900.7 *Radio Interface for White Space Dynamic Spectrum Access Radio Systems Supporting Fixed and Mobile Operation.* This standard defines the radio interfaces used for dynamic access to free dune spaces and the rules of operation for mobile and fixed radio networks [72]

LSA and CBRS

It is foreseen that in the future, the static models of spectrum management and licensing schemes, e.g., license-exempt (as applied for, e.g., Industrial, Scientific, Medical (ISM) band or for Unlicensed National Information Infrastructure (U-NII) band) and exclusive use (as, e.g., for regular cellular operators), will be complemented by flexible ones [73]. Although the static solutions are easy to implement and manage, it is envisaged that the introduction of spectrum flexibility is necessary to accommodate the expected traffic growth for future wireless networks. In this context, infrastructure and spectrum sharing have been widely investigated in the previous years, leading to significant achievements. This research is highly associated with the concept of cognitive radio, which was introduced almost two decades ago, and which assumes the inclusion of some artificial intelligence into the communication system [1, 74]. The key concept of a cognitive approach to spectrum utilization is to create an opportunity for flexible spectrum access based on various utilization goals or optimization criteria (such as the maximization of spectrum usage or minimization of mutual interference).

It is also assumed that for the protection of existing data transfers between the transmitter and receiver (in general so-called primary systems), an efficient algorithm that utilizes detailed information about the surrounding environment must be provided. The information may be achieved through spectrum sensing [7] or received from a dedicated database [75, 76]. Two approaches to flexible spectrum sharing have gained particular attention, mainly Licensed Shared Access (LSA) [77] and Spectrum Access System (SAS) applied to Citizen Broadband Radio System (CBRS), denoted hereafter as CBRS-SAS [78]. Various surveys have been published discussing the key achievements of the scientific society working in that domain, e.g., [79–81]. Next, in [82], the authors have surveyed various licensed spectrum sharing schemes from the point of view of their applicability by mobile network operators. An interesting discussion on the selection of the best access strategy for various spectrum bands is presented in [83]. LSA was originally introduced by the European Commission (EC) [84] to respond to the interests of the industry. In this model, additional licensed users are introduced. They can utilize spectrum bands used by other incumbent systems as long as they follow the dedicated spectrum sharing license. The first frequency band being studied for LSA is 2.3-2.4 GHz in Europe. As a result of efforts made by the Conférence européenne des administrations des Postes et des télécommunications (CEPT) and the European Telecommunications Standards Institute (ETSI), the sharing framework for LSA contains, e.g., harmonized technical conditions, cross-border coordination aspects, etc. From the architecture perspective, the implementation of the LSA concept assumes the presence of two components on top of the existing cellular architecture, mainly, LSA Repository and LSA Controller. Let us mention that the Authorized Shared Access (ASA) concept also falls under the LSA umbrella [85,86]. LSA evolution is also being developed to provide user priorities and a more dynamic overall approach to access shared spectrum resources [87, 88]. A simple schematic of the LSA architecture can be seen in Fig. 2.7. There are two main elements shown as LSA repository - which contains information on the use of spectrum by primary (existing) users in time, frequency and space and LSA controller - which processes and calculates spectrum availability and generates final rules for spectrum usage.

The second one of the most popular spectrum allocation and sharing schemes is considered within the CBRS-SAS, where the sharing model with three tiers of users is introduced by the Federal Communications Commission (FCC) in the US for the 3550-3700 MHz band [89, 90]. Unlike LSA, it enables additional usage of both licensed and license-exempt-like spectrum, as long as the incumbent's rights are protected.

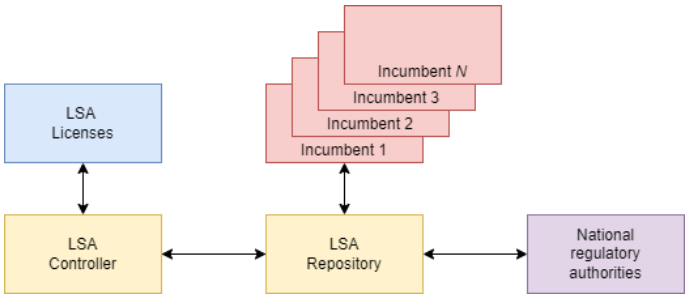

FIGURE 2.7: Basic architecture of Licensed Shared Access

Two types of spectrum uses are introduced here, Priority Access Licenses (PALs, being the licensed users operating along with the rules similar to those in the LSA concept) and license-exempt - like General Authorized Access (GAA). The dedicated Spectrum Access System (SAS) controls the spectrum access for both PAL and GAA users. The main difference is that PAL users are protected from the interference caused by other PAL and GAA users, and in general the GAA users are not. However, recently, new approaches to managing interference between GAA users have been considered, mainly CBRS Alliance discusses the need for the introduction of dedicated coexistence manager [91] responsible for spectrum management among CBRS-SAS users.

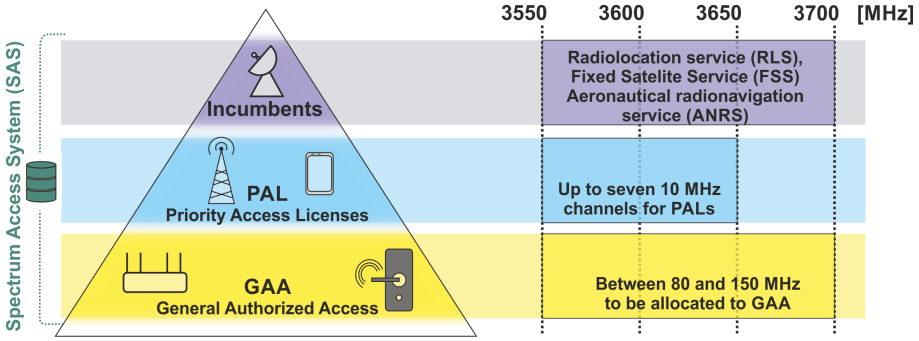

FIGURE 2.8: Three tiers of spectrum access in CBRS

A diagram presenting the hierarchical relations between the three layers of CBRS-SAS users is depicted in Fig. 2.8 (source of diagram [92]). One can observe that the CBRS-SAS sharing model enables additional transmissions to be realized on both licensed and license-exempt bases while protecting the incumbent's rights. Following [93, 94], all incumbent systems have to be protected by the Citizens Broadband Radio Service Device (CBSD), i.e., the devices, fixed stations, or network of such stations that are granted functioning in the shared frequency band. Two classes of CBSDs are defined (class A and B), which differ, i.e., in the maximum allowed transmitting power. The exemplary incumbents to be protected are navy radars or other Department-of-Defence (DoD) systems, Fixed Satellite Services, and so-called Grandfathered Wireless Broadband Licensee. As the CBRS-SAS model introduced additional licensed users, i.e. Priority Access License (PAL) users, they should meet additional requirements. PAL users should protect the incumbent systems. However, at the same time, they should be entitled to protection from GAA users (third tier of users) and other PALs *within the defined temporal, geographic, and frequency limits of their PAL, consistent with the rules outlined in this part* [94]. One may state that the PAL users have operational certainty similar to the LSA licensees. The GAA users are simply one of the CBSD users (regardless of the CBSD class) and have to protect the other transmission realized within higher tiers. The PAL and GAA systems have to accept the interference originating from any systems operating in higher layers of the CBRS-based model.

The key component in the management of interference in this concept is the Spectrum Access System (SAS) that coordinates the spectrum usage of CBRS-compliant devices to protect the incumbents and PALs from other CBRS users. In principle, SAS is a combination of controlling functions and a database for the coordination of interference. Numerous detailed features of SAS are defined in [94], such as:

- determination and provision to CBSDs of permissible channels or frequencies, as well as maximum permissible transmit power level at their location
- registration and authentication of the identification information and location of CBSDs
- retention of information on so-called exclusion zones and protection zones
- resolving of any conflicts in using the frequency band while maintaining a stable radio frequency environment

It is worth mentioning that the CBRS-SAS concept has adopted the Environmental Sensing Capability (ESC) for monitoring the incumbent activity, which would detect the appearance of specific incumbents.

Related Work

Focusing more on the CBRS-SAS domain, one of the fundamental papers [90] investigates the perspectives of the CBRS-based system for the 3.5 GHz frequency band. Next, Sahoo in [95] investigated two approaches (i.e., static and one called max-min fairness) used for the fair treatment of GAA requests. This is due to the requirements expressed by FCC [94] to ensure the spectral efficiency and non-discriminatory coexistence of various CBSD. Our approach presented in this thesis extends this problem towards much more flexible resource allocation among the CBSDs - we allow not only for flexible power allocation but also for the adjustment of the transmit power to meet interference constraints. It is worth mentioning the recent trends investigated within the Wireless Innovation Forum (WInnForum), e.g. [96–98], which deal with the ways of applying spectrum coordination between GAA users in the CBRS-SAS system. It is widely considered to apply tools from the network theory to create interference graphs and apply various graph coloring solutions. The main goal of these approaches is to deal with GAA spectrum channels to maintain better and coordinate the interference between GAA users. In this thesis, we follow this approach as well; however, the proposed solutions assume a much higher level of flexibility given to SAS and the spectrum controller.

In the recent paper, i.e., [99], the authors have presented a design of the so-called hybrid centralized and distributed Medium Access Control (MAC) scheme for SAS. In their approach, the proposed self-organized spectrum sharing scheme applies the benefits of learning algorithms based on game theory and reinforcement learning. In particular, in the first approach, the achievement of Nash equilibrium within a non-cooperative game is considered for interference minimization and fair spectrum sharing among CBSDs. In the second approach, N_Q-learning with a decision-making process modeled as a Markov decision process is considered. By incorporating various sources of interference (adjacent and co-channel interference) and by analyzing the overhead introduced by the proposed solutions, the authors claim to propose a tool for future wireless networks. This thesis does not apply any of the aforementioned tools for spectrum sharing and channel allocation; contrarily, we assume a centralized approach where graph theory is considered. The same authors in [100] considered the application of a broadcast message termed rejects request to send. This approach modifies the solution known in the IEEE 802.11 Distributed Coordination

Function (DCF) mechanism and adjust it for SAS to maximize the system throughput for GAA CBSDs operating in an unlicensed spectrum. In [101], the preliminary results for the application of the maximum weighted independent set principle known from graph theory have been presented. The study of SAS-assisted centralized carrier allocation among CBSDs was evaluated in two ways, by an analysis of two metrics: first, the min-demand service ratio, and second, the max-demand service ratio as a function of the managed CBSDs. The so-called super-radio formation algorithm was proposed to identify the set of radios coexisting in the same channel. What is worth mentioning in that context is that the authors have considered a carrier sensing mechanism known from the WiFi domain. An extended version of this thesis is presented [102].

The considerations of various user categories (associated with various requirements set to the minimum acceptable throughput) were presented in [103]. The proposed dynamic algorithm allocates the resource blocks among all stakeholders to achieve the minimum requirements assigned to each category. In order to achieve this goal, the fulfillment of the traffic requirements is evaluated by determining the transmission path-loss and shadowing effects. This paper discusses the CBRS-SAS approach in the context of 5G networks through carrying out experiments using a proprietary 5G, system-level simulation tool calibrated according to the 3GPP technical report 36.814. Hardware experiments, and dedicated field trials evaluating the implementation of the CBRS-SAS model were proposed in [104, 105], as well as in an our other paper, i.e., [106]. Finally, the problem of reliable detection of the incumbent radar systems operating in the 3.5 GHz band is discussed in [107].

2.4 Radio environment maps for TVWS — experimental implementation

To provide the rationale for creating and deploying the indoor and outdoor REM databases, one may need to perform a detailed measurement campaign to estimate the potential availability of specific frequencies for the considered. This section covers the entire process of creating a REM map for a particular case. The description includes all the steps from taking measurements through their processing, interpolating missing data, and creating ready maps. The analyzed case is the power received in the television band. Here the database has been prepared based on the measurement campaigns carried out in Poznan, Poland. The power of all detectable received Digital Video Broadcasting - Terrestrial (DVB-T) signals has been measured in specific locations inside and in close vicinity of the building of the Faculty of Computing and Telecommunications (the Faulty of Electronics and Telecommunications at that time) of Poznan University of Technology (PUT). Then, a crucial step was to analyze the collected data. Based on such measurements, the kriging algorithm has been applied to calculate the approximated values of the received power in any place inside the building. Once such a reception map has been created, it is used to calculate the maximum allowable transmit power of the new wireless transmitter operating in a selected TV channel.

2.4.1 TVWS-based dynamic spectrum access

Observation of the low use of the television band and the stationary (slowly changing) nature of this network (positioning of transmitters and channel assignment) was the motivation to perform some long-term investigations on the possibilities of actual deployment of secondary systems with associated REMs that will operate in TV band while protecting the DVB-T receivers. The goal was to verify various factors which may influence the practical deployment of such a secondary system and to identify how these factors map the design of the secondary system. To meet these goals, we have conducted various measurements (e.g., the received power of the DVB-T signal was measured), both inside and outside of the building. We have tested the stability of the signal (changes of the signal in time). Moreover, to diversify the results, the experiments have been done in two European cities - Poznan in Poland [108–112], where the number of occupied TV channels (also denoted hereafter as multiplexes) is relatively low, and Barcelona in Spain, where the number of active multiplexes is high. Since the latter measurements were not performed directly by the PUT team, their detailed description is not included here, and it can be found in [75]. Based on the achieved results, we were able to draw some conclusions on the practical consideration associated with the creation of the REM databases for secondary systems inside and outside buildings. Moreover, the measurements have been performed for a longer time; thus, we were able to observe the influence of the change of the channel plan on the REM structure.

2.4.2 Measurements in terrestrial television band

The measurement campaigns have been performed in two European cities, namely Poznan in Poland and Barcelona in Spain. As the latter is an excellent example of a city with a high number of inhabitants, Poznan represents an eastern European city with a medium number of inhabitants. Barcelona's example is not the main topic of this work, so that the description will focus on Poznan city. Moreover, the whole urban area counts around 5 million people. From the wireless communication point of view, these numbers mean high traffic requirements and the need for spectrum for delivering new services.

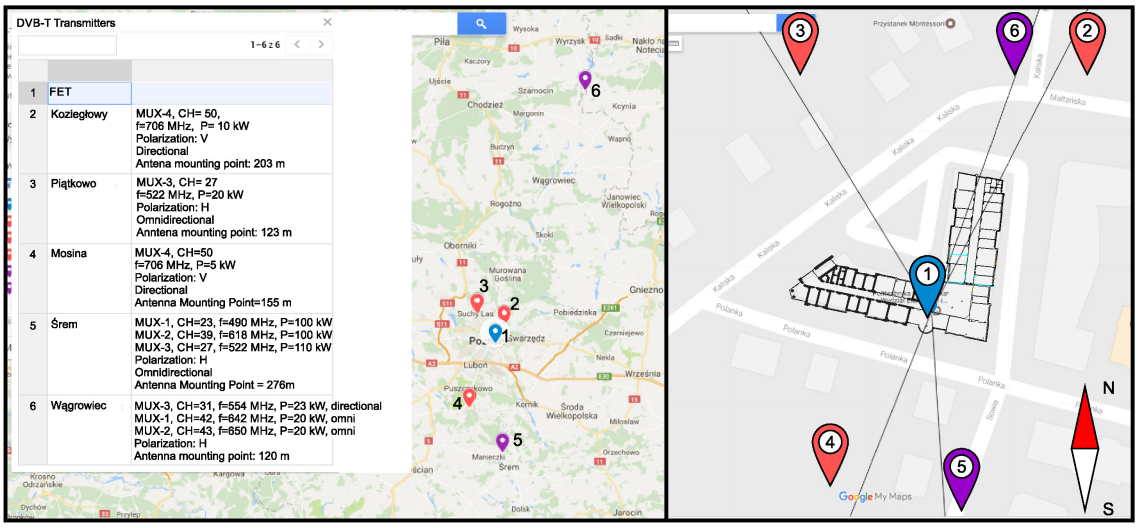

FIGURE 2.9: Location of DVB-T transmitters with regards to the PUT premises

On the other side, the city of Poznan has around 540 thousand inhabitants living in the area of 261 km^2 (resulting in the density of around 2076 persons per squared kilometer, whereas in the city of Barcelona, such density equals 16000 persons per squared kilometer); the whole agglomeration has around 1 million people. One may observe that in Poznan, the average number of people per squared kilometer is much smaller than in Barcelona, resulting in less demanding requirements for wireless communication systems. From the perspective of the study, these two cities are good representatives of two completely different deployment scenarios, which increases the diversity of this analysis. A detailed description of the measurement campaign in the city of Barcelona in Spain can be found in [75].

To effectively analyze the achieved results, one needs to be aware of the key parameters of the deployed DVB-T transmitters. In the case of Poznan, the exact coordinates for the measurements are 52°24′1.58″ N, 16°57′21.06″ E. The measurements have been done in two phases, first set of campaigns have been carried out in 2014, whereas some new results have been achieved in 2016. While the deployment of the TV towers did not change, the frequency plan of the TV channels is different. This is a highly beneficial situation as one may observe the influence of the change of frequency plan on the database creation. The location of the DVB-T transmitters, as well as the important parameters, are summarized in Table 2.2 and Fig. 2.9.

TABLE 2.2: Currently available DVB-T channels at PUT premises (status for the date: 30.11.2016)

TV channel	Center Frequency [MHz]	MUX Number	Location (city)	Transmit power [kW]	Approx. distance from PUT [km]	Azimuth
50	706	MUX-4	Poznan "Karolin"	10	4.6	42.45°
27	522	MUX-3	Poznan "Piatkowo"	20	7.4	319.26°
50	706	MUX-4	Poznan "Mosina"	5	19.2	212.65°
23	490	MUX-1	Poznan "Srem"	100	31.5	173.71°
39	618	MUX-2	Poznan "Srem"	100	31.5	173.71°
27	522	MUX-3	Poznan "Srem"	110	31.5	173.71°
31	554	MUX-3	Wagrowiec "Chojna"	23	71.7	28.54°
42	642	MUX-1	Wagrowiec "Chojna"	20	71.7	28.54°
43	650	MUX-2	Wagrowiec "Chojna"	20	71.7	28.54°

The coloring of the pins used on the Google map has the following meaning - blue pin represents the location of the PUT premises, and violet pins represent the DVB-T towers which did not change the transmit parameters. In contrast, the red pins correspond to the DVB-T towers for which the transmit setup has been modified during experiment time. The fundamental changes are the following: first, the new transmitter has been mounted (location 3 at Piatkowo); second, the change of the TV channel from 36 (594 MHz) to 50 (706 MHz) has been applied to stations (pins 2 and 4). Let us note that channel 36 is a scheme of Single Frequency Network (SFN) and the signal comes from two transmitters distanced by 4.6 km and 19.2 km with transmitting powers of 10 kW and 5 kW, respectively (locations denoted by pins 3 and 5 at the map).

As the location of the building is known, as well as the location of the TV towers, let us now discuss the key building parameters. The indoor measurements were performed in each room and along the corridors of a typical university building (which can be treated as the example of the office building), where many rooms of similar size are present. The building contains three tiers, i.e., the ground floor and two upper levels. The building is relatively new - the premises of the PUT were constructed in 2006. The outer (load-bearing) walls are bricks and concrete, whereas the rooms are spit through thinner partition walls. Each room has a big window and wood-based doors. The floor plans and photographs for a selected tier are shown in Fig. 2.10.

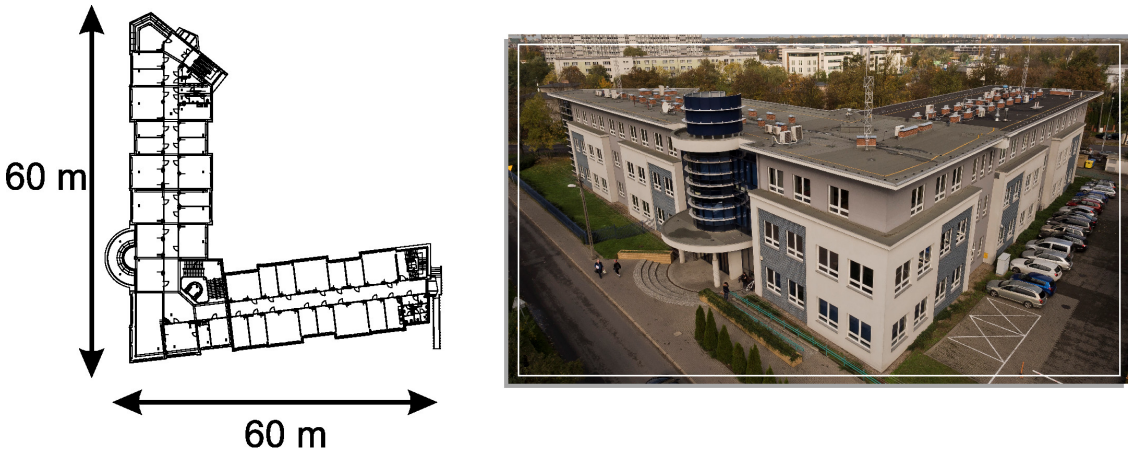

FIGURE 2.10: Floor plans and photos of the PUT premises

In general, the goal was to measure the received power of the present DVB-T signals both indoors and outdoors. The TV signal was measured by the omnidirectional antenna of type AOR DA753, covering the frequency range from 75 to 3000 MHz, and then sent to the spectrum analyzer (Rohde & Schwarz FSL6). Collected samples have finally been stored on the computer via Matlab. The resolution and video bandwidth of the spectrum analyzers were the same and equal to 30 kHz. Moreover, to mitigate the multipath effect in indoor campaigns, for each point, the measurements have been spatially averaged over a small area, i.e., the antenna has been randomly moved within a square area of around 30 cm. The system setup is shown in Fig. 2.11.

To assess the distribution of the received power of DVB-T signal in any potential point inside and around the building, a set of reference measurement points have been identified. In general, two main assumptions have been made: first, it was agreed that one measurement point was associated with an area of around 20 m^2; second, if there were smaller rooms, at least one measurement point was associated with every room in the building. The exact locations have been selected on each floor of the building as far as possible (i.e., the differences in room locations between the levels sometimes influence the location of the measurement point); however, the differences were negligible. The set of reference points for a certain level is shown in Fig. 2.12.

FIGURE 2.11: Measurement setup applied in Poznan

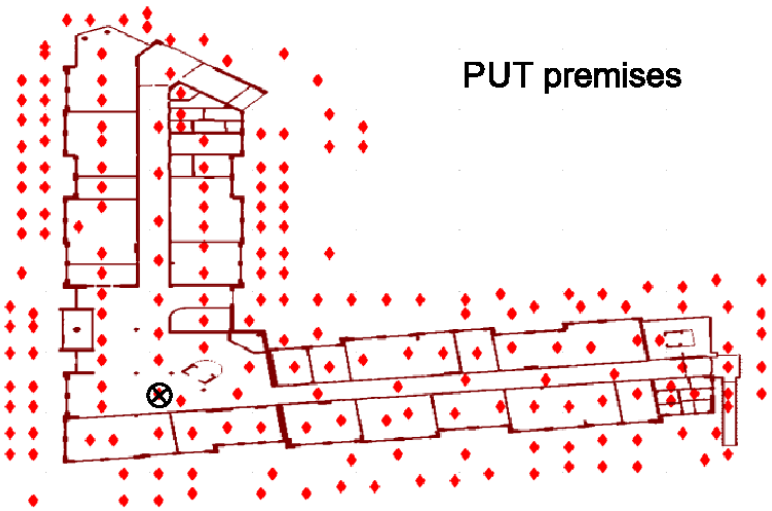

FIGURE 2.12: Measurement points identified for PUT premises

The most important is information about the average or median received power level in each measurement point. The description of another interesting phenomenon, such as its stability over time or the impact of humans moving inside the building, can be found in [75]. From the perspective of the performed measurements, the term "point" is relatively imprecise. It should be noted here that the measurement in a given location lasted less than a minute and consisted of collecting in-phase and quadrature samples. During this time, the entire measuring system was shifted by several to several centimeters on each side to average the impact of the multipath effect and thus the fading selective. The collected samples were saved on the computer's hard drive to calculate the received signal strength later. Thus, 100 values of received power were obtained for each measurement site on each of the seven tested TV channels. The median of such a set of 100 numbers was considered the final value of the power received in a given channel. As part of this work, the measurement base was supplemented with data inside the building, with its measurements made outside. As it is impossible to measure the received signal at every point of the building, we decided to apply one of the algorithms used for the creation of GIS products; namely kriging [59, 113]. In order to do this, one needs to measure exact values in a particular set of points and then interpolate the results in two or three dimensions.

2.4.3 Radio environment maps

Various interpolation and geostatistical techniques can be applied for the creation of the digital map, such as inverse distance weighting or kriging, as mentioned in Sec. 2.2. They all rely on the limited set of measured points (treated as known values) and calculate the approximated value in any requested point where the value is unknown (no measurement has been made there). In this work, we applied the ordinary kriging algorithm adopted to indoor scenarios, i.e., where the influence of the wall-attenuation has been considered [59], as well as where the knowledge of the location of the signal source was used. From various types of kriging (such as universal kriging or kriging with the trend, simple kriging, multivariate kriging, etc.), we selected the ordinary kriging as in this approach it is assumed that the mean value of the observed metric is constant in the local neighborhood of the considered point, for which the value is calculated. In our derivations, we consider the 2D case. Let us associate any point in space i having coordinates (x_i, y_i) with the investigated metric (here - a value of received power) z_i. The set of all N_m known points will be denoted as V_m. Let us also denote by u the point for which the considered metric is unknown, i.e., the value of z_u is not known and will be a subject of possible calculation. Finally, by V_u we denote the set of indexes of points in the vicinity of point u for which the value of a considered metric is known. The elements of this set are selected according to the specific rule, e.g., this set will contain the N_u closets points in terms of Euclidean distance. In the ordinary kriging the idea is to find the value of z_u as the weighted sum of known values, i.e., $z_u = \sum_{i \in V_u} w_i z_i$, where the weighting coefficients sum up to one: $\sum_{i \in V_u} w_i = 1$. The kriging algorithm is designed to find the optimal weights through the formula:

$$\boldsymbol{\Upsilon} \mathbf{W} = \boldsymbol{\Psi}, \tag{2.1}$$

where $\mathbf{W} = [w_1 w_2 ... w_{N_u} \kappa]^T$, $\boldsymbol{\Psi} = [\gamma(d_{1,u})\gamma(d_{2,u})...\gamma(d_{N_u,u})1]^T$, and $(\cdot)^T$ is an operation of matrix transposition, and $d_{i,j}$ is the distance between points i and j. Furthermore, κ used in matrix $\mathbf{W}$ definition is the Lagrange multiplier used to minimize the so-called kriging error. Moreover, function $\gamma(\cdot)$ represents the spatial correlation between the points, thus it is usually the (semi)variogram of selected type. Finally, let us define the matrix $\boldsymbol{\Upsilon}$

$$\boldsymbol{\Upsilon} = \begin{bmatrix} \gamma(d_{1,1}) & \dots & \gamma(d_{1,N_u}) & 1 \\ \vdots & \ddots & \vdots & 1 \\ \gamma(d_{N_u,1}) & \dots & \gamma(d_{N_u,N_u}) & 1 \\ 1 & \dots & 1 & 0 \end{bmatrix}. \tag{2.2}$$

The semivariogram function shall be selected in such a way that the correlation between two points shall increase with the reduced distance. Following [59], we applied the exponential semivariogram model defined below:

$$\gamma(d_{i,j}) = \begin{cases} 0 & \text{for} \quad d_{i,j} = 0 \\ \gamma_{\text{nugget}} + (\gamma_{\text{sill}} - \gamma_{\text{nugget}}) \exp\left(1 - 3\frac{d_{i,j}}{\gamma_{\text{range}}}\right) & \text{for} \quad d_{i,j} > 0 \end{cases}. \tag{2.3}$$

In the equation above the constant values $\gamma_{\text{nugget}}, \gamma_{\text{sill}}$ and γ_{range}, are the so-called *nugget* (so the value associated with the distances smaller than the typical spacing between the two points), *sill* (the maximum value of the semivariogram function) and *range* (which identifies the distance above which the correlation between two points is negligible), respectively. These constants are adjusted based on the conducted measurements. Now, the ordinary kriging algorithm applied in this work can be briefly summarized as follows: for the new point u we identify the set of N_u measurement points i which are closest to the point u in a Euclidean sense. Then the weights associated with each identified point are calculated, and finally, the value z_u is computed.

However, as the measurements have been made inside and outside the building, there is a need to include the potential impact of the walls in the kriging algorithms. Following the approach from [59], we decided to increase virtually the distance between the two points if the walls separate these points. In other words, the attenuation introduced by the wall acts as a virtual shift of the point by the distance corresponding to the distance at which the signal will pass at a given frequency in the path-loss model. For example, if there will be N_w walls between two points i and j, each wall will be characterized by the attenuation in dB $W_l, l = 1, 2, \cdots, N_w$, then for a considered free space attenuation coefficient η the final distance between the two points will be defined as:

$$d_{i,j} = L_E + 10^{\frac{\sum_{l=1}^{N_W} W_l}{10\eta}}, \tag{2.4}$$

where L_E is the Euclidean distance between these points. In our calculations, we set η to 3.5. In Fig. 2.13 we show the coverage map for the ordinary kriging algorithm for $N_u = 10$, where for the outer walls, we set the attenuation arbitrarily to 25 dB, whereas for the walls inside - to 10 dB. One may observe that the coverage map created in the way described above is not so accurate; in principle, one may observe that the interpolated values outside the building are lower than those achieved by measurements - strange spikes are observed close to the outer walls. The difference between the peak and surrounding values is at the level of some decibels, but still, the indoor samples' influence seems to be incorrect. Intuitively, there shall be no spikes, and the values of the power outside should be similar to those samples where the received power has been measured. Moreover, we have observed that the inclusion of wall attenuation in the procedure of virtual distance extension has led to some numerical problems inside the ordinary kriging algorithm. Let us note that we expressed the building sizes in decimeters. This corresponds to the calculation raster used in the ordinary kriging algorithm - we have calculated the approximated value of received power on each point of the size 1 dm × 1 dm.

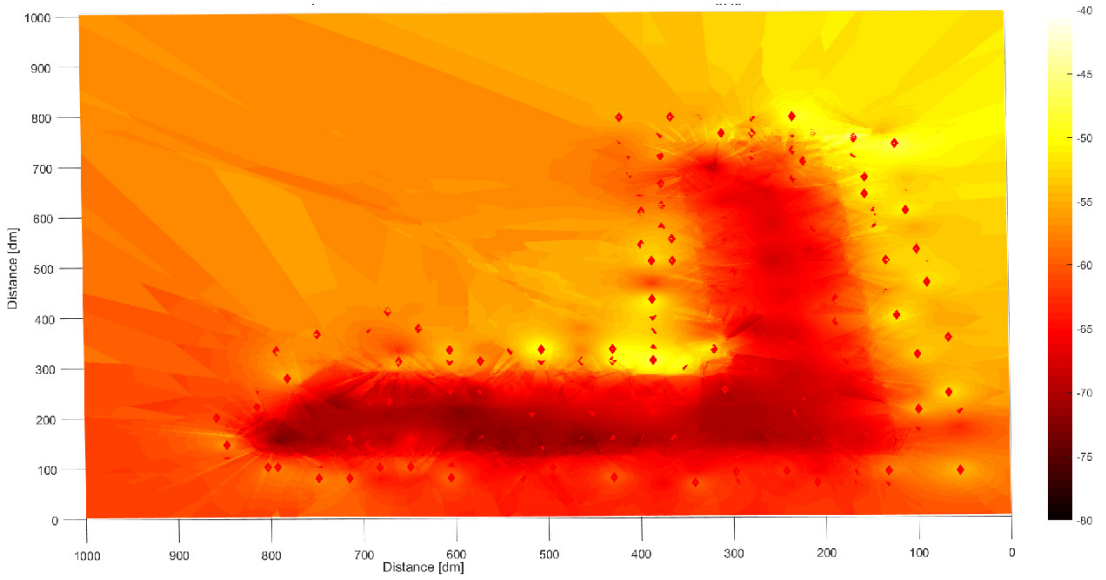

FIGURE 2.13: Coverage map for the channel 27 at the ground floor; $N_u = 10$

Based on the above observations, we have proposed two modifications that allow us to reflect better the influence of walls in the ordinary kriging algorithm:

- first, we split the map into two non-overlapping parts, i.e., indoor and outdoor fragments, and then merged them afterward. In consequence, the coverage map outside is created based only on the outside samples, and the inner part of the map relies on the samples gathered from

indoor measurements; one may say that we intentionally treat these samples as uncorrelated or that we do not utilize the whole available information

- second, we consider in our calculations the location of the transmitter; the rationale behind such an approach is the following - in the ordinary kriging, we take into account the correlation between the given points (where the measurements have been made). In the approach proposed in [59], every wall causes a virtual shift of the affected point. However, suppose we assume the presence of the dominant path in two neighboring rooms, where the ray that originates from a distant transmitter enters the rooms via windows. In that case, the value of the observed power should be very similar in both cases. Consequently, the correlation should be high, and the effect of the inside wall separating these two rooms (leading to virtual distance extension) should be omitted. Thus, as long as the inside walls are quasi-parallel to the direction indicated by the DVB-T transmitter, these walls shall be discarded from the calculation in the kriging algorithm. On the other side, the perpendicular walls shall be taken into account. To analyze this aspect, one needs to identify first the location of the DVB-T transmitters and the angle between the transmitter and the building walls

Creation of Radio Environment Maps

In Fig. 2.14, the results for the first proposal are shown. Let us notice that we intentionally reduce the size of the map to the selected fragment of the building to observe the map's details better and simplify the analysis; for the same reason, we do not show the walls. One may observe that the map created in such a way is free from the phenomena identified in Fig. 2.13 - the map is smoother. However, the drawback of such an approach is that the impact of all samples is not included; thus, only the part of available information is utilized.

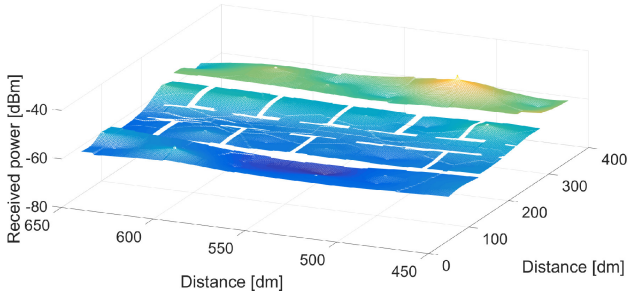

FIGURE 2.14: Coverage map achieved by concatenation of two maps: the one created based on indoor samples, and the second created based on outdoor samples

The goal is to exclude the unintended influence of internal walls that are quasi-parallel to the received signal from the distant transmitter from the ordinary kriging algorithm. We have selected channel 27, as this is the one that is transmitted from two directions in a single-frequency manner. Thus, we have selected two angles (related to the building position) which correspond to the locations of the DVB-T transmitter in Srem and Piatkowo (in Fig. 2.9 these TV towers are denoted with numbers 5 and 3, respectively). The achieved results are shown in Fig. 2.15 for Srem transmitter and in Fig. 2.16 from Piatkowo transmitter. When comparing these two figures, one may observe that, first, the unintended influence of walls has been minimized, i.e., the whole coverage map is smoother, and there are no high spikes on the coverage map. However, the differences between the coverage maps in these two cases are unexpectedly not so high. This may result from the fact that we have (intentionally) selected the channel for which the signal is generated from two transmitters.

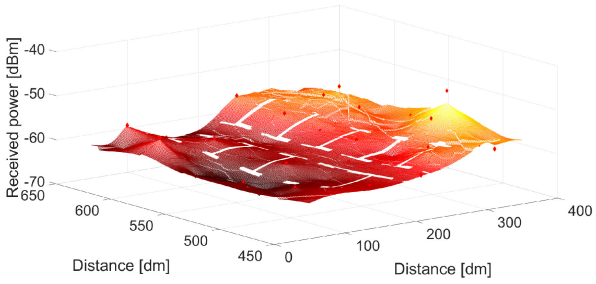

FIGURE 2.15: Coverage map — considering transmitter location (Srem)

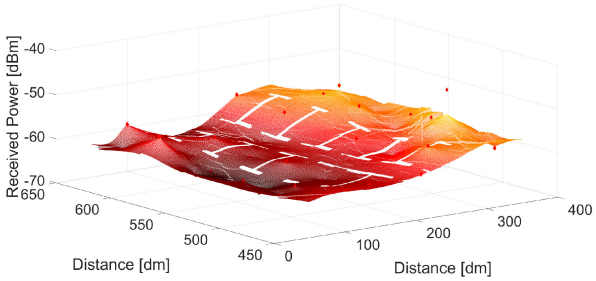

FIGURE 2.16: Coverage map — considering transmitter location (Piatkowo)

These observations lead to the conclusion that it is worth comparing the results for advanced kriging (where the direction of the dominant path is included) with the pure kriging and with the approach proposed in [59]. The coverage maps achieved for the former case are shown in Fig. 2.17, whereas the map for the latter in Fig. 2.18. When comparing the four coverage maps, one may state that their differences are not so significant - the key difference between all the algorithms is mainly in the spikes around the building. These are eliminated when the influence of walls is treated in the way proposed in that work. In other words, the algorithm generates more reliable results but at the price of higher complexity.

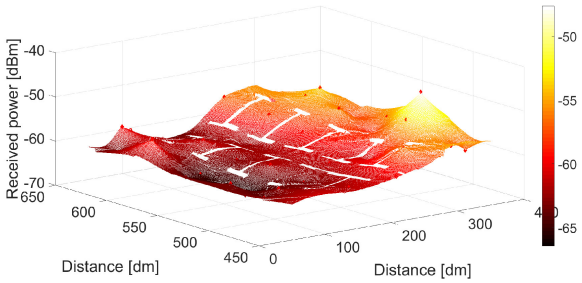

FIGURE 2.17: Coverage map — impact of the walls not considered

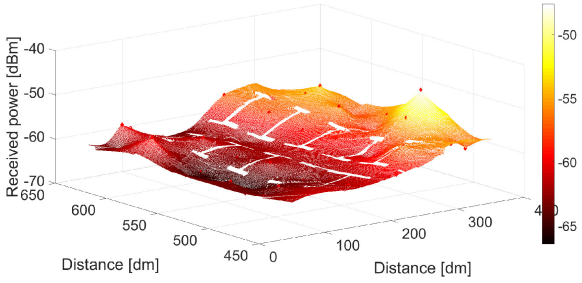

FIGURE 2.18: Coverage map — considered impact of the walls in the kriging algorithm

However, there is a need for a metric that will numerically characterize the quality of such a coverage map created for REM databases. One of the possible metrics could be the mean square error calculated for some reference points applied in the kriging algorithm. In other words, the metric will reflect the average difference between the measured value at the known point and the value obtained by the kriging algorithm when this point was treated as unknown. Unfortunately, in all scenarios considered in that work, after removing the gross errors (caused by numerical instability), the mean absolute values of the error achieved for all points were very similar and equal to around 2.3 dB. At the same time, the range of the errors varied from around -15 to +15 dB. Such results, together with the subjective analysis of the coverage maps, entail the need for a definition of another, more accurate metric that can be used to assess the quality of the coverage map.

The achieved results allow us to draw some initial conclusions regarding the applicability of the maps created utilizing an ordinary kriging algorithm. First, one may observe a strong need for a proper assessment of the real impact of walls on the kriging algorithm. The solution proposed in [59] seems to be valid in a case where the transmitter is localized inside the building and operates at relatively small transmit power levels (and the corresponding coverage area will be relatively small). An excellent example will be the analysis of WiFi signals. However, in the case of TV signals, which are broadcasted from the TV towers typically located far away from the building of interest, such a model may not be valid, as the impact of walls on the virtual extension of the distance between points is significantly reduced. At the same time, improper consideration of external and internal walls leads to the wrong assignment of weights by the kriging algorithms and, consequently, improper interpolating of the unknown values. These problems can be mitigated by utilizing the knowledge of the direction from which the TV signal comes. The achieved results proved the correctness of this approach; however - as shown in this work - it is not easy to apply this strategy in the Single Frequency Networks where more DVB-T transmitters deliver the same signal from various directions.

Thus, if there is a need for a detailed coverage map, a more advanced approach should be proposed on how to treat the walls to calculate the weights by the ordinary kriging algorithm. However, as the differences between all considered approaches are not so high, the immediate question appears if such a detailed map is needed anyway. It may be a simplified model for coverage maps tailored to REMs would be sufficient for practical application. This final statement is essential when we consider the possible change in the usage of TV channels. As it has been observed by comparing the two tables shown in this work, the setup of TV channels for the considered area in Poznan has been essentially changed for over two years. If the REM database relies significantly on the detailed and accurate coverage map, there will be a need for the creation of a new map whenever there is any change in the channel setup. Moreover, this would make the practical deployment of REMs intractable, as every time, new measurements should be performed. Thus, as a conclusion from that work, one may state that there is a need for a mid-accurate and straightforward way to calculate the coverage map for a certain frequency band.

Summary

This section discusses REM creation process. A detailed measurement experiment in the television band has been described. Based on the performed measurements, a set of REMs was created, which:

- have an approximately regular grid defined
- are static in the long term
- use kriging as an interpolation method to complete map points where there are no measurement points collectively present the power map of the received DVB-T signal
- use contextual information about the position of TV transmitters during interpolation

This is a very good example of REMs that do not need to be updated very often due to rare changes to the TV broadcast network. Most importantly, the created REMs lay the groundwork for further investigation on using contextual information to improve wireless transmission, and in particular to improve the spectral efficiency of the entire network.

Chapter 3

Theoretical approach to context information utilization in DSA systems

Leaving aside the challenges posed by existing networks and standards, we present considerations on DSA systems. Assuming the presence of the already created radio environment database in the television band, we present proposals for the DSA system that uses it. Moreover, the problem of the simultaneous allocation of radio resources and power in the DSA system has been extensively analyzed, as well as, the possibility of selecting the waveform was considered.

DSA system allows spectrum allocation for system users in a dynamic manner, which is beneficial as the spectrum can be split between different users based on current user demands, environment, time, etc. In this chapter, we propose the utilization of CI in the algorithm of spectrum allocation, which is part of the DSA system. Analysis of our proposal is split into three research topics. The first research topic assumes the usage of DSA for simultaneous spectrum usage of primary and secondary users in the TV band. Such research is based on a measurements campaign described in Sec. 2.4, and is investigated in two ways: through simulations, described in Sec. 3.1, and through experiments, described in Sec. 3.2. The second research topic, described in Sec. 3.3 deals with the problem of coordinated resource allocation and power control among a set of available base stations. A detailed definition of the problem is provided, followed by a discussion on the heuristics proposed for solving the problem. Four solutions are presented that are based on existing standards as well as on the approaches described in the literature. Next, a new multi-selection (multi-choice) algorithm is proposed and discussed. In the third research topic, described in Sec. 3.4, we discuss the idea of waveform flexibility in future wireless networks utilizing cognitive radio functionality. Mainly, we consider the possibility of adjusting the shape of the waveform based on the information about the surrounding environment stored in a dedicated CI database.

3.1 Research topic 1a: Algorithm for dynamic spectrum access

This chapter presents a proposal for a system for the dynamic allocation of frequency resources. The main idea for developing this algorithm is to use the previously collected measurement data regarding the received power of the signal in the TV band. By simulating the placement of several transmitters in the measurement area (within REM), the maximum allowable transmit power of these transmitters is calculated. During the calculations mentioned above, the need to protect TV receivers by ensuring a sufficiently low level of interference, and protect transmission receivers from unlicensed users previously added to the system, are taken into account. In order to carry out such simulations, several assumptions described below were adopted, and an algorithm was proposed that allows to decide on granting access to the spectrum for a new unlicensed user. This proposal includes a detailed description of the proprietary algorithm and the results of simulations carried out in Matlab, where unlicensed users are placed in the same building as the measurement campaign was done, i.e., in the building of the Faculty of Computing and Telecommunications (FCT) of the Poznan University of Technology. The proposed system is based on a map of the TV signal strength created from actual measurement samples and supplemented based on spatial interpolation - kriging, presented in the Sec. 2.4 of this thesis. The work considered here is also described in authors papers [75, 114–117].

The presentation of the algorithm of dynamic resource allocation, operating on a ready map of the radio environment, should be preceded by several assumptions:

- the data presented in Sec. 2.4 were used in this analysis, mainly the power maps of received digital TV signals
- spectrum resources are only allocated to users inside the building
- the system operates on ten arbitrarily selected digital television channels. Channels 21 to 30 were selected (470 - 550 MHz), but it is assumed that only on channels 23 (486 - 494 MHz) and 27 (518 - 526 MHz) the TV signal is detectable, so the others were considered undeveloped. In addition, at almost all measurement points inside the building, the signal strength on channel 23 was insufficient for the operation of the TV set (an external antenna is required). Therefore we recognize that channel 23 can also be used in this system for unlicensed users inside the building. Consequently, only the signal on channel 27 is a protected signal here
- the power selected for new users must be such that the recipients of television available on the protected channel do not experience a decrease in image and sound quality
- The allocated power must be limited from the top. In the experiment, this limit was set at 20 dBm (an acceptable European level for 802.11 transceivers operating in the 2.4 GHz band)
- the power for which we consider the proper operation of the TV set is -84 dBm. This value results from the modulation and coding mode used in DVB-T (i.e., 64-Quadrature Amplitude Modulation (QAM) with 3/4 efficiency), for which the minimum signal level is -59 dBm. By increasing this value by a margin related to the problem of correct detection of the so-called hidden terminal (the assumed value is 25 dB [118]), we get the value -84 dBm
- the noise power level was set to -97.9 dBm. This value is the average power received at all measurement points in channels where no TV signal is received

- the assumed emission mask of unlicensed users is such that in the directly adjacent channels (± 1), the received power is 50 dB lower than the transmitted, while in the further adjacent channels, separated by (±2) the power is 70 dB lower. The power emission mask is shown in Fig. 3.1

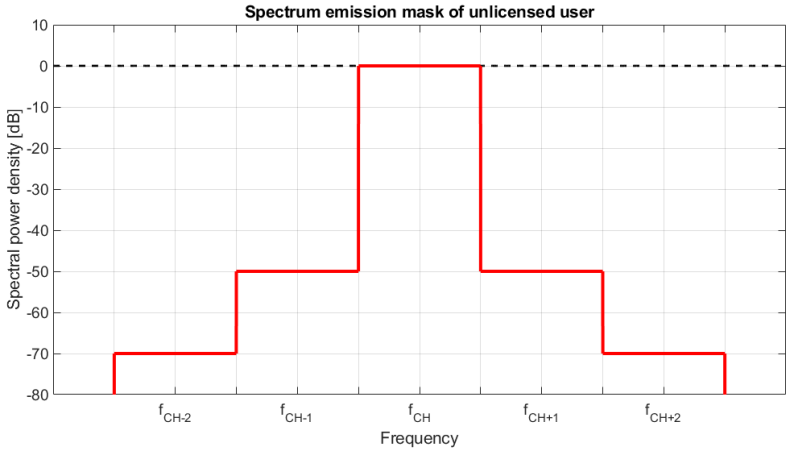

FIGURE 3.1: Spectrum emission mask of secondary user

- the interference that an unlicensed user may introduce to another (previously added) user must not cause Signal-to-Interference-plus-Noise Ratio (SINR) to drop below 0 dB (in any place where the SINR of the protected transmitter exceeds 0 dB)

The proposed algorithm of the spectrum allocation system is described in detail below. It describes the procedure necessary to be followed to decide to grant access to the spectrum to an unlicensed user while ensuring the protection of the licensed users and unlicensed users previously added to the system described. A simplified block diagram of such an algorithm in Fig. 3.2. All values used in the formulas are expressed on a logarithmic scale.

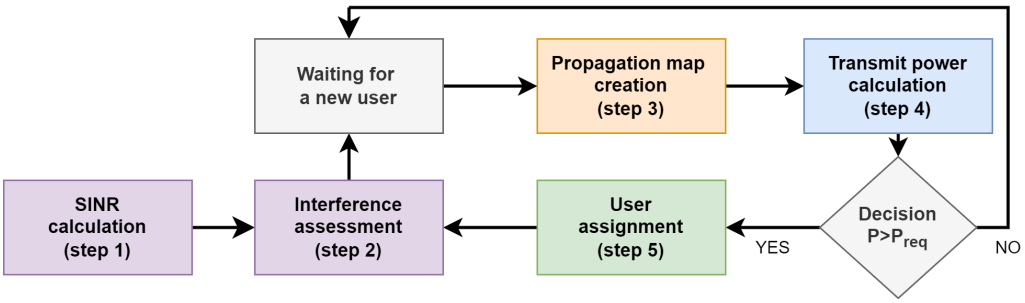

FIGURE 3.2: Simplified algorithm of Dynamic Spectrum Access

Step 1. *SINR calculation*: The first step is TV signal receivers SINR calculation for each of the considered channels and for each analyzed location (that is protected).

$$SINR(x,y,ch) = \begin{cases} P(x,y,ch) - P_{\text{noise}}, & P(x,y,ch) \geq P_{\min} \\ 0, & P(x,y,ch) < P_{\min}, \end{cases} \tag{3.1}$$

where $P(x,y,ch)$ is the measured power at (x,y) in the ch channel, P_{noise} is the measured noise power (-97.9 dBm) and $P_{\min}$ is the minimum power needed to properly receive digital TV set as a value of -84 dBm

Step 2. *Interference assessment*: The interference margin I, understood as the permissible interference power observed by the protected system, which will not lead to interference with the TV signal reception, should be determined.

$$I(x, y, ch) = P(x, y, ch) - P_{\min}. \tag{3.2}$$

Such a margin can be represented in the form of a map, which we understand as the power reserve for interference potentially coming from other systems, in this case, from new users to whom resources will be allocated

Step 3. *Propagation map creation*: After the appearance of a new user, the propagation map of his signal (attenuation map) is computed. The free space propagation model supplemented with wall loss is used in this case. The L attenuation for the position at point (x, y) for the ch channel is equal to

$$L(x, y, ch) = L_{fs}(x - x_u, y - y_u) + SEM(ch - ch_u) + \sum_{l=0}^{N_w} W_l, \tag{3.3}$$

where (x_u, y_u) is the u-th user location, ch_u is the channel on which the u-th user transmits, SEM is the spectrum emission mask, L_{fs} is the free space propagation model, N_w is the number of obstacles (walls) between the user and the analyzed point, and W_l loss of a specific obstacle

Step 4. *Transmit power calculation*: In the next step, one should calculate the allowed transmitting power P_{TX}, taking into account the presence of other system users. This is a value that will not cause the SINR to drop below the required level in any position in the building. This value is determined by plotting the signal attenuation map on the maps created in the second step.

$$P_{TX} = \min[\sum_{x=X_{\min}}^{X_{\max}} \sum_{y=Y_{\min}}^{Y_{\max}} \sum_{ch=CH_{\min}}^{CH_{\max}} (I(x, y, ch) + L(x, y, ch) + P_{\text{noise}})], \tag{3.4}$$

where the x and y coordinates take all possible values from the range $<X_{\min}; X_{\max}>$ and $<Y_{\min}; Y_{\max}>$ respectively, and the ch channel accepts all analyzed channels from the range $<CH_{\min}; CH_{\max}>$. At the same time, adjacent channels are also checked with the emission mask of unlicensed users. Of course, if we cannot meet these conditions on any of the available channels, the potential user will not be served

Step 5. *User assignment*: In the last step, the new user decides whether the power determined in the previous step by the database is sufficient to ensure correct transmission. The P_{req} threshold value for this decision is application-specific. If the power is sufficient, the user is added to the system, which implies updating the maps from steps one and two. The new user signal is now treated as a protected signal.

Simulation Result

To verify the correctness of the proposed algorithm, an experiment was carried out consisting of adding three users to the system created according to the steps and assumptions presented in the previous section. Fig. 3.3 shows the interference margin for the first floor of the building (for channel 27). The analysis of this map shows that outside the building, we have a Signal-to-Interference Ratio (SIR) "margin" of 35 dB above that required for proper reception.

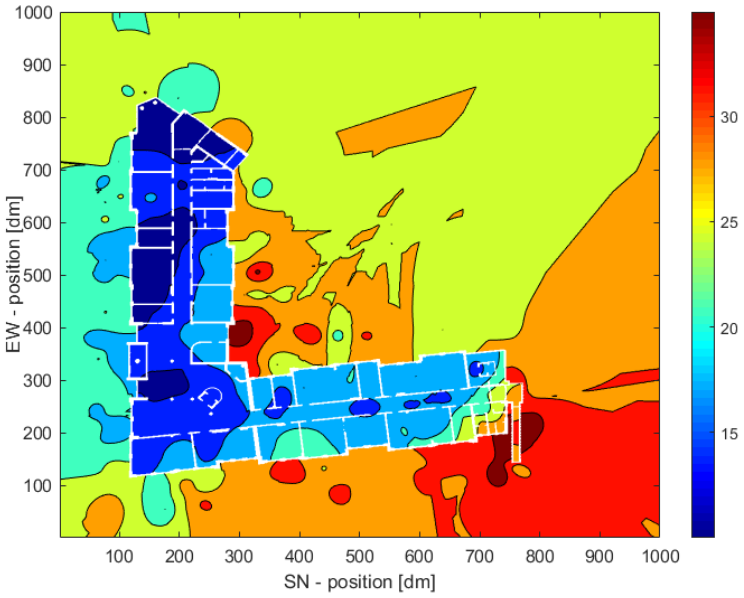

FIGURE 3.3: Map of interference margin [dB]

Inside the building, this value does not exceed 20 dB. These values are not sufficient for transmitting signals of unlicensed users on the same channel. This is because the algorithm described above will allow for transmission with a maximum of a dozen or so dB above the noise and interference level, which gives a signal with a power of about -80 dBm. It is too low a value to speak of a satisfactory transmission. However, we can successfully consider the use of adjacent channels. We do not try to add a user on channels that are very distant from the protected channel during the experiment because such a procedure does not add anything. The algorithm will allow the user to transmit at maximum power with the given assumptions.

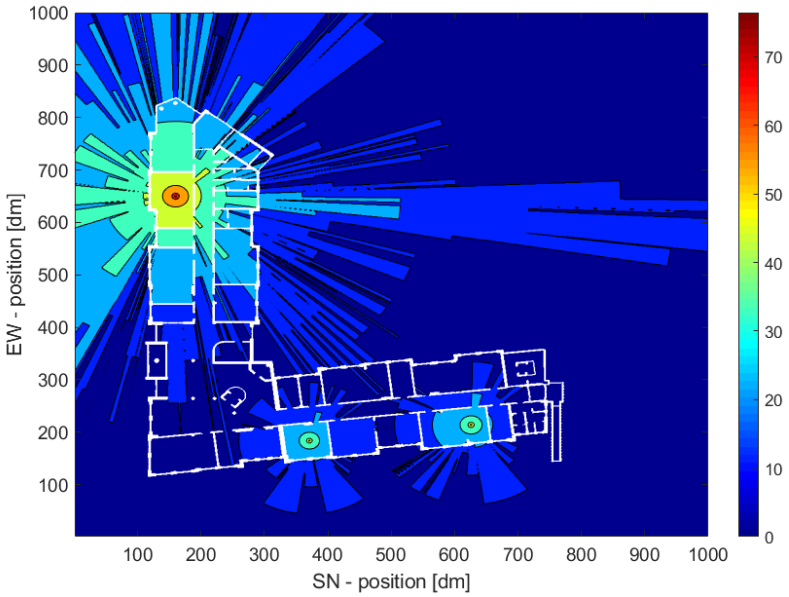

FIGURE 3.4: Map of Signal-to-Interference-plus-Noise Ratio [dB] for secondary users

First, the first user was added at the point (*160*, *650*) (x-axis - SN position, y-axis - EW position), for which the algorithm determined the maximum power of -10.5 dBm (on channel 25). Then an attempt was made to add a second user with a position at the point (*371*, *184*) on channel 25, which was enabled by the algorithm with a power of -34.5 dBm.

Finally, the last user has been added in the position (*626*, *214*) for which the maximum power on channel 25 is -33.8 dBm. Fig. 3.4 shows a SINR map of all three users.

Analysis of the protected channel SINR map leads to the following conclusion. The value at points where new users have located drops to 0 dB. This means that there is no 'reserve' of power (margin) for additional disturbances in exactly these places. However, at points one dm (pixel) away from users, the SIR value is unchanged from its original value. This situation concludes that transmitting with a power of about -40 dBm (with the assumed spectrum mask) does not cause large crossings to the adjacent channels. This value is insufficient in most applications; however, using another channel (leaving one or several channels free) allows for achieving much higher powers. Knowing about the position of digital TV receivers would significantly increase the maximum power (by increasing the margin) with which unlicensed users can transmit, which would make the system more practical (due to possible longer transmission range). An important observation about the operation of this system is the effect of the order in which users appear, typical of multiple access methods. Changing the order of the moment of appearance of the user, for example, the first with the third, results in setting completely different values of the maximum power. It remains an open question to establish rules (for example, margin) regarding interference between unlicensed users. The adoption of a different method may significantly change the algorithm's functioning.

Summary

A compact summary of the use of contextual information to improve spectral efficiency is presented in Table 3.1 below.

Ph.D. candidate's publications considering problems discussed in this section	[75], [114], [115], [116], [117]
Context information used in this section	Set of received power from DVB-T transmitters; location of TV transmitters; location, minimal required received power, maximum transmit power, frequency channel of secondary users; list of already allocated channels for secondary users.
Influence on the system	Allowing access to spectrum for unlicensed users; protection of primary (TV receivers) and secondary users.
Impact on spectrum efficiency	Higher spectrum utilization through more devices that's uses the same band.
Comment	By using exactly the same frequency range, it is possible to increase the number of users, which leads to an increase in the total system throughput, and thus to improve the spectral efficiency of the entire system. In this thesis, the possibility of using such a system was presented by means of a computer simulation.

TABLE 3.1: Summary of work presented in chapter 3.1

3.2 Research topic 1b: Experiment of DSA system utilization

This section presents the results of the experiment performed using the actual equipment and algorithm described in Sec. 3.1. The experiment was performed on two white-space subsystems in an arbitrarily selected laboratory in Poznan, Poland. Following the decisions made by the REM manager, such subsystems established a connection in the form of video transmission. A detailed description of this experiment can be found in the following author's publications [75, 117, 119].

3.2.1 Experiment setup

The ultimate goal of the conducted experiment was to increase the spectrum utilization by establishing new indoor white-space wireless links in the TV band such that the DVB-T signal is not distorted. The experiment was carried out on the ground floor of the Faculty of Electronics and Telecommunications premises at Poznan University of Technology, Poland, on the last day of April 2017. The Block diagram of the experimental setup is shown in Fig. 3.5.

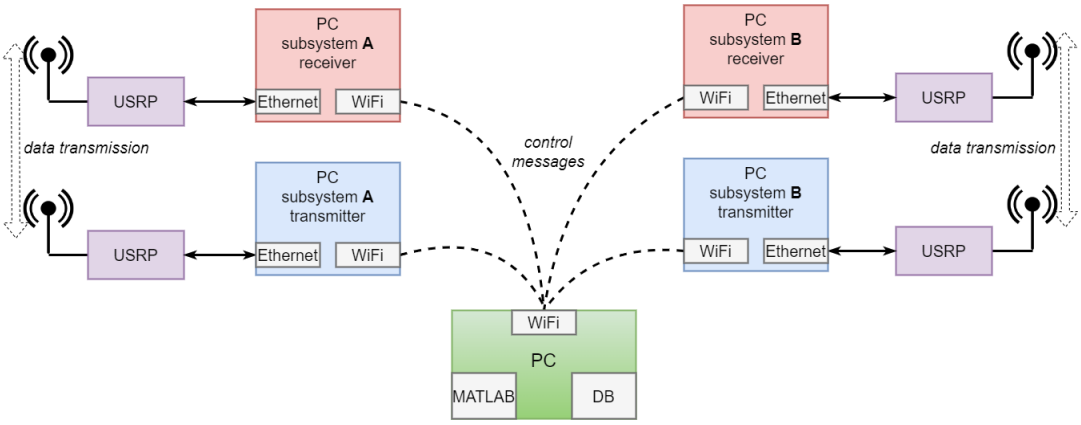

FIGURE 3.5: Block diagram of the experiment setup.

The white-space transmitter was implemented in the GNU Radio environment that steered the connected Universal Software Radio Peripheral (USRP) N210 board equipped with the wide bandwidth transceiver WBX board [75,119]. Some of the functions have been delivered by National Instruments in the form of dedicated blocks in GNU Radio Companion; however, the new blocks (e.g., those for database querying) have been implemented in C++. For data transmission, we have selected a freely available Big Buck Bunny media sequence [120], which was streamed via User Datagram Protocol (UDP) port, coded, and modulated with a Gaussian Minimum Shift Keying (GMSK) modulation scheme. Such a selection allows us to analyze the influence of potentially interfering signals observed by the white space receiver; thus, we do not apply any coding or advanced modulation schemes. In other words, we can observe how the potential interference coming from the primary system and other simultaneous secondary systems influences the white space receiver and vice-versa - how the out-of-band transmission of a simple modulation scheme impacts the primary system. Please notice, however, that the selection of the transmission scheme is not critical in our experiment. One can easily exchange the GMSK modulation scheme with the one widely considered for white space transmissions, such as multicarrier schemes like Orthogonal Frequency-Division Multiplexing (OFDM) from IEEE 802.11af, or its filtered version Filter Bank MultiCarrier (FBMC) from IEEE 1900.7 standard. If allowed by the database, the GMSK signal was delivered to the USRP block and broadcasted over the air inside the building using an omnidirectional antenna. An analogous approach has been applied to the white-space receiver, whose connection diagram is shown in Fig. 3.6.

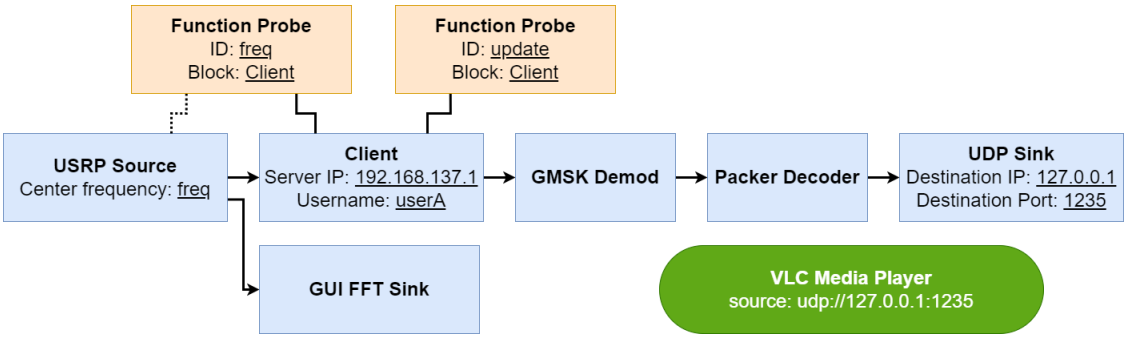

FIGURE 3.6: Schema of the receiver; the GNU Radio based structure is shown jointly with and the VLC media player used as video transmission receiver

Besides the blocks similar to those applied at the transmitter (such as the GMSK demodulator, decoder), one may observe the presence of the parallel chain of blocks used for maintaining the connectivity with a remote database. Moreover, it can be noticed that the software spectrum analyzer has also been applied, which shows the Power Spectral Density (PSD) of the received GMSK signal. Finally, the VideoLAN Client (VLC) media player is visible that visualizes the decoded stream collected at the UDP port. Please note that the whole communication was steered by the remote database, implemented on a dedicated laptop with Matlab installed on it. This REM server was accessible via Ethernet connection and was responsible for granting access to the white spaces depending on the given location. To guarantee connectivity between the remote REM server and the white-space devices, each computer emulating such white space device was equipped with a dedicated Wireless Local Area Network (WLAN) dongle. Such a solution was necessary as the only way to provide communication between USRP and a personal computer is via Ethernet cable, so two simultaneous network connections were needed. The experimental scenario has been illustrated in two consecutive figures, Fig. 3.7 and Fig. 3.8.

FIGURE 3.7: Photograph of the first white-space transceiver (left side computer with USRP board put on it) and REM database (right computer connected with Internet via Ethernet cable); the left-side computer communicates with database using WLAN-dongles stick into it

In a broader scope, the experiment consisted of two key phases. The first step was to establish the first white-space connection with the use of REM databases and observe the spectrum inside the room using the Rohde & Schwarz FLS6 spectrum analyzer. In the second step, another white-space link was established in the same room such that neither the DVB-T signal nor the existing white-space transmission was distorted.

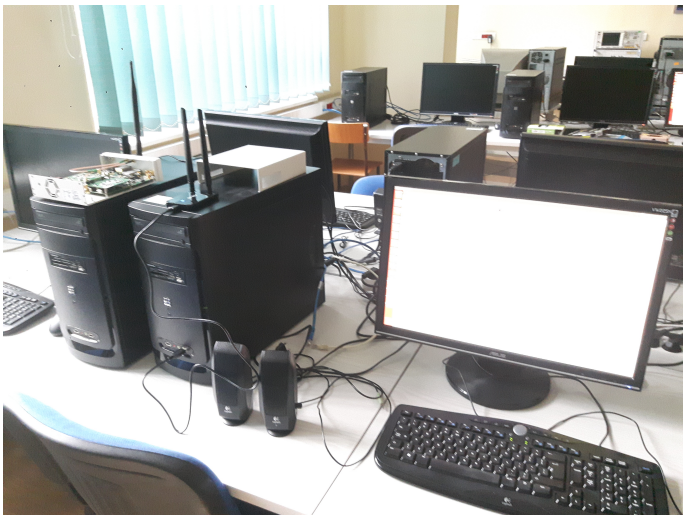

FIGURE 3.8: Photograph of the second white-space transceiver (the one with USRP board laying on it); the computer communicates with database using WLAN-dongles

Each key phase consisted of a sequence of smaller steps:

1. first, the new white-space transmitter sends a query to the remote database (via WLAN connection) with a request for a new transmission grant
2. second, after receiving the request, the database calculates the allowed maximum transmit power and sends this message back to the transmitter; at the same time, the database stores the parameters of the new prospective link (including center frequency, etc.); this information will be then later delivered to the white-space receiver
3. third, the white-space receiver periodically checks the database for any new entry indicating new transmissions to it; the reception parameters may be adjusted if needed according to the stored parameters

3.2.2 Experiment results

The procedure described in the previous section has been applied in the real-time experiment. In the first phase, the new white-space device asked for new transmit grants, and once it had received them, it started data transmission. Next, the second white-space device tries to get a positive response for the spectrum access requests. In both cases, a centralized remote REM database controlled the whole process. As the messages stored in a log file of the remote database present the consecutive steps of the experiment, we list the key messages of this log file below:

  - No new requests // *database awaits new request from new transceivers*
  - No new requests
  - ...

- Phase I (first user's request)
  - New request with coordinates A = $\{20, 276, 468, 5, 0\}$ // *coordinates inside the building, i.e. {ID, x, y, channel, request state}*
  - Allowed transmit power *result* = -8.9391 dBm
  - No new requests

  - Adding new user A = $\{20, 276, 468, 5, 3\}$
  - No new requests
  - ...

- Phase II (second user's request)
  - New request with coordinates A = $\{21, 310, 407, 6, 0\}$
  - Allowed transmit power *result* = -47.8770 dBm
  - No new requests
  - Adding new user A = $\{21, 310, 407, 6, 3\}$
  - No new requests
  - ...

One may observe that the database provides a periodic update on the status of the whole REM-based spectrum management system. If a new request comes, it calculates the maximum transmit power in dBm for a given location. Unfortunately, in the conducted experiment, the duration of the server response was long and would not be applicable in practice. The database's response for the spectrum inquiry was in the range of tens of seconds. Such a long server reply is since we applied very high accuracy of the applied algorithm. The space granularity (raster) applied for calculation of potential interference induced to the primary system by prospective TVWS transmitter was set to 1 decimeter, resulting in 10^6 calculation points.

In Fig. 3.9, one the left side, the PSD of the observed signal after the first key-phase (once the first white-space link has been established) is shown where the center frequency of the white-space link was set to 507 MHz, relatively close to the visible DVB-T signal spectrum with the center frequency of 522 MHz. We did not observe any noticeable noise increase in the TV band.

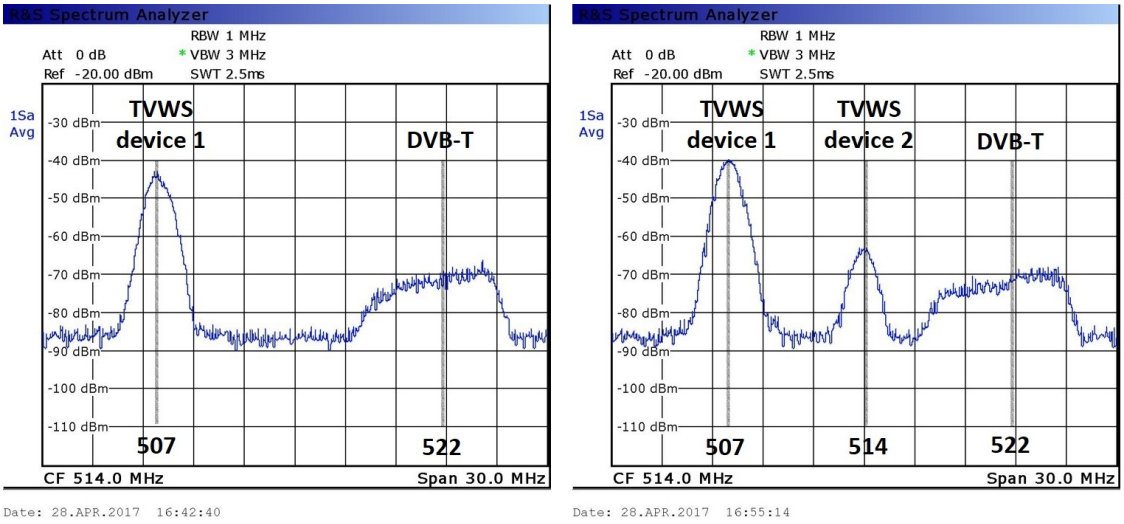

FIGURE 3.9: Power spectral density observed inside the room after the first and the second white-space link has been established

In Fig. 3.9, on the right side, we show the PSD of the observed signals again, but for a case when two white-space links have been established. The second link operates on the center frequency equal to 514 MHz. One may observe that the allowed transmitting power was lower as compared to the previous case, as the database needs to protect now two systems, both DVB-T one and the existing white-space transmission. Again we did not observe visually any changes in the DVB-T spectrum.

Also, in both white-space links, the reception of the transmitted video streaming was possible. It means that the out-of-band interference was relatively low and negligible. Consequently, such a simultaneous spectrum usage, as shown in Fig. 3.9 is possible. Finally, once the first white-space transmitter has been granted by the REM based system, the latter has to create a new or update the existing table with the spatial distribution map of the observed signal to noise ratio - see Fig. 3.10. Let us stress that we successfully transmitted the video stream with the requested quality in both transmissions.

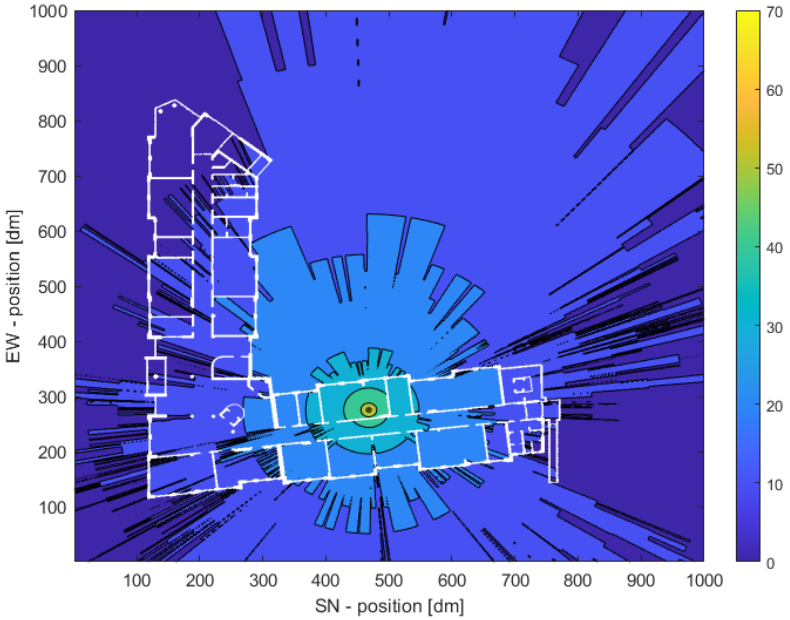

FIGURE 3.10: Spatial distribution of the observed SINR [dB] when one white-space device is active

Discussion and summary

In this work, we have presented the achieved results of the conducted experiment, where two white-space links have been established and managed using a dedicated remote REM database. It may be concluded that it is technically possible to practically deploy real-time indoor cognitive radio systems parallel to the existing legacy systems. The remote REM-based system manages the whole deployment process; in particular, it calculates the maximum acceptable Effective Isotropical Radiated Power (EIRP) values for any new user and adds this user to the dedicated database. However, the process of calculating new allowed values of EIRP was, in our case, very slow (in terms of tens of seconds), which makes the application of such a system challenging. This problem is a subject for further analysis and investigation, as access to the database must be very fast and reliable. In general, however, the experiment has proved that it is justified to consider low range white-space transmission that relies on REM based management system. This experiment also showed that a database created on the basis of measurements (Sec. 2.4), supplemented by kriging, can effectively provide CI for transmission in DSA.

A compact summary of the use of contextual information to improve spectral efficiency is presented in Table 3.2 below.

Ph.D. candidate's publications considering problems discussed in this section	[75], [117], [119]
Context information used in this section	Set of received power from DVB-T transmitters; location of TV transmitters; location, minimal required received power, maximum transmit power, frequency channel of secondary users; list of already allocated channels for secondary users; last connection time of secondary user to database.
Influence on the system	Allowing access to spectrum for unlicensed users; monitoring of secondary users connection to database; protection of primary (TV receivers) and secondary users.
Impact on spectrum efficiency	Higher spectrum utilization through more devices that's uses the same band.
Comment	By using exactly the same frequency range is possible to increase the number of users, which leads to an increase in the total system throughput, and thus to improve the spectral efficiency of the entire system. In this work, the possibility of using such a system was presented by means of an experiment performed in a laboratory using real equipment.

TABLE 3.2: Summary of work presented in chapter 3.2

3.3 Research topic 2: Joint spectrum and power allocation in CBRS-based DSA

In this chapter we deal with the proposal of several algorithms for efficient resource (frequency and power) allocation among Citizen Broadband Radio System (CBRS) Spectrum Access System (SAS) so-called CBRS-SAS [78] base stations operating as General Authorized Access (GAA) users in the three-layer model. Here, rich context information is stored and processed in the SAS.

The description of the work is organized as follows. First, we present assumed system model (see Sec. 3.3.1), and a detailed definition of the optimization problem for frequency and power allocation in the CBRS-SAS model for GAA users (see Sec. 3.3.2). Next, in Sec. 3.3.3 we present in detail four considered heuristic solutions for resource allocation among base stations, whereas in Sec. 3.3.4 we discuss the power optimization procedure and the proposed multi-choice algorithm. Finally, Sec. 3.3.5 provides a performance evaluation of the proposed schemes for various scenarios, and discusses the potential of using rich CI.

3.3.1 System model and problem formulation

This section presents the analyzed system's model, a mathematical description of the problem under consideration, and a heuristic analysis. The description of the CBRS system and related work is presented in Sec. 2.3.

General assumptions

In this thesis we consider the CBRS-SAS model [93] for spectrum sharing, where SAS is designed to manage Priority Access License (PAL) users within the second tier and the Coexistence Manager (CxM) is considered for interference management among GAA users [91]. Following the nomenclature used in the FCC directive [93], we will hereafter use the term CBSD, which represents either a fixed station, or a network of such stations, operating in PAL or GAA mode. In terms of available resources, 150 MHz of frequency band split into 30 channels each of 5 MHz bandwidth are available for tier three CBSDs, and 10 channels each of 10 MHz can be assigned for PAL users. In particular, GAA users may operate in the entire spectrum range (from 3550 to 3700 MHz), whereas PAL users can work only in the lower 100 MHz subband (from 3550 to 3650 MHz). In this work we only consider the allocation of resources to GAA users, although indirect information about higher tier users is available through the information of allowed power from SAS. It is assumed that the spectrum allocated (used) by the CBSD has to be contiguous. In our analysis, we consider a certain square area of a given size (in our case, 40 km) split into N_Q square subregions. Following the required accuracy of CBSDs defined in [93], the size of a square is set to 100 m. There are N_C CBSDs deployed over the considered area, whose coordinates are known. Again, following the guidelines from [93], the borders of the (circular) cell associated with a certain CBSD are defined as the set of points for which the observed received power measured in the 10 MHz band is above the available limit, i.e., -96 dBm (if we consider a narrower channel of 5 MHz band, this limit is set to -99 dBm). For path loss estimation, we follow the Free-Space Path Loss (FSPL) model, where the distance is calculated utilizing the Haversine formula. Furthermore, for each CBSD the aggregated interference in its coverage area from other CBSDs cannot exceed -99 dBm per 5 MHz.

Moreover, although resource allocation for CBSD devices of the PAL class is out of the scope of this work, we take into consideration the guidelines regarding the available transmit power defined by SAS. In particular, SAS provides the maximum allowed power for each frequency channel in each location. In addition, there are two classes of CBSD, i.e., in class A the maximum transmit

power is 30 dBm per 10 MHz (or 27 dBm per 5 MHz, respectively), whereas class B allows 47 dBm per 10 MHz band (or, analogously, 44 dBm per 5 MHz) [93]. However, a given CBSD can have its own hardware (device) specific maximum transmit power, which cannot exceed the values specified for its CBSD class. Finally, the maximum effective transmit power will be the minimum of these three values. From the perspective of CBSD, the power spectral density function is flat and constant in the entire assigned spectrum band. Moreover, the brick-wall transmit mask is defined. Adjacent Channel Leakage Ratio (ACLR) describes the ratio between the power transmitted in the nominal band of the system to the power observed in the adjacent band. Thus for bands adjacent to the channel assigned to the device for signal transmission, the ACLR is set to -42 dB, and for more distant channels, we assume that there is no spectrum leakage (ACLR is set to minus infinity). Adjacent Channel Selectivity (ACS) instead informs us about the ratio of receiver filter attenuation on the band of interest and filter attenuation on the adjacent channel frequency. These two factors are often represent jointly as Adjacent Channel Interference Ratio (ACIR), defined in linear scale as

$$\frac{1}{\text{ACIR}} = \frac{1}{\text{ACLR}} + \frac{1}{\text{ACS}}. \tag{3.5}$$

It can be measured as a ratio of interference powers in the whole band at the RX antenna to effective interference disturbing transmission. Typically ACS is obtained indirectly as a result of ACLR and ACIR measurements. In our investigation DownLink (DL) transmission will be considered. Moreover, our system model assumes the application of LTE transmission based on Time Division Duplex (TDD) as assumed in the CBRS-SAS standard [91]. In particular the so-called CBRS configuration 7 is assumed.

Mathematical description

There are N_C CBSD devices indexed $i = 1, ..., N_C$. The whole bandwidth is divided into N_{ch} channels each of $B_{CH} = 5$ MHz bandwidth indexed $n = 1, ..., N_{ch}$. In general it creates $2^{N_{ch}}$ options for bandwidth utilization by each of N_C CBSD devices. However, we assume that each CBSD is active and it can utilize only the continuous band. In consequence, there is only one option of using all N_{ch} channels, 2 options of using $N_{ch} - 1$ channels, 3 options of using $N_{ch} - 2$ channels etc. It gives in total $N_K = \sum_{n=1}^{N_{ch}} n = \frac{(1+N_{ch})N_{ch}}{2}$ options of 5 MHz channel usage. An $N_{ch} \times N_K$ matrix $\mathbf{\Gamma}$ consists of binary values with $\Gamma_{n,k} = 1$ if the n-th subchannel is active in the k-th spectrum utilization scheme. Otherwise, $\Gamma_{n,k}$ equals 0. The allocation of spectrum schemes to CBSDs is stored in an $N_C \times N_K$ binary matrix β with $\beta_{i,k} = 1$ if the k-th spectrum allocation scheme is used by the i-th CBSD. As such, the total bandwidth B_i used by the $i - th$ device can be calculated as $B_i = B_{CH} \sum_{n=1}^{N_{ch}} \sum_{k=1}^{N_K} \Gamma_{n,k}\beta_{i,k}$. Each CBSD transmits with power P_i per a single 5 MHz channel. The maximal power is limited by a regulatory authority, i.e., P_{REG} (see two classes of devices discussed in the prior subsection), device specification, i.e., $P_{\max} \leq P_{\text{REG}}$ per 5 MHz, and by information obtained from the SAS database. The maximum power provided by the SAS database, denoted as $P_{\text{SAS}i,n}$, is specific for a given device location, i.e., (x_i, y_i) in Cartesian coordinates and for a given frequency channel n. It is assumed that a CBSD transmits equal power in each of active channels. As such the maximal power of the i-th CBSD is minimum out of $P_{\max}$ and all $P_{\text{SAS}i,n}$ for which $\beta_{i,k}\Gamma_{n,k} = 1$ (true for all frequency channels active for the i-th device). Depending on the allocated power P_i, the range R_i of useful transmission of the i-th CBSD varies. The sensitivity of the receiver, equal to P_{SEN}, i.e. -99 dBm per 5 MHz in our case [93], is related with the R_i using the Friis propagation formula as

$$P_{\text{SEN}} = \frac{G_T G_R \lambda^2}{(4\pi)^2} R_i^{-\gamma} P_i = \alpha R_i^{-\gamma} P_i, \tag{3.6}$$

where G_T, G_R and λ are the transmitter antenna gain, receiver antenna gain and wavelength, respectively. γ is the environment dependent pathloss exponent, equal to 2 for free space propagation. The point (x, y) is within the useful range of the i-th CBSD (located at (x_i, y_i)) if

$$\sqrt{(x_i - x)^2 + (y_i - y)^2} \leq R_i. \tag{3.7}$$

In such a case, according to [93], the total interference from all CBSD devices $j \in \{1, ..., N_C\}$ is to be below the predefined level P_{INT}, which in our case equals -99 dBm per 5 MHz. Assuming ACIR between the k-th reception scheme and $\tilde{k}$ transmission scheme is $\text{ACIR}_{k,\tilde{k}}$, the interference constraint for each point (x, y) within the useful range of the i-th CBSD can be written as

$$\sum_{\substack{j=1 \\ j \neq i}}^{N_C} \alpha P_j \left((x_j - x)^2 + (y_j - y)^2\right)^{-\frac{\gamma}{2}} \cdot \sum_{k}^{N_K} \sum_{\tilde{k}}^{N_K} \text{ACIR}_{k,\tilde{k}} \beta_{i,k} \beta_{j,\tilde{k}} \leq P_{\text{INT}}. \tag{3.8}$$

The ACIR depends on the transmitter power spectral density PSD (including out-of-band radiation) and the receiver selectivity. In the case of OFDM transmission, the method of calculation is given in [121]. Typically it will be a value in the range $(0; 1\rangle$ with 1 for $\tilde{k} = k$. Most importantly, this condition is to be met for each point (x, y) within the useful range of the $i-$th CBSD. It is possible to define a dense enough grid to meet this interference constraint for practical considerations.

3.3.2 Joint spectrum and power allocation - problem statement

Our main optimization goal is to maximize the widths of the spectrum bands (thus, in consequence, available channel capacity) assigned to the CBSDs over possibly the broadest geographical area (that is directly proportional to the assigned transmit power). However, as the CBSDs can belong to various operators having various requirements, the goal function can be case-specific. Examples can be the maximization of the sum of allocated powers $\mathbf{P}$, the sum of allocated bands B_i or average throughput over the analyzed area. Each of these definitions has some drawbacks, e.g., maximizing the sum of allocated powers minimizes the bandwidth spanned by each device.

In general, an utilization function $f(\mathbf{P}, \beta)$ is to be maximized by a proper choice of transmit powers $\mathbf{P}$ and spectrum utilization scheme β. Considering the minimum set of constrains defined above, the optimization problem is

$$\max_{\mathbf{P},\beta} f(\mathbf{P}, \beta) \tag{3.9}$$

$$s.t. \forall_i \forall_{(x,y):\alpha P_i((x_i-x)^2+(y_i-y)^2)^{-\frac{\gamma}{2}} \geq P_{\text{SEN}}} \tag{3.10}$$

$$\sum_{\substack{j=1 \\ j \neq i}}^{N_C} \alpha P_j \left((x_j - x)^2 + (y_j - y)^2\right)^{-\frac{\gamma}{2}} \cdot \sum_{k}^{N_K} \sum_{\tilde{k}}^{N_K} \text{ACIR}_{k,\tilde{k}} \beta_{i,k} \beta_{j,\tilde{k}} \leq P_{\text{INT}}.$$

$$\forall_i \forall_{n:\beta_{i,k}\Gamma_{n,k}=1} 0 \leq P_i \leq \min\{P_{\max}, P_{\text{SAS}i,n}\} \tag{3.11}$$

$$\forall_i \forall_k \beta_{i,k} \in \{0, 1\} \tag{3.12}$$

$$\forall_i \sum_{k=1}^{N_K} \beta_{i,k} = 1. \tag{3.13}$$

The first constraint (3.10) refers to the interference limitation which has to be fulfilled for each CBSD in the network, i.e., the allowed interference at any point within the useful range of the i-th CBSD has to be limited. Constraint (3.11) describes the allowable ranges of the transmit power assigned to each CBSD dependent on the chosen spectrum utilization scheme β.

Finally, constraints (3.12) and (3.13), guarantee the selection of the contiguous band by each of the CBSDs. The problem defined above belongs partially to the class of binary integer programming because of β nature. However, the whole problem does not resemble any specific optimization problem class. The most problematic are constraints active under some conditions. Consequently, it is hard to solve the problem in that form by employing the well-known optimization tools regardless of the final definition of the optimization function f. Thus in the following part, we will propose a heuristic analysis, which is later refined by applying optimization algorithms for simplified optimization problems.

3.3.3 Heuristic analysis

As the joint spectrum and power allocation problem has been identified as a complicated optimization problem, we provide a comprehensive analysis of the four proposed heuristic algorithms. These are, by assumption, not optimal, but they deal with the research problem in various ways. In the first three cases, the considered solutions rely on graph theory. Mainly, the first proposal is the realization of the approach defined in [91], where a dedicated interference graph is created, and its chromatic number is used in the frequency allocation process. The two following solutions are our modifications of the first algorithm. The latest algorithm considered here is the extended version of the iterative approach proposed in [122]. All proposals have been published in the author's paper [92].

A. Graph coloring and finding the chromatic number

In this subsection, we rely on the general approach defined in [91]. Mainly, assuming the knowledge of the detailed location of CBSDs, the coexistence manager may create a so-called interference graph as proposed in, e.g., [96, 123]. In such a case, every CBSD will be represented in the undirected graph as a node. There will be an edge between nodes i and j if node i introduces interference to any point within coverage radius R_j of node j higher than P_{INT} or the other way round. While the coverage radius of the i-th CBSD R_i is defined in (3.6) we can define an interference radius $R_{\mathrm{INT},i}$, i.e., the distance from the i-th transmitter where the received power equals the interference limit P_{INT}, as

$$P_{\mathrm{INT}} = \alpha R_{\mathrm{INT},i}^{-\gamma} P_i. \tag{3.14}$$

Nodes i and j are interfering (connected in the graph) if the sum of $R_{\mathrm{INT}i}$ and R_j or $R_{\mathrm{INT},j}$ and R_i is greater than or equal to the distance between those CBSDs denoted as $d_{i,j}$.

One may observe that in this case, the interference graph will be a simple graph (i.e., neither loops nor multiple edges between two nodes are allowed). Thus such a graph may be represented in the form of the adjacency matrix $\mathbf{A}$, which is an $N_C \times N_C$ square matrix, and whose elements equal one if there exists an edge between two nodes. It is created using (3.14) and (3.6) as

$$A_{i,j}=\begin{cases}1 \;\; if \;\; \max\left(\left(\frac{\alpha P_i}{P_{\mathrm{INT}}}\right)^{\frac{1}{\gamma}}+\left(\frac{\alpha P_j}{P_{\mathrm{SEN}}}\right)^{\frac{1}{\gamma}},\left(\frac{\alpha P_j}{P_{\mathrm{INT}}}\right)^{\frac{1}{\gamma}}+\left(\frac{\alpha P_i}{P_{\mathrm{SEN}}}\right)^{\frac{1}{\gamma}}\right)\geq d_{i,j} \\ 0 \qquad \text{in other cases}\end{cases} . \tag{3.15}$$

In general, three ways of removing an edge from the graph may be considered: either the transmit power of the interfering nodes will be reduced, or the locations of these nodes can be changed, or the available spectrum band can be split orthogonally between these two nodes. In our case, we assume that the device's location is fixed (i.e., even for nomadic networks, the coexistence manager can suggest the available band for a specific location provided by the device in the query).

It can be assumed that the distance between nodes $d_{i,j}$ and requirements on the sensitivity level P_{SEN} and interference level P_{INT} are fixed. However, the potential interference depends additionally on the allocated band (carrier frequency changes α) and allocated power P_i and P_j as visible in (3.15). A worst-case scenario is assumed here with the minimum center frequency out of the available band, i.e., $f = 3652.5$ MHz, guaranteeing the maximum interference range. Additionally, the worst-case power $P_{\mathrm{WC}i}$ is defined as being the maximum out of all possible frequency channels n, i.e.,

$$P_{\mathrm{WC}i} = \min\{P_{\max}, \max_{n}\{P_{\mathrm{SAS}i,n}\}\}. \tag{3.16}$$

The worst-case power provides the highest interference radius and the highest protected area (defined by radius R_i). Two nodes are linked in the interference graph if there is any spectrum and power allocation scheme that can cause such an interference. In order to find the minimum number of orthogonal sets in any graph, the algorithms for node coloring and finding the so-called chromatic number can be applied. The chromatic number defines the minimum number of colors required to color each node in a given graph, assuming that always different colors are used in connected nodes. In our case, the calculated chromatic number X defines the minimum number of non-overlapping frequency subbands. In the final step, the division of the whole available bandwidth into X subbands and the assignment of those subbands to colors have to be performed, which is equivalent to the assignment of frequency bands to certain CBSDs. It is not a straightforward problem, as interference from adjacent channels has to be considered. In the worst case, it will be necessary to allocate two adjacent subbands to close CBSDs, and such a situation may entail the need for creation of a dedicated guard band, e.g., of bandwidth B_{CH}. One solution is to consider all possible combinations of color-band assignment (giving $X!$ options) and select the one that minimizes the guard band.

An exemplary interference graph and the resultant subband allocation among colors are shown in Fig. 3.11. One may observe the presence of 9 CBSDs, grouped into three subgraphs. The dashed circles represent the coverage area of the CBSD the assuming maximum allowable transmit power. The edges between the nodes indicate the presence of interference (if both nodes use the same band), and different colors represent different frequency subbands. In the provided example, one may observe that the chromatic number is $C = 3$. On the right side of the figure, one may observe the frequency allocations, i.e., the vertical axes represent CBSDs, and the horizontal one - represents the frequency blocks. The white color in this figure means that a given frequency block has not been assigned to this certain CBSD, and the various tones of copper color define different frequency blocks. One may observe that for CBSDs with indexes $\{1, 2, 3, 4, 6\}$ the entire spectrum has been split into three orthogonal subblocks. Analogously, devices $\{5, 7, 8\}$ split the band into three bands, and CBSD 9 can use the entire band. These three groups of nodes are indicated in the right-side plot by various shades of color (i.e., light brown, and dark brown). Graph coloring and band allocation are carried out separately for each subgraph. Next, looking at the left part of the figure, one may notice that nodes 5, 7, and 8 are marked with various colors, which means that three non-overlapping frequency blocks have been assigned to them. At the same time, pairs of node $\{1, 2\}$ and $\{3, 6\}$, are colored with blue and red, respectively, which indicates that the same frequency bands are assigned to each node in the group. Finally, let us notice that there was no need to introduce guard bands for nodes $\{5, 7, 8\}$. It was, however, necessary to add guard bands (one block of 5 MHz) between frequency blocks allocated to node 4 and pairs $\{1, 2\}$ and $\{3, 6\}$.

The presented solution is described in the form of an Algorithm 3.1. It relies on the approach proposed in [91] and may be the basis for further analysis and improvements, as we discuss in the following sections.

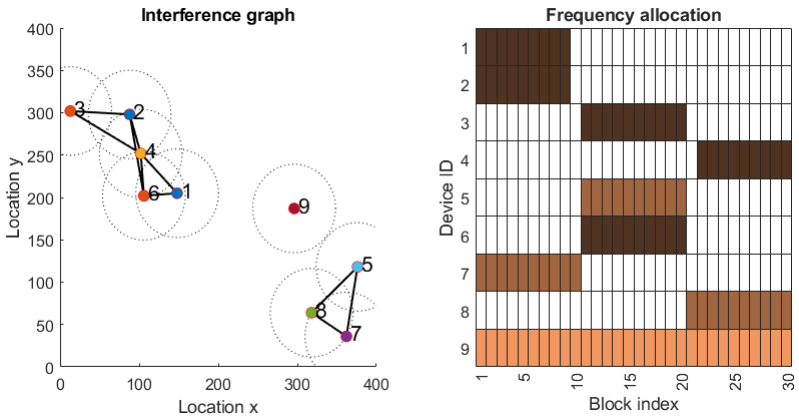

FIGURE 3.11: Example of interference graph

Algorithm 3.1: Interference Graph Creation and Coloring

Data: CBSDs setup (location, transmit power)
Result: Colored Interference Graph and Initial Resource Allocation
1 Deploy N_C CBSDs in the give area;
2 **foreach** *pair* (i, j) *of CBSD* **do**
3 | create an edge in the graph according to (3.15)
4 **end**
5 Once the graph is created, apply the coloring algorithm and find the chromatic number X;
6 Assign frequency subbands to colors;
7 Add guard bands if necessary;

B. Aggregated interference problem - heuristic approaches

The graph coloring approach in the form presented above does not consider the problem of aggregated interference. Although the interference from another CBSD transmitting in the adjacent band is somehow considered by the application of the guard bands, it does not solve the problem of aggregated interference. The interference graph consists of edges representing the presence of interference between two particular nodes. However, it does not reflect the issue of summation of the interference power originated from many, even not connected nodes. As shown in Fig. 3.11, there is no violation of the interference requirements between nodes 5 and 9. However, the total aggregated interference observed by node 5 appeared to be above the limit. In order to deal with this problem, we have proposed two heuristic approaches described below.

1) Graph coloring with add-edge algorithm

In the first case, we assume that the entire interference graph will be updated so that the aggregated interference (that causes problems) is also considered. In order to update the interference graph, for the violated CBSD i (i.e., the node that observed too severe aggregated interference), we create a list of interferers not connected to a given node and find the most distorting node j. Once it has been identified, an edge between nodes i and j is added to the graph, and the adjacency matrix is updated (i.e., $A_{i,j} = A_{j,i} = 1$). Thus, we call this approach an *add-edge* procedure. Next, graph coloring and band allocation as in Algorithm 3.2 are executed. The *add-edge* procedure is repeated as long as there are some CBSDs that observe too severe aggregated interference. The entire procedure may be summarized as in Algorithm 3.2. The interference graph from Fig. 3.11 is then modified as shown in Fig. 3.12, where the additional edge between nodes 5 and 9 is created. The corresponding frequency allocation among nodes 5, 7, 8, and 9 is also changed.

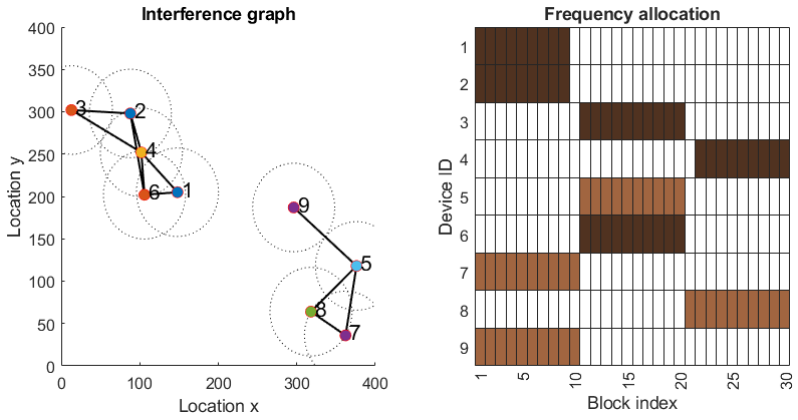

FIGURE 3.12: Interference graph after executing "add-edge" procedure

Algorithm 3.2: Graph Coloring with Add Edge Algorithm

Data: CBSDs setup (location, transmit power)
Result: Colored Interference Graph, Resource Allocation with Acceptable Aggregated Interference

```
Apply Algorithm 3.1;
Calculate aggregated interference;
while too severe aggregated interference in the network do
    Find strongest interferer j (not connected previously) for selected most violated node i;
    Add edge between nodes i and j in interference graph;
    Find chromatic number X and apply the coloring algorithm;
    Assign frequency subbands to colors (including guard bands);
    Calculate aggregated interference;
end
```

2) Graph coloring with Reduce Power algorithm

In the second proposed approach, the interference graph is not modified; thus, the spectrum split (achieved as the outcome of Algorithm 3.1) is not changed. The elimination of the harmful aggregated interference is achieved here by the proper adjustment of the transmit power of interfering nodes. Similarly to Algorithm 3.2, the most violated node has to be detected; in the next step, the most influencing node (with respect to the identified violated one) has to be identified, and in consequence, its transmit power has to be reduced by, e.g., 1 dB (this is an arbitrarily chosen value that can be adjusted due to various circumstances). After the power reduction step, the presence of too strong aggregated interference has to be checked, and if necessary, the entire loop has to be repeated one more time. The entire procedure has been summarized in Algorithm 3.3.

C. Iterative approach

In [122], an Iterative Allocation Process (IAP) is proposed to deal with the CBSDs resource allocation. Following IAP, SAS takes iteratively all requests expressed by the CBSDs and checks if the allowable levels for aggregated interference are violated at any identified protection point. Suppose, for a given request the interference levels are not violated for any existing CBSD at any protection point. In that case, such a request is accepted, and requested resources are granted for this CBSD. Next, the consecutive request is processed. In the case of violation of the allowable interference level at any of the referenced points, SAS reduces the allowable transmit power for the considered CBSD and verifies the interference levels again. The last steps are repeated iteratively until the interference requirements are fulfilled or the transmit power falls below threshold.

Algorithm 3.3: Graph Coloring with Reduce Power Algorithm

Data: CBSDs setup (location, transmit power)
Result: Colored Interference Graph, Resource Allocation with Acceptable Aggregated Interference

```
Apply Algorithm 3.1;
Calculate aggregated interference;
while too severe aggregated interference in the network do
    Find strongest interferer j for selected violated node i;
    Reduce the transmit power P_j of node j by a certain value, e.g., 1 dB;
    Update interference graph;
    Find chromatic number X and apply the coloring algorithm;
    Assign frequency subbands to colors (including guard bands);
    Calculate aggregated interference;
end
```

It is worth noticing that IAP does not assume a change of the frequency bands when the interference requirement is not satisfied. In order to improve the performance of this iterative algorithm, we have slightly adjusted it to consider the availability of multiple frequency channels. First, it is assumed that the entire available bandwidth is divided between CBSDs in such a way that for each CBSD a certain predefined (equal) number of 5 MHz width, adjacent frequency blocks may be assigned from the total $N_{ch} = 30$ blocks. This approach may be easily modified to a more flexible case, where each CBSD provides an individual spectrum request. The key idea in the updated algorithm is that the coexistence manager tries to allocate the contiguous frequency band (with maximum possible power) before it decides on transmit power reduction. In particular, the algorithm starts with the index of the first frequency block and checks if the particular fragment can be allocated to this CBSD with given maximum power P_i. If not, it increments the block index and checks the transmit opportunities again, i.e., if the interference constraints are met. Suppose the algorithm reaches the last possible frequency block and allocation is impossible. In that case, the requested transmission power is reduced as in the original IAP algorithm, and the search starts again from the first frequency block. The modified IAP algorithm is presented as Algorithm 3.4.

3.3.4 Optimized power allocation and proposed multi-choice algorithm

The presented meta-heuristic algorithms find by default only one solution, which may not always fulfill each CBSD's requirements. For example, suppose there is a requirement that the minimum reasonable bandwidth allocated to the CBSD be above some certain value. In that case, the solutions found by the above algorithms may not be acceptable. Analogous conclusions could be drawn for the situation where the minimum radius of the cell (thus transmit power) is also defined. For this reason we have proposed the Multi-Choice Algorithm that produces $M_{\max}$ solutions, where $M_{\max}$ is limited either by the number of available channels or the chromatic numbers, so $M_{\max} = \min(X, N_{ch})$. Such an approach will deliver the entire spectrum of solutions, starting from the situation where all nodes use the same frequency band and ending when the available spectrum is split orthogonally among all CBSDs.

Let us observe that the problem of efficient resource allocation among CBSDs consists of two (associated) subproblems. The first one is related to the right split of the available frequency band and assignment of the resulting subbands into CBSDs. The second one deals with power optimization in each frequency band. We will present the proposed power optimization algorithm, which will be widely applied in the proposed multi-choice algorithm once the frequency assignment has been done.

Algorithm 3.4: Updated IAP

Data: CBSDs setup (location, maximum transmit power)
Result: Resource Allocation with Acceptable Aggregated Interference

foreach *CBSD requesting* $R \leq N_{ch}$ *frequency blocks.* **do**
  Set frequency block index $n = 1$;
  Set the transmit power P_i to minimum value from the vector of R+1 constrains as $P_i = \min\{P_{\max}, P_{\mathrm{SAS}i,n}, \dots P_{\mathrm{SAS}i,n+R-1}\}$;
  while *frequency resources are not allocated for considered i-th CBSD* **do**
    if *there is no possibility to assign R blocks starting from index* $n \leq N_{ch} - R$ *due to violation of interference constraints* **then**
      if $n \leq N_{ch} - R$ **then**
        Increase index $n = n + 1$;
      else
        Reduce transmit power P_i for considered CBSD by e.g. 1dB;
        Set frequency block index $n = 1$;
      end
      if *allowable transmit power is below acceptable threshold* **then**
        Discard this CBSD request;
      end
    end
  end
end

A. Power optimization

It is possible to simplify the optimization problem (3.9) for a case of $\tilde{N}_I$ devices operating in the same band. This is a subset of all devices, i.e., $\tilde{N}_I \leq N_C$. It can be the result of a fixed β matrix and choosing a common activity band. In the final algorithm, power optimization will be carried out for each frequency channel (out of N_{ch}) separately. However, it is possible to optimize the power for a wider band as well. Fixed β removes the requirement of constraints (3.12) and (3.13). Additionally, the upper limit of power P_i is a fixed number denoted as $P_{\mathrm{MAX}i}$. It is a solution of the optimization problem $\forall_i \forall_{n:\beta_{i,k}\Gamma_{n,k}=1} \min\{P_{\max}, P_{\mathrm{SAS}i,n}\}$. Finally, the interference constraint (3.10) can be simplified. It is not required to check for an exceeded interference level inside the cell (for multiband optimization interference can occur as a result of, e.g., Out-Of-Band (OOB) radiation from adjacent band). It is enough to check the interference on a cell border. ACIR in this case equals 1. This significantly reduces the number of constraints. The goal function is only dependent on a vector $\mathbf{P}$. It is chosen to maximize sum of P_i values weighted by power coefficient ρ. High ρ values prioritize CBSDs transmitting with high power, while lower values promote equality between CBSDs' powers. This is one of the implementations of the goal function $f(\mathbf{P}, \beta)$ with constant β, chosen for practical purposes. These simplifications allow us to define the optimization problem as

$$\max_{\mathbf{P}} \sum_{i=1}^{\tilde{N}_I} {P_i}^{\rho} \tag{3.17}$$

$$s.t. \, \forall_i \forall_m \, \alpha \sum_{\substack{j=1 \\ j \neq i}}^{\tilde{N}_I} {g_{i,j,m}}^{-\gamma} P_j \leq P_{\mathrm{INT}} \tag{3.18}$$

$$\forall_i \, 0 \leq P_i \leq P_{\mathrm{MAX}i}, \tag{3.19}$$

where $g_{i,j,m}$ is distance between the j-th CBSD and m-th point on the border of the i-th CBSD.

Let us define N_M protected points on the border of each CBSD. Each of these is defined by an angle θ_m for $m = 1, ..., N_M$ and cell radius R_i in polar coordinates for i-th CBSD as shown in Fig. 3.13. The distance between i-th and j-th CBSD equals $d_{i,j}$ and angle of vector between i-th CBSD and j-th CBSD in polar coordinates equals $\varphi_{i,j}$. Using law of cosines, the distance $g_{i,j,m}$ can be calculated as

$$g_{i,j,m} = \sqrt{d_{i,j}^2 + R_i^2 - 2d_{i,j}R_i \cos(\theta_m - \varphi_{i,j})}. \tag{3.20}$$

Observe that the above optimization problem depends only on P_i variables after substituting R_i using (3.6). This problem is solved by means of function *fmincon* available in Matlab.

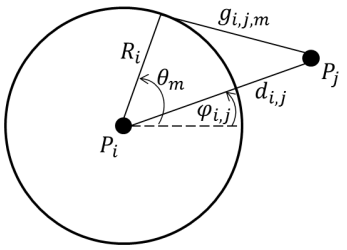

FIGURE 3.13: Scheme for calculation of distance $g_{i,\tilde{i},m}$, i.e., between j-th CBSD and m-th point on the border of i-th CBSD

B. Concept of a multi-choice algorithm

Once the power optimization algorithm has been discussed in detail, let us now present the entire multi-choice algorithm, which is illustrated in Fig. 3.14. It is split conceptually into two main phases, the first one, where Graph Coloring with Add-Edge Procedure is applied (Alg. 3.2), and the second, where node clustering is applied iteratively. In the first phase, only one solution is generated, i.e., the one where all devices transmit with the maximum allowable power (this is obtained by maximal band fragmentation). In the second phase, the remaining $M_{\max} - 1$ solutions are created. The entire algorithm is discussed in the following subsections.

1) Initialization and graph coloring

As in the previous algorithms, as the input to the algorithm, we take the limitations coming from SAS and CBSDs specifications mainly the maximum equivalent transmits power for each device is provided. Next, as the parameter, we take the acceptable interference level P_{INT}. We start the creation of an interference graph and calculation of chromatic number X.

2) Phase 1 - assignment of colors to frequency bands

Next, the algorithm enters the step of assigning frequency subbands to the colors. Currently, this is realized by generating all $X!$ possibilities and selecting the best one minimizing the number of the required guard band. In particular, we check each combination of color pairs if they can occupy adjacent frequency bands or need one channel of separation as a guard band to prevent excessive out-of-band interference. Next, we try all combinations of color pair order and search for the one that requires the minimal number of guard bands. When we know the order of colors and places for the guard bands, we only need to choose how many channels (subbands) are assigned to each color. We used two solutions. The first one assumes that every color should have the same amount of spectrum. The second one assumes assignment is proportional to the number of devices utilizing a given subband, i.e., colors with a higher number of devices should have more spectrum.

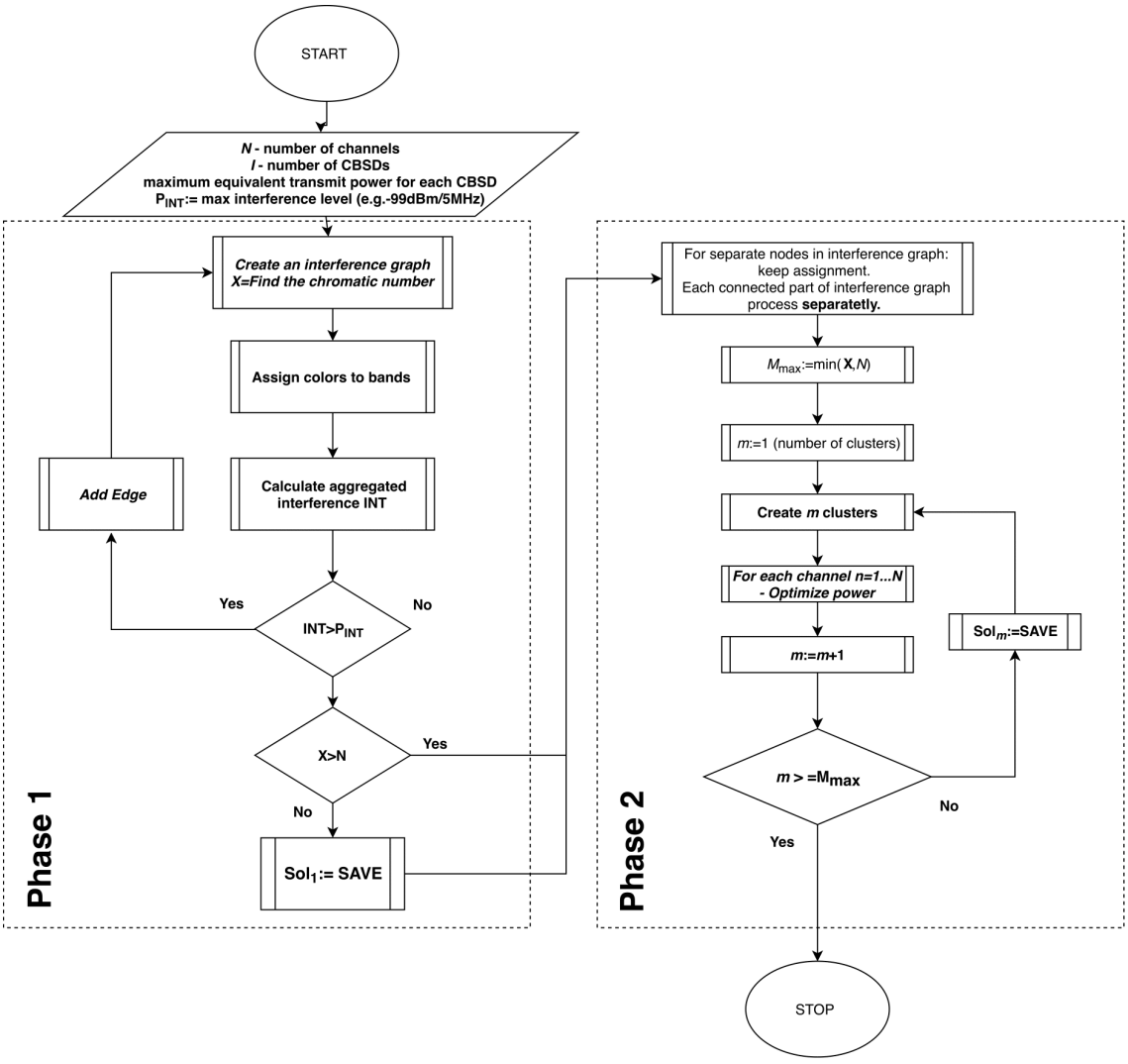

FIGURE 3.14: Multi-choice algorithm

For example, if we have three devices associated with two colors, one color should get 1/3 of the spectrum and the second one 2/3 of the spectrum. The former approach is hereafter called *Equal assignment*, whereas the latter - *Proportional Assignment*. One may observe that the order of coloring and assignment of frequency bands to colors matters. Thus, there may be some channels left, for example, because the number of channels (without guard bands) is not always divisible by the number of colors X. In such a case, we simply add these free channels to random colors (CBSDs). Observe that the above-described procedure is carried out for each subgraph (not connected to another subgraph) separately.

3) Phase 1 - Add Edge procedure

In order to verify the correctness of the created graph and resultant frequency assignment, the total observed aggregated interference (denoted in the algorithm as P_{INT}) is calculated for each node on its coverage area. Suppose the aggregated interference from many CBSDs violates the interference constraint. In that case, it has to be eliminated, and this is done by the application of the Add Edge algorithm (Algorithm 3.2), repeated as many times as the aggregated interference occurs. Once this constraint is fulfilled, the created graph is treated as the outcome of the first phase of the Multi-Choice Algorithm and delivered as input to the second phase.

One may notice that this graph and its corresponding chromatic number guarantee interference-free transmission with the maximum power for all N_C CBSDs. The available spectrum has to be split into X orthogonal, not necessarily equal, subbands of the bandwidth being the integer multiplication of 5 MHz. If such a division is possible, we treat such a spectrum assignment as the first possible solution and store it. The created solution may be, however, not possible if the number of CBSDs is large and the interference graph very dense. To be more precise, when the final chromatic number X is greater than the number of available 5 MHz channels N_{ch}, then it is impossible to split the spectrum as described earlier. In such a case, the outcome of the first phase of the algorithm is the interference graph that guarantees the lack of an aggregated-interference problem. No possible solution for frequency assignment will be created then.

4) Phase 2 - iterative procedure

The outcome from Phase 1 of the Multi-Choice Algorithm is, first, a network graph that may be colored so that there is no aggregated interference; second, the chromatic number X, and third, if applicable, a unique solution for the maximum transmit power. The ultimate goal of Phase 2 is to show the trade-off between the allocation of power and frequency to the CBSDs. The algorithm calculates the optimal power assignment for all potentially applicable numbers of frequency divisions. In other words, it starts with the case where all CBSDs are clustered together (i.e., they use the same frequency or, equivalently, the number of colors in the graph is one) and optimizes the transmit power in the network, taking into account each 5 MHz bands individually. If by m we denote the current number of CBSD clusters, then the algorithm starts with $m = 1$. Next, the number of colors is incremented, which is equivalent to increasing the total number of CBSD clusters by one ($m = 2$). In other words, the entire band will now be split into two parts. Again, the optimal power assignment is applied. This procedure is repeated $M_{\max}$ -1 times, thus as long as the number of clusters equals the chromatic number X or when the number of clusters equals the number of available 5 MHz channels.

5) Phase 2 - merging colors

The critical issue is to find the way for cluster creation; mainly, how should the CBSDs be assigned to the cluster? It is done to decrease spectrum fragmentation. The input is the colored interference graph from Phase 1. It contains X various colors. In order to achieve m colors, $X - m + 1$ colors have to be merged, and we propose to do this iteratively. The main idea is to merge the two least interfering colors in the interference graph every time. It is achieved through the maximization of the minimum pathloss between the CBSDs of two colors to be merged. Observe that the frequency allocation obtained in Phase 1 or previous iterations of Phase 2 is not used at this stage.

Let us define matrix $\mathbf{W}^{a,b}$ of size $C_a \times C_b$. Indexes a and b denote a given graph color, i.e., $a, b \in \{1, ..., X\}$. The number of CBSDs utilizing the $a - th$ color is denoted by C_a. A matrix element $W^{a,b}_{g,h}$ denotes the pathloss between the $g - th$ CBSD of color a and $h - th$ CBSD of color b, where $g \in \{1, ..., C_a\}$ and $h \in \{1, ..., C_b\}$. This pathloss is calculated based on a proper element $d_{i,j}$. The following dedicated metric has been used to rate any pair of colors a, b:

$$\bar{w}_{a,b} = \min_{g,h} \mathbf{W^{a,b}}. \tag{3.21}$$

The result $\bar{w}_{a,b}$ can be interpreted as a interference attenuation between colors a and b. Although in total X^2 combinations are possible, it can be observed that $\bar{w}_{a,b} = \bar{w}_{b,a}$ and there is no point in calculating $\bar{w}_{a,a}$.

It is only required to do the above optimization for $\frac{X(X-1)}{2}$ pairs of colors, i.e., $a \in \{1, ..., X-1\}$ and $b \in \{a+1, ..., X\}$. The pair of colors to be merged $\left(\bar{a}, \bar{b}\right)$ is chosen based on the above set as

$$\left(\bar{a}, \bar{b}\right) = \arg \max_{\substack{a \in \{1,...,X-1\} \\ b \in \{a+1,...,X\}}} \bar{w}_{a,b}. \tag{3.22}$$

The pair of colors guaranteeing the maximal minimal pathloss between CBSDs is chosen (max-min problem). This procedure is repeated until the required number of clusters m is obtained. Using this method we can create any cluster count from 1 to $M_{\max}$.

6) Power optimization

Once the colors are merged, the next step is to assign frequency subbands to the merged colors, as described in Phase 1. After that the power optimization algorithm from Sec. 3.3.4 is applied for each frequency channel n independently. The power of the i-th CBSD P_i is the minimum out of all power values obtained as a result of poorer optimization carried out for each active channel (for $i-th$ CBSD), i.e., $\forall_{n:\beta_{i,k}\Gamma_{n,k}=1}$. While in the first phase, the algorithm generates potentially only one feasible solution (i.e., the one where all transmit powers are maximal), in the second phase, one will achieve $M_{\max} - 1$ solutions. The Coexistence Manager will then need to decide (based on given decision criteria) which solution is the most suitable. We discuss the performance of this algorithm and various selection criteria in the following section.

3.3.5 Performance evaluation

In this section, we discuss the results of computer simulations. The entire simulator has been implemented in the Matlab environment, where several toolboxes have been utilized, e.g., for solving the power optimization problem. We start our discussion with the presentation of the results from the exhaustive search simulation and compare the allowed system configurations with the results of the proposed algorithms (Algorithms from 3.2 to 3.4 and the Multi-Choice one). Finally, we discuss in detail the features of the proposed multi-choice algorithm in various scenarios.

Let us recap that in our simulation we use the system model described in detail in Sec. 3.3.1, mainly, each CBSD may be allocated with a contiguous band in the range from 3.550 GHz to 3.7 GHz, split into $N_{ch} = 30$ channels, where the bandwidth is set to $B_{CH} = 5$ MHz. The interference limit $P_{\mathrm{INT}} = -99$ dBm/5 MHz, the coverage area of each CBSDs is defined as a circle of the radius defined in (3.6) for the free space path loss model with $\gamma = 2$. The CBSDs are deployed over the square area of size 40 km $\times$ 40 km, split into $N_Q = 160000$ subregions of size 100 m $\times$ 100 m. Moreover, in the simulations we consider the guidelines delivered by SAS, mainly for each CBSD location a vector of size N_{ch} is created that contains the maximum power that can be potentially used by the $i-th$ CBSD on each frequency channel, i.e., $P_{\mathrm{SAS}i,n}, n = 1 \ldots N_{ch}$. The values of $P_{\mathrm{SAS}i,n}$ were chosen as a random variable uniformly distributed in the range $\langle 17, 44 \rangle$ dBm confirming correctness of the proposed solutions. However, the results presented below are obtained for constant $P_{\mathrm{SAS}i,n}$ values both over the frequency range and CBSD index. It simplifies the interpretation of the results. This removes randomness caused by SAS. If not stated differently, we have considered CBSD from Class B, i.e., the maximum power defined in [93] cannot exceed $P_{\mathrm{MAX}} = 44$ dBm measured in the 5 MHz band. It is assumed the CBSDs TX and RX use omnidirectional antennas of gains $G_{\mathrm{TX}} = 1$ and $G_{\mathrm{RX}} = 1$. Power optimization utilizes $\rho = 0.5$, providing a relatively high equality of assigned powers between CBSDs.

A. Exhaustive search and solution space

In order to visualize the space of feasible solutions, we have applied the brute force algorithm. For the defined number of frequency channels N_{ch} and the number of possible transmit power levels N_{chP}, considering all possible locations of the assigned spectrum blocks in the available range, i.e., $(N_{ch}+1)N_{ch}/2$ as shown previously, we calculate the value of corresponding interference and aggregated interference. The total number of system configurations is $\left((1+N_{ch})\frac{N_{ch}}{2}N_{chP}\right)^{N_C}$. If there is no violation of any of the assumed constraints for the given setup, such a setup is included in the space of available solutions. Otherwise, it is marked as a prohibited setup.

As the total number of options significantly increases with the increase of the number of CBSDs, available channels, and power range, as shown above, we have decided to show the brute force results for a simplified scenario. However, such a simplification has no impact on the overall conclusion which can be drawn. In this subsection we have assumed the presence of $N_C = 3$ CBSDs, which may use up to $N_{ch} = 5$ available frequency channels with $N_{chP} = 7$ steps of transmission power (from 10 dBm to 40 dBm, step 5 dBm). Two location options showed in Fig. 3.15 and Fig. 3.16 were considered.

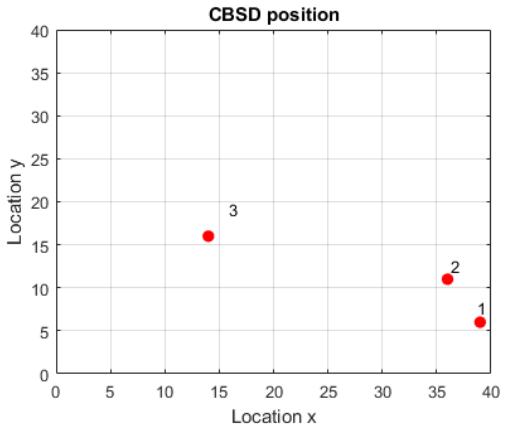

FIGURE 3.15: CBSDs position (Scenario I)

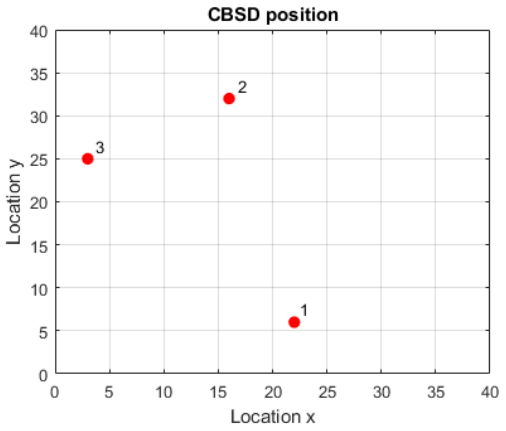

FIGURE 3.16: CBSDs position (Scenario II)

In Fig. 3.15–3.20, the red dots represents all tested setups for frequency and power assignment not meeting interference constraints, whereas the black dots constitute the domain of feasible solutions. One may notice that the space of available solutions is discrete, as the input data for the brute force algorithms are also discrete. Moreover, on the horizontal axis the sum of allocated bandwidths for all CBSDs, i.e., $\sum_{i=1}^{N_C} B_i$ is considered, and on the vertical axis the mean PSD is shown, i.e., $\frac{1}{N_C}\sum_{i=1}^{N_C} P_i$. It may be concluded that the points generated in the brute force algorithm may overlap (regardless of the color of the nodes). The same mean PSD and total bandwidth may be achieved for various setups with some of them obeying constraints and other not.

Solution spaces in these cases are showed in Fig. 3.17 and Fig. 3.18. One issue to be discussed is the presence of black *tails* in the horizontal direction, a sequence of black dots surrounded by red dots. An immediate question may appear how is it possible that the point, e.g., 35 dBm per 5 MHz for 35 MHz, is acceptable, and 33 dBm (for the same summarized bandwidth) is not allowed? The reason is the fact that this result has been achieved for a discrete set of power values, i.e., value 33 came from averaging, e.g., two high power values and one close to zero, and this solution may not be possible. In general, it is visible that it is impossible to provide a maximum bandwidth, i.e., 25 MHz while keeping the maximum transmission power, i.e., 40 dBm, in each device (upper right corner in Fig. 3.17 and Fig. 3.18) as a result of interference constraints not met.

On the other hand, results in the lower-left corner, providing a minimum bandwidth and transmit power, are acceptable from the constraints perspective. However, they provide low spectral efficiency. Depending on the construction of the goal function $f(\mathbf{P}, \beta)$ the optimal solution will differ; however, it is expected that it will be located close to the *border* between red and black dots areas.

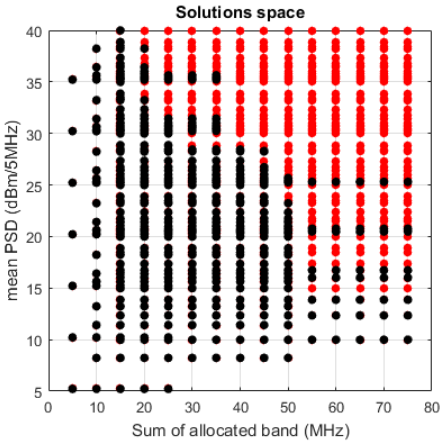

FIGURE 3.17: Solution space (Scenario I)

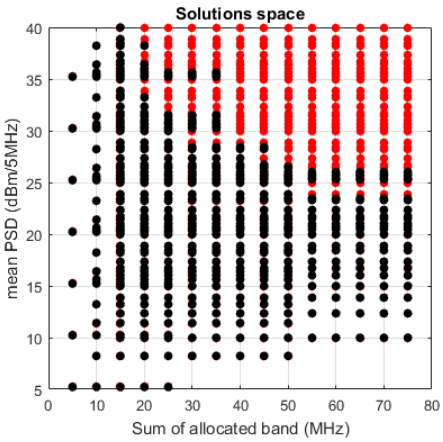

FIGURE 3.18: Solution space (Scenario II)

B. Performance comparison

Let us now compare the performance of the above-proposed algorithms. It can be based on the solution set presented above. However, as proposed in Sec. 3.3.2, the maximization of the mean throughput over the whole area can be used as a goal function. Let us define the summarized rate for the i-th CBSD over its cell area as

$$S_i = \int\int_{A_i} B_i log_2\left(1 + \frac{\alpha P_i \left((x_i - x)^2 + (y_i - y)^2\right)^{-1}}{P_{\text{noise}} + \sum_{\substack{j=1 \\ j \neq i}}^{N_C} \alpha P_j ((x_j - x)^2 + (y_j - y)^2)^{-1} \sum_k^{N_K} \sum_{\tilde{k}}^{N_K} \text{ACIR}_{k,\tilde{k}} \beta_{i,k} \beta_{j,\tilde{k}}}\right) \quad (3.23)$$

where P_{noise} is thermal noise power over the 5 MHz band and integration area is

$$A_i = \left\{(x, y) : (x, y) \neq (x_i, y_i) \wedge \alpha P_i \left((x_i - x)^2 + (y_i - y)^2\right)^{-1} \geq P_{\text{SEN}}\right\}. \quad (3.24)$$

Observe that the point coinciding with the i-th CBSD location is excluded from calculation, as the FSPL propagation model works erroneously in this point, i.e., causes infinitive received power for $(x, y) = (x_i, y_i)$. Additionally, formula (3.23) is simplified in the frequency domain. It considers neither frequency selective channel fading, nor interference changing between 5 MHz blocks.
The mean interference in the whole band is considered. This throughput has to be averaged over the whole area, i.e., 40 km × 40 km, and all N_C CBSDs, giving

$$\overline{S} = \frac{1}{N_C} \frac{1}{(40)^2} \sum_{i=1}^{N_C} S_i. \quad (3.25)$$

We want to project the solutions generated by the considered algorithms onto the space of available solutions. The first three plots in Fig. 3.19 and Fig. 3.20 represent the results of the Algorithms 3.2 (i.e., Add Edge algorithm), 3.3 (i.e., Reduce Power algorithm) and 3.4 (i.e., updated IAP algorithm) achieved for the two considered scenarios, respectively.

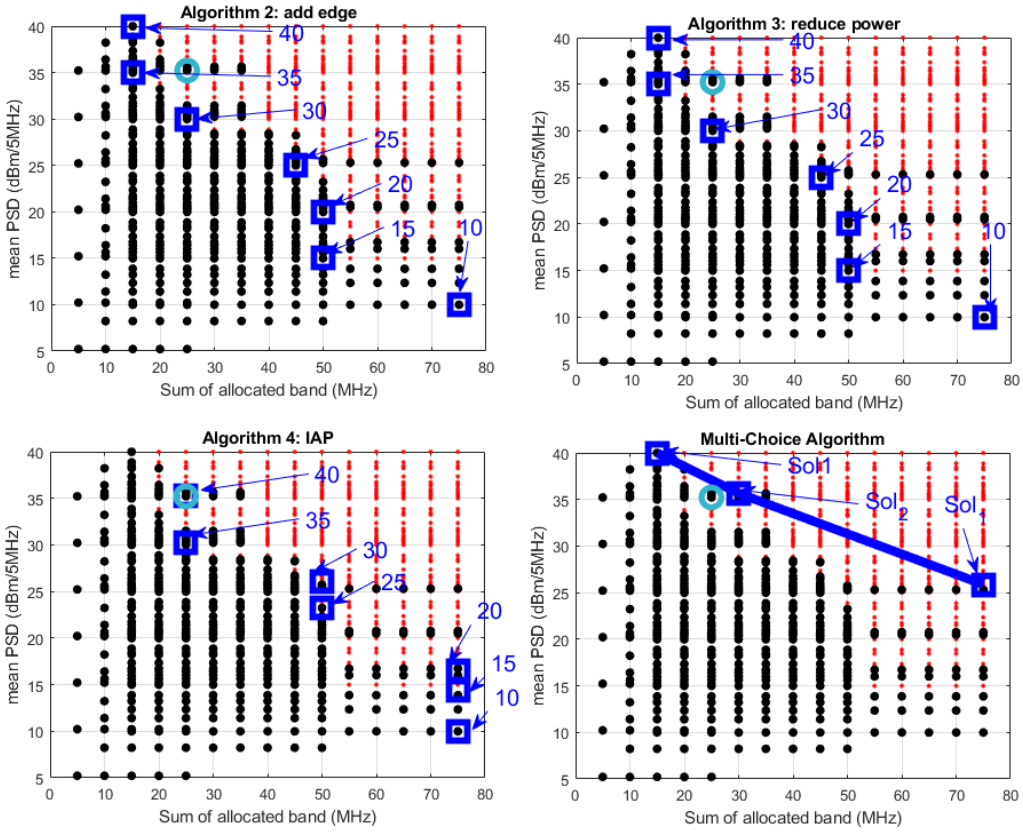

FIGURE 3.19: Performance comparison (first scenario)

The results for the seven power levels are denoted by blue squares. One may, in general, observe that all results lay on or close to the so-called Pareto Frontier, i.e., the line connecting the solutions which are optimal for various limiting criteria. In addition, we marked by the light blue colored circle the allowable solution with the highest mean throughput, as defined by (3.25), which equals 34.109 and 32.243 $\frac{\text{Mbps}}{\text{km}^2}$ in the first and second scenarios, respectively. It is worth noting that these points are also located close to the Pareto Frontier. Also, one may observe that the first algorithm utilizes maximum allowable power, whereas the Reduce Power algorithm and updated IAP propose solutions that do not always use the maximum available transmit power. The first two algorithms (i.e., Add Edge and Reduce Power) considered with the highest available transmit power (40 dBm) achieved the same mean rate over the whole area of 17.54 $\frac{\text{Mbps}}{\text{km}^2}$. In comparison, the updated IAP algorithm achieved 24.82 $\frac{\text{Mbps}}{\text{km}^2}$ with the same simulation setup. The fourth plot in Fig. 3.19 and Fig. 3.20 shows the results achieved by the Multi-Choice Algorithm. It produces only three solutions, one from the first phase (left top solution-whole band divided into three orthogonal subbands) and two from the second phase (2 and 1 frequency subband, respectively).

The general conclusion that can be drawn is that these results are *shifted right*, so in practice, it means that they should guarantee much better performance. It shows the potential of the proposed Multi-Choice algorithm. The mean throughput over area is equal 17.54, 14.76 and 11.80 $\frac{\text{Mbps}}{\text{km}^2}$ for 3 clusters, 2 clusters and 1 cluster, respectively. The proposed algorithms achieve around half of the maximum value of this metric found by an exhaustive search. However, the maximum is obtained for the case of the whole band and maximum power allocated to a single CBSD and deactivation of others. The fairness of resource allocation is much higher in the proposed algorithms, showing that the mean rate over the area cannot be treated as an ultimate goal function for the whole network optimization.

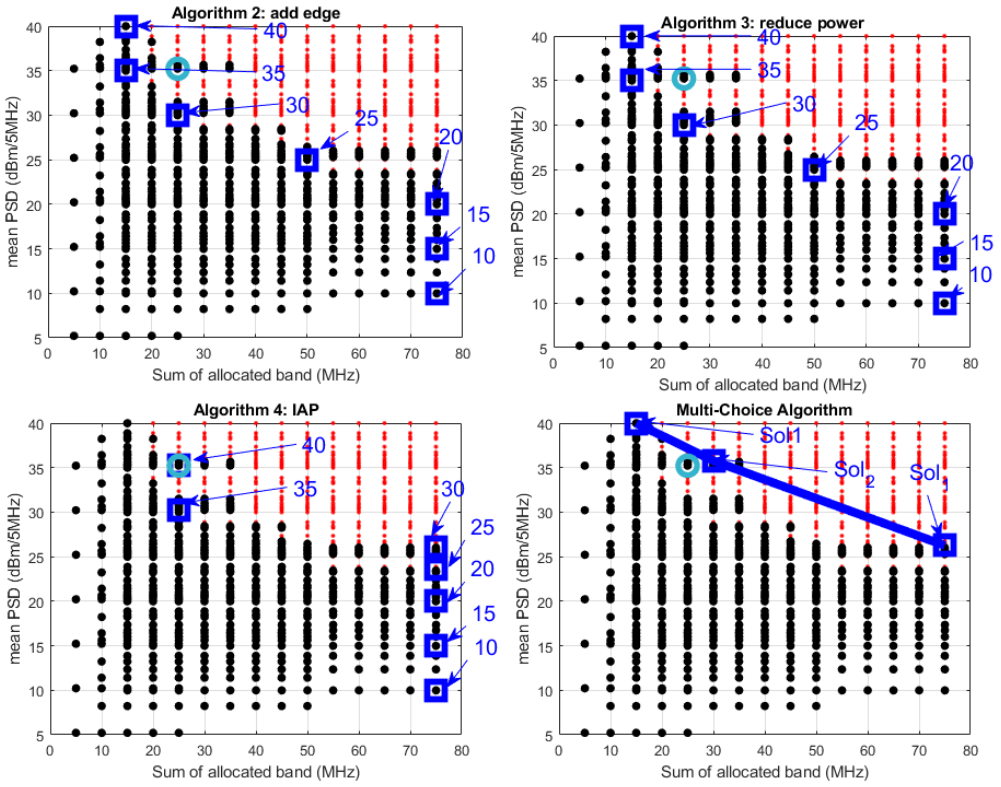

FIGURE 3.20: Performance comparison (second scenario)

C. Multi-choice performance analysis

As we see that the Multi-Choice Algorithm outperforms the other solutions, we would now like to discuss its features in a more detailed way. We have increased the number of CBSDs to 5, and we have set the maximum to transmit power per 5 MHz to 44 dBm, equal to the whole available bandwidth of 150 MHz. A single, random generation of CBSD locations is considered. As the number of figures is relatively high (it is done intentionally to reflect in detail the algorithm's behavior), we split the description of them into two parts.

1) Fig. from 3.21 to 3.25

For the single, exemplary deployment of CBSDs (shown, e.g., in Fig. 3.21), the calculated chromatic number equals $X = 5$, thus the 5 steps of the Multi-Choice Algorithm can be extracted. We show in Fig. 3.21 (for five clusters, each cluster utilizing a separate band) to Fig. 3.23 (for one cluster of CBSDs) a few selected steps. In each figure, one may observe the coverage area of each CBSD, the corresponding interference graph, which has been already colored, and the final split of frequencies among devices. When necessary, the algorithm adds the one-channel frequency gap (guard band) between two adjacent blocks of frequencies. Furthermore, in order to obtain statistically meaningful results, the Multi-Choice Algorithm was run for 100 random deployments of 10 CBSDs. In Fig. 3.24, Empirical Cumulative Density Functions (ECDF) of allocated bandwidth and power are shown for the changing number of CBSD clusters from 1 to 10. Expectedly, for a low number of clusters, high bandwidth is assigned (e.g., 150 MHz for each device for 1 cluster) at the cost of reduced transmit power (e.g., about 80 % of CBSDs transmit with power below 20 dBm for 1 cluster). High transmission power is possible for a high number of clusters but with significantly reduced bandwidth. The proposed Multi-Choice Algorithm allows a single setup to be chosen based on a specific goal function or minimum requirements of each CBSD.

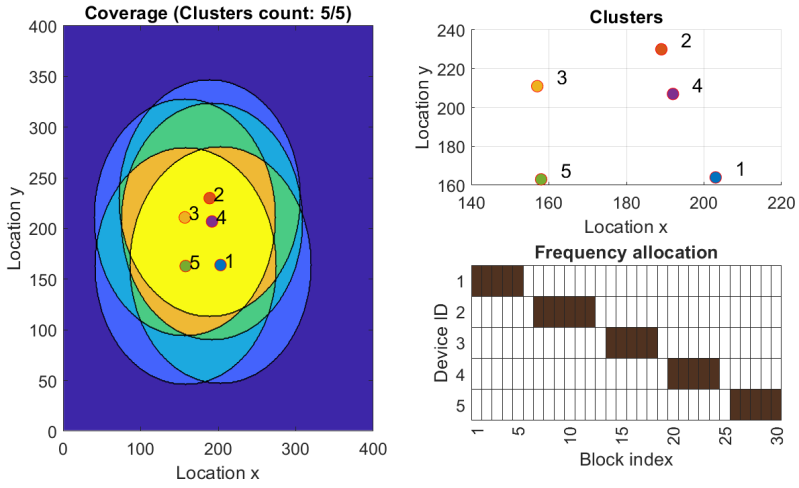

FIGURE 3.21: Clustering algorithm (5 clusters)

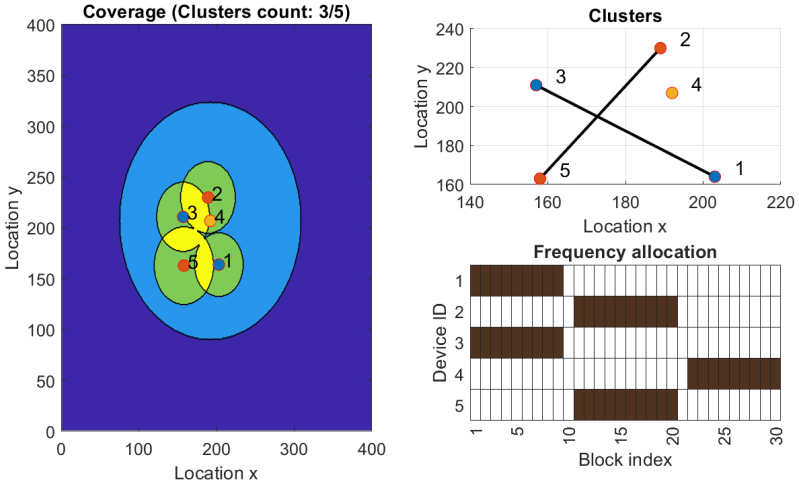

FIGURE 3.22: Clustering algorithm (3 clusters)

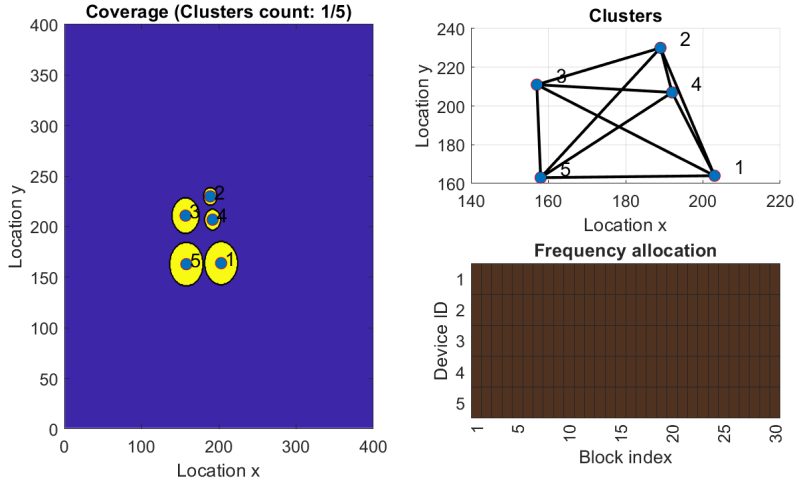

FIGURE 3.23: Clustering algorithm (1 cluster)

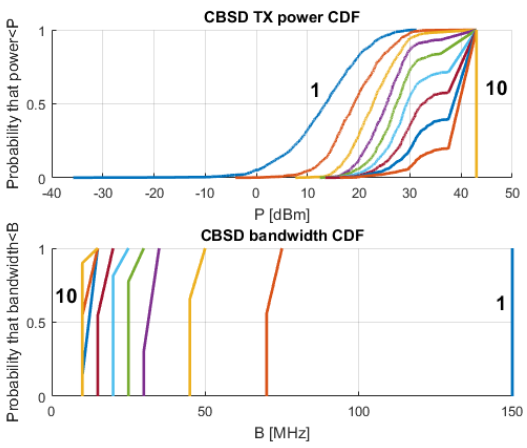

FIGURE 3.24: Transmit power and bandwidth of CBSDs

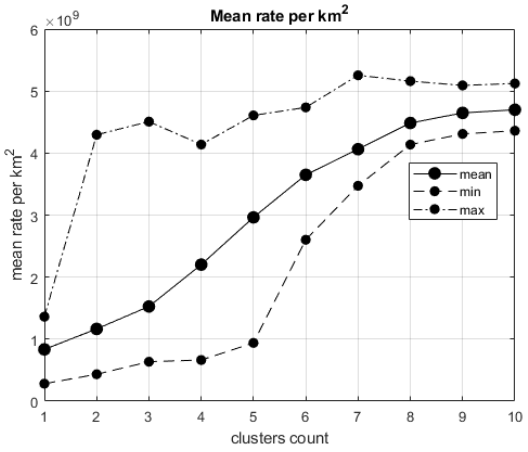

FIGURE 3.25: Bitrate per km^2 of CBSDs

As an example, rate averaged over the whole simulation area and all $N_C = 10$ CBSDs is calculated as defined in (3.24). The minimum, mean and maximal values (over 100 random runs) are plotted in Fig. 3.25. One may observe that the highest rate is achieved for the highest number of clusters. Maximal band partitioning is optimal from the perspective of this metric and uniformly distributed CBSDs. However, for different CBSD distributions, this can change. An analytical derivation of the mean area rate for the case of two base stations utilizing the same or orthogonal frequency bands can be found in Appendix of [92]. The conclusion is that for two CBSDs located close to each other (distance smaller than about $0.7 \cdot 2$ of the maximum cell radius obtained for the maximum allowed power), it is advantageous to use a narrower but orthogonal band. However, for wider distances, it is advantageous to reduce the transmission power but use the whole bandwidth in each CBSD. This can be the case encountered in a real network where base stations are significantly distanced to increase coverage. Overlapping is typically used only for handover purposes.

2) Fig. from 3.26 to 3.28

An example of such a deployment (i.e., the one where it will be beneficial to reduce the transmit power) is shown in Fig. 3.26. All CBSDs can transmit with the maximum power of 16 dBm per 5 MHz resulting in the maximum cell radius of 3.7 km.

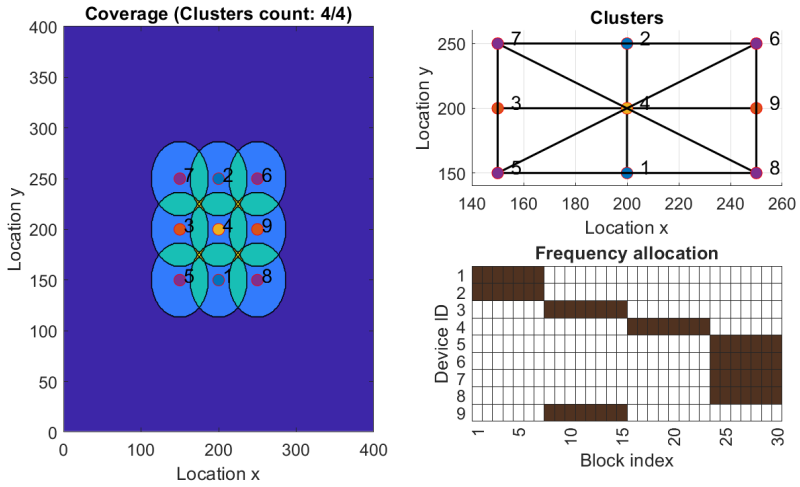

FIGURE 3.26: Clustering algorithm on grid (4 clusters)

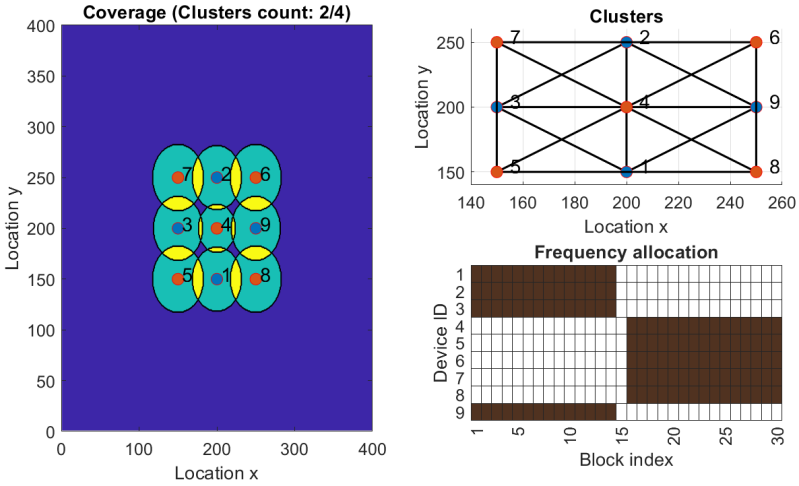

FIGURE 3.27: Clustering algorithm on grid (2 clusters)

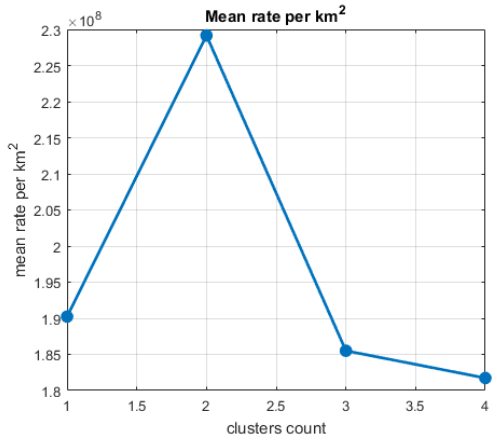

FIGURE 3.28: Bitrate per km^2 for regular grid of $N_C = 9$ CBSDs

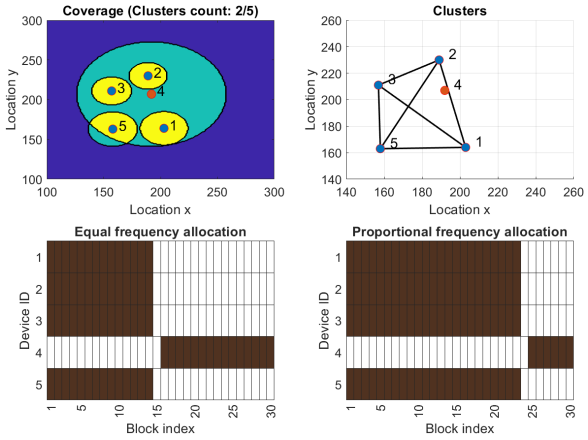

FIGURE 3.29: Comparison proportional and equal assignment

The distance between two closest CBSDs equals 5 km. This is about $0.68 \cdot 2$ of the maximal cell radius, i.e., close to the border value obtained in Appendix to [92]. The grid-like deployment of CBSDs resulted in a densely connected graph, and the chromatic number equals $X = 4$. Fig. 3.26-3.27 show selected results of the graph coloring, cell areas and band distribution for the number of clusters decreasing from 4 to 1, respectively. The mean area rate calculated according to (3.24) is shown in Fig. 3.28. The maximization of this metric is obtained for two clusters of CBSDs.

Finally, let us compare the performance of the Multi-Choice Algorithm when the *traditonal* and *proportional* approach to channel allocation among CBSDs is considered. Let us remind that in the former case, the set of available resources is split equally between CBSDs. In contrast, in the latter case, the amount of frequency resources is directly proportional to the number of CBSDs in each cluster. The comparison of these two approaches is shown in Figs. 3.30-3.31. As could be expected, both algorithms guarantee the same performance for the minimum number of clusters (i.e., all CBSDs are in the same cluster) and for the maximum number (i.e., the number of colors equals the number of CBSDs, $X = N_{ch}$). In all other cases, the mean rate per one squared kilometer is higher for the traditional approach, but the span between the maximum and minimum rate is high. In the proportional case, this span is much narrower, i.e., the distribution is fairer. the corresponding frequency allocation among CBSDs is shown in Fig. 3.29.

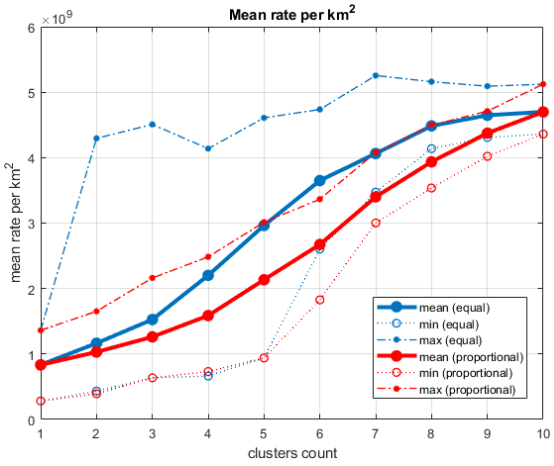

FIGURE 3.30: Bitrate per km^2 (comparison proportional and equal assignment)

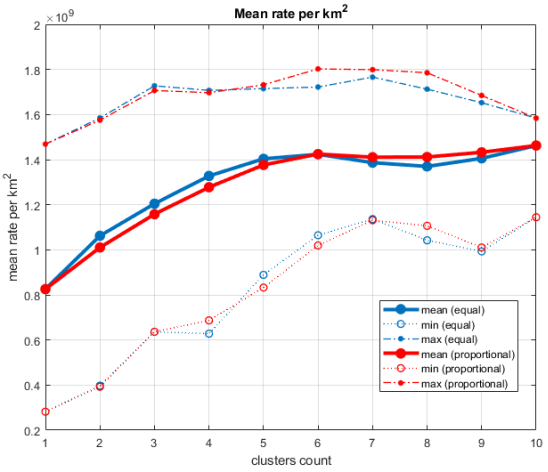

FIGURE 3.31: Bitrate per km^2 for max power 30 dBm (comparison proportional and equal assignment)

Conclusion and summary

In work, we dealt with the efficient allocation of resources (power and frequency) among CBSDs under the control of the coexistence manager. We have compared the performance of the four presented heuristic algorithms with new multi-choice solutions. Based on the achieved results projected onto the available solutions space, we can draw the following conclusions. First, the four heuristic algorithms provide only one, typically suboptimal solution which lays close to the Pareto optimal frontier curve of the solution space. The proposed Multi-Choice Algorithm delivers multiple solutions (all located on the optimal frontier curve), giving the coexistence manager a new degree of freedom in selecting the best solution based on the chosen selection criteria.

A compact summary of the use of contextual information to improve spectral efficiency is presented in Table 3.3 below.

Ph.D. candidate's publications considering problems discussed in this section	[75], [117], [119], [123]
Context information	Position, type, and transmitting parameters of all CBSDs; maximum transmit power from NRA; spectrum occupation; list of already transmitting PAL and GAA users; list of transmission requests from new devices; allowed interference level.
Influence on the system	Clustering of CBSDs; different schemes of spectrum allocation between clusters of CBSDs; different allowed transmit power selection of each cluster of CBSDs.
Impact on spectrum efficiency	Increase of the total throughput in the network when the same bandwidth is used multiple times; maximization of mean bitrate per km^2, therefore maximization of spectrum efficiency over a given unit of area.
Comment	The work proposes an algorithm for the allocation of frequency and power to cells, the aim of which is to maximize the average power density (among cells). As a result of such action and control of the number of clusters created by the algorithm, it is possible to maximize the average bit rate in a given area.

TABLE 3.3: Summary of work presented in chapter 3.3

3.4 Research topic 3: Waveform flexibility in context-aware network

In Sec. 3.2 and 3.1 we discuss the role of CI for generic, DB-supported DSA. In Sec. 3.3 we extend it and propose an algorithm for spectrum sharing in the CBRS-SAS model, which assumes rich CI saved and processed by SAS. Now we discuss the idea of waveform flexibility in future wireless networks utilizing cognitive radio functionality. Mainly, we consider the possibility of adjusting the shape of the waveform based on the information about the surrounding environment stored in a dedicated context-information database. In the proposed approach, the cognitive terminal has an option to select one of four available waveforms to adapt itself in the best way to the constraints delivered by the database. This section presents the key concept of waveform flexibility, the proposed algorithm for waveform selection, and the achieved simulation results. The description of the presented algorithm was also published in the following author's works [124, 125].

3.4.1 Database-supported waveform adaptation

The idea of waveform adaptation

Contemporary wireless communications systems utilize various adaptation procedures while transmitting data. Closed and open loops for power control or application of various Modulation and Coding Scheme (MCS) are the most popular examples. One may, however, consider the case when other signal parameters are adjusted to optimize the utilization of frequency resources. We propose to apply waveform flexibility. Mainly, each cognitive terminal may decide to select one of four available waveforms for data transmission: traditional Orthogonal Frequency-Division Multiplexing (OFDM) signaling or Filter Bank MultiCarrier (FBMC) [126] based schemes, and their non-contiguous version, namely Non-Contiguous Orthogonal Frequency-Division Multiplexing (NC-OFDM) [127] and Non-Contiguous Filter Bank MultiCarrier (NC-FBMC) [128]. As OFDM is characterized by its maturity and is widely applied in many communication schemes, one of its main drawbacks is high Out-Of-Band (OOB) power emission. Contrarily, FBMC signals are said to guarantee very strong attenuation of the OOB, but at the price of higher complexity due to the application of the per-subcarrier filtering. Depending on the situation in the environment (in particular, on the allowable level of interference that can be induced to neighboring systems), the transmitter in the first step can select either choose OFDM or FBMC. Furthermore, if the selection of the contiguous band will not be possible, the non-contiguous versions of these two multicarrier schemes can be applied [129]. In this case, the spectrum of the transmit signal is not contiguous, and it is interwoven with frequency bands occupied by other transmissions. As the system has four transmission options, the decision will be made based on the available information about the environment stored in the dedicated context information database, CI DB.

Interference analysis

Let us assume the presence of incumbent users, which utilize specific frequency resources in a given band B, coexisting with the secondary users wanting to transmit within the same frequency range. The latter have to protect the primary systems; thus, they cannot induce too much interference into their receivers. Nevertheless, some signal quality degradation at the primary link may be acceptable if it is above some defined threshold. At the same time, secondary users have to accept any interference signal originating from the primary transmission. The interference observed between neighboring frequency channels is caused due to the imperfections of the real transmitter (e.g., characteristic of the impulse shaping filter and nonlinearities at the radio front end lead to

OOB emission) and receiver (e.g., non-ideal selectivity of the reception filters). The problem at the transmitter side is controlled by providing (typically in the standards) the definition of the Spectrum Emission Mask (SEM), which specifies the requirements on the minimum transmitted signal attenuation at a given frequency. However, the design of the reception filters at the receiver side (thus, its transmittance) is typically left to manufacturers, and its characteristics (averaged over various designs) can be retrieved by measurements. As an interesting exception, in LTE minimum selectivity of receiver is specified [130]. These two sources of imperfections correspond to two sources of interference observed. SEM will inform us how much power will be introduced to the neighboring channels if the transmitter sends the signal with power P_T. Analogously, the frequency response of the effective reception filters defines the amount of unwanted power intercepted by the receiver from the neighboring bands. These two phenomena are typically described mathematically by the following parameters: ACLR, ACS, and especially ACIR (see equation 3.5) which combines two previous. A description of these parameters can be found in Sec. 3.3.

3.4.2 Proposed algorithm for database-oriented waveform adaptation

The entire algorithm is split conceptually into two phases. The first one is related to the definition of the maximum allowable interference power that may be induced to a given licensed system and will be realized in the database. The second one aims at the decision-making process on band, power, and waveform selection. We consider a frequency band B split equally into N non-overlapping channels of bandwidth B_n.

Calculation of the maximum transmit power

In the design of the algorithm, we take into account the following assumptions. First, we consider that any of the existing transmissions may accept some additional distortions (due to the aggregated interference originating from various sources) as long as its minimum required signal-to-interference-plus-noise ratio for n-th licensed system, $\mathrm{SINR}_{\mathrm{min},n}$, is not violated. Knowing the noise level and the wanted signal received power, one may calculate the current SINR, and then - the amount of power (interference) that can be induced ΔP_n in any prospective location of a given primary system receiver (we assume unknown licensed system RX location; if the RX location is known the protection is required only in a single point of the map.). Knowing this value (one can understand it as interference margin), as well as assuming given SINR value (the result of band and waveform selection for a licensed system of given reception performance, as explained later), one may calculate what could be the maximum transmit power (for a given location of the transmitter in space and transmission in frequency) which will not exceed the limit ΔP_n. In order to compute this value, the exact location of the transmitter and the victim receiver has to be known (or at least the distance d between them), as well as some assumptions regarding the path-loss value L_d between these two devices have to be made. As the position of the transmitter is easy to obtain, the receiver's position is typically unknown; thus, the procedure described below has to be repeated for each possible location of the receiver to be protected. Minimum transmit power, i.e., assuming worst-case victim receiver location, is utilized out of all prospective victim receiver locations.

1. in the first step, the noise power σ_n^2 at n-th victim system receiver and each location (where the receiver to be protected can be deployed) has to be defined. It may be done through calculation (where only thermal noise will be included, i.e., $\sigma_n^2 = kTB_n$, where T is the temperature in Kelvins, and k is the Boltzmann constant equal to $1.23 \cdot 10^{-23}\frac{\mathrm{J}}{\mathrm{K}}$) or through measurements. In the latter case, the power of the entire noise (including ambient inter-

ference) observed at a given location will be measured. These values may be stored in the database

2. for each potential point of the victim receiver location, the database stores power of the observed wanted signal, i.e., P_{Rn}, and in consequence, the current SINR value (as a result of division with noise/interference floor available as described in the previous step). This, in turn, allows for calculation of the interference margin for n-th licensed system receiver as follows: $\Delta P_n = P_{R,n} - \mathrm{SINR}_{\min,n} \cdot \sigma_n^2$. When the value of ΔP_n is below zero, it suggests that the quality of the received licensed signal is unacceptable even without secondary transmission; thus, theoretically, there are no restrictions on the interference. The measurements may be done either in the dedicated measurements campaigns (applicable for broadcasting systems that are stable and unchanged for a long time period) or can be done permanently by the densely deployed sensing modules

3. assuming that the transmit power of the k-th cognitive user is denoted by $P_{TX,k}$, the interference power induced to n-th licensed system receiver can be defined by the following formula $I_{\mathrm{ACIR},n,k} = P_{TX,k} L_d^{-1} \mathrm{ACIR}(k,n)^{-1}$, where $\mathrm{ACIR}(k,n)$ comes from the SEM function and receiver effective filter characteristics. Maximum allowed transmit power can be calculated using following formula $P_{TX,k} \leq \Delta P_n L_d \mathrm{ACIR}(k,n)$. The calculated value is correct only for the distance d. Thus this step has to be repeated for each possible location of the receiver to be protected. Once this loop is done, the final allowable transmit power is the minimum of these values

4. once the final maximum allowable power is calculated, the values of the interference margin have to be updated. This can be easily done by updating the observed equivalent noise power (we treat interference as noise), $\hat{\sigma}_n^2 = \sigma_n^2 + I_{\mathrm{ACIR},n,k}$ for each location on the map

Based on the CR location, CI DB can calculate the most harmfully interfered with licensed system receiver location. These results in value $\Delta P_n L_d$ and licensed system reception filter characteristics sent to the CR. The CR can adjust ACIR value (by proper waveform selection) and transmission power as long as $P_{TX,k} \leq \Delta P_n L_d \mathrm{ACIR}(k,n)$ is met.

ACIR calculation

Knowing the effective reception filter characteristic, it is possible to calculate effective interference caused by every single subcarrier both in OFDM and FBMC systems as shown in [129]. Most importantly, the interference coupling (after normalization equal to ACIR) can be calculated for each subcarrier independently and added to the set of active subcarriers. In the case of contiguous band allocation ACIR is calculated for each possible "starting" subcarrier (for known required bandwidth, the last subcarrier can be easily found). The allocation maximizing ACIR is chosen. In the case of non-contiguous allocation, the subcarriers are sorted according to their impact on interference power. The required number of subcarriers (to obtain the needed bandwidth) is chosen, starting with those with the smallest interference coupling. While this scheme can result in high fragmentation of allocated spectrum, the obtained ACIR value is greater or equal to the optimal value assuming contiguous allocation.

Band and waveform selection process

In Fig. 3.32 a simplified block diagram of waveform selection algorithm is shown. As we assumed a transmit power and bandwidth as parameters of cognitive device request. It means that if, for the specified bandwidth, the required power can be met by OFDM for a given device position, then the cognitive device selects this type of transmission. Suppose the calculated power value is too small. In that case, the cognitive device considers a FBMC transmission, which typically allows for higher power usage (as a result of reduced OOB radiation). If power for FBMC transmission is still too small, cognitive device checks the possibility of NC-OFDM selection, and later - of NC-FBMC.

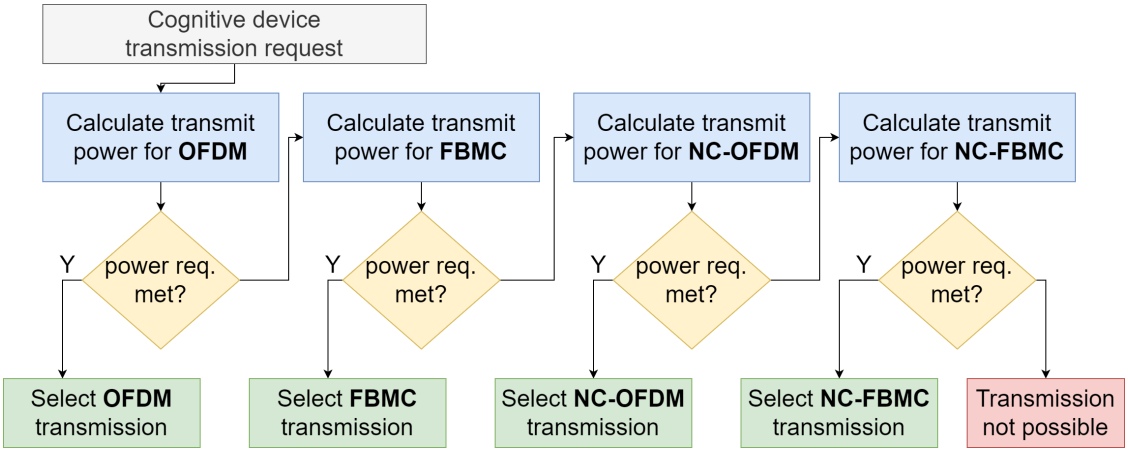

FIGURE 3.32: Simplified block diagram of waveform selection algorithm

3.4.3 Simulation results

Simulation setup

Our simulation is focused on TVWS and is performed over a square area of size 100 m, split further into smaller squares with a grid of 10 cm. As a simulation scenario, we consider the L-shaped building with a known coverage map of DVB-T received power, as discussed in Sec. 2.4. Analyzed digital television power comes from measurements placed on the ground floor and outdoor of the building. Based on measurements, we set up the noise level to -97.877 dBm (it is an averaged value of measured received power in empty 8 MHz DVB-T channel, marked as B_{DVBT}). Please note that the thermal noise in room temperature for 8 MHz bandwidth equals -104.969 dBm, so we assume that noise figure NF of DVB-T receiver is around 7 dB. Base bandwidth unit (channel size) B_{ch} is set up as 1 MHz.

The detailed coverage map of DVB-T signal power comes from kriging interpolation of real measurements done around Poznan University of Technology (PUT) building, as shown in Sec. 2.4. We assume minimal SNR required to proper digital television reception SNR_{req} is equal 15 dB. In our simulation, we considered path loss model proposed for TVWS indoor solutions based on measurements in the same building (presented in [131]). It is defined by the following formula $PL = 34.88\log(d) - 28 + 20\log(f_c)$ in dB, where d is a distance in meters, and f_c is a carrier frequency expressed in MHz. Moreover, we assumed minimum distance between cognitive radio transmitter and DVB-T receiver of 2 meters as in [132]. In our simulation we considered four adjacent DVB-T channels, mainly the considered frequency range is $\langle 502; 534\rangle$ MHz, where band occupied by DVB-T system is around central frequency of 522 MHz.

Frequency allocation

In our investigation, we considered three cases: in the first one, we assume that a cognitive device (located at the arbitrarily selected point of coordinates $(215, 590)$ on the 10 cm grid mentioned above) sends a request for a small amount of bandwidth of 2 MHz. In that way, only OFDM and FBMC transmission is considered. For the non-contiguous schemes, the same bands as in contiguous schemes are optimal. Applying the algorithms defined in Sec. 3.4.2, the allowable transmit power in the whole bandwidth of 2 MHz for OFDM and FBMC schemes equals -1.7465 dBm and 22.7118 dBm, respectively. The second scenario assumes that the cognitive device wants to occupy a contiguous band of 16 MHz. With OFDM transmission device can set up transmission power to -7.7549 dBm while with FBMC to 6.4470 dBm. The third scenario assumes that the cognitive device wants to use 18 MHz of bandwidth. This amount of spectrum can be assigned with OFDM and FBMC transmission with very small power (-34.4422 dBm in both cases) and we need to consider usage of NC-OFDM or NC-FBMC. In consequence, the device can transmit with power -3.7293 dBm using NC-OFDM or with 9.3460 dBm using NC-FBMC. Corresponding frequency allocation is shown in Fig. 3.33.

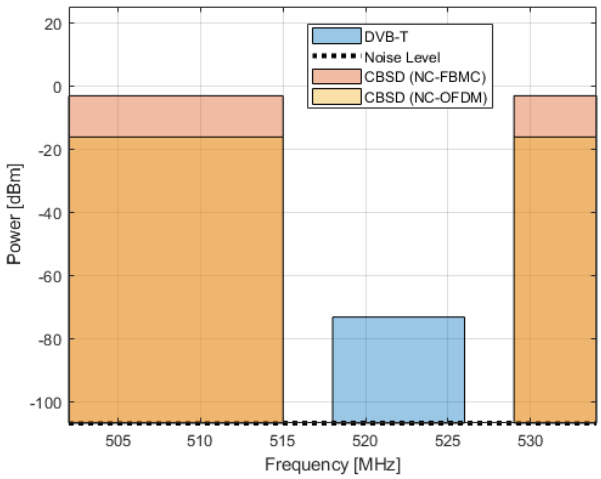

FIGURE 3.33: Transmit power and spectrum allocation in the third scenario (power in dBm/1 MHz)

Waveform selection

Let us now analyze the waveform selection algorithm, as discussed in Sec. 3.4.2. Our analysis set the minimum required to transmit power to 5 dBm in our analysis. In Fig. 3.34, on the left side, we show the map of the allowed transmission type for every possible position inside the building when the cognitive device requires 2 MHz bandwidth. We can see that in almost every position, we need to use FBMC transmission because OFDM allows for too small power. The power constraint is fulfilled in only 1.592% of locations in addition to non-continuous modes of transmission are not needed here (when FBMC is sufficient). Allowed transmission mode for widest bandwidth request of 18 MHz is shown on the right side of Fig. 3.34. Here we can find that in almost every position TVWS device needs to use NC-FBMC transmission, and only in few places it can use NC-OFDM. In Fig. 3.35 map of allowed transmit power for FBMC transmission is shown. It varies within the building from about 16 to 36 dBm.

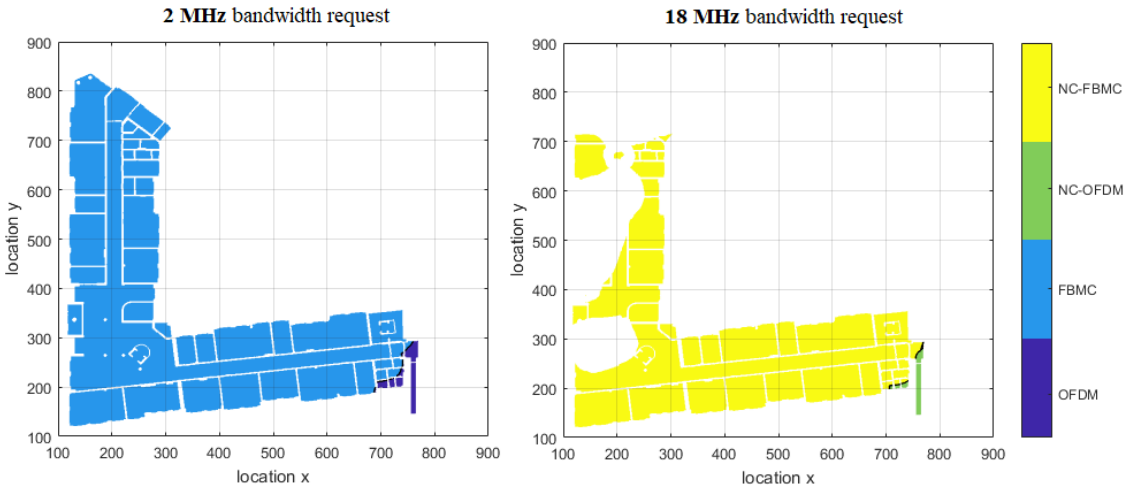

FIGURE 3.34: Allowed transmission mode for 2 and 18 MHz bandwidth request

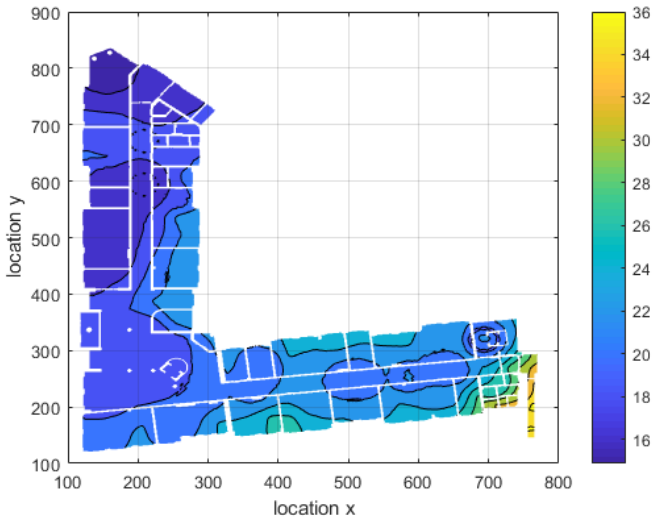

FIGURE 3.35: Allowed transmission power [dBm] for 2 MHz bandwidth FBMC request

Conclusion and summary

We have proposed the application of waveform flexibility, where the cognitive user may adaptively select the best waveform. The selection process is performed at the terminal side based on the information retrieved from the dedicated context information database. Our simulation results showed that such an approach allows for selecting such waveform that optimizes given criteria. This promising achievement leads the way toward more advanced schemes. The waveform selection procedure will consider other degrees of freedom (e.g., adaptation of the pulse shape in the multicarrier scheme).

A compact summary of the use of contextual information to improve spectral efficiency is presented in Table 3.4 below.

Ph.D. candidate's publications considering problems discussed in this section	[124], [125]
Context information	Received power from DVB-T transmitters; waveform capabilities, transmission, and reception parameters of cognitive devices; transmission requirements of cognitive devices; list of already transmitting devices; maximum interference level which can be introduced to TV band.
Influence on the system	Waveform, bandwidth, channel, and transmit power selection for each cognitive device, that requests transmission opportunity.
Impact on spectrum efficiency	Increasing the number of users which simultaneously utilize the same spectrum
Comment	The waveform selection algorithm allows you to select the appropriate modulation for individual users, which makes it possible to increase the number of users using a given part of the band (the possibility of reducing the protection bands between users).

Table 3.4: Summary of work presented in chapter 3.4

Chapter 4

Practical approach to context information utilization in DSA systems

In chapter 3 we intentionally omitted challenges and requirements defined by the existing networks and standards. Now we describe a DSA system that was designed, implemented, and verified in the field tests in the area of a real network of licensed users that should be protected. Moreover, modifying the scheduler's decisions and user association mechanism improved spectrum efficiency in the LTE and LTE-A networks, respectively.

As we initially verified the possibility of CI utilization in DSA systems, to which chapter 3 is devoted, we investigate this topic further by applying DSA to the network which already exists or has some strict requirements. This chapter is split into three research topics. In the first research topic, described in Sec. 4.1 we propose CBRS-based system that allows unlicensed user GAA, represented by a programmable radio, i.e. USRP, access to the spectrum. The proposed system was tested in field tests, where the car, together with an unlicensed user, tried to gain access to the spectrum in the area where protected primary network devices (WiMAX) were present. In the second research topic, described in Sec. 4.2, we simulate an indoor and outdoor network where the spectrum was shared between indoor and outdoor users. Using contextual information about user locations and allocation history made it possible to optimize the method of allocating spectrum resources, by modification of scheduler's decisions. In this approach, the main challenge was the adopted transmission standard (i.e., LTE network) and, therefore, the necessity to use resource blocks (RB). In the third research topic, described in Sec. 4.18, we propose an algorithm for the users to cells assignment, which increases system throughput. The most challenging factor was the application of the LTE-A standard, where only by influencing the CRE parameter was it possible to change the methods of assigning users.

4.1 Research topic 1: Experiment of CBRS-based system utilization - field trials

Within the first research topic, the primary aim was to confirm that the concept of dynamic spectrum access (using contextual information) can be practically applied in an existing network. For this purpose, field tests were carried out using real and operating radio infrastructure, which was the main challenge of the planned spectrum access system. In this thesis, we show the results of advanced field trials carried out near Poznan in Poland, which prove the applicability of CBRS-like databases and protocols for advanced spectrum sharing in real-world scenarios. It is worth highlighting that the extensive experiments have been conducted with fully operational, working commercial wireless networks, where all important performance metrics have been permanently monitored for their correctness. The tests were conducted in rural areas. The ultimate goal was to deliver customized services (e.g., multimedia services) at the 3.6 GHz band to the countryside users utilizing the spectrum band licensed (and used) for other services. The successful experiment showed the expected benefits of flexible spectrum usage in 5G networks and beyond, but it also emphasized the challenges that still require attention. It is worth mentioning that this work, being a continuation of the initial tests discussed in [106], presents the final results of the full experiment with improved spectrum sharing algorithms. These have been presented in Ph.D. candidate original publications [133, 134].

4.1.1 Considered spectrum sharing scheme

The ultimate goal of the conducted field trials was to verify in practice the reliability and performance of the application of dedicated remote databases for flexible spectrum management. In particular, our target was to carry out an experiment where three networks of completely different types operate in the same geographical area utilizing the same resources (in both time and frequency domains) with various privileges. Mainly, we consider the licensed multicarrier (i.e., OFDM-based) network for wide-band Internet delivery, point-to-point MicroWave (MW) link for high-rate communication and nomadic Small-Cell (SC) network for delivering customized services. Such a selection is important from the perspective of 5G wireless networks and beyond, as it illustrates the convergence of various types of networks and, at the same time, presents the possibility of the coexistence of various operators (service deliveries). By assumption, the frequency operation of all considered networks is controlled by the dedicated spectrum management tool, guaranteeing that the required quality-of-service metrics for these systems are satisfied. In our experiment, we have implemented CBRS-based solution for vertical spectrum sharing, where the network operator owning the license for wireless data transmission shares its band (dynamically) among two primary services and also allows that this already shared spectrum may be elastically utilized by the GAA-like users. As the assumption for the field trials was to verify the performance of the flexible spectrum sharing in practical scenario, we decided to apply the chosen CBRS-based spectrum sharing scheme to adjust it to the existing, commercially deployed networks and to conduct the test during the typical day when the network is utilized *as every day* by the end-users. This, in turn, allows us to monitor the impact of the proposed CBRS-based, flexible spectrum management scheme on the overall network performance.

Scenario setup

The whole experiment was conducted near Poznań, Poland, where the network operator INEA is granted the license to deliver Internet services in the 3.6 - 3.8 GHz band (which is close to the

frequency bands considered for 5G, also in terms of typical path-loss values), and agreed to test the dynamic spectrum management scheme in their business networks. INEA has delivered its services in the Greater Poland area in Poland via WiMAX network since 2010. So far, it has provided fast and affordable connectivity for Internet and telephony services to almost 6000 households across the 30,000 km^2 regions. As the deployed WiMAX network is now at its technological end, INEA sees real benefits in more effective utilization of its spectrum. Although INEA does not provide LTE-A access to the users, we can treat WiMAX signal as the representative of OFDM-based network. Fortunately, from the system-level perspective, the technological details of chosen OFDM-based system is not that important, as we will concentrate more on high-level interference analysis between coexisting systems; as a result, dynamic spectrum sharing. The second business network considered in the experiment is the point-to-point MW link located within a close coverage area of the WiMAX base station. This connection is also based on OFDM technology, and it benefits from the high directivity of transmitting and receiving antennas. These facts have been considered in the spectrum management system. Finally, the GAA tier of users in the experiment has been realized by means of nomadic deployment of SC broadcasting video stream over in the local area (maximum radius depends, of course, on the agreed maximum transmit power for certain location). Both, GAA transmitter and receivers have been implemented utilizing the USRP N210 boards. Fig. 4.1 shows the considered scenario for experimentation. One may observe the presence of the WiMAX Base Station (BS) with the connected Customer-Premises Equipment (CPE), as well as the MW link and the exemplary location of the GAA system (i.e., the GAA transmitters and receivers).

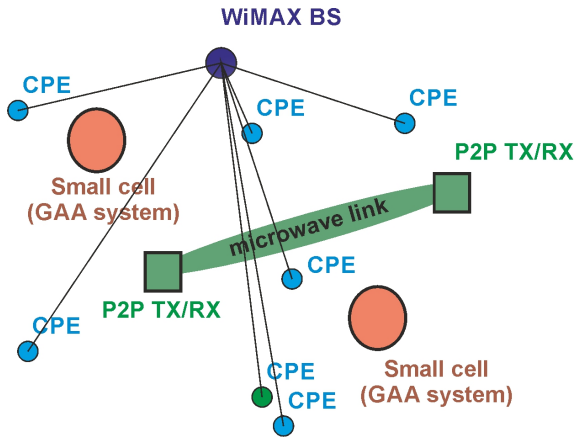

FIGURE 4.1: Network schema in considered experiment scenario

Supporting databases

For the spectrum management purposes we have selected and modified the CBRS-model, where the remote database is used for coordination of the three systems under control. The database itself has been delivered for the experiment by the Fairspectrum company located in Finland. The entire communications and message exchange between the database and the two legacy (WiMAX and MW link) networks have been realized via Simple Network Management Protocol (SNMP), where all the steering and control instructions are sent via Management Information Base (MIB) messages by addressing appropriate Object IDentifier (OID). At the same time GAA system communicates with the database by application of the modified CBRS protocol. In particular, as illustrated in Fig. 4.2, the SNMP client implemented within the database domain, talks to the WiMAX and MW link Network Managements systems through a Virtual Private Network (VPN) client.

It stores the status data in Structured Query Language (SQL) Database (DB). Clocked Control uses SNMP client to change the center frequency and channel bandwidth of WiMAX and MW devices based on the daytime. Next, the SAS server - also implemented at the database side - reads protocol information from SQL DB and stores protocol information there. The following commands, standardized in the CBRS protocol [135], are used here -*Register* (for registering new users), *Spectrum Inquiry* (for inquiring about the available spectrum resources), *Grant* (for granting the GAA transmitter the usage of requested spectrum band), and *Heartbeat* requests (for periodic update of the GAA transmitter state). These commands invoke DB Engine, which in turn queries the measurement data from WiMAX and MW links with SNMP client. In the considered setup WiMAX reports Carrier-to-Interference-and-Noise Ratio (CINR) in both downlink and uplink, whereas for the MW link, estimated potential throughput is reported. It is worth mentioning that the two processes, i.e., communication with MW and WiMAX, and communication with SC are realized simultaneously.

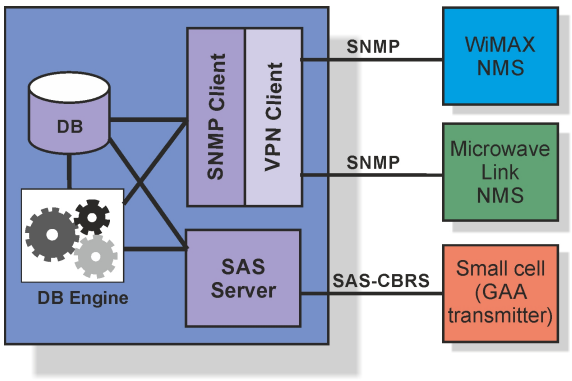

FIGURE 4.2: Diagram of interfaces in the analyzed system

Applied spectrum management algorithm

The details of the implemented algorithm for dynamic spectrum management have been described in [106]. They are now concisely summarized, and the improvements are presented (mainly the database system's ability to learn and adjust decisions based on learned data). In order to start transmission, the SC device sends the registration request, and once accepted, it sends spectrum inquiries asking for allowable transmit opportunities, i.e., maximum transmit power for preferred frequency bands. We have applied the joint open- and closed-loop algorithm for power control in our approach. If the returned parameters satisfy the SC needs, it sends the grant request for selected spectrum resources, which, once granted, can be used for data transmission by the SC network. We call this scheme an open-loop for power control by the SC systems. SAS server is permanently monitoring the performance of all networks under control and informs (through the heartbeat message) if the SC device has to modify its transmit parameters. Moreover, the above process, on the one hand, guarantees the protection of the legacy systems; on the other - it allows for optimization (boost) of the SC systems performance. It is realized by the application of the iterative procedure, where - assuming that the heartbeat message is positive - the GAA device sends the request to the database subsystem asking for agreement on increased transmit power. In our trial, we assumed that the SC device might request for additional 3 dB of transmit power in each iteration. This option is a closed-loop power control scheme. In the initial field tests ([106]) free space loss propagation model has been applied for the calculation of the initial limitations on the transmit power sent to the SC devices as the reply to the grant request message.

As the Free Space model was too restrictive (it does not consider the presence of buildings and other scatterers), in the current experiment, we have assumed Hata propagation models for these calculations, which appeared to be much closer to realistic scenarios [136]. However, the application of the propagation model and the usage of the calculated values of the transmit power have to be verified in practice for each location of the SC (i.e., from where the grant request is being sent). The initial computed values, being some approximation, have to be verified for correctness in terms of induced interference to all affected CPEs (higher tier devices) in the vicinity. It may happen that the computed initial values will be too restrictive, and the GAA may transmit with a higher power, and vice-versa - the initial value may be too high and have to be reduced. In both cases, it will be efficient to store the real values of the allowed maximum transmit power in the database subsystem and use it as the initial value in case of future requests and inquiries (for calibration of the applied propagation model). We have applied this approach in our algorithm. The final maximum transmits power is stored in the repository for each measurement point. When the next spectrum request appears in the close vicinity of that point, the database replies with the saved value. The applied solution is presented in the form of a pseudo-code in Algorithm 4.1.

Algorithm 4.1: Applied algorithm for *i*-th SC

```
   Data: SC, MW, WiMAX setup (location, transmit power)
 1 while i-th SC wants to transmit data do
 2     SC sends spectrum inquiry message;
 3     if No entry in the database for SC location then
 4         Database informs about the calculated initial transmit power based on Hata model;
 5     else
 6         Database informs about the stored value of the maximum transmit power;
 7     end
 8     if There is positive reply to Spectrum Inquiry message then
 9         SC sends Grant message for one selected frequency band from all defined in the
             response to Spectrum Inquiry;
10         if No entry in the database for SC location then
11             Database responses with initial transmit power based on Hata model;
12         else
13             Database responses with stored value for the maximum transmit power;
14         end
15         if There is positive reply to Grant message then
16             SC starts transmission with received setup; while i-th SC is transmitting do
17                 if i-th SC causes too much interference then
18                     SC is forced to reduce transmit power to last acceptable value, or to stop
                         transmission;
19                 else
20                     Database stores the value of the maximum, safe transmit power for
                         given location;
21                     SC may send Grant Request message for higher transmit power;
22                 end
23             end
24         else
25             SC may either try to again ask for certain frequency sending new grant
                 message, OR it can move to another frequency band defined in the response to
                 the Spectrum Inquiry OR it may restart the procedure;
26         end
27     end
28 end
```

4.1.2 Experiment results

Field tests have been conducted in two locations in the countryside close to Kórnik in the west part of Poland, shown in Figs. 4.3 and 4.4. Two legacy commercial networks involved in the experiment have been set up. The 802.16e-2005 WiMAX base station by Cambium Networks PMP320, where the spectral efficiency of each connect CPE changes in time as function of dynamically selected modulation, Forward Error Correction (FEC) coding and MIMO mode. It worked in 2x2 MIMO mode on a center frequency set to 3.664 GHz with 10 MHz channel bandwidth and with the transmit power of the base station within the range from -40 to 27.5 dBm. The directional antennas had 16 dBi gain. During the simulations, only control data have been transmitted. The MW link by RADWIN operated at 3.674 GHz center frequency and occupied 10 MHz bandwidth. The applied antennas had 19.5 dBi gain and allowed for 2x2 MIMO transmission. The center frequencies and the bandwidths of these two networks may be modified, as we previously proved in [106]. However, in our field trial, we focused on the inter-tier spectrum management and GAA layer; thus, we kept them fixed. The measurements have been conducted through dedicated hardware, mainly the SC was implemented on the Ubuntu-powered laptop with the GNU Radio running on it. The negotiations with the database subsystem through the dedicated control channel have been realized by using a cellular network. The SC transmitter and the SC receiver have been realized similarly, i.e., two laptops with Ubuntu system have been connected to N210 USRP boards with SBX daughterboard, covering 3.6 GHz band. The field trials have been realized using the INEA car, where we have mounted the above SC transceivers. One of the measurement points is shown in Fig. 4.5. Moreover, during the whole experiment, the performance metrics (i.e., uplink and downlink SINR, in the protected devices, levels of modulation and coding schemes, etc.) have been permanently monitored in real-time through a dedicated web-based interface. All measurements have been realized at a carrier frequency of 3.7675 GHz, i.e., the worst case was selected as we consider the same frequency as the frequency assigned to the nearby WiMAX sector.

Field trials in the first area

In the first area, we have collected 18 measurements in the locations depicted on the map in Fig. 4.3 as blue pins. In each location, we have first identified the closest CPEs that have to be protected and which may be affected by the particular SC if it starts transmission. The locations of three identified CPEs are shown by orange markers. Next, for each measurement point, we have applied the algorithm provided in Algorithm 4.1 to identify the maximum allowable transmit power for a given location. Once this value is found, we store it in the database subsystem. When there is a *Grant Request* message sent in the future from that location, the system will not use the Hata propagation model for initial rough approximation but will read the stored values.

The measurement results for each point in the first location have been summarized in the upper part of Table 4.1. In the first column, the distances $d_{i,j}$ to the closest CPE has been shown, which has been calculated based on the geographical coordinates of the j-th CPE $(\theta_j^{\mathrm{CPE}}, \varphi_j^{\mathrm{CPE}})$ and i-th measurement point $(\theta_i^{\mathrm{MP}}, \varphi_i^{\mathrm{MP}})$, where (θ, φ) denote the latitude and longitude in radians. The so-called Spherical Law of Cosines have been applied here with Earth radius set to $R_E = 6371$ km as defined below:

$$d_{i,j} = \arccos\left(\sin\theta_j^{\mathrm{CPE}} \cdot \sin\theta_i^{\mathrm{MP}} + \cos\theta_j^{\mathrm{CPE}} \cdot \cos\theta_i^{\mathrm{MP}} \cdot \cos\left(\varphi_j^{\mathrm{CPE}} - \varphi_i^{\mathrm{MP}}\right)\right) \cdot R_E. \tag{4.1}$$

Although in the table we show only the distance to the closest CPE, the database subsystem takes into consideration all CPEs that may be affected by new signal transmission.

FIGURE 4.3: First area of field trials — map of measurement points

FIGURE 4.4: Second area of field trials — map of measurement points

FIGURE 4.5: Field trials — exemplary measurement point at the countryside

The initial values of the maximum acceptable transmit power P_{TX} have been computed by the database subsystem based on the Hata propagation model and are shown in the third column. These values initialized Algorithm 4.1 to find the final value of the allowed transmit power, $\tilde{P}_{TX}$, which is then stored in the repository of the database subsystem. The fourth column shows the achieved values of the maximum transmit power based on online WiMAX and MW quality-of-service reports. In most cases, one may observe that the initial values achieved based on the Hata propagation model were more restrictive compared to the final allowable values. However, in some places, the situation was the opposite. The conclusion from this experiment may be the following: although the actual values of the allowed transmitting power have to be verified and possibly stored in the database subsystem, the application of the Hata propagation model, in most cases, *speeds up* the algorithm, and is a safe approximation of the final value. Finally, our goal was to create a detailed map indicating the maximum allowable power in each prospective point of the considered area. For that purpose, we have interpolated the measured values between measurement locations. We have followed the natural interpolation method based on Delaunay triangulation. Before interpolation, all measured values have been transformed from logarithmic to a linear scale. Achieved results are shown in Fig. 4.6. Such a map may be further used for a better approximation of the allowed maximum transmit power instead of applying the Hata propagation model.

Field trials in the second area

As the goal of the first experiment was to create a detailed map with the values of maximum transmit power, in the second field trial, we intended to deliver wireless services by the real deployment of SC in the rural area. Five measurement points have been selected for evaluating the environmental context (see Fig. 4.4). Achieved values of the maximum transmit power have been presented in the second part of Tab. 4.1. One may observe that due to the relatively short distance to the two closest CPEs, the calculated and measured values of the maximum transmit power are rather low. Regardless of this fact, we have selected the last location for deployment of the SC transmitter, which shall deliver wireless services to the SC users in its close vicinity (around 100 m as in classical WLAN access points). This particular location was selected intentionally, as it was close to the countryside bus stop and close to a small shop with small car parking (see Fig. 4.7). Thus, the SC transmitter could act as a local, high-rate wireless service provider.

TABLE 4.1: Measurement results — in both locations

Point no.	**Distance [m]**[a]	P_{TX} **[dBm]**[b]	$\tilde{P}_{TX}$ **[dBm]**[c]
Location 1			
1	133	- 11	$(>) -\infty$
2	256	22.1	$(=)22.1$
3	60	-10.62	$(>) -\infty$
4	180	6.12	$(<)$ 22.1
5	182		22.1
6	186	9.52	$(<)$ 22.1
7	94	-3.6	$(<)$ 22.1
8	48	$-\infty$	$(=) -\infty$
9	53	-6.46	$(<)$ 4.1
10	178	6.96	$(>)$ -4.9
11	253	9.67	$(<)$ 10.1
12	134	3.8	$(<)$ 7.1
13	159	6.77	$(<)$ 22.1
14	106	0.75	$(<)$ 22.1
15	301	11.05	$(<)$ 22.1
16	182	10.15	$(<)$ 22.1
17	121	2.22	$(<)$ 16.1
18	161	6.09	$(>)$ -1.9
Location 2			
19	261, 316	15.05	$(>)$ -10.9
20	151, 265	6.97	$(<)$ 10.1
21	161, 306	7.27	$(>) -\infty$
22	177, 320	8.25	$(>)$ -4.9
23	108, 239	1.08	$(>)$ -3.9

Green color represents the situation where $\tilde{P}_{TX} > P_{TX}$
and red when $\tilde{P}_{TX} < P_{TX}$
[a]Distance to the closest affected CPE
[b]Calculated maximum transmit power based on propagation model
[c] Calculated maximum transmit power based on real-measurements - stored in REM

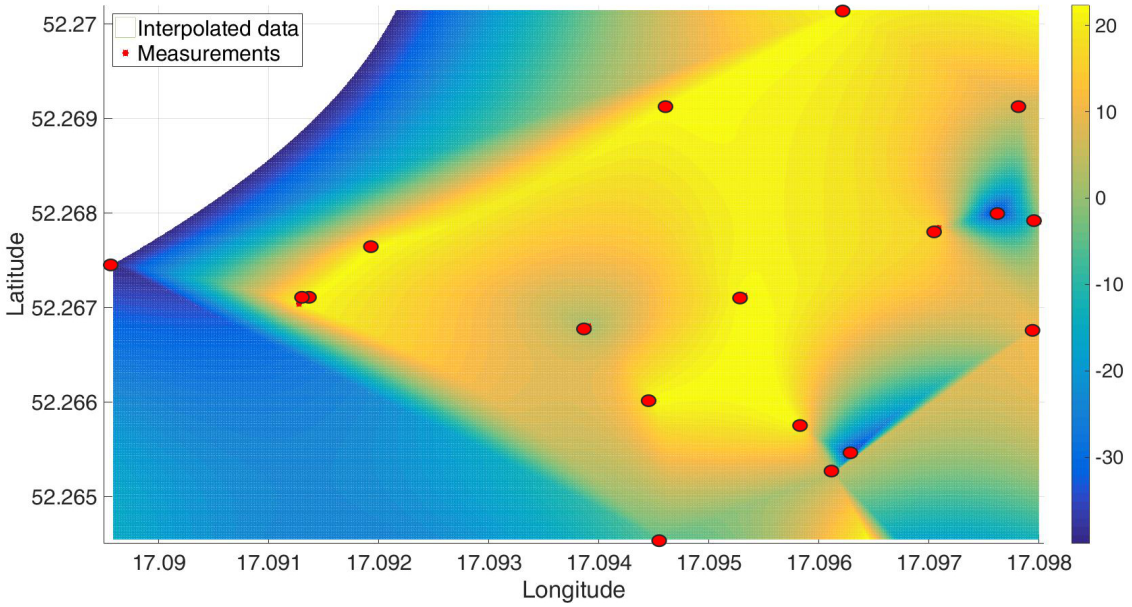

FIGURE 4.6: Maximum allowed transmit power in dBm — interpolation result

After the application of Algorithm 4.1, the maximum transmit power was identified, and the SC transmitter started streaming the video. The SC receiver was realized by means of laptop with Uninterruptible Power Supply (UPS)-powered USRP N210 board. The transceiver was located in the INEA car, distant by some tens of meters from the receiver (Fig. 4.8). It was possible to transmit and receive the video signal during the experiment.

FIGURE 4.7: Photograph of SC receiver location at the countryside bus-stop

FIGURE 4.8: Photograph of SC transmitter inside the INEA car

Conclusions and summary

In our experiment, the remote database was implemented to monitor the performance of all considered wireless networks, mainly two commercial networks and the small-cell-based, nomadic network. The database was also used for dynamic spectrum management. In the first step, we have created and verified how this database can be utilized for spectrum sharing. It was proved that the considered propagation model was too restrictive in most cases. In reality, higher transmit power can be used. Once the database is filled with the values of maximum transmit power, it can be used in the future for faster spectrum management. However, the transmit power has to be properly adjusted in case of any performance disturbance. For this purpose, permanent monitoring and closed-loop power control have been applied. Next, besides filling up the database, we have

deployed the SC transmitter and started streaming video locally. The transmission was successful. However, the coverage area was limited by the allowed maximum transmit power. Overall, we think that the field tests carried out in a real scenario with commercial networks proved the expected benefits of flexible spectrum usage. Mainly, the new SC network can be dynamically deployed, increasing the overall spectrum usage.

A compact summary of the use of contextual information to improve spectral efficiency is presented in Table 4.2 below.

Ph.D. candidate's publications considering problems discussed in this section	[133], [134]
Context information	QoS reports, location of CPE; location, and current transmit power of SC; location, and maximum transmit power based on propagation model and measurements for each analysed location.
Influence on the system	Decision to allow access to spectrum to unlicensed users (SC); additional users that uses the same spectrum; interference cased by SCs and observed by CPEs.
Impact on spectrum efficiency	Increasing the number of users which simultaneously utilize the same spectrum; marginal interference introduced to CPEs causes a little bitrate reduction, which in terms of spectrum efficiency is much smaller than improvement due to new SC deployment.
Comment	As a result of field tests, it was possible to design and test a spectrum access system. Thanks to the observation of the quality of service for primary users (in real time), the system allowed access to the spectrum for the new user (unlicensed) in most test sites, thus ensuring protection against interference for the primary user.

Table 4.2: Summary of work presented in chapter 4.1

4.2 Research topic 2: RSM in wireless network simulator

In the second practical research topic, we assumed that the main challenge is to adopt telecommunications system by using the radio resource blocks allocated to users as specified in the LTE standard. The results discussed has been published in the following author's papers [117,137,138].

Where 6G radio and IoT overlap – example scenario considerations

Let us consider an example scenario with two operators (see Fig. 4.9). Mobile IoT-network operator deployment aims at delivering Machine-Type Communication (MTC) [1] traffic services to users located outdoors. It is provided by dedicated roadside units operating at frequency f_1, and their coverage areas are depicted in green in Fig. 4.9 b). The coexisting mobile broadband MBB operator delivers MBB services to both indoor and outdoor users. The outdoor users are primarily served by macro-BSs working at frequency f_2 (depicted in red). However, as a result of frequency f_1 not being utilized indoors, the set of indoor hotspots is deployed in the band originally assigned to the IoT operator to improve the end-user performance (coverage depicted in orange). The MBB operator deploys multisystem 4G/5G/6G BSs, denoted for simplicity and backward compatibility as eNB or New Radio (NR) BSs. Although the investigation has been carried out for the case where an indoor operator may deploy multi-system nodes (allowing for switching between the systems), the results presented in this work concentrate intentionally on the case when an indoor operator deploys NR base stations.

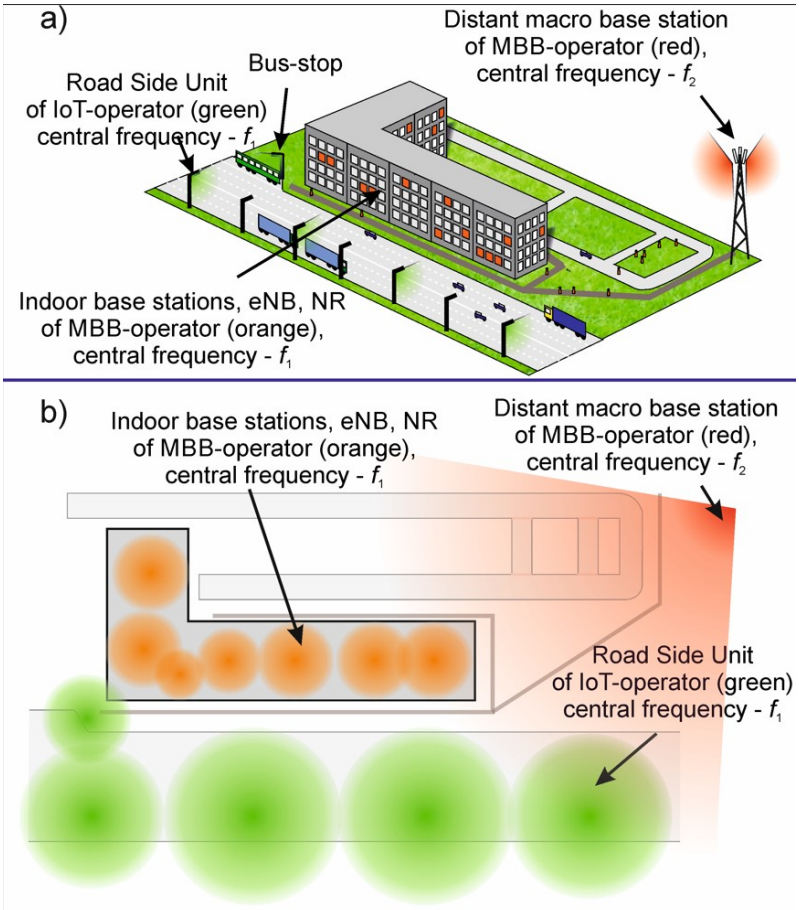

FIGURE 4.9: Example scenario: a) 3D deployment view, b) Top view of the radio coverage.

[1] We use the terms Mobile BroadBand (MBB) and MTC to preserve backward compatibility with 4G and 5G networks' nomenclature, however in the context of 6G network new schemes may be defined

4.2.1 Simulation results

Use-cases and setup

In order to evaluate the performance of the proposed context-aware communications with the spectrum shared between IoT and MBB networks, we have considered three use cases:

1. real-time LSA spectrum sharing: Application of LSA policies for the considered scenario, where the policies define the spectrum sharing rules between both operators

2. outdoor user interference reduction: Application of the RSM-based subsystem where an outdoor user is moving along the building (in this case, the trajectory, history, and handover maps are applicable)

3. advanced spectrum management: Application of traffic maps for better spectrum management by the MBB operator through advanced scheduling under constraints introduced by the IoT operator

Below, we provide some representative system-level simulation results for these use-cases. As the technical details for 6G are not available at this stage, for simulation purposes, we consider a setup tailored to 4G and 5G to illustrate the expected gains and benefits. The simulations represent at least 1 second, with scheduler decisions every 1 ms. The inter-cell interference cancellation algorithm has been applied (a version of the soft frequency reuse scheme), and Winner II channel models [139] have been used. Arbitrarily, the central frequencies have been set to $f_1 = 3.5$ GHz (typical for 5G systems, also called NR), and $f_2 = 2.6$ GHz (for conventional systems, i.e., LTE-A). The multicarrier single-input single-output communication of 20 MHz channels has been simulated. Thus, some assumptions have been made, as stated in Table 4.3. Both cooperating systems (IoT and MBB operators) follow the specific LTE-A/NR spectrum access schemes, i.e., the standardized modulation and coding schemes are selected based on Effective Exponential SNR Mapping (EESM) [140], and implemented jointly with the Proportional Fairness (PF) scheduler [141].

Table 4.3: Simulation parameters used in experiments

Parameter	**Value / notes**
Path loss channel model	Winner II channel model for indoor/ indoor-outdoor propagation schemes;
Channel changes	Extended Pedestrian A model (EPA) with 7 tabs implemented by means of Jakes model
Central frequency	$f_1 = 3.5$ GHz (NR) and $f_2 = 2.6$ GHz (LTE-A)
Channel bandwidth and its utilization	20 MHz / 98% (as for NR)
Corresponding number of RBs	108 (as for NR)
Scheduling method	Proportional Fair with $\beta = 0.5$; decisions made every 1 ms
SNR mapping	EESM tailored appropriately to NR with 15 MCS levels
Maximum transmit power	21 dBm
BS height	10 m (above ground for outdoor micro BS), below ceiling (for indoor BS)
Minimum distance between UE and BS	10 m (for outdoor BS), 3 m (for indoor BS)
User distribution	Uniform, 20% of static users (no movement), 80% of pedestrian users (approx., speed 0.8 m/s)
User Data Traffic	Full Buffer mode

The β parameters used for weighting instantaneous and averaged rate of each user was set to 0.5. Please note that at the time of conducting the investigation, not all of the physical-layer-specific parameters of the NR have been known. All the simulations have been carried out in the Matlab environment.

Application of the LSA changing in time

In this considered use-case, the database can be utilized to adapt to the changes in the LSA policy in real-time. Assume that the MBB operator borrows a particular fragment of the spectrum from the IoT operator for a given period of time. Once this period is over, new policies are applied. Each record in the database defines the ID of an indoor BS, the time range when the frequency band can be used by the BS, the maximum transmits power, and other transmit power constraints, and the frequency range that can be used. For demonstration purposes, we have defined an arbitrary sequence of frequency changes.

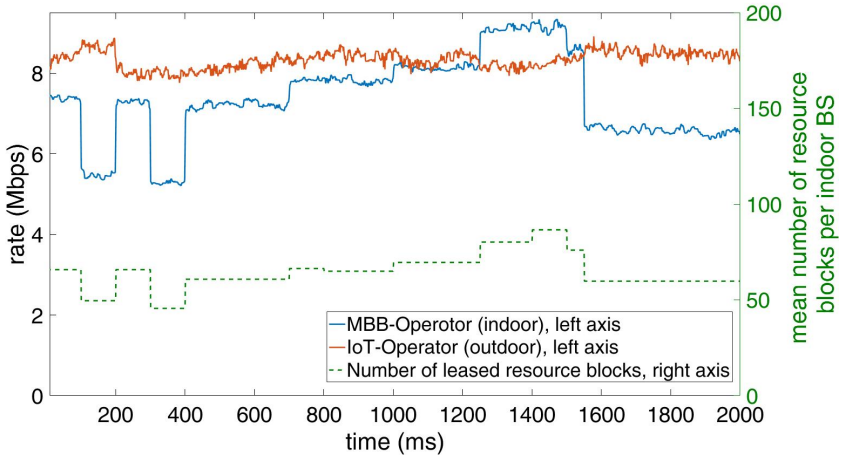

FIGURE 4.10: Average rates for indoor and outdoor UEs as the function of time in the advanced LSA

Fig. 4.10 shows the achieved rate variations in time as functions of changes in the assigned bandwidth for indoor BSs. At the bottom of the figure, the average number of resource blocks available for indoor-BSs of MBB operator is plotted as a reference to justify the time changes in indoor-user rate. The results show that the application of the RSMs allows for real-time configuration of BSs. Thus, one may conclude that it is possible to apply very frequent changes in terms of frequencies assigned to BSs; thus, adaptive frequency allocation provides new prospective benefits for performance.

Application of the RSM databases with an outdoor user moving along the building

Let us now evaluate the applicability of RSMs for controlling interference generated to the moving outdoor user associated with the IoT operator (it may be a pedestrian or a bus moving along the street as in Fig. 4.9). One may observe that when the bus/pedestrian is close to the building corners, indoor BSs deployed close to these corners have the strongest impact on the induced interference. The influence of BSs deployed in the central part of the building is smaller, and there is practically no influence of BSs located in the opposite corner of the building. At the same time, when the moving user is close to the central part of the building, it observes interference coming from the highest number of indoor BSs.

In this use-case, the optimization algorithm [138] takes the trajectory map of the outdoor user into account and finds the transmit power of all indoor BSs to maximize the sum rate while keeping the interference induced to the outdoor user below the agreed level. This result is compared with the situation when there is no indoor network. In our demonstration scenario, we consider a bus driving 50 km/h along with the building, which takes 6 seconds. The mean indoor/outdoor UE rate is calculated over periods of 200 ms. The achieved mean rates are shown in Fig. 4.11. While analyzing the results, please notice that we have intentionally limited the number of outside UEs to one – this allows for the evaluation of the impact of this particular UE on the overall system performance.

- there is a slight degradation in the achievable rate for outdoor users due to spectrum sharing (see the results denoted in the legend as "Adaptive outdoor protection")
- when there is no protection for the outdoor users, there is a strong degradation of the outdoor-user rate as a function of location, whereas the indoor-user rate is unchanged
- because the optimization algorithm requires the knowledge of the outdoor user position, the mean outdoor rate is unchanged regardless of the outdoor user position in the "Adaptive outdoor protection" scenario. At the same time, the rate of the indoor users is the worst when the outdoor user is close to the central part of the building where indoor-BSs power is limited

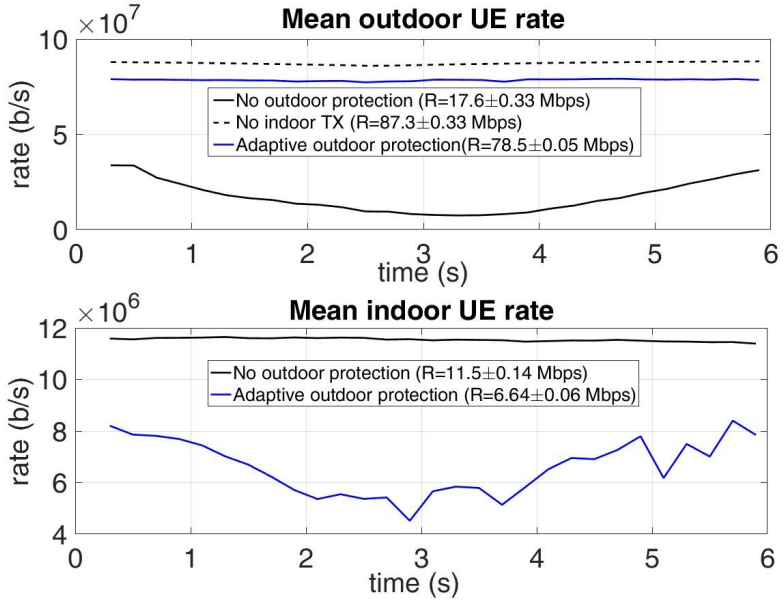

FIGURE 4.11: Mean indoor and outdoor UEs rates vs. time (one outdoor UE)

Application of traffic maps for better spectrum management

Let us now consider the use-case in which the RSM subsystem is applied with the traffic maps for resource scheduling simplification. In the baseline LTE (4G) system, the scheduler makes its decision every 1 ms [138]. Such frequent decision-making is not necessary if the scheduler can predict a user's behavior. Mainly, it is beneficial in the office scenario, where the users (or IoT devices) do not move in a period much longer than 1 ms. In our use-case scenario, apart from static or slowly moving users, we consider an MBB clustered user consisting of 10 non-moving

devices, resulting in relatively slowly-changing channel coefficients. The following algorithm has been proposed, implemented, and verified:

- in the initialization step, an observation period is applied for about 10 seconds, during which the RSM subsystem collects the decisions made by the scheduler on each resource block
- then, the RSM manager algorithm determines the average MCS index assigned to each resource block for a certain location, and calculates the standard deviation of the assigned MCS index; the MCS average and the standard deviation maps are shown in Fig. 4.12. The historical decisions and the current ones are weighted in order to replace older decisions with updated ones smoothly
- once the map is created, the algorithm selects the set of static devices (with the smallest standard deviation and non-zero mean) and assigns the resources to these UEs, so that their traffic demands are satisfied. In consequence, the set of resources is split into two parts: one assigned to the static users for a longer time (5 seconds in our simulations), and the other – assigned to the moving or new users based on the traditional PF algorithm [142]. After 5 seconds, the algorithm checks if there are any changes in the currently observed traffic distribution and adjusts its behavior to the new situation

In summary, access to this kind of context information (e.g., the traffic map) allows the scheduler to reduce the number of its scheduling decisions by simply omitting static users in the dynamic resource allocation phase. Static users are allocated with previously defined parameters.

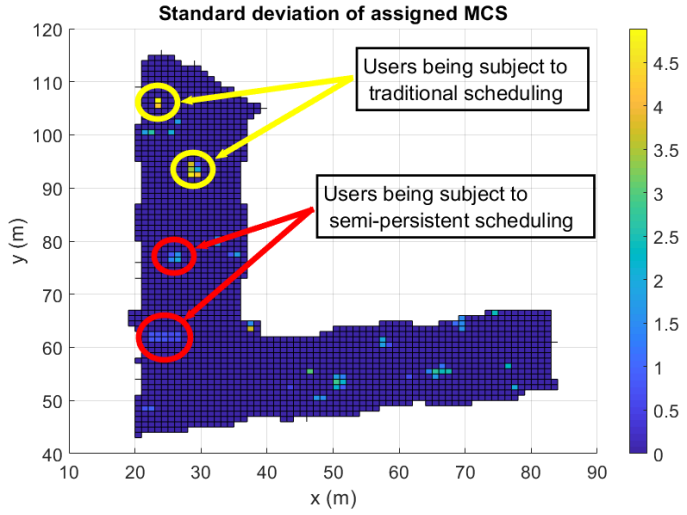

FIGURE 4.12: Traffic map -– the standard deviation of the MCS index after 15 s of observation; each point represents 1 m x 1 m square

In Fig. 4.13, the sum rates for indoor and outdoor users are shown. As expected, there is no change in the achieved rate for both indoor and outdoor UEs. The complexity of the scheduler is reduced without any negative impact on the system performance. Observe the dashed vertical line denoted as "Update", indicating the periodic update of the decision on the assignment of users to two scheduler groups. The average number of resources allocated by the PF scheduler to indoor users is reduced from 510 in the initial phase to 446 in the second phase (12.5% reduction of the processing cost). Such a reduction means a huge gain in the entire processing in the MBB system for the same outdoor system performance.

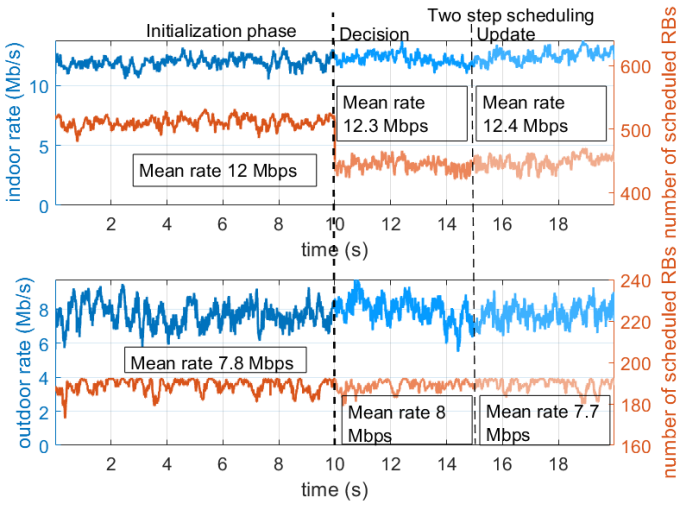

FIGURE 4.13: Sum-rates achieved for indoor and outdoor UEs using RSMs with traffic prediction

Discussion on RSM and database subsystem

The presented discussion and results show the benefits of context-information availability in databases. However, the trivial conclusion that the more information available, the more opportunities for efficient communication, is not straightforward in practical implementation. It entails challenges for wireless communications, which stem from big data processing, especially if mobility aspects are considered. Access to accurate and valid data in dynamically changing environments emphasizes the need for efficient design of the RSM subsystem, where all potential delays in collecting data are minimized. Moreover, statistical databases should be replaced with more advanced solutions tailored to rapidly varying scenarios. At the same time, a big amount of data to be available in various locations implies either information caching (to reduce delay) or high backhaul traffic. One may foresee that once the availability of rich context information is guaranteed, numerous algorithms from various domains of wireless communications can be enhanced for better performance. The concise summary of the design aspects of the RSM is sketched in Table 4.4. Moreover, in Table 4.5 we have presented a brief analysis of the prospective load from the operator perspective due to the application of the RSMs for each of the considered use cases. As the real load is highly implementation-specific, we presented the worst-case analysis, i.e., no storage optimization is applied, and no advanced data structures were considered.

Conclusions and summary

As in the context of 5G networks, the sixth-generation networks are envisioned to support a large number of services that pose divergent requirements. Collectively, these services are expected to demand more and more capacity, while the networks must be more energy-efficient. As an enabler for the converged multi-operator and multi-service networks, big-data processing for context-aware communication with radio service maps is considered to play a key part. In this article, we have presented an application of RSM for dynamic spectrum management in future context-aware communication networks. Taking the radio service context and operators' priorities into account, we have shown that, complementary to long-term mechanisms that benefit from legacy applications, RSM also shows a high value for mid- and short-term RRM schemes. The combination of radio-environment-, traffic- and trajectory maps with prediction functionalities offers a huge potential for efficient resource management and flexible sharing of resources between operators according to their priorities, needs, and dynamic changes in the spectrum usage scenarios. Thus,

we claim that 6G systems may strongly benefit from applying big-data processing algorithms that utilize dedicated, context-information database subsystems.

TABLE 4.4: Selected aspects of the RSM subsystem design

RSM design issue	**Notes on implementation**
RSM as a separate subsystem	Contemporary networks have already implemented procedures for data collection and utilization. The trend towards the application of big-data solutions and the need for data exchange with other systems and operators prompts a separate RSM subsystem to be created, as it is done today for an operations/business support system (OSS/BSS).
RSM management	RSM subsystem functionality can be delivered by a company specialized in data collection, environment monitoring, management, and storage, i.e., the network operator can outsource such tasks to companies delivering data processing services.
The need for standardization of RSM databases	The ways of collecting some specific types of data may be subject to standardization (e.g., feedback information about the channel state). However, each operator may propose tailored solutions for better data aggregation and storage. Nevertheless, there should be an interconnection between various systems and operators (e.g., for a better gathering of data about the ambient environment), and the communication interfaces should be defined.
Centralized or distributed architecture	The advantages and disadvantages of centralized and distributed architectures are well investigated. Considering the specific features of a wireless network (e.g., user mobility, multipath propagation, and large scale of the communication networks), the hybrid solution could be the best option, where long-term data are stored centrally, whereas short-term information is cached locally.
Consistency and availability	Following the well-known CAP theorem on consistency, availability, and partition tolerance, the design of the distributed database should take these aspects into account.
Delay and accuracy	In mobile wireless networks, the key functional problem is the reliable access to accurate data exactly at the right time (measured in milliseconds). The requirements for end-to-end delay constrain the RSM subsystem architecture. It may be required to apply advanced data processing and data mining algorithms for efficient data delivery.
Data gathering	The RSM subsystem is beneficial only when it is populated with updated data. Thus, methods of efficient monitoring and storage must be implemented. Standalone sensors may complement the information collected within the wireless network by mobile agents or BSs/access points.
X-Haul traffic	The presence of an RSM subsystem responsible for big-data processing in wireless networks immediately generates the need for efficient front- and back-haul (X-haul) traffic management. This aspect is directly related to the subsystem architecture design, whether centralized or distributed. However, access to big data also assumes that there is a dedicated communication channel through which the context data are transferred.
Security	Collection, and storage of big data require the application of advanced security algorithms for better privacy protection. The anonymization of collected data is a good approach. However, it has to be supported by proper security procedures.

Table 4.5: Storage and AI tools analysis (worst case scenario)

Use case	**Brief Load Analysis (Worst Case analysis)**	
Note: we map each use case to a few of the Seven Patterns of AI [143], which consists of: 1. Recognition, 2. Conversation and Human Interaction, 3. Predictive Analytics and Decisions, 4. Goal-Driven Systems, 5. Autonomous Systems, 6. Patterns and Anomalies, 7. Hyper-Personalization.		
Use case	**Storage**	**AI algorithm**
1. Real-time LSA spectrum sharing	In this case, the leasing operator specifies the rules (i.e., allowed transmit power per location and resource block – 8 bits, spectrum masks - 40 bits) for spectrum sharing. For the defined number of base stations (12) and resource blocks (100), and considering that the change of configuration may be done every ms, the required storage speed is around 57 MB/s (i.e., such an amount of data has to be updated in RSM every second). This value depends on the scenario assumptions, and its optimum is implementation-specific.	As humans prepare the general policy rules for spectrum sharing in a human-understandable way (may be done by a system administrator), and rules may be written in a fuzzy way, the considered algorithms use declarative programming from one hand and fuzzy logic on the second side. From the seven patterns of AI, this set falls within the Conversation and Human Interaction group.
2. Outdoor user interference reduction	Here, the policy rule is fixed so that it can be omitted in calculations. Moreover, the trajectory map, which defines the typical routes of the bus, is also negligible in the overall load. In this case, in the assumed worst-case scenario, the heaviest burden is the transfer of the values of the observed signal quality for each resource block. Even assuming only 5 bits per resource block (following channel quality indicator reporting procedure), the RSM will need to receive 0.5 Mbps per user, then process around 6 Mbps (in total for all 12 BSs), and send back to each secondary user around 0.5 Mbps. The above values scale proportionally with bandwidth (number of resource blocks) and are limited by implementation-specific constraints.	In this case, the clue is to predict the behavior of the outdoor-user trajectory and utilize this information for better spectrum sharing. After the learning phase (training), the typical values of allowed power and resource allocation can be done, promising pattern matching schemes. Within the seven patterns of AI, the algorithms here fall into predictive analytics and decisions and pattern detection.
3. Advanced spectrum manage-ment	In this case, the RSM utilizes the map of the building (separate per each floor) with a given raster. It has to store and process the historical MCS value per each location, as well as its variance. Assuming a raster of 1 dm, 5 bits per MCS index, and 8 bits per variance, it will need only around 21 kb per resource block, so around 2.1 Mb per all resource blocks. These values will increase accordingly with bandwidth. The data processing speed is at an analogous level (i.e., around 2 Gbps).	As the locations of the users may change in time, the AI algorithms applied fall again in the pattern and anomaly recognition group within the seven patterns of AI.

A compact summary of the use of contextual information to improve spectral efficiency is presented in Table 4.6 below.

Ph.D. candidate's publications considering problems discussed in this section	[117], [137], [138]
Context information	Location, floor, history of MCS allocation, history of throughput, and cell's association of users; list of LSA rules.
Influence on the system	Modified process of spectrum allocation (scheduling of RBs among UEs); number of decisions made by scheduler.
Impact on spectrum efficiency	Possibility of using the same spectrum by users inside and outside the building; reduction of control data amount.
Comment	The use of a semi-persistent scheduling method made it possible to reduce the number of decisions made by the scheduler, which in turn reduces the amount of control data sent over the network. At the same time, no decrease in user throughput is observed, so as a result application of this scheduler is neutral for users and beneficial from the point of view of spectral and energy efficiency of the network (less redundant information is transmitted).

Table 4.6: Summary of work presented in chapter 4.2

4.3 Research topic 3: RSM in M-MIMO LTE-A network simulator

Deployment of small cells in a heterogeneous network is directly related to the problem of right user association between macro- and small-cell base stations. In order to force just the selection of an appropriate base station, an additional component is added to the measured path loss (signal strength) to modify, i.e., virtually extend or squeeze, the cell radius. In the third research topic, we present the concept of using the Cell Range Extension (CRE) [144] parameter in coordinated LTE-Advanced (LTE-A) networks. Within the coordination area that covers numerous base stations, the values of CRE are tuned in such a way that the achieved network throughput is improved by proper User Equipment (UE) assignment to the Base Station (BS). The research results described here were published in one of Ph.D. candidate papers [145].

The UE to BS association in the LTE-A standard is performed by default based on the received power level (received signal reference power - Reference Signal Received Power (RSRP) indicator). With the introduction of the heterogeneous network structure including small BS, it became clear that such approach is not the optimal one when traffic offloading to smaller BS is desired. Therefore, the CRE parameter has been introduced to prioritize small (e.g. pico) BS in the cell selection process. The CRE is an additive modifier applied to the RSRP value, that can be set individually for each BS. By setting high CRE value for the small BS, the cell-edge users, that would have been assigned to the macro BS, select pico BSs instead.

The idea behind CRE is to deal with the problem of different coverage areas in UpLink (UL) and DownLink (DL) directions observed in the situation when the small BS is deployed within the coverage area of the macro BS. The virtual cell range of each site may be modified by adding a dedicated value of CRE parameter used in calculation of the received signal power from macro and pico BSs. Following the 3rd Generation Partnership Project (3GPP) standard [146, 147], two kinds of parameters may be used for that purpose depending on the UE mode. In particular, in idle mode (parameter used for BS selection) – there is a parameter called: *q-OffsetCell* within *IntraFreqNeighCellInfo* (in System Information Block (SIB), i.e. SIB4) and within *InterFreqNeighCellInfo* (in SIB5). SIB4 defines the information regarding intra-frequency neighboring cells, and SIB5 - information regarding inter-frequency neighboring cells. The range of the *q-OffsetCell* is from -24 dB to 24 dB. On the other hand, in the connected mode there is a parameter called *cellIndividualOffset* used for cell reselection, and specified in *measObjectEUTRA*. It is used in handover events, such as A3 (i.e, neighbor becomes offset better than *Pcell*) and A4 (i.e., neighbour becomes better than threshold). Its range is again from -24 dB to 24 dB. Both parameters are set for the BS (not for UE).

The method of choosing the base station based on RSRP and fixed CRE values, while allowing for traffic offloading to the small BSs, is not always the best solution. An example might be the case when an UE is very close to a certain base station (which results in high receive power) that already supports a large number of UEs at its capacity limits. In contrast, another station, at a slightly greater distance, does not support any or supports less UEs. In such a situation, the UE of interest could get more radio resources and, consequently, achieve higher throughput when assigned to BS with lower RSRP. Such a mechanism has not been provided for the LTE-A standard, although different cell load balancing methods are discussed in the literature [148–150]. The possibility of adaptation of CRE to provide load balancing between the BSs is one of the considered options. However, the main problem with such an approach is that any changes to CRE value for one BS may impact associations for all the neighboring BSs. CRE is a parameter specific for a single BS, not for a single UE, hence, it is not really feasible to force cell reselection for only a selected UE unless the UE association is optimized jointly for all the BSs.

System model

In order to design the CRE adaptation mechanism and the related modified cell selection procedure, we consider a dense urban scenario represented using Madrid Grid Model (MGM) [151]. It is based on observations regarding the city structure of Madrid and comprises such elements as buildings of different heights, roads, or parks with several trees. The MGM structure is outlined in Fig. 4.14 with dimensions of 387 x 552 m and buildings' heights varying from 28 m to 52.5 m. One may also observe the location of the macro base station (mBS with id 1) that is placed on the rooftop of the building in the central part of the analyzed area, and five pico base stations (pBS with ids from 2 to 6). The deployment of the BSs has been optimized to provide coverage in the whole area and to increase system capacity on the right side of the modeled city fragment, where a pedestrian walkway is present. There are 60 UEs uniformly distributed on the streets of the considered area, so only outdoor-to-outdoor transmission is taken into account.

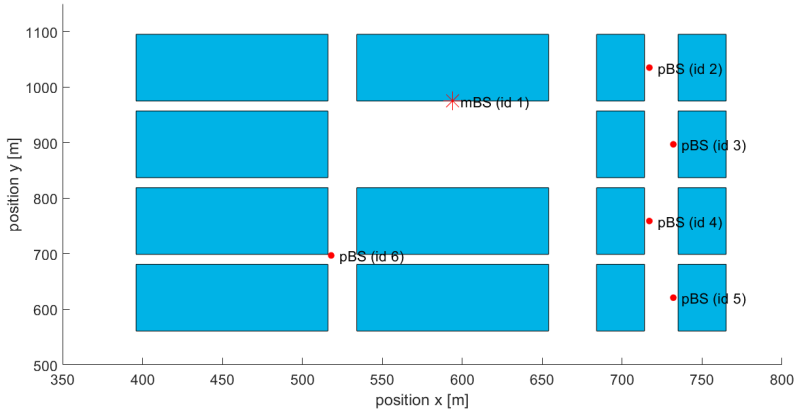

FIGURE 4.14: Illustration of the considered scenario: blue boxes represent buildings, red star is the location of macro BS (on rooftop of the building) and red dots indicate the pico BSs

We consider MIMO LTE-A heterogeneous system with eight antennas available at the macro BS and four antennas mounted at each pico BS site. All UEs are equipped with single antennas. We assume Time Division Duplex (TDD) communication with the UL/DL configuration number 5, with 10 ms DL to UL switching periodicity (i.e., DL subframe followed by special subframe, uplink subframe and seven DL subframes: DL SS UL DL DL DL DL DL DL DL) [152]. The assumed bandwidth shared between all BSs is 20 MHz, and, in consequence, the number of available resource blocks is 100. As multiple antennas are used at the BS, we apply Maximum Ratio Transmission (MRT) precoding and allocate resource blocks according to the Proportional Fairness (PF) criterion. The association of UEs to BSs is made based on the RSRP measurements, taking into account the CRE modifier for each BS. When the combined received power and CRE from the other BS exceeds the corresponding value for the currently serving BS (including small margin), the handover procedure is initiated.

The considered scenario is a dense urban one with MIMO employed; thus, very accurate modeling of signal propagation is required to capture all significant properties of the wireless channel. In this work, we use a ray-tracing approach with Qamcom Channel Model (QCM) tool [153] employed that provides a full 3D propagation scenario definition, including buildings and other obstacles. The identification of propagation paths is up to the second-order (two reflections), with the higher-order paths modeled stochastically.

4.3.1 Radio service maps for CRE adaptation

In our proposal we have used Radio Service Map (RSM) for selection of the best association pattern of UEs to BSs based on the UE location. The best assignment in this context means maximizing the throughput of the entire network. In other words, for a given set of all UEs locations served by the network within the coordination area, the algorithm finds the best association of UEs to BSs by searching through stored RSMs. In such an approach, the first step is to create the representative set of patterns (i.e., allocation of UEs to BSs), store them in the database and, next, match the current deployment of UEs to the stored patterns. In such a case, the network will utilize AI-based solutions to analyze the historical data to find the best UE association. However, the knowledge what is the best potential association of the BSs to UEs has to be realized using the mechanisms from LTE-A standards. Knowing these limitations, we propose to modify the values of CRE for each base station in such a way that the resultant UEs association to BSs will be as close as possible to the optimal one. In the following considerations, we assume that the RSM has been built, for example, based on an exhaustive search, so the best possible UEs to BSs assignment for each set of UEs location is known. RSM has a grid structure. Therefore the location of each UE is known with accuracy to the grid size. Two sets of UEs locations are distinguishable in RSM if at least one UE has locations from a different grid cell than the other set.

In order to show CRE value impact on UEs to BSs assignment, the following example was prepared. On top of Fig. 4.15 one may observe three rows with possible allocation patterns of UEs (vertical axis) to the BSs (specified in form of color coding, where black color represents lack of association); also the number written in each cell represents the index of the associated BSs (i.e., 0 – lack of association, 1 – association to mBS, 2-6 – association to corresponding pBS). In the first row, we show the best-stored pattern of UE assignment to BSs for a certain location, so the first row is the result of RSM utilization in our LTE-A use case. In the middle row, one can see the association of UEs to BSs for a given location when the classic, standardized method is applied, i.e., when the UE is associated with BSs based on the received signal strength without CRE. One may observe eight differences between these two rows, e.g., UE number 3 is allocated

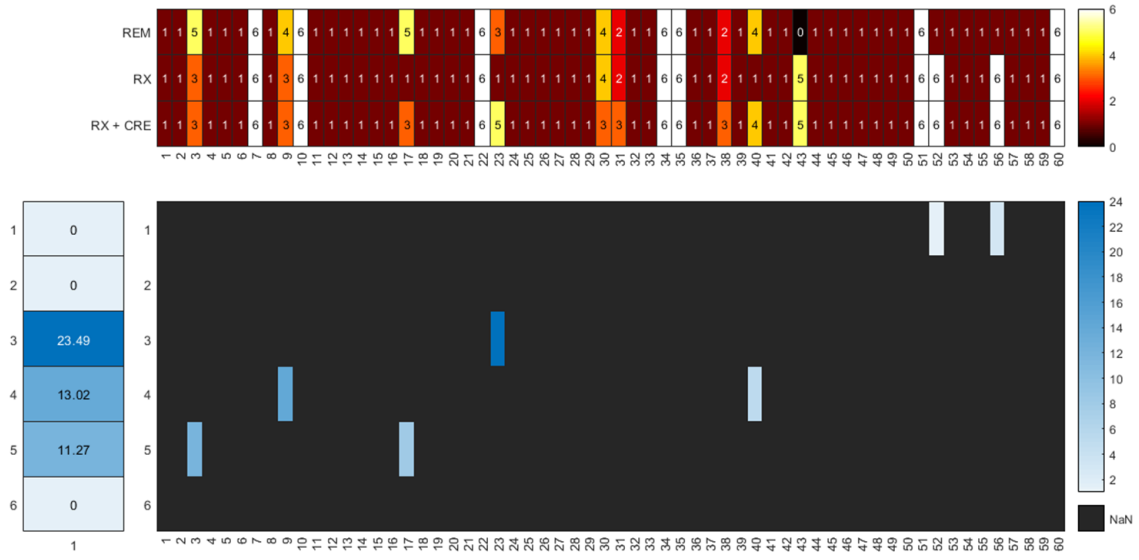

FIGURE 4.15: Illustration of the calculation of CRE values based on RSMs: the top part presents the association of UEs to BSs with different methods applied; the bottom part shows the calculated desired CRE values, with the vertical axis indicating the BS indexes and the horizontal representing the individual UEs; the left site shows the calculated CRE values for each BSs

to pBS number 3 based on signal strength, but for a given location of UEs, it will be better if this UE is associated with pBS number 5. Considering that the stored RSM contains a better UE assignment pattern, the algorithm should now modify the values of CRE-related offsets to guarantee its realization. Based on the location of the UE, the assumed path loss model, and the location of BSs, we have calculated the required value of the offset to reassign all wrongly associated UEs. Assuming that only cell range extension is possible, only positive values of the offset can be achieved. The calculated values are shown in the bottom part of the figure. Using the color-coding (with values in logarithmic scale from 0 to 24 dB), the corresponding values of the offset are presented (also in a numeric form on the left side of the figure). However, as it could be foreseen, modification of the CRE-related offset in one BS has an impact on many UEs in its vicinity; thus, direct application of the map is not possible, what is illustrated in the third row on top of the analyzed figure. Unfortunately, direct application of the RSM indications does not lead to any special improvement. Thus, we propose another solution to this problem.

Since we assume the best possible UEs to BSs assignment is known for a specific set of UE positions, the only remaining issue is to apply this assignment scheme in a particular network. For this purpose, in the LTE-A network, it is necessary to select the CRE values in such a way that the UEs to BSs assignment is as close as possible to this assignment indicated by RSM. It can be expected that the overall rate in the network will increase at the price of a more frequent cell reselection procedure compared to classical LTE-A UEs to BSs assignment. The CRE determination procedure starts by setting a random CRE value for each of the BS. We also assume that we do not change the CRE parameter settings for macro BS but only for pico BS. For each UE which is not assigned to the target BS, the minimum value of the power change that would cause the current to target assignment change is determined. Next, from all the values required to change the assignment to target one, all that require too high CRE change (outside the range from -24 dB to 24 dB) are rejected. From the list of potential CRE changes, the one that requires the least absolute value change to a single CRE parameter is selected and applied. This process is repeated many times, both for the stage of randomizing the initial CRE values for each base station and for the stage of introducing changes to the CRE value. At each stage of the search, the current list of CRE values for each BS is saved along with the number of UEs assigned not according to the target assignment set by RSM. After many iterations, the CRE parameter set is selected for which the minimum number of erroneously assigned UEs has been reached.

4.3.2 Simulation results

In order to verify the performance of the proposed CRE adaptation mechanism, computer simulations of the LTE system for the considered scenario have been carried out using Matlab, with a single simulation run duration of 500 time slots (0.5 s). First, it is worth looking at how UEs are assigned to BS during the simulation. Fig. 4.16 shows the UE to BS assignment using the standard LTE-A assignment method based only on received power level. Fig. 4.17 shows the UEs to BS assignment, choosing the CRE value so that the assignment is as close as possible to that obtained from RSM. The figures show that with the standard UEs to BSs assignment method (LTE-A) the number of UEs switching between stations is less frequent.

In Fig. 4.18 one may observe the increase in the overall performance of the network – the CDF plots of the UE average rate is shifted right at every point, meaning that each UE in the network observed gain is achieved rate. It is worth noting that an increase in the 10th percentile of UEs average rate from 3.13 Mbps to 3.5 Mbps is observed ($\approx$11.5 % of improvement). At the same time, the mean rate is improved by $\approx$5 % and the rate for the 90th percentile of UEs – by $\approx$2.5 %.

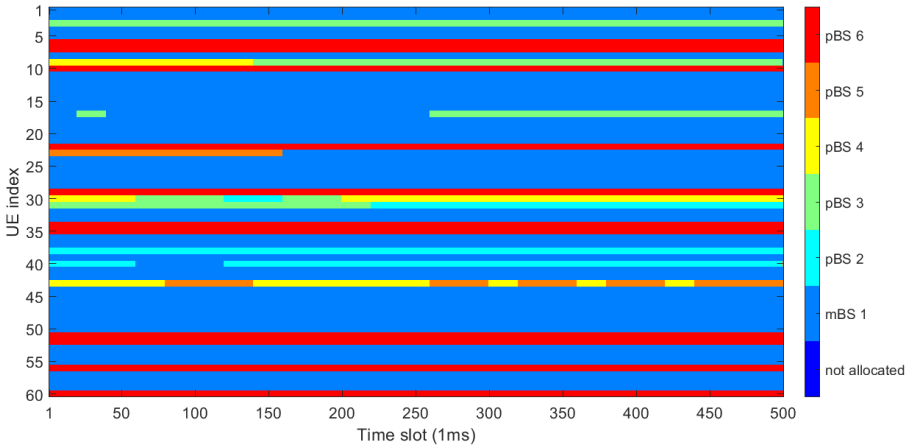

FIGURE 4.16: Illustration of the time evolution of RSRP-based UEs allocation to BSs

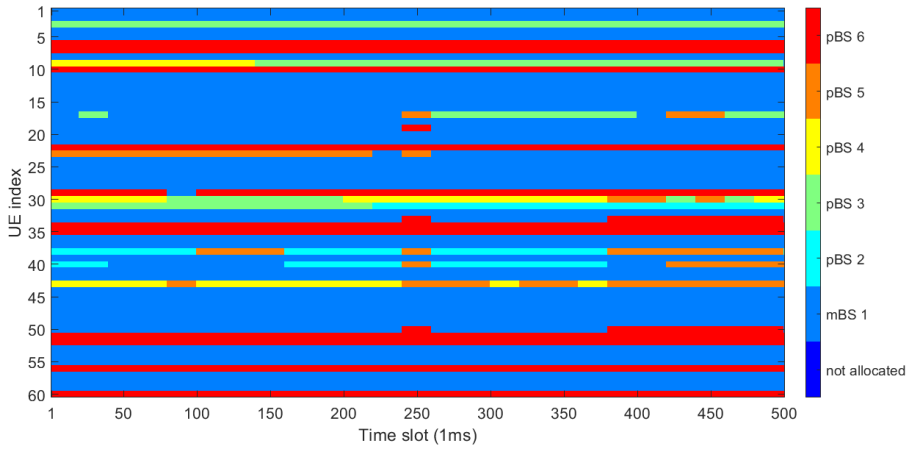

FIGURE 4.17: Illustration of the time evolution of RSM-based UEs allocation to BSs

The cost of such a promising gain is the increased number of triggered cell-reselection procedures – it is sometimes necessary to reselect the cell even if the observed power values do not justify such behavior. In our experiment, for the 500 time slots, the number of initiated handovers was approximately doubled, reaching the value of 52 changes, as seen in Fig. 4.19. This phenomenon can be observed by analyzing Fig. 4.16 and Fig. 4.17 where the associations' changes in time are shown for a pure LTE-A system and the system supported by the RSMs.

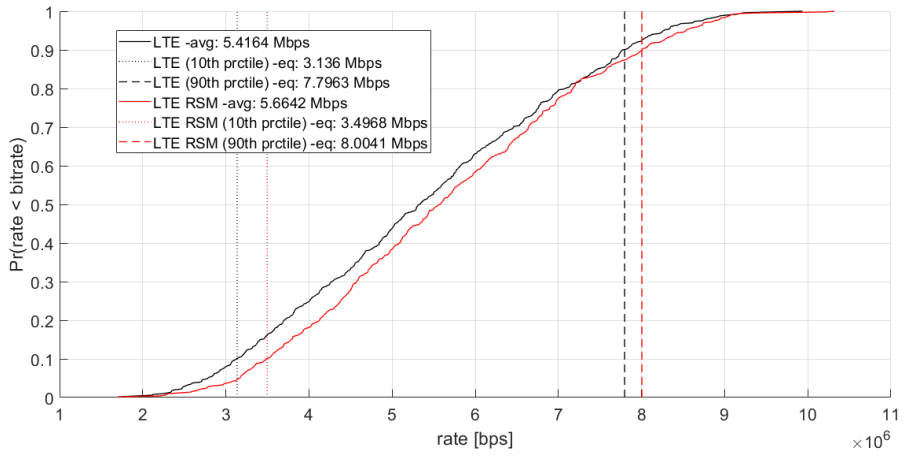

FIGURE 4.18: Empirical cumulative distribution function of UEs data rates without and with RSM-aided CRE adaptation

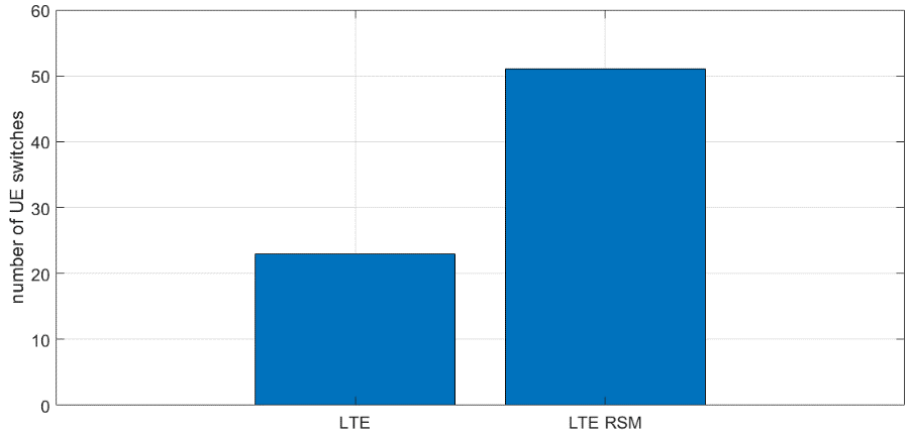

FIGURE 4.19: Number of cell reselections (handovers) for the conventional RSRP-based association and RSM-aided association

Conclusions and summary

In this work, we have discussed the opportunity to improve CRE mechanism applied in LTE/LTE-A networks in schemes, where strong coordination between the base stations is considered. Although CRE offset is set per-base station, so its value is applied to all UEs associated with given BS, it has been proved that there exists optimal association of UEs to the BS. Such association can be achieved by the proper setup of the CRE offset. In our scheme, we applied an exhaustive search approach to optimize the CRE parameter selection, with the results later stored in the dedicated database. This approach has increased the UEs average rate by approximately 5 %, and the 10th percentile of UEs rate by approximately 11.5 %. In future work, machine learning algorithms can be applied to reduce the complexity of the brute-force approach.

A compact summary of the use of contextual information to improve spectral efficiency is presented in Table 4.7 below.

Ph.D. candidate's publications considering problems discussed in this section	[145]
Context information	Set of users location; sumaric throughput in the system; UE to cell association setup; setup and available range of CRE parameter;
Influence on the system	Modified process of UEs to cells assignment, which changes distribution of interference and bitrate of UEs; modification of CRE of pico-cells.
Impact on spectrum efficiency	Increased sumaric thoughput of the network; increased number of reselections of cells.
Comment	Modification of a default way of UE to cell assignment (by modification of CRE parameter) allowed to create improved set of assignment and hence improved throughput (and improved spectrum efficiency).

TABLE 4.7: Summary of work presented in chapter 4.3

Chapter 5

Context information utilization in ultra-dense wireless networks

Considering the trend in wireless transmission, which consists of increasing the density of devices while reducing their range, the ultra-dense radio network is considered, for which inspirations from the operation of the human nervous system were used. Even with the fact that the human nervous system is more similar to a wired than a wireless network, we present visionary and new approaches to using contextual information in future dense wireless networks.

One of the challenges identified for future wireless networks beyond 5G is to achieve extremely low energy consumption while keeping the required level of quality of service, expressed in terms of reliability and system throughout [154]. Inspired by the functioning of the human brain and nervous system, we consider a highly dense wireless network in this work. The distance between the nodes is reduced so that as simple as possible transmission schemes can be applied, i.e., with simple modulations, lack of error-coding, and no re-transmissions. Two types of contextual information have been used in this work. Firstly, the backup devices use the information they observe about neighboring nodes (e.g., delays in sending messages) and take an active part in the transmission in case of any irregularities. The second type of contextual information is external information (non-existent in a specific system but having a potential impact on this system), which, when observed by a dedicated device, allows for the modification of the operation of the analyzed network (e.g., change of power, message transmission route, etc.). Both types of contextual information are most importantly used to improve the reliability of the radio network. However, this behavior has a significant impact on spectral efficiency, as only a properly functioning radio network ensures correct user data flow, which is necessary for the spectral efficiency of the entire network. In this chapter, we analyze the reliability of the network, which utilizes proposed HNS-inspired nodes. In the first research topic considered within this chapter, described in Sec. 5.1, we assess the reliability and availability of the particular network by means Reliability Block Diagram (RBD) analysis. In the second research topic, described in Sec. 5.2, the reliability of random realizations of such network is analyzed utilizing percolation theory.

5.1 Research topic 1: Reliability and availability analysis in ultra dense network

Motivation and related work

Wireless communication systems are facing permanently increasing requirements not only in terms of offered throughput but also regarding other performance metrics, such as low latency, reduced overall energy consumption, or high reliability [154, 155]. The proliferation of smartphones and other wirelessly connected devices in the community is greater from one year to another. However, at the same time, the network infrastructure becomes continuously more heterogeneous - densely deployed micro- support services offered by the macro-base stations and pico-base [156–159]. Moreover, the cloud-based solutions gained popularity in practice, where the centralized baseband unit is associated with several connected Remote Heads (RHs) [160]. One of the justifications for this situation is that the reduction of distance between the network edge and the end-user leads to better transmission opportunities. It is expected that the number of wireless nodes (mainly infrastructure elements like base stations, repeaters, etc.) will also increase in the future. When the number of deployed nodes is high, and the network is often considered as *very*, *ultra* or even *extremely* dense [161], the inter-node distance maybe even so short that highly simplified transmission schemes can be applied. Thus, in this chapter, we consider ultra-dense wireless networks [162, 163], where the density of transmitting nodes per certain area is as huge that in most cases, line-of-sight transmission is possible, and in consequence, the resultant transmit power at each hop may be significantly reduced compared to the contemporary nodes. Moreover, following the recent concept of so-called integrated-access-backhaul transmitters, we assume that each wireless node may act relay [164]. It is essential from the perspective of the reduction of the overall energy consumption in the entire network. Such an aspect is of particular importance from the perspective of future wireless networks, as recently *zero-energy* paradigm has been seriously considered as one of the key research challenges for the networks beyond 5G [165–167]. Advanced processing algorithms and solutions can, of course, combat the impact of a harsh environment on signal propagation, but at the expense of increased node complexity and energy consumption. In this thesis, we investigate the vision of a highly dense wireless network that could be, at least partially, applied in future wireless networks. In consequence, in this chapter, we focus on ultra-dense wireless networks, where each node may act as a source, sink, or relay in the network.

The idea of such a futuristic network, specified by the above assumptions, sprouted out from the observations of the neuronal communications within the human brain and Human Nervous System (HNS), which is fairly effective in achieving high energy efficiency (per one information bit), required throughput and high reliability. Nowadays, the main research trend in this domain concentrates on artificial neural networks, on their improvements and modifications [168, 169]. They are often applied for decision-making in various scenarios, learning, and general improvement of the artificial intelligence domain. Numerous focused solutions inspired by HNS are also considered in the literature, such as advanced routing protocols in wireless sensor networks [170] or in general in wireless networks [171]. Nice overview of various practical applications of HNS in wireless systems is presented in [172–175]. In our approach, however, we rather focus on HNS only, and in particular on specific components of the neural system, such as microglia cells or astrocytes [176], and try to project their functions on the wireless world. Observation of the human body's operation, particularly how information is transmitted in the body (which makes us move our hands, see, and feel), seems to be highly similar to such ultra-dense telecommunication networks. Many elements of the human body are interconnected and exchange information with

each other. A fundamental observation is that this information exchange occurs in the nervous system, which consists mainly of a very dense network of neurons. Additionally, this transmission is very simple yet complete. This is reminiscent of the notion that nature has developed the nervous system in such a way that information is transmitted by simple transmission over a large number of (independent/separate) connections instead of complicated transmission over a small number of paths (usually common). The considered neural network is not used for, e.g., decision making, but we utilize it for data transmission. Our ultimate goal is to achieve high network reliability in a dense wireless network with reduced energy consumption (e.g., achieved through simplified coding and lack of retransmissions) by the application of dedicated mechanisms observed in HNS. Initial findings on the HNS inspirations applied to wireless communications have been discussed already in our previous papers. In those works, we analyze such a network's throughput and energy efficiency. The novelty of this work is the reliability evaluation of such a network by applying the Reliability Blocks Diagram method and comparing the results for cases where the proposed microglia and astrocyte functionality is activated [177, 178].

5.1.1 Inspirations from the nervous system

The human nervous system is a very complex network with an enormous number of nodes and links. At the same time, it uses a relatively very simple scheme for data transmission - through electrical impulses and chemicals - which carry short, and non-coded information [176]. In addition, there is no re-transmission method applied. Although the structure of the nervous system is more of the *wired* than *wireless* type, in terms of a very dense wireless communication network, an analogy can be fairly considered. Many useful features or mechanisms in terms of communication can be found in the nervous system (both central and peripheral). Below we briefly present some of the prospective inspirations.

Neuron

The *neuron* is the basic, most common, and most important cell in the nervous system. Its main function is to receive information from other neurons (through chemicals - neurotransmitters received by neuroreceptors in neuron dendrites). In the Fig. 5.1 the neuron structure and elements are shown. If the signal is strong enough, send the same information further to other neurons.

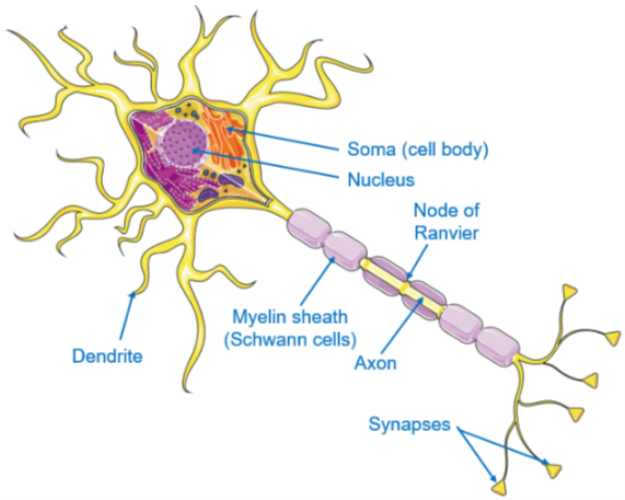

FIGURE 5.1: The neuron cell schema[1]

[1]Servier Medical Art, `https://smart.servier.com/` (CC BY 3.0)

More precisely, information is sent further if the action potential, which depends on the number of received neurotransmitters, is above the threshold. Propagation of information in a neuron is realized through electrical impulses in axons and then by releasing neurotransmitters (chemicals) in axon ends - synapses.

Inspiration from neuron analysis for a dense wireless network

Neurons can be simply mapped to network nodes, which receive, process, and transmit information. A high-density neural network is an analogy to a very dense wireless network. Next, the neuron's cell body represents the wireless transceiver, whereas the wireless link corresponds to the dendrites and synapses. We follow the fact that a new neuron will be fired (activated) to transmit the received message further only when the received signal is strong enough. In particular, we set a threshold for the minimum power of the received signal, which is required to transmit the message further.

Astrocyte

The *astrocyte* [173] is a glial cell which is one of the components of the Blood-Brain Barrier (BBB). The smallest blood vessels are surrounded by astrocyte feet. An astrocyte can detect some chemicals in the blood (such as glucose) through dedicated receptors. Using this knowledge, astrocytes can communicate with each other and can influence the transmission between neurons. It means that the information about, e.g., glucose, influences the neuron's transmission utilizing astrocytes' capabilities, but it does not initiate data transmission in neurons.

Inspiration from astrocyte analysis for a dense wireless network

The astrocyte function can be treated as a virtual switch at the junction of two domains (e.g., networks, subnetworks, or even planes, e.g., control and data plane). It means that some parameters within one domain (e.g., network) can influence the functionality of another one. As an example, we can point out a situation when sensors detect an emergency in some location. Then the second network can react to this observation by redirecting the data traffic to bypass this location to reduce the probability of connection failure (e.g., in the case of a sudden power failure). In other words, this function can be implemented as a short-term scale control plane that can reconfigure some parts of the network in sudden situations.

Microglia

Another very important glial cell in Human Nervous System (HNS) is the *microglia*. It is the first and main form of human active immune defense in the central nervous system. The microglia cleans the brain from unnecessary and damaged neurons or cells. It occurs in two main forms: a sense form when it observes surroundings and an active form when it takes action. What is very important, the microglia can communicate with other microglia cells, astrocytes, or even neurons [179].

Inspiration from microglia analysis for a dense wireless network

In a wireless network, we can find a lot of useful applications of microglia, such as providing some fault tolerance in the network. However, the most straightforward one is to create a dedicated device that observes the surroundings (more specifically, power level, interference, packet flow) of a given network and, in the case of detecting some crucial changes (e.g., one device suddenly stopped responding), it can react. It can be realized in several ways.

First, it may inform other nodes, administrators, or controllers about the detected problem. Additionally, it could take over tasks that were performed by the currently non-responding device. The microglia functionality, in this case, is very similar to the astrocyte functionality. However, a microglia-inspired device is a device that works in its own network, and an astrocyte device is an external trigger from other networks.

5.1.2 Proposed application of HNS elements for high network reliability

Based on the discussion in the previous section, we model the wireless communication network as follows. First, only the simplified transmission between the nodes is allowed (i.e., no dedicated channel coding and decoding algorithms are applied, and no advanced signal processing techniques are considered); moreover, the re-transmissions are not permitted. If the required signal power is observed at the receiver side, the data is assumed to be delivered correctly. Second, the nodes are stated to be static, so no mobility of nodes can be assumed to improve reliability in case of network failure. Next, the nodes may act as a source of the message or may act as a simple relay. Finally, the network nodes may malfunction due to, e.g., hardware damage or simply device fatigue, resulting in a decrease in network reliability; this kind of failure can be classified as *long-term issue*. The degradation of link quality (due to increased power of distortions, such as observed interference) entails breaks in communications reducing the network reliability; such a situation reflects the *short-term issues*. Thus, we assume the presence of dedicated nodes (such as microglia or astrocytes) to overcome the network mentioned above failures, both *short-* and *long-term* in their nature. Both of them do not take part in data transmission in the HNS, but in specific moments they enable special functions to, e.g., increase network reliability. We propose the application of dedicated microglia-inspired and astrocyte-inspired network nodes (which may also be realized as a software function within an existing device), which can modify the functioning of the network in the case of an emergency. In particular, they can detect malfunctioning or damage of a node, i.e., they react when the transmitter has observed no acknowledgment of the correct reception of sent messages. In such a dense wireless network, the damage of a node can be observed in various cases, such as mechanical damage to the device or simply a fully drained battery. These situations often occur in military applications. When such a situation is detected, the microglia-inspired node activates its transceiving functionality (trying to replace the damaged node). The astrocyte-inspired node can alert neighboring devices to, e.g., use higher transmission power, so the message could bypass (or *jump over*) the place with a higher risk of failure (less reliable path). The analogous system has already been considered in our previous works (such as [177, 178]); in this work, however, we concentrate on the reliability and availability enhancements of such a dense wireless network. The results of this analysis have been included in [180].

System reliability and availability

Nowadays, there is a need for very reliable transmission in wireless communications. In the fifth-generation network, the "five-nines" reliability is one commonly spoken of. Five nines refer to the reliability (or even more correctly, availability) of the level 99.999% [154, 155]. The definition of reliability says that it is the probability of a network operating properly without any device or link failure [181, 182]. The availability, in turn, is defined as the proportion of time a system is in a functioning condition. It is appropriate to use the term reliability for network devices, while the availability should be used for a wireless link. Among various approaches for reliability assessment and evaluation, we selected the Reliability Block Diagram (RBD) [183]. Let us analyze the following illustrative example.

5.1.3 Reliability block diagrams - an example

RBD is a block diagram that represents all elements of a network in terms of reliability in the form of fault dependencies. Blocks can be connected in a series (if the fault of one such element causes the system's fault) or in parallel (if the fault of one element does not cause the system's fault). To demonstrate this feature, the exemplary RBD of a very simple wireless network consisting of four nodes (A, B, C, and D) is presented in Fig. 5.2.

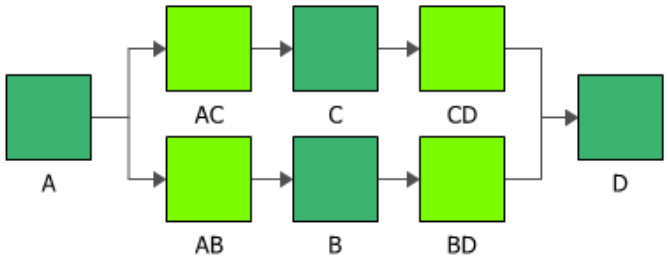

FIGURE 5.2: Reliability Block Diagram of the exemplary network

One can find that there are two parallel paths between nodes A and D through device C or device B. Each path has three blocks in a series that represent the reliability of the device and two links: between the source and device (AC or AB) and between the device and sink (CD or BD). In this case, the reliability of this system ζ_s can be expressed by the following formula:

$$\zeta_s = \zeta_A \zeta_D (\zeta_C \zeta_{AC} \zeta_{CD} + \zeta_B \zeta_{AB} \zeta_{BD}), \tag{5.1}$$

where ζ_i is the reliability of device i, and ζ_{ij} is the reliability of the link between devices i and j [182]. In the case of simple exemplary network, where the Binary Phase Shift Keying (BPSK) transmission method is used (only to demonstrate idea), the reliability of the wireless link is expressed by the formula:

$$\zeta_{ij} = 0.5 \cdot erfc(\sqrt{E_b/P_{\text{noise}}}). \tag{5.2}$$

where E_b is a signal energy, and P_{noise} is a noise power. In this example we assume for simplicity that the probability of device fault does not change over time, so the reliability of a device (network node) can be expressed as a constant value. Next, the considered distances between devices are equal to: $d_{A,C} = 28.43$ m, $d_{C,D} = 31.11$ m, $d_{A,B} = 30$ m, $d_{B,D} = 24.08$ m. The transmit power of each device equals -26 dBm (i.e., let us remind that we consider a highly dense wireless network, so the transmit power is also reduced to avoid interference), central frequency - 3.5 GHz, and assumed bandwidth - 20 MHz. FSPL model is considered. Applying these parameters, the achieved values for reliability of links equal: $\zeta_{AC} = 0.972$, $\zeta_{CD} = 0.959$, $\zeta_{AB} = 0.965$, $\zeta_{BD} = 0.988$. When the reliability of each device is equal to 0.99, the final reliability of the whole system is then equal to $\zeta_s = 0.975856$.

Wireless link modeling

In the above example, the non-realistic assumption was made - the probability of failure in the network did not change over time. Such an approach is wrong, especially in the context of a wireless link whose quality changes dynamically over time. Moreover, node fatigue and prospective battery depletion should be considered. In such a case, the network reliability should be replaced by the network availability to simulate the average time when the network is available. The reliability in this context is inappropriate because it considers only a period of time before the first wireless link unavailability occurs.

To ensure accurate simulation results, a log-normal model of shadowing was used [184]. Thus, in the first step, it is necessary to calculate the operating range using the Friis formula:

$$R = \frac{\lambda}{4\pi} \cdot \sqrt{\frac{P_{TX}}{P_{RX}}}, \tag{5.3}$$

where λ is an operating wavelength, P_{TX} is a transmission power of transmitter in mW and P_{RX} is a minimal power at receiver can receive information in mW. Then, the reliability of the wireless link is described by following equation:

$$\zeta_{ij} = 0.5 \cdot \left[1 - erf\left(3.07 \cdot \frac{\ln(r/R)}{\sigma/\eta}\right)\right], \tag{5.4}$$

where r is a distance between transmitter and receiver, R is a transmission range of the transmitter, σ is a standard deviation of shadowing, and η is a pathloss exponent [185].

5.1.4 Simulation results

In order to validate the concept of microglia-inspired and astrocyte-inspired devices, we have generated a random network topology shown in Fig. 5.3. Please note that the reliability and availability of the network are highly related to topology. Thus, to guarantee statistical correctness, we repeated the simulations analyzing 100000 different realizations of failure sequences that appear in the network, assuming various node failure probabilities as specified later. The "new link" created through astrocyte-inspired devices means increased transmit power (increased transmission range and additional nodes are accessible). The "new link" in the case of microglia-inspired devices means the utilization of links in data transmission, which were not available when the microglia-inspired node was not active. The task of this network is to send messages from source to destination. We assume that if there is a path between the source and the destination, this task is feasible, abstracting from the routing algorithm used (any routing algorithm should be able to find a path between the source and the destination if it exists).

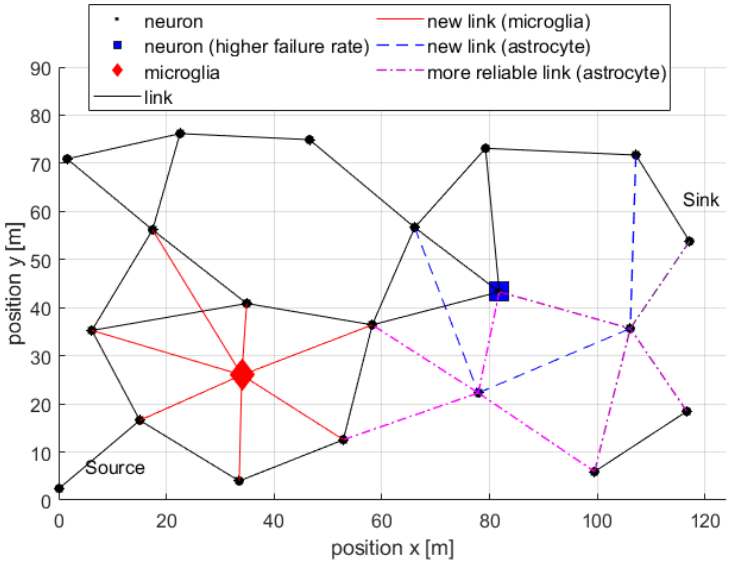

FIGURE 5.3: Simulated network topology

Because the analyzed network contains a large number of nodes and links (in the context of RBD), the determination of reliability in an analytical way is too complicated. For this reason, all results were obtained in a simulation manner utilizing Matlab, and BlockSim environments [186].

A specific single device was added to play the role of a microglia, and an astrocyte function was added to simulate the reaction to an emergency. All other devices play the role of a neuron - they receive and send further messages. The transmit power of the neuron was set to 8 dBm, and of microglia and neurons with increased transmit power (as a reaction to the astrocyte function) to 10 dBm. The key simulation parameters were set: operating frequency 3.5 GHz, bandwidth 10 MHz, and required minimum signal-to-interference-noise threshold -5 dB. System parameters have been selected to achieve dense wireless, where the distance between adjacent nodes is approximately equal to 20m. Moreover, the Additive White Gaussian Noise (AWGN) channel was considered and FSPL model with parameter $\alpha = 2$ was used. Let us remind one that no dedicated channel coding or signal equalization etc., is applied; also, retransmissions are not permitted.

The microglia device does not take action in message transmission until at least one of the neighboring neurons (in its transmission range) stops working properly. The microglia detects this situation by observing the message flow in its neighborhood. Then it turns on the transmission functionality and acts like a neuron in the network. A node with the astrocyte functionality receives information about some problems in its vicinity, which can increase the failure rate in the system. In our approach, the astrocyte ensures that a less reliable area can be bypassed through other paths or even *leaped over* (using higher transmission power). To validate this concepts, four network scenarios have been checked:

— Scenario 1 — without astrocytes and microglia (used as reference)

— Scenario 2 — with microglia turned on

— Scenario 3 — with active astrocyte function

— Scenario 4 — where both microglia and astrocytes worked

Two use cases have been evaluated, mainly use case A - for analysis of the microglia-inspired and astrocyte-inspired nodes' impact on improving network reliability and use case B when the network availability was investigated (i.e., node reliability changes in time).

Use case A - reliability

In the following simulations, we assumed the value of reliability represents the probability of the device surviving a certain number of days. Mean Time To Failure (MTTF), introduced to clarify the meaning of the reliability values [187], may be defined by the following formula:

$$MTTF = \frac{t}{-\ln \zeta}, \tag{5.5}$$

where t is an observation time, and ζ is the reliability. Equation (5.5) can be used to calculate MTTF of the network when $\zeta = \zeta_s$, the device when $\zeta = \zeta_i$ or the wireless link when $\zeta = \zeta_{ij}$. Typically ζ_i has an exponential distribution, which is the most commonly used life distribution in reliability analysis. For numerical evaluation, we arbitrarily assumed observation time equal 1 day (may be changed to another justified period). The reliability of neurons was set to 0.99 (MTTF equals around 100 days), and the reliability of neurons in an area with a higher failure rate was set to 0.8 (MTTF equals around 5 days). The reliability of microglia was set to 0.999 (MTTF equals around 1000 days). The achieved results are shown in Fig. 5.4. The main conclusion from obtained results is that application of microglia or astrocyte can increase the mean time to failure of the system by about 7.35%.

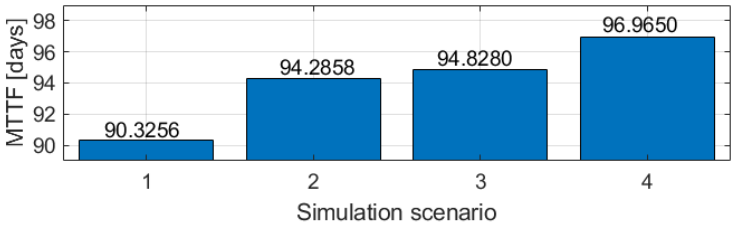

FIGURE 5.4: Simulated network mean time to failure

To illustrate the possibilities of the proposed approach, we changed the reliability models of devices from constant values to distributions (i.e., to model the situation when the probability of device failure changes in time). The reliability of a node (i.e., a battery-powered device) can be represented as 2P exponential distribution with ρ parameter (being a scale parameter) and ϱ parameter (being a location parameter) [182] specified as

$$f(t) = \rho e^{-\rho(t-\varrho)}. \tag{5.6}$$

In Fig. 5.5, the reliability distribution over time of each device used in the simulation can be found. The parameters of the reliability distribution of particular devices are the following: for neuron $\{\rho = 9515.5, \varrho = 904.4\}$, for neuron with increased failure rate $\{\rho = 2195.9, \varrho = 977.9\}$, and for microglia $\{\rho = 16835.1, \varrho = 830.8\}$. The values of the average lifetime of each device are typical for electrical devices and are equal to around 2 years for microglia-inspired node, one year for wireless transceivers (corresponding to neurons) and three months for neurons in an area with a higher failure rate. The gamma parameter shifts the reliability distribution to prevent a situation where a just deployed network fails.

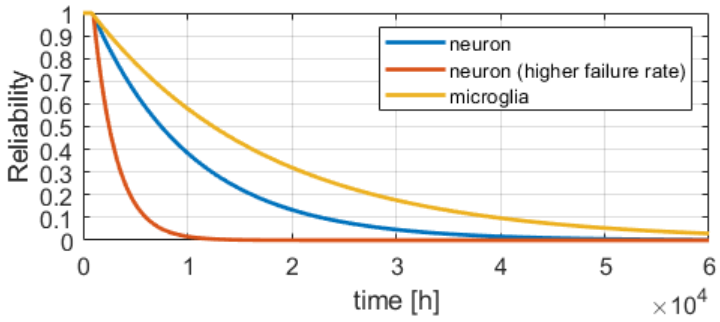

FIGURE 5.5: Use case A — reliability of devices

In Fig. 5.6 we can find that the reliability of the network in each moment of time is higher, when we use microglia or astrocyte nodes. The highest value of the reliability can be achieved using both microglia and astrocyte nodes.

Use case B - availability

In order to verify our solutions in more realistic scenario we changed link reliability model from simple one (equation 5.2) to log-normal shadowing radio propagation model (equation 5.4). The standard deviation of shadowing was set to $\sigma = 2$, and the pathloss exponent was set to $\eta = 2$. The required signal-to-interference-plus-noise ratio was specified as 13.2 dB. The operating frequency of the system was - as previously - set to 3.5 GHz. Exponential distribution was used to model the reliability of the devices in the network. The mean time of exponential distribution was set to 1000, 2000, 700 hours, respectively, for neurons, microglia, and neuron in an area with a higher failure rate.

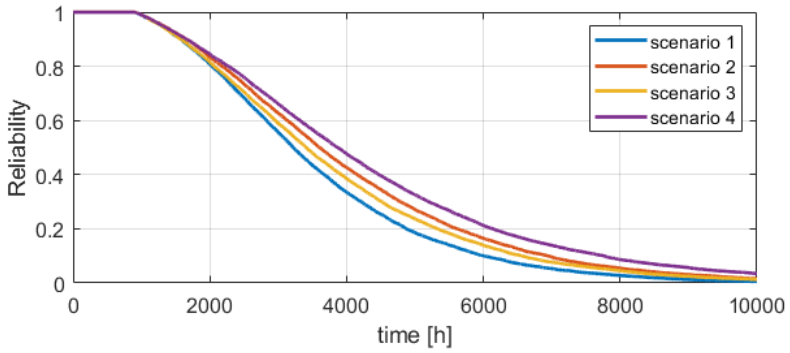

FIGURE 5.6: Use case A — reliability of the analyzed network

In Fig. 5.7, one can notice that the system with a more realistic link model behaves similarly to the simple link model. In particular, the system in the reference scenario (Scenario 1) achieves the lowest availability, and the system is operating in the fourth scenario - the highest availability. Moreover, the availability values achieved in the second and third scenarios are between the first and fourth scenarios.

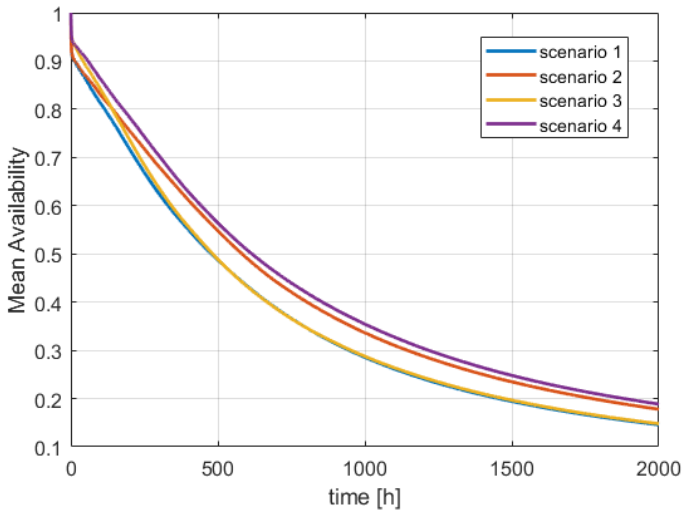

FIGURE 5.7: Use case B — mean availability of proposed network

Mean availability in different time stamps behaves in the same way, as presented in Fig. 5.8. Mean time required to achieve availability equal to 0.5 is lowest in reference scenario (first one), the application of microglia or astrocyte increases this value, and the highest value can be achieved using both of them. It is worth noting that the mean availability at time 2000 hours is almost 30% higher in fourth scenario than in first scenario. The mean availability at time 800 hours is around 20% higher in fourth scenario than in first scenario. It shows that proposed solutions can bring higher benefits in long time of the network operation.

Conclusions and summary

This work has evaluated a futuristic vision for wireless communications in dense wireless networks. We stated that in such a scheme, one could benefit from observing HNS and applying specified solutions. We have proposed the application of microglia and astrocyte nodes for achieving high system reliability while keeping the communication process highly simplified. We have shown that the inspiration from the human nervous system could be implemented in wireless networks and, at the same time, improve system performance.

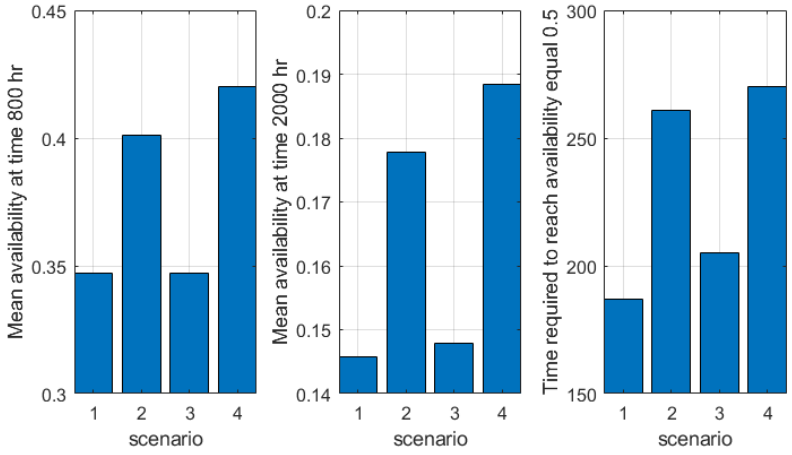

FIGURE 5.8: Use case B — simulation results

However, proper node placement in the proposed solution is critical and should be widely investigated (particularly in various network topologies). The proposed application was evaluated in the case with a realistic wireless link model. Both within a network with a constant failure rate (typical network) and within a network with exponential failure rate distribution, using proposed solutions, there is the possibility to improve the network's reliability.

A compact summary of the use of contextual information to improve spectral efficiency is presented in Table 5.1 below.

Ph.D. candidate's publications considering problems discussed in this section	[177], [178], [180], [188], [189], [190], [191]
Context information	The delay in the transmission of messages by neighboring nodes; emergency situations outside the analyzed network
Influence on the system	Use of additional (emergency / backup) network nodes; increasing the power of some nodes (increasing the range)
Impact on spectrum efficiency	Increased network lifetime; possibility of longer maintenance of spectral efficiency
Comment	By using inspiration from the operation of the nervous system (glial cells), it is possible to extend the life of the dense radio network and thus improve the spectral efficiency (over a long period of observation)

TABLE 5.1: Summary of work presented in chapter 5.1

5.2 Research topic 2: Brain-inspired data transmission in dense wireless network

The previous section analyzed the reliability and availability of dense networks modeled through HNS inspirations. Now we focus on the performance analysis of such an approach in two ways. First, the theoretical limits have been derived based on stochastic geometry, in particular - based on the percolation theory. Additionally, computer experiments have been carried out to verify the performance of the proposed transmission schemes in four simulation scenarios. Achieved results showed the prospective improvement of the reliability of the wireless networks while applying proposed bio-inspired solutions and keeping the transmission extremely simple.

The type of contextual information in this work is identical to the work described in the previous chapter; however, in this work, the analysis of the network for reliability was performed in a completely different way. The percolation theory was used here, which statistically shows the impact of the proposed solutions on the reliability and general operation of networks with random nodes location. Therefore, the presented considerations concern the general structure of the dense network - and not its specific implementation. The influence of the presented solutions on the spectral efficiency is such that the minimum number of devices has been determined through the percolation theory, which enables the proper functioning of the network - i.e., the possibility of sending messages between the ends of the network. Minimizing the number of devices in such a network minimizes the interference generated by other nearby networks, improving overall spectral efficiency in a given area.

Motivation and state-of-the-art analysis

In today's network deployment, reliability plays a significant role, as already described in Sec. 5.1. The messages have to be delivered correctly with a very low level of possible transmission failures [192, 193]. In order to correctly assess the reliability of the proposed solutions, deterministic methods such as Fault Trees, RBD, or Markov chains are often used [194]. RBD has been discussed in Sec. 5.1. Unfortunately, in the case of dense networks with a significant number of nodes, the problem of the high computational complexity of these methods becomes crucial. For this reason, the authors used stochastic geometry [195, 196], or more precisely, the percolation theory, to assess the reliability of the dense wireless system. Particularly noteworthy here is the percolation threshold, which can be used to determine the critical number of nodes necessary for the correct operation of the assumed network. Initial results have been presented in [177, 180, 197], wherein [197] the percolation was applied to evaluate the reliability of wireless network under different nodes density, in [177] the impact of microglia inspired nodes were tested in case of distributed antenna systems, and in [180] network nodes was evaluated in terms of reliability in the case of the limited lifetime of nodes. All mentioned initial works use an idealistic transmission model, which omits a very important aspect in the case of a dense wireless network - interference. In this research, we extend this work by including an analysis of interference impact on reliability.

Moreover, in [180, 191, 197], we have applied two research methodologies to evaluate the performance of the biology-inspired dense wireless networks. In particular, we have adjusted the classic LOAD - next generation (LOADng) [198] and implemented it in the considered dense wireless transport network. In this case, four different types of HNS-based inspirations for dense wireless networks have been tested. Next, the theoretical analysis using percolation theory has been applied and verified through extensive computer simulations. However, none of our prior work evaluated the real impact of mutual (self-)interference on the system's overall performance.

As we consider a fully distributed system (i.e., the one with no central coordination), the probability of simultaneous data transmission by many nodes in their close vicinity may be high. Thus, it is necessary to consider the presence of such phenomena. The main contribution of this work is the evaluation of the impact of interference on the system performance. We did it in two ways; first, we verify the impact of interference in such dense wireless systems by application of the percolation theory, and second, we carry out extensive computer simulations, where the LOADng algorithm is modified by adding a back-off procedure.

We present our system model and scenarios selected for investigation and discuss the research problem, i.e., evaluating the expected impact of self-interference phenomena. Next, we deal with the reliability analysis, including percolation theory and its implementation in dense wireless networks. Achieved simulation results are then discussed in the following section, and finally, the work is concluded.

Related work

As emphasized already, humans have been consistently highly inspired by the functioning of our world and nature, particularly the human body; these inspirations led to numerous significant findings and discoveries. In computer science, various algorithms and solutions are motivated by observing nature. One can mention, for example, solutions based on the behavior of bees, bumblebees, or ant-colony, in general, swarm intelligence [199–201], an algorithm based on findings in genetics, but also solutions like simulated annealing which mimics the behavior of the fabric processing. Recently, the most popular solutions are related to the application of the neural networks in their various configurations (like convolution neural networks, recursive neural networks, etc.), and implementation contexts (computing, feature recognition, automation, networking) [202–204]. It is also worth mentioning that the behavior of bees (swarm) has inspired the design of the whole communication and networking frameworks and protocols, like ZigBee [205]. However, when projecting the brain inspiration on wireless communications, the number of publications is not that high, suggesting that this research domain is still unexplored.

Ultra-dense wireless networks and their biological counterparts

In this part of the thesis, we consider a highly dense network consisting of N wireless nodes deployed randomly over a certain square area of size D, as illustrated in Fig. 5.9. Each wireless network node may act as a transmitter (source), a receiver (sink), or relay the message. In other words, the network of all wireless nodes may be treated as some sort of transport network. These wireless nodes operate in the same frequency band (central frequency f_c and bandwidth B); thus, when transmitting at the same time, they may cause mutual interference. Moreover, we assume that any two wireless nodes which are close enough to receive the signal with the power above some threshold create the wireless link.

The illustrative situation is shown in Fig. 5.9, where the light-green circle represents the coverage area of the transmitting node, and the common part of two such areas are marked by orange and represents the interference area. All nodes within the interference area are susceptible to harmful interference and degradation of the signal-to-interference-plus-noise metric. Without loss of generality, in our further analysis, we select one of the nodes as the transmitter and the other distant node as the destination node for the reception of this message; the other nodes lying between them are treated as relays. As the network is dense, we follow our prior inspirations from the HNS, which we recap briefly below.

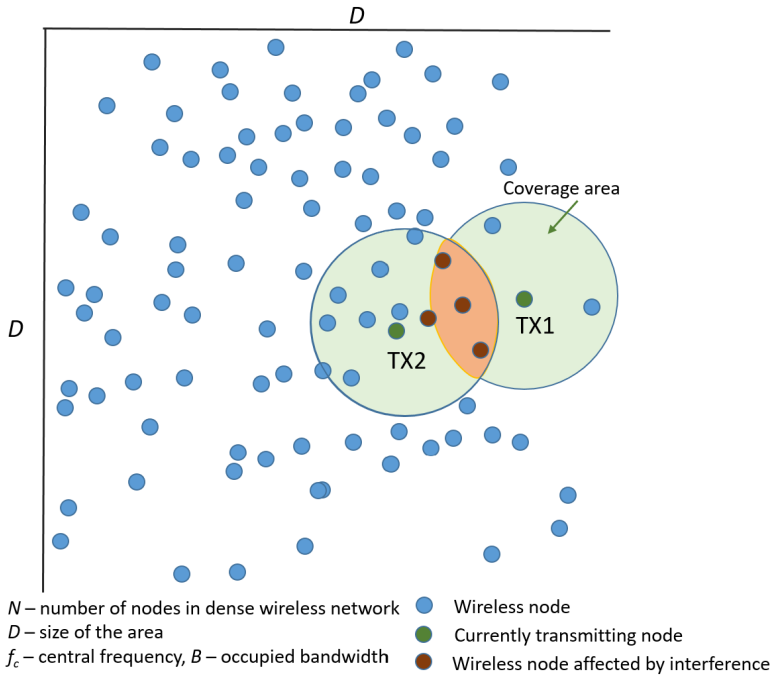

FIGURE 5.9: Considered dense wireless network

5.2.1 Network reliability assessment through the percolation theory

As discussed in Sec. 5.1, one of the seriously considered metrics in terms of evaluating future wireless networks is reliability. Various methods can be used for reliability assessment, e.g., Markov Chains, Fault Trees, or RBD. However, these approaches do not reflect well or easily the stochastic nature of such dense wireless networks, whose performance strongly depends on the current node distribution and node load.

Application of the percolation theory

Stochastic geometry allows modeling and interpreting the impact of various processes and the random variables characterized by various spatial distributions. In other words, the impact of randomness in the spatial domain can be evaluated. Among various tools known from stochastic geometry, percolation theory allows specifying the value of the probability when the network will become blocked (no path may be identified between the source and the destination) for a given network structure (i.e., the spatial distribution of nodes) [206–208].

As a physical phenomenon, percolation describes the mechanism by which porous material is permeated. Here, a very common example may be the coffee brewing process, where the water flows through coffee beans to extract the appropriate ingredients. Depending on the type of coffee and its amount (densely or loosely grounded coffee, amount of coffee, etc.), the percolation process will run differently. One may apply percolation theory to describe this process, where the path in the graph defines the liquid flow, and the graph represents the material (coffee in this example). In the case of wireless networking, the theory of percolation allows analyzing the message passage through networks with various densities and spatial distributions, which we can call permeability. In that context, one may observe that a critical parameter called percolation threshold exists for a given material (network structure), which specifies the limit, and exceeding this limit informs about the lack of permeability.

In particular, the percolation threshold defines the percentage of nodes that must be active to guarantee permeability. Thus, for a given set of nodes N and the achieved percolation threshold p_T, the minimum required a number of nodes that guarantee the proper functioning of the network is equal to $\lfloor p_T \cdot N \rfloor$, where $\lfloor \cdot \rfloor$ is the floor function.

Let us assume that the wireless network is represented in the form of a graph, where the wireless transceiver corresponds to the node and the valid wireless link to the graph edge. The corresponding transmission range will be achieved by assuming some fixed maximum transmit power. One may observe that, for the fixed range, when the density of nodes decreases, the probability of lack of permeability decreases. Analogous observations can be made when reducing the effective transmission range (e.g., reduced transmit power or increased observed interference at the reception node). The network graph contains some clusters (subgraphs) if the permeability is not achieved. Following the authors of [206–208], the percolation threshold is reached at the moment when the size of the second-largest cluster (denoted hereafter as SG) in the graph reaches its maximum.

Following [197], we derive the percolation threshold for the dense wireless node to show the reliability of the bio-inspired communications schemes; however, in this thesis, we consider a significant aspect, mainly the presence of self-interference, as illustrated in Fig. 5.9. We assume that the network nodes are distributed according to the spatial Poisson process and are operating asynchronously. In our simplified case, we state that there exists a reliable wireless link between two wireless nodes, when the observed SINR is above some threshold θ^*, i.e., SINR $\geq \theta^*$. As in [208], the desired signal may be expressed as $S = \frac{P_0 \prod_k X_k}{R^{2b}}$, where X_k represent the existing propagation effects in the wireless channel (such as path loss $X_k = 1$ or log-normal fading $X_k = e^{2\sigma G}$, for G being the normally distributed random variable of zero mean and unit variance). Moreover, R is the distance and η amplitude loss exponent. Analogously, the total sum-interference from all $j = 1, 2, ..., J$ simultaneously transmitting nodes can be computed as $I = \sum_{j=1}^{J} \frac{P_I \Delta_j \prod_k X_{j,k}}{R_j^{2b}}$, where $X_{j,k}$ represents propagation effects in link to device j. In our case we assume that the network is not synchronized, thus, in order to describe the transmission profile (i.e., the duty cycle) we introduce the random variable $\Delta \in [0, 1]$. Thus, the total aggregated interference I can be defined utilizing the skewed stable distribution [208]:

$$I \sim S\left(\alpha = \frac{1}{\eta}, \beta = 1, \gamma = \pi\lambda C_{1/b}^{-1} P_I^{1/b} \mathbb{E}\left\{\Delta_j^{1/b}\right\} \prod_k \mathbb{E}\left\{X_{j,k}^{1/b}\right\}\right). \tag{5.7}$$

where Δ_j is the duty-cycle factor associated with interferer j. Here, in this generic formula, the term C_α is defined as

$$C_\alpha = \begin{cases} \frac{1-\alpha}{\Gamma(2-\alpha)\cos(\pi\alpha/2)}, & \alpha \neq 1 \\ 2/\pi, & \alpha = 1 \end{cases}, \tag{5.8}$$

where $\Gamma()$ denotes the gamma function. Next, the P_I term stands for the transmit power of the interfering nodes. However, we assume that the maximum power is the same for the desired node and the interferers. The introduced skewed distribution $S(\alpha, \beta, \gamma)$, valid for $\alpha \in (0, 2]$, $\beta \in [-1, 1]$ and $\gamma \geq 0$, can be characterized by its skewness β, and it possesses the corresponding characteristic function

$$\omega(w) = \begin{cases} \exp\left(-\gamma |w|^\alpha \left[1 - j\beta \text{sign}(w) \tan(\frac{\pi\alpha}{2})\right]\right), & \alpha \neq 1 \\ \exp\left(-\gamma |w| \left[1 + j\frac{2}{\pi}\beta \text{sign}(w) \ln(w)\right]\right), & \alpha = 1 \end{cases} \tag{5.9}$$

It is well known that the probability density function of our searched random variable I can be calculated using inverse Fourier transformation

$$f(x) = \frac{1}{2\pi} \int_{-\infty}^{\infty} e^{-isx} \omega(s) ds. \tag{5.10}$$

In our case, we assume that the nodes are densely deployed over a certain area, thus the dominant channel effect will be path loss at the line-of-sight link, i.e., $X_k = 1$. Again, following the authors of [208], the probability of SINR above-assumed threshold θ^* can be derived as

$$P\left\{\text{SINR} \geq \theta^*\right\} = F_I\left(\frac{P_0}{r_0^{2b}\theta^*} - \sigma_n^2\right), \tag{5.11}$$

where σ_n^2 is a noise level, r_0 is a distance between nodes, η is a propagation environment coefficient, P_0 is a transmit power of the desired signal, and F_I is a cumulative distribution function of random variable I. Consequently, Formula (5.7) can be simplified as

$$I \sim S\left(\alpha = \frac{1}{\eta}, \beta = 1, \gamma = \pi\lambda C_{1/b}^{-1} P_I^{1/b} \mathbb{E}\left\{\Delta_i^{1/b}\right\}\right), \tag{5.12}$$

where α, β, and γ are charac-teristic function coefficients. Consequently, the corresponding characteristic function can be derived as

$$\omega(w) = \begin{cases} \exp\left(-\gamma\left|w\right|^{\frac{1}{\eta}}\left[1 - j\text{sign}(w)\tan(\frac{\pi}{2b})\right]\right), & b \neq 1 \text{ (nonlineofsight)} \\ \exp\left(-\gamma\left|w\right|\left[1 + j\frac{2}{\pi}\text{sign}(w)\ln(w)\right]\right), & b = 1 \text{ (lineofsight).} \end{cases} \tag{5.13}$$

In our highly dense wireless network, we assume the presence of line-of-sight, and the above formula for $b = 1$ is selected. Moreover, the value of γ is defined as:

$$\gamma = \pi\lambda C_1^{-1} P_I \mathbb{E}\left\{\Delta_i\right\} = \frac{\pi^2}{2}\lambda P_I \mathbb{E}\left\{\Delta_i\right\} \tag{5.14}$$

as $C_1^{-1} = \frac{2}{\pi}$. Thus, the distribution of the aggregated interference can be expressed as:

$$I \sim S\left(\alpha = 1, \beta = 1, \gamma = \frac{\pi^2}{2}\lambda P_I \mathbb{E}\left\{\Delta_i\right\}\right). \tag{5.15}$$

Finally, the probability density function can be computed as:

$$\begin{aligned} f\left(x\right) &= \frac{1}{2\pi}\int_{-\infty}^{\infty} e^{-iwx}\omega(w)dw \\ &= \frac{1}{2\pi}\int_{-\infty}^{\infty} e^{-iwx} e^{-\gamma|w|\left[1+j\frac{2}{\pi}\text{sign}(w)\ln(w)\right]}dw \\ &= \frac{1}{2\pi}\int_{-\infty}^{\infty} e^{-iwx} e^{-\frac{\pi^2}{2}\lambda P_I \mathbb{E}\{\Delta_i\}|w|\left[1+j\frac{2}{\pi}\text{sign}(w)\ln(w)\right]}dw. \end{aligned} \tag{5.16}$$

The above formula can be calculated numerically and tabulated, allowing for direct calculation of the searched probability $P\left\{\text{SINR} \geq \theta^*\right\}$.

Experiment setup

We conducted extensive computer experiments to evaluate the investigated concept of highly simplified transmission in dense wireless networks. The whole simulator was prepared using Matlab version with standard libraries, and all simulation runs were carried on the standard personal computer PC with specification i7-6500u, 12 GB RAM, under Windows 10 system. In our experiment analysis, we apply normalized values to generalize it and make it independent from the applied physical values. Thus, the analyzed system consists of a network of $N = 30$ randomly distributed neuron nodes. These devices mirror neurons in the nervous system, i.e., they are designed to transmit information to each other. Moreover, once the neuron-nodes are deployed, $M = 0.1N$ microglia-nodes are added, also deployed uniformly in the same area. Please note that we intentionally do not deploy astrocyte nodes in this investigation phase.

TABLE 5.2: Simulation parameters used in the first phase of the study

Parameter	Description	Value
N	number of the neuron nodes	30
M	number of the microglia nodes	$M = 0.1 \cdot N = 3$
D	size of the considered area (related to the cell range size)	10 [distance units]
r	transmission range (cell range)	1 [distance unit]
$P_0 = P_I$	transmit power of any node	1, 10, 30, 40 or 50 [power units]
σ^2	noise power	1 [power units]
θ^*	required SINR level	1 [linear scale] or 0 [dB]

The analyzed area is a square with the side $D = 10$. The devices are characterized by the transmitting power $P_0 = P_I$ and the range $r = 1$. The required signal to noise and interference level was set at $\theta^* = 1$ (in a linear scale) and the noise level at $\sigma_n^2 = 1$. All simulation parameters used in this part of our work are summarized in Table 5.2. During the experiment, we assume that the simulations search for the percolation threshold value that ensures the correct operation of the network. The simulations were averaged (repeated) over different topologies and device operation probability levels. An example of the analyzed topology is shown in Fig. 5.10. One may observe the presence of wireless nodes (neurons, denoted by black dots), the source, and the destination.

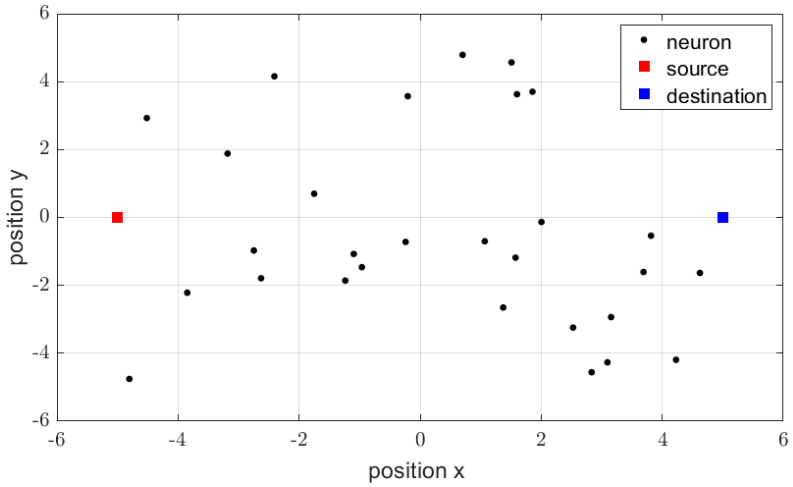

FIGURE 5.10: Example of the analyzed topology

In the following results, we show the size of the SG cluster as the function of the probability p_c, which is the probability of proper functioning of any wireless node. Each simulation result is presented as a solid line, and the additional dashed line is a fourth-degree polynomial approximation. As mentioned above, the greatest value of SG is achieved at the percolation threshold, i.e., $p_T = \arg\max_{p_c}(SG(p_c))$. The smaller the p_T, the better the network's reliability (i.e., fewer nodes are required to guarantee permeability). In other words, when the percolation threshold decreases, the network will be able to operate in heavier conditions (with greater error probability at a certain link). In Fig. 5.11 and Fig. 5.12, one may observe the changes of SG as function of different transmit power levels and for different number of neuron-nodes. One may observe that when the transmit power increases (so the coverage area increases as well, and, in consequence, for the fixed node density, the number of nodes located in interference areas increases), the percolation threshold slightly shifts left. However, the minimum is achieved for $p_c \approx 0.25$. However, the change in node density shifts the curves left and emphasizes the effect that for higher transmit power, the percolation threshold also decreases.

In Fig. 5.13, one may observe the changes of SG as function of different number of nodes. These results are mainly two selected lines in Fig. 5.11 and Fig. 5.12 for the same level of power $P_0 = P_I = 30$ but for different number of nodes, i.e., $N = \{30, 100\}$.

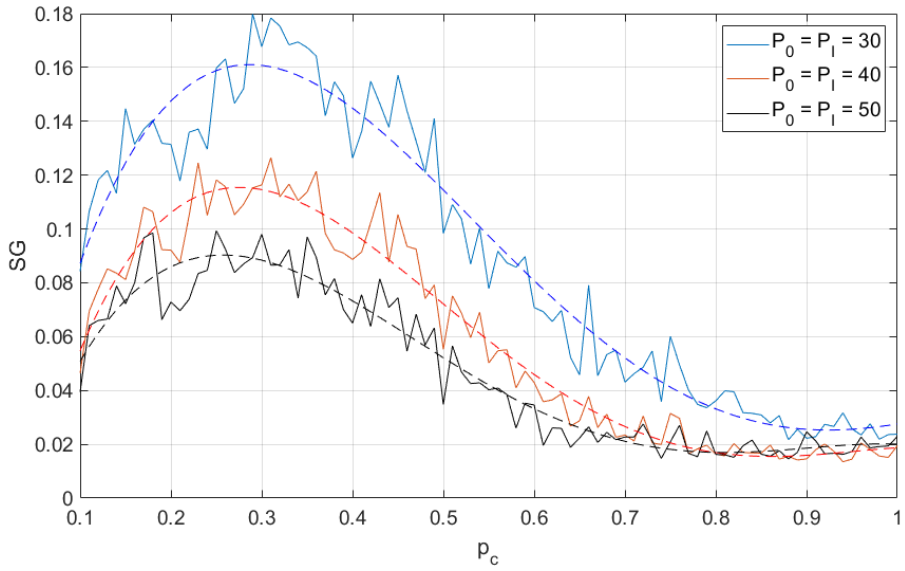

FIGURE 5.11: Second largest cluster size as function of node operation probability (different transmit power levels); 30 neuron-nodes. Dashed lines are a fourth-degree polynomial approximation

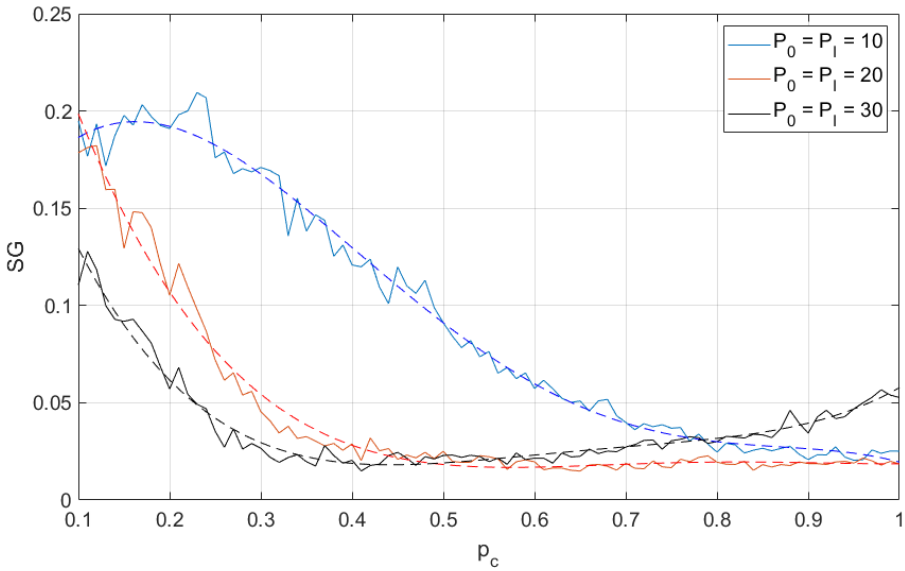

FIGURE 5.12: Second largest cluster size as function of node operation probability (different transmit power levels); 100 neuron-nodes. Dashed lines are a fourth-degree polynomial approximation

Finally, in Fig. 5.14, the impact of the duty cycle on the network reliability is shown. Interestingly, as the SG size changes with the mean duty cycle change, the network reliability (expressed employing the percolation threshold) is rather unchanged (around 0.2).

In this section, we derive theoretically how the percolation threshold can be derived in the dense wireless network, as discussed in detail in [208]. However, the percolation threshold provides only some insights into the overall theoretic limits of the dense wireless network. Thus, in the following section, we investigate the network reliability by utilizing extensive computer simulations.

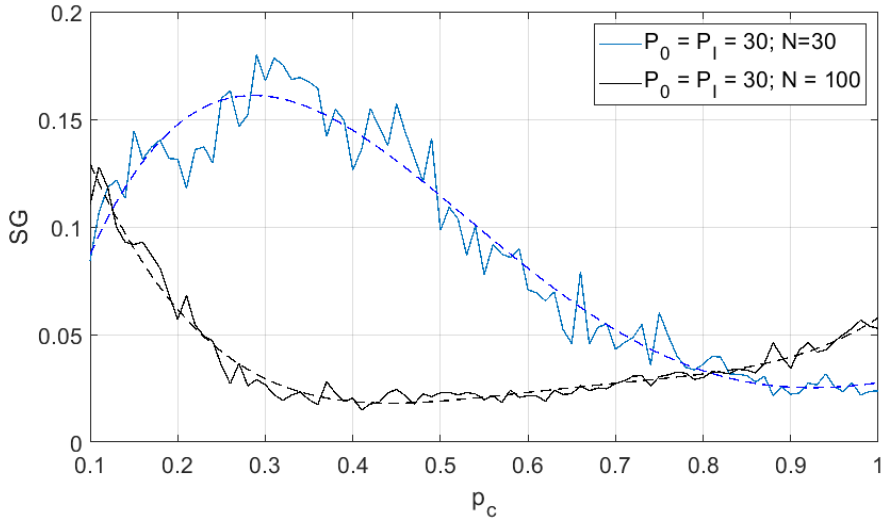

FIGURE 5.13: Second largest cluster size as function of node operation probability (different number of nodes). Dashed lines are a fourth-degree polynomial approximation

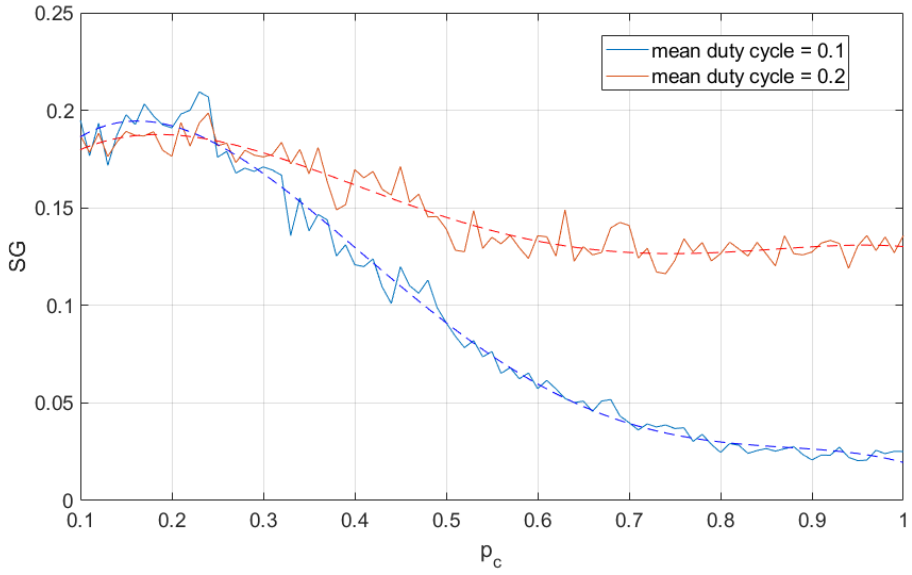

FIGURE 5.14: Second largest cluster size as function of node operation probability (different mean duty cycle). Dashed lines are a fourth-degree polynomial approximation

Bio-inspired wireless network reliability—analysis by means of computer experiment

As the previous section discussed some theoretical limits for the reliability of the dense wireless network, in this part, we analyze it through computer simulations and experiments. We have incorporated self-interference in the research. Thus, this section describes the simulation results in which the proposed concepts were tested in the network where the messages are sent. This network consists of many nodes and enables the communication between users who are at the edge of the network using the LOADng routing protocol. In particular, a single random network topology includes 400 basic network nodes (neurons) and 80 additional network nodes (microglia). These devices are distributed over an area of 30 km by 24 km on a grid with a side of $N_Q = 1$ km. The adopted carrier frequency for this system is $f_c = 2.45$ GHz, the band is $B = 5$ MHz, the required signal-to-noise ratio and interference is $\theta^* = 3$ dB, and the transmission power is 2 dBm.

We assume that the connection between any two points may be corrupted with some probability. The probability of a node breakdown is arbitrarily fixed to 0.05, and the mean time to failure is set to 5000 iterations. The simulation time is 10,000 iterations. The average time between messages is 50 iterations. As above, for the sake of clarity, we collect all important simulation parameters used in this part of our work in one table (Table 5.3). To deliver data from source to the destination, the well-known LOADng algorithm was selected.

Table 5.3: Simulation parameters used in the second phase of the work

Parameter	**Description**	**Value**
N	number of the neuron nodes	400
M	number of the microglia nodes	80
A	number of the astrocyte nodes	1
$x \times y$	sizes of the considered area	30×24 km
N_Q	grid size	1 km
f_c	center frequency	2.45 GHz
B	frequency bandwidth	5 MHz
$P_0 = P_I$	transmission power	2 dBm
θ^*	SINR threshold	3 dB

Mainly, in the beginning, the network nodes do not have any information about neighbor nodes. When some node discovery is necessary, a broadcast message is sent to find a specific node. Nodes that are not a destination of such message simply transmit this broadcast message further, and the node which is a destination of such message replies with different types of message. Such reply selects a route based on some metric (commonly the distance in the form of hop count), and each node on this route updates its routing table. In the case of problems in the existing routing map, e.g., one node does not respond, another type of message is sent, which informs all nodes on the route about the problem. The reaction to this message can be turning on microglia-based nodes and dropping routing entities due to such node activation. Then, a new route to the destination needs to be discovered in the same way as described. However, to deal with interference problems in the network, the applied LOADng algorithm was modified. Mainly, the Binary Exponential Backoff algorithm was implemented. In the case of collision (i.e., when at least two transmitters start their transmission at the same time causing harmful interference and degrading effective SINR), the current value of the backoff-window is randomly selected from the allowed range of integer values, and another try for data transmission is repeated after the back-off time is over. Such binary exponential back-off time increases the network reliability, as it introduces some sort of collision mitigation, but it is achieved at the price of longer message processing time. Thus, it increases the average data delivery time within the network and degrades the energy consumption.

For performance evaluation, we consider again four scenarios:

- Scenario I: Only neuron-nodes are deployed; this scenario is also used as reference
- Scenario II: Both neuron- and microglia-nodes are available
- Scenario III: Both neuron- and astrocyte-nodes are deployed
- Scenario IV (the complete scenario): All kinds of nodes are deployed (i.e., neuron-nodes, microglia-nodes, and astrocyte-nodes)

As mentioned above, neuron-nodes and microglia-nodes are deployed uniformly over a certain geographical area, where the number of microglia-nodes constitutes 10% of neuron nodes. If astrocyte nodes are applied, we assume the presence of one centrally deployed astrocyte node.

Moreover, in our experiments, we assume that a certain level of reliability has to be achieved, and we observed its cost in all scenarios. The structure of the simulator was prepared in such a way that it operates in a slotted mode; mainly the time is split into equal time slots (called iterations). One message may be sent and received during one iteration by each node. The analysis of the simulation results was carried out in two ways. First, the delay in delivering packets expressed as the difference between the iteration number in which the message was sent and the iteration number in which the message reached its destination was analyzed. Second, the analysis of the energy consumption was expressed by the sum of the transmission power in subsequent iterations. In the simplified transmission model, we treat transmitting power as the only component of the consumed power because it is the largest part of the consumed power in such systems.

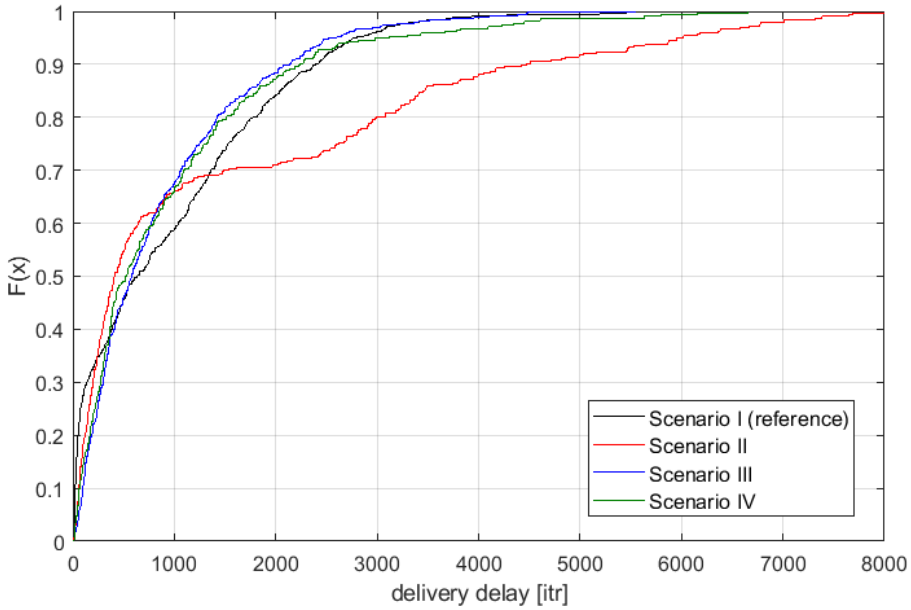

FIGURE 5.15: Distribution of delivery confirmation delay

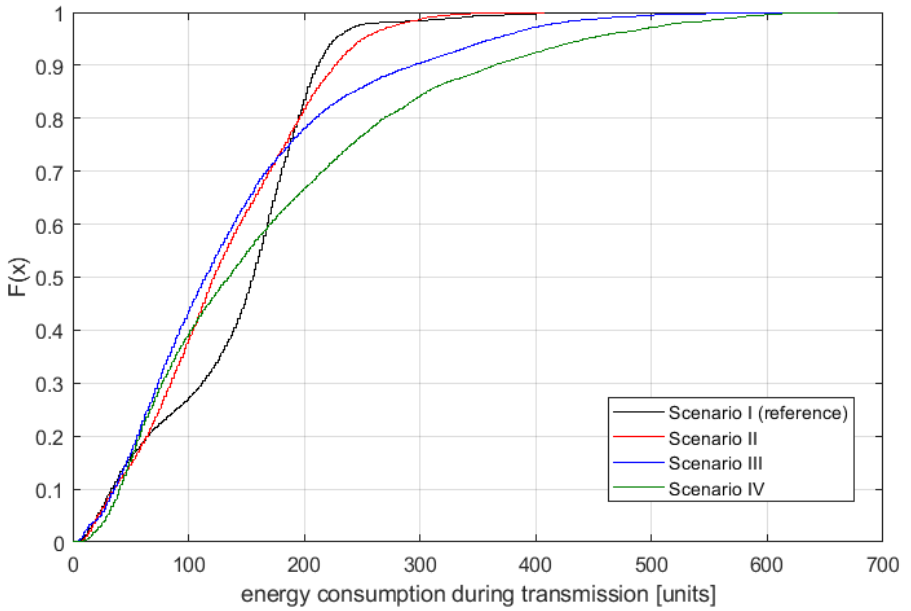

FIGURE 5.16: Distribution of energy consumed during transmission

In Fig. 5.15, the distribution of the delivery confirmation delay is plotted for the four scenarios. One may observe that the inclusion of either microglia or astrocyte nodes improves the performance in some ranges compared with the reference scenario (black line). For example, in Scenario II, there are more situations where very small delivery delays are present. At the same time, the addition of astrocyte-node improves the overall performance significantly. The best results are achieved in general in Scenario III. However, these results cannot be analyzed without association with the overall energy consumption, as shown in Fig. 5.16. Here, one may observe that, to some extent, Scenarios II-IV are better than the reference one, where only neuron nodes are considered. However, the most important conclusion is network reliability when applying the highly simplified transmission procedures. This analysis has to be done for specific assumptions; for example, one may request that the maximum allowed delay in the considered networks is less than 100 hops (iterations) or that the total consumed energy during packet transmission is below 100 energy units. Having such constraints allows us to "slice" vertically the results shown in Fig. 5.15 and Fig. 5.16. For example, if only 100 energy units are allowed, then Scenarios II and III provide the best results. Moreover, the reference scenario seems to be the best for highly stringent scenarios. It proves that the simplified transmission scenario allows a certain reliability level.

Discussion

In this work, we analyze the reliability of biology-inspired dense wireless networks. Our considered network is characterized by extreme simplicity of data transmission, i.e., no advanced channel coding is applied. It means that network reliability has to be achieved differently. First, we can gain from the high density of deployed nodes, and in most cases, the line-of-sight transmission is possible. It has been proved that such a simplified transmission scenario can achieve reasonable performance expressed in terms of observed message delivery delay or overall energy consumption for a given reliability level. Second, besides deploying only simple neuron nodes (whose basic functionality is to relay messages as only the received signal-to-interference-plus-noise ratio is above some threshold), one may also deploy some nodes with improved functionality.

If we look at the results of the percolation experiment, we can see that it is a very good method for assessing the reliability of a wireless network. For example, when we analyze the impact of the number of nodes on the reliability of the network, we see that increasing the number of nodes (in this case from 30 to 100) significantly lowers the percolation threshold—that is, it is possible to use less reliable devices in this case. However, the analysis of the power of the nodes shows that increasing the power increases the range of the nodes, which improves the reliability (as a single node has the chance to connect through more distant nodes). On the other hand, however, we do not observe a significant decrease in the percolation threshold (increase in reliability) because higher power also means a greater level of observed interference—which prevents (or at least limits) reliable transmission. Thanks to the use of percolation, we can analyze the behavior of the wireless network—what is important—regardless of its topology (we assume that it is a random value). In this area of the conducted experiments, it would be worth considering a network where we have the ability to control power levels, which would allow to some extent, to manage interference throughout the network. Of course, this approach would improve the network's performance, but at some cost—increasing the complexity of the entire network. Another aspect worth investigating is the analysis of the radio environment in which there is not always a direct line of sightline.

The analysis of the part concerning the simulation of a specific wireless network shows that in terms of message delay and energy consumption, a network using only basic nodes inspired by neurons performs satisfactorily. Median message delay does not significantly deviate from

the minimum values (given the presence of interference in the network); however, some large or extreme delays also occur (e.g., 95th percent delays). In some specific applications or network configurations, however, it is possible to improve the underlying performance of the neurons themselves by applying some kind of support or intelligence in the network (using devices other than neurons as part of the devices). The same situation occurs in the human nervous system, where transmission between neurons takes place and is possible; however, it is improved by the use of glial cells. In the case of the simulations carried out, it can be noticed that, for example, the use of additional devices inspired by microglia (scenario two) reduces the lowest network delays so far. However, at the same time, extending the longest delays in the network—i.e., it is possible to obtain lower delays at the price of lower delay stability. In general, these simulations have shown that replacing some devices with more extensive ones (but not all devices) allows for improving or adjusting the behavior of the entire network. As in the case of percolation analysis, it is possible to consider introducing some kind of node control (e.g., power control) here.

Conclusions resulting from the presented results concerning the modeling of a dense wireless network are certainly the possibility of using percolation theory to check the network behavior (in a stochastic way). Secondly, in dense networks, we can achieve higher reliability when we apply reduced requirements for data processing (simplification of transmission). This aspect is extremely important in relation to sensor networks where energy consumption is crucial, especially in the case of networks where we cannot replace the battery and each node is limited by the energy reserves it has, and energy harvesting solutions are considered in these networks. In this type of network, the presented simplification of transmission is the most promising. Of course, this requires further research, particularly the analysis of the impact of the radio environment, the analysis of the aging of devices, and the analysis of failure rates. Device aging and failure frequency are often expressed as reliability versus time, which adds another dimension to the analyses presented in this article.

Summary

Summarizing the overall results, one may conclude that when the dense wireless network is considered, there is a space for applying highly simplified transmission schemes while keeping the network reliability at an assumed level. Thus, there is a space for further research towards the implementation of other HNS-focused solutions.

A compact summary of the use of contextual information to improve spectral efficiency is presented in Table 5.4 below.

Ph.D. candidate's publications considering problems discussed in this section	[191], [194], [197], [209], [210]
Context information	Observation of a malfunction (no response) of a neighboring nodes; emergency situations outside the analyzed network; received transmission statistics and routes.
Influence on the system	Use of additional (emergency or backup) network nodes; modification of routes used in the network.
Impact on spectrum efficiency	Increased network lifetime; possibility of longer maintenance of spectral efficiency; minimizing the number of devices necessary for the operation of the network.
Comment	By observing neighboring devices and information outside the network, it is possible to provide an overall (static) improvement in network reliability.

Table 5.4: Summary of work presented in chapter 5.2

Chapter 6

Spectrum virtualization - spectrum management application

In parallel to the trend of reducing cell size, radio access virtualization is considered. A particularly interesting part of the virtualization concept is the radio network management applications and, in particular, the Spectrum Management Application (SMA). Such application can utilize context information to improve its operation, i.e., spectrum management, thus spectrum efficiency.

Taking into account another trend in radio communication, which is virtualization, we present an approach to using contest information for spectrum management in the form of a SMA. In this approach, a certain part of the radio network functionality responsible for spectrum allocation is handled by applications. It also offers a more flexible approach to creating a radio system because if the various functionalities of the system are implemented simply by a specific piece of code, it becomes much easier to modify, replace, and update than in the case of replacing physical devices. With the help of such an SMA it is possible to manage access to the spectrum for individual devices dynamically. Moreover, context information access and utilization can improve this dynamic spectrum management process. The considerations described in this chapter have been divided into three research topics. In first research topic, described in Sec. 6.1, we investigate an experiment that involved applying a SMA to a real network created with the help of the OAI. For this purpose, an application was proposed that, based on information about the available spectrum along with several additional parameters (e.g., the price of using a given spectrum, width, etc.) and a selected set of rules (which defined the current needs of the operator, e.g., cost reduction) decision to choose one of the available frequency ranges. In the second research topic, described in Sec. 6.2, we present an innovative concept for the design of a SMA, where the operator band is distributed between base stations (and, consequently, users) according to the freemium concept. This concept is particularly popular in mobile services and applications. It assumes free access to the service for all users, with a limited scope of these services or a wider range of services and improved quality of service for an additional fee. In the third research topic, described in Sec. 6.3, we show the use of an application (so-called xApp) managing user traffic in an open radio network.

6.1 Research topic 1: SMA as a flexible and efficient resource utilization

Dynamic spectrum access and management is one key enabler to constitute the foundation for a multi-service architecture with a high level of flexibility. In this section of the dissertation, we design and implement the Spectrum Management Application (SMA) as an efficient tool to manage and process different policies and rules defined by various stakeholders such as national regulatory authorities, operators, and licensed shared access. The SMA is an open-source and clean-slate replacement for legacy platform-dependent spectrum management solutions and can provide custom control programmability and agile resource utilization. We also elaborate on the design details of the SMA and show how it can dynamically select the optimal spectrum offers based on different applied rules in time series. Finally, we demonstrate two specific use cases via integrating the implemented SMA prototype on top of the Mosaic5G [211] and OpenAirInterface (OAI) [212] platforms. A detailed description of the proposed solution can be found in the author's paper [213].

Motivation

A dedicated Spectrum Management Application is designed and implemented, based on the generic concept in [214], as a network common control service that operates on top of the Software Defined Network (SDN) i.e., softwarized mobile network. The SMA can manage and process different defined policies and rules. For instance, the National Regulatory Authority (NRA) can define some specific policies for spectrum usage in a particular geographical area to facilitate proper service delivery during a scheduled mass event. Another possibility is that one license owner (operator) may define its policies for spectrum sharing with other interested players, or two collocated operators can define their mutual agreements for spectrum sharing in between. In all cases, the SMA can interpret these policies and make decisions on the eligible ways of spectrum use; which are weighted based on a set of rules defined by the service providers to describe the desired relationships among the interesting parameters (e.g., bandwidth, available time). Finally, the control decisions are enforced toward the underlying Radio Access Network (RAN) by the logically centralized coordinator and controller. At the time of design, the SMA is the first open-source spectrum management tool implemented with a high level of flexibility.

Related works

Traditionally, the usage of a certain frequency band shall follow the set of policies defined by the authorized regulatory authorities, e.g., NRA, and is typically controlled by the dedicated licensing mechanism. Two distinct variants are practically applied in contemporary wireless networks, mainly *license-only* and *license-exempt*. In the former case, the licensee has the only right to exclusive spectrum use, which guarantees that the licensed system is protected from uncontrolled interference within the same band. Contrarily, in the license-exempt case, specific spectrum bands are relaxed from any constraint, and thus anyone who owns certified devices can use these bands. A well-known example is the allocation of WLAN communication in the ISM and U-NII bands, around 2.45 GHz and above 5 GHz, respectively. However, the average spectrum occupancy is still low, even in densely populated areas. Thus various approaches to enable the flexible spectrum access can be applied [215], such as sensing, prediction, and inferring. Hence, a compromise between above two cases can be made, and many solutions have been provided [216], such as LSA, and SAS for CBRS. A more detailed description of related works can be found in Sec. 2.3.

SMA overview

The SMA aims to provide the flexible and agile control logic for utilizing radio spectrum resources in heterogeneous networks. It processes several types of input information (i.e., short-term and long-term policies, sensing data) aggregated through well-defined interfaces, derives spectrum management control decisions (called hereafter *SMA-policy*), and enforces the applied policies via interacting with local or remote RAN Real-Time Controller (RTC). The development of SMA relies on the platform SDK with well-defined Application Platform Interfaces (API) to reveal the virtualized network information and provide network programmability.

Following [214], a high-level architecture of SMA is shown in Fig. 6.1, which includes the spectrum management rules and decision making algorithm. The former relies on several criteria (e.g., from input spectrum management rules) to manage available spectrum offers. For instance, it can pre-exclude some ineligible spectrum offers when their price (e.g., Euro per second) is larger than a pre-defined maximum value. The latter can generate the output *SMA-policy* based on the input short/long-term policies and sensing data to be applied toward the underlying heterogeneous RAN. To enable SMA, we rely on the platform mentioned above SDK to provide a software development environment to simplify the design, development, test, and update of applications. It also includes a group of libraries to provide specific functions/methods to be accessed through one or more API calls. As for the RAN controller, it provides the required control functionalities and interfaces to abstract the underlying network (i.e., north-bound interface, NBi), deploy the spectrum management and sharing policies to the underlying networks through dedicated agents (i.e., south-bound interface, SBi), and exchange information for coordinating spectrum management decisions between network domains (i.e., east-west interface, EWi). Finally, the underlying agents can enforce the *SMA-policy* on the heterogeneous RAN, either being macro cell, small cell or radio unit (controlled implicitly through the Centralized Unit (CU) and Distributed Unit (DU)[1]).

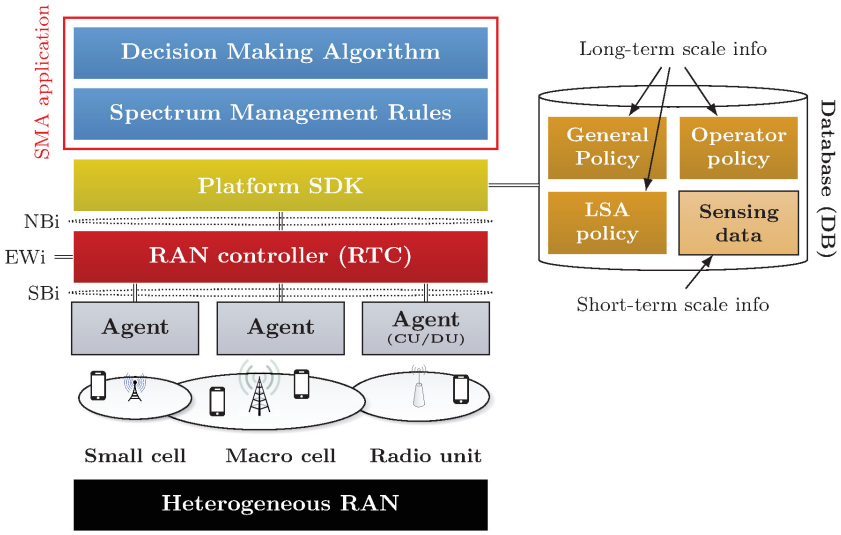

FIGURE 6.1: High-level architecture of SMA

In Fig. 6.2, the processing flow of SMA is shown. First of all, the DB located at the SDK can collect and populate the spectrum-related information, and the SMA can utilize the SDK to load the policy and rules that shall be followed when generating its control logic. Then, the RTC can register to the agent in order to get the latest status that can be loaded from the underlying RANs. These statuses include the spectrum information such as available bandwidth and sensing

[1]Defined by third-generation partnership project (3GPP) in TR38.801.

data to be exposed to the SMA to make the control decisions. After all, the *SMA-policy* will be provided by SMA, validated by RTC, and enforced by agent to the underlying RANs. Further, the base stations (BSs) can optionally provide feedback information (e.g., unfeasible policy, conflict decision) back to the SMA in order to adapt the decisions.

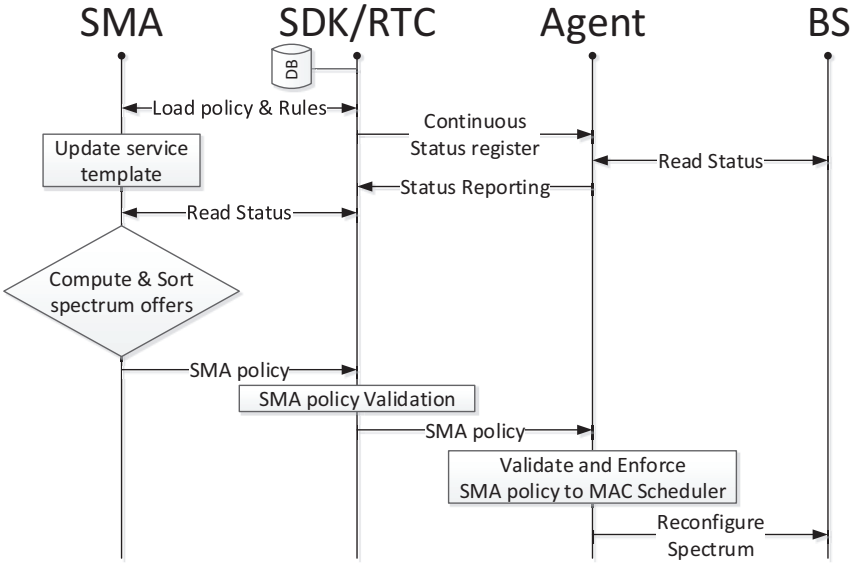

FIGURE 6.2: Processing flow of SMA

To sum up, SMA can leverage the underlying SDK, RTC and agents to utilize available spectrum resource. Specifically, it takes into account various entries stored in the dedicated DBs, and it can analyze the following information:

(a) general policies defined by the NRA for a given region and time

(b) mutual agreements between any two (or more) operators regarding the spectrum sharing

(c) open (for public) spectrum sharing rules, such as those following the LSA, or CBRS approaches, that define how any allowed stakeholder may bid or request from the spectrum licensee on a certain amount of spectrum resources

(d) priorities to be applied while allocating the spectrum among the BSs (for instance, the operator and frequency preferences)

More design and implementation details of SMA are given in the next section.

6.1.1 SMA design and implementation

We hereby provide the design details of SMA and show how the implemented SMA can dynamically select optimal spectrum offers based on different applied rules.

Input and output

In Fig. 6.3, the inputs of SMA include policy and rules. Based on the input policies defined by interested stakeholders, various opportunities for spectrum usage are created, i.e., spectrum offers. Moreover, the input rules can provide the patterns to calculate the weight of each spectrum offer that is defined for each group to select the optimal offer.

- **general policy**: It contains a list of general spectrum usage policies of a specific region or country (provided by Federal Communications Commission (FCC) for US, and Electronic Communications Committee (ECC) for Europe). More specifically, `freq_min`, `freq_max`, `frame_type` and `max_tx_power` correspond to the minimum carrier frequency, maximum carrier frequency, applicable frame type (e.g., Frequency Division Duplex (FDD) or Time Division Duplex (TDD)) and maximum transmission power, respectively

- **operator policy**: It contains the parameters for a list of spectrum offers. These spectrum offers can be shared by several operators with certain utilization rules, which is defined by the same group of operators. Followings are the specific parameters for each spectrum offer:

  - `operator`: Name of operator that defines this policy
  - `freq_min`: A list of lower boundaries of possible bands
  - `freq_max`: A list of higher boundaries of possible bands
  - `busy`: Option that will be used when the activity of other BSs of the same operator is detected between `freq_min` and `freq_max`
  - `idle`: Option that will be used otherwise
  - `sub_freq_min`, `sub_freq_max`: Define a band (possibly sub-band) which can be used when in the "`busy`" state
  - `power_mask`: Define the transmission power mask (interference to the narrowest channels)
  - `min_lease_time`: It serves as the minimal time interval (for example, in the level of millisecond [ms]). After this time interval, new spectrum request (query) has to be send. Such mechanism can provide the periodic update scheme like the CBRS model
  - `max_lease_count`: Maximum count of intervals (for example, 200×100 ms) that such band can be used
  - `max_time_to_leave`: Maximum time to leave this band when detecting other BSs using the same band
  - `price`: The price (for example in Euros) to use such band for a single `min_lease_time` time duration
  - `sensing_sensitivity`: Sensing sensitivity in dBm.

- **sensing data**: It contains the detected BS information (i.e., not controlled by the same RTC) with specific frequency spectrum range and the corresponding operator name. It can be used to identify aforementioned "`busy`" or "`idle`" state

- **LSA policy**: It includes the same parameter set as in the **Operator policy**, but without breakdown for option `busy` and `idle`. Such policy is used to identify the ways to activate licensed spectrum sharing

- **spectrum management rules**: Include several parameters:

  - `mvno_group`: Name of the set of rules
  - `pattern`: A custom pattern to calculate the weights of spectrum offers when one does not want to use the default pattern, for instance, custom costs
  - `use_pattern`: It indicates whether to use the aforementioned custom pattern; otherwise, the default pattern will be used

  - `cost`: It includes the weights for each parameter in the spectrum offer as the default pattern. This parameter is ignored when using the custom pattern
  - `operator_preference`: It represents the preferences among different spectrum owners. This value can be set to a "do-not-care" value to be fair among operators
  - `criteria`: It includes a list of criteria that can pre-exclude some offers beforehand. For instance, the maximum "price" value can be set and some offers will be excluded when their price is larger than this value. The same mechanism can be set for other parameters
  - `freq_preference`: It indicates the preference of band in term of the absolute normalized distance (Hz in frequency domain) between offered frequency bands and the preferred band. For instance, if there are two feasible offers over 3.5 GHz and 2.6 GHz and we prefer 2.8 GHz frequency, then the 2.6 GHz offer is more preferable.

- **BS group membership**: It determines to which Mobile Virtual Network Operator (MVNO) group, a given BS (with a particular cell identity) belongs to.

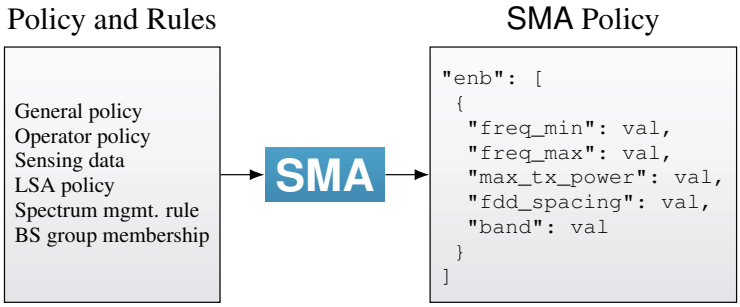

FIGURE 6.3: Input and output of SMA

As for the output of SMA in Fig. 6.3, the *SMA-policy* includes several parameter values: `freq_min`, `freq_max`, `max_tx_power`, `fdd_spacing`, `band` correspond to the minimum frequency, maximum frequency, maximum transmission power, spacing between uplink and downlink direction in FDD mode, and the band identity, respectively. Such *SMA-policy* output will then be applied through the RAN controller and agent toward the underlying BSs.

Decision making algorithm of SMA

Afterwards, we design the decision making algorithm of SMA shown in Alg. 6.1. All spectrum offers, criteria and parameters are formed in the set $\mathcal{L}$, $\mathcal{C}$ and $\mathcal{P}$, respectively. Before computing the weights for each offer, we firstly exclude ineligible offers s_j from $\mathcal{L}$. For the k-th parameter (e.g., `price` and `min_lease_time` mentioned in the **Operator policy**), we multiply its normalized value v_k by the cost c_k and sum all resulted products to get the weight (i.e., w_j for the j-th offer). Moreover, we apply the preference in terms of the operator and frequency mentioned beforehand: `operator_preference` and `freq_preference`. Finally, the optimal offer s_{opt} is selected as the output SMA policy *SMA-policy*.

Implementation

Following aforementioned design, we implement the SMA prototype from scratch. Specifically, the SMA is developed as a virtualized network function in Python 2.7 and can be found in the Mosaic5G Store repository[2].

[2] `https://gitlab.eurecom.fr/mosaic5g/store`

Algorithm 6.1: Decision making algorithm of SMA

Input : *Policy* is the input policy and rule
Output: *SMA-policy* is the output SMA policy

begin
  for $bs \leftarrow 1$ **to** *number of BSs* **do**
    Add all spectrum offers in *Policy* to the offer list $\mathcal{L}$;
    $cId \leftarrow$ getCellId(bs);
    $rules \leftarrow$ getRules(cId, *Policy*);
    Add all pre-excluded criteria in *rules* to the criteria list $\mathcal{C}$;
    Add all parameters in *rules* to the parameter list $\mathcal{P}$;
    for $c_i \in \mathcal{C}$ **do**
      for $s_j \in \mathcal{L}$ **do**
        if $\sim$ *CheckOffer*(s_j, c_i) **then**
          $\mathcal{L} = \mathcal{L} \setminus s_j$; /* Pre-exclude offer s_j due to criteria c_i */
        end
      end
    end
    for $s_j \in \mathcal{L}$ **do**
      if *use_pattern* **then**
        /* Use custom pattern to compute weight */
        $w_j \leftarrow$ calcWeightUsingPattern $(rules, s_j)$;
      end
      else
        $w_j \leftarrow 0$;
        for $p_k \in \mathcal{P}$ **do**
          /* Get normalized value of k^{th} parameter from offer s_j */
          $v_k \leftarrow$ GetNormParam (s_j, p_k);
          /* Get cost of the k^{th} parameter from *rules* */ $c_k \leftarrow$ GetCost $(rules, p_k)$;
          $w_j \leftarrow w_j + c_k \times v_k$;
        end
        $w_j \leftarrow w_j \,/\, \left(\sum_{k=1}^{|P|} c_k\right)$; /* Normalized to cost sum */
        /* Apply normalized operator & frequency preference */
        $w_j \leftarrow w_j \times$ operator_preference $(s_j) \times$ freq_preference (s_j);
      end
    end
    $opt \leftarrow \arg\max_j w_j$; /* Select optimal offer based on weights */
    $SMA\text{-}policy_{cId} \leftarrow s_{opt}$; /* Apply offer s_{opt} to cell cId */
  end
end

The implemented SMA can be executed on top of the FlexRAN and OAI platforms as a local or remote application, and thus supporting the LTE/LTE-A radio access technology. Note that to dynamically apply a new *SMA-policy*, a "soft-restart" operation is performed for the considered LTE BS (eNB). Such "soft-restart" refers to restart only the RAN part of LTE eNB, without affecting the connections to the core network or the controller.

SMA selection results for different rules

Based on our implemented SMA, we show how different spectrum offers can be selected according to different applied rules. Via applying different rules, a given LTE eNB can be associated to different MVNO groups in order to select the most suitable spectrum offer to be deployed. In particular, there are four considered rules as follows:

Rule A — select the cheapest spectrum offer regardless of the bandwidth

Rule B — select the spectrum offer with the largest bandwidth regardless of the cost

Rule C — select the spectrum offer with the lowest minimum lease time

Rule D — select the spectrum offer with the highest minimum lease time

Note that the rules mentioned above are spectrum-oriented, and more complex rules can be derived to further incorporate the perceived user performance. In Fig. 6.4, we can see that there are five available spectrum offers with respective prices in terms of Euros per second from 2.6 GHz to 2.7 GHz. These five offers will be selected from time to time based on aforementioned rules applied in the order: Rule A → Rule B → Rule A → Rule B → Rule C → Rule D. Fig. 6.5 shows the costs spent on the selected band based on the above time-varying applied rules.

When applying Rule A (refers to 5 s to 75 s and 100 s to 155 s in Fig. 6.5), the one with the lowest price (refers to the highlighted band in Fig. 6.4a) is selected. Further, when Rule B is applied (refers to 80 s to 95 s and 160 s to 265 s in Fig. 6.5), the one with the largest bandwidth (refers to the selected band in Fig. 6.4b) is chosen. Rule C (refers to 270 s to 350 s in Fig. 6.5) aims to select the offer with the lowest minimum lease time to match its desired utilization duration (e.g., a service may only need a short peak throughput to carry a single big file) as highlighted band sown in Fig. 6.4c. Finally, the selected band (highlighted band in Fig. 6.4d) of Rule D (refer to 365 s to 480 s in Fig. 6.5) is the one that can last longer in terms of the lease time. To sum up, SMA can act as a key tool to easily adapt different rules.

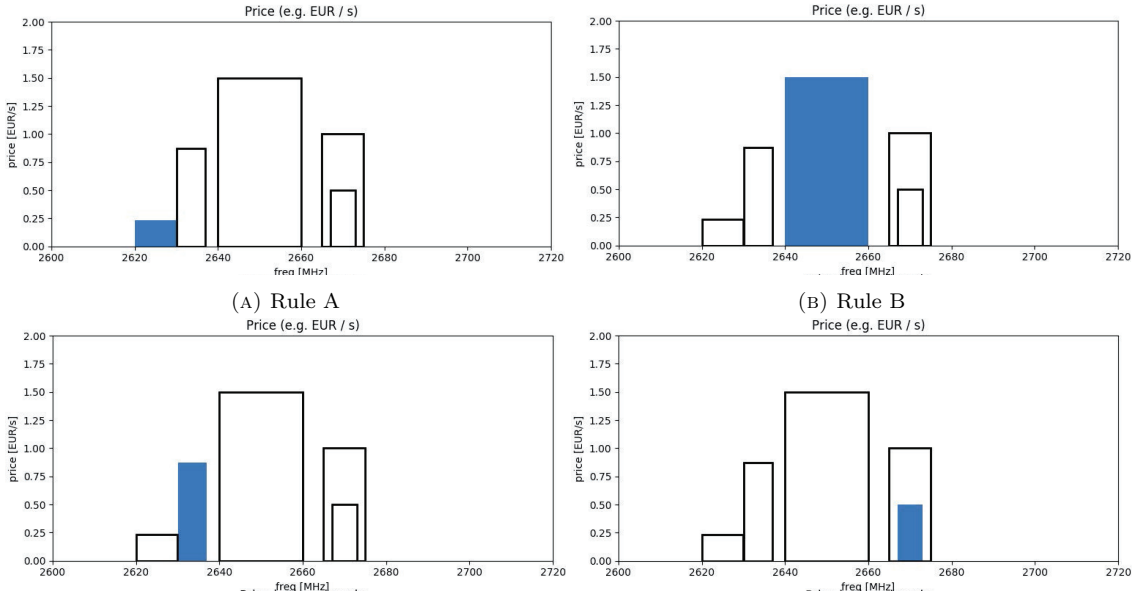

(A) Rule A (B) Rule B

(C) Rule C (D) Rule D

FIGURE 6.4: SMA band selection based on policy rule

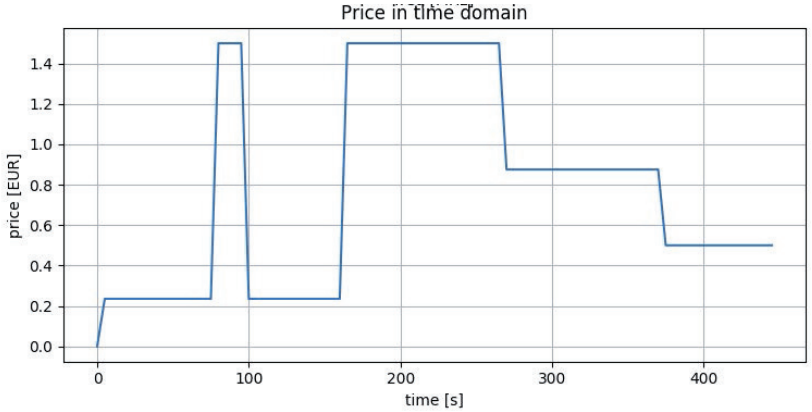

FIGURE 6.5: Normalized spectrum costs based on dynamic rules

6.1.2 SMA use cases

The implemented SMA is integrated locally on top of the Mosaic5G [211] and OAI [212] platforms to manage the spectrum usage in a real-time manner. Once the new *SMA-policy* is decided by SMA, it will be validated and enforced toward controlled eNBs (cf. Fig. 6.2). Afterwards, these affected BSs will be reconfigured and "soft-restarted", thus a new cell is switched on. Each eNB has a single antenna and is operated in FDD mode to serve the COTS UEs. In following, we show how the SMA can be applied in two use cases: (a) phantom cell and (b) cell zooming.

Phantom cells

The *phantom cell* [217] notion separates control plane (C-plane) and user plane (U-plane) processing to be provided through macro and small cell, respectively. The C-plane is served in a low frequency band to maintain better connectivity and mobility, while the U-plane is mainly provided by small cells utilizing high frequency bands to boost user data rate[3]. Note that these small cells are not configured with cell-specific signals or channels, and hence termed "phantom" cells. The SMA can provide dynamic policies toward phantom cells in specific situations, e.g., more capacity has to be offered to the UEs. Before examining the benefits of such dynamicity, we firstly review the time spent on reconfiguring *SMA-policy*. In Fig. 6.6, the overall reconfiguration time is made up of five components in the time-line. First of all, the SMA period represents the duration to collect sensing data for decision making by SMA. Then, the SDN time from t_{SMA} to t_{SDN} is to deliver the new *SMA-policy* through controller and agent (cf. Fig. 6.2) toward underlying BS, depending on the collocation of SMA, controller and agent (e.g., locally or remotely). While the BS re-start time from t_{SDN} to t_{BS} aims to "soft-restart" the RAN part at BS. It depends on the underlying RAN service platform and Software Defined Radio (SDR) infrastructure. The average value is 4 second when we integrate SMA over OAI platform with USRP B200mini SDR. Finally, there are two UE-related components, i.e., cell re-selection time ($t_{\text{UE},1}$ to $t_{\text{UE},2}$) and UE attach time ($t_{\text{UE},2}$ to $t_{\text{UE},3}$). An overlapping between BS re-start time and cell re-selection time is observed due to the UE radio connection loss at $t_{\text{UE},1}$ before "soft-restart" is completed.

To quantitatively see the impacts of reconfiguration on UE side, we measure these two UE-related components on two different COTS UEs with different numbers of supported band and UE category, i.e., Samsung Galaxy S6 (UE category 6, supports 13 LTE bands) and Samsung Galaxy S5 (UE category 4, supports 6 LTE bands) in three respective trials as shown in Fig. 6.7. A larger delay for Galaxy S6 is observed, which may be due to the number of supported band, i.e., Galaxy S6 spends more time to measure all supported bands to decide the best one for cell re-selection[4].

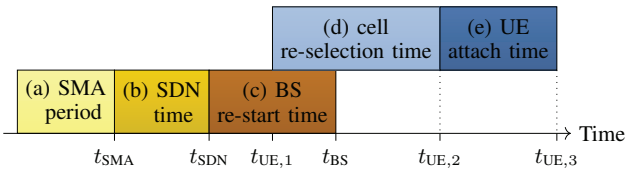

FIGURE 6.6: Reconfiguration time-line

Next, we reconfigure the underlying eNB via SMA and compare two scenarios to show the advantages of phantom cell. First of all, the phantom cell is deployed at a higher frequency band and can utilize larger bandwidth to boost the U-plane performance when compared with the macro cell.

[3]Macro cells support both C-plane and U-plane signaling.
[4]Average UE attach time is normally less than 500 ms in our measurement.

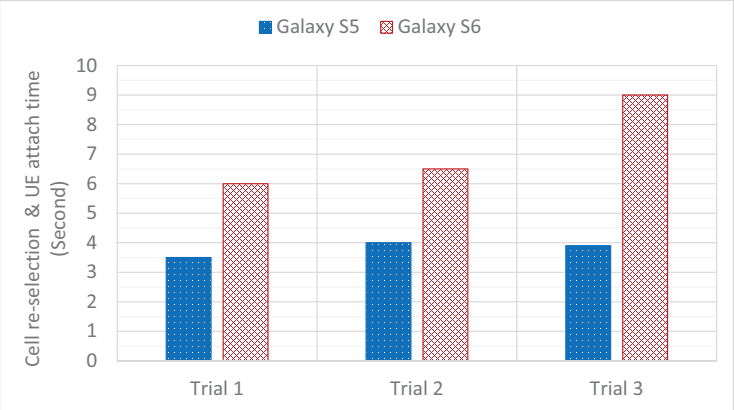

FIGURE 6.7: Indicative UE-related delay for different COTS UEs

Specifically, the phantom cell is deployed at band 7 (2.6 GHz) and can utilize a larger bandwidth (i.e., 10 MHz), while the macro cell is deployed at band 13 (750 MHz) and can only use a smaller bandwidth (i.e., 5 MHz). The measured good-put and delay jitter at the UE side are provided in Fig. 6.8a using the Nexus 6p COTS UE that receives the UDP traffic in the downlink direction. We can see that using phantom cell can show a better user experience via exploiting a larger available bandwidth. This benefit would be more distinct when the phantom cell uses a much higher carrier frequency (e.g., mmWave) with an even larger radio bandwidth.

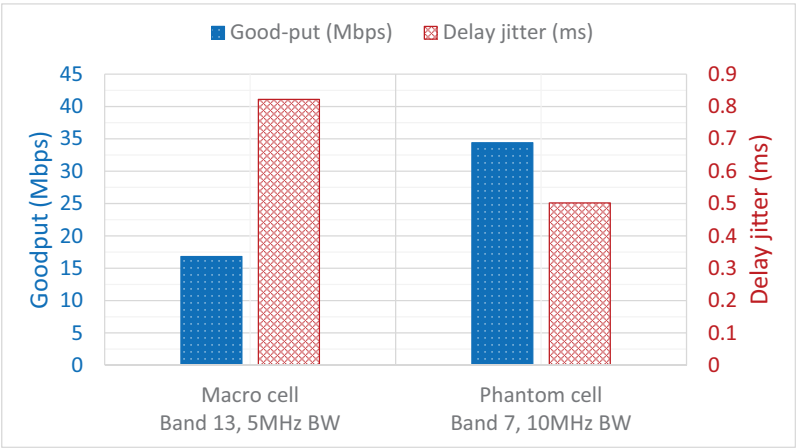

(A) Different applied bandwidths for macro/phantom cell

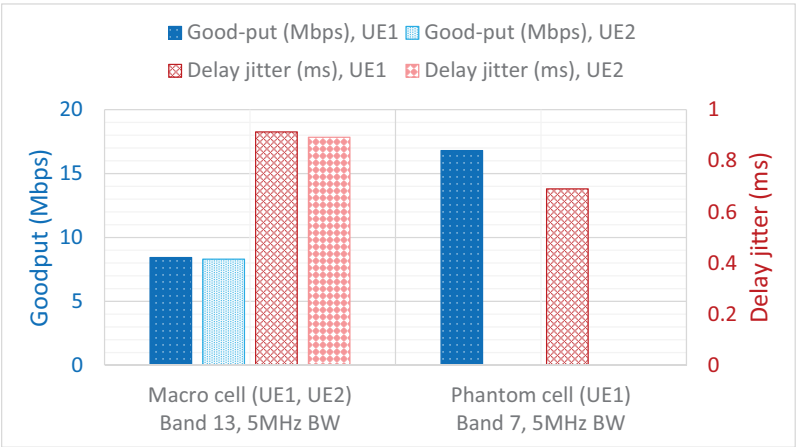

(B) Different numbers of connected UE for macro/phantom cell

FIGURE 6.8: Benefits of phantom cell via applying SMA

In the second scenario, we consider another benefit of phantom cell. For macro cell, it shall support more users as it has a larger coverage area; however, the phantom cell can serve users in a limited range with regard to the macro cell thus boosting the experience of nearby users. Specifically, the phantom cell is deployed at band 7 (2.6 GHz) with 5 MHz bandwidth to serve a single UE and the macro cell is deployed at band 13 (750 MHz) with 5 MHz bandwidth to serve two UEs at the same time. Here, we use identical Nexus 6p COTS UEs for fairness comparison and the downlink UDP traffic is transported toward the UEs. The results for these two cases are shown in Fig. 6.8b. We can see that both UE1 and UE2 in the macro cell individually have a lower good-put when compared with the phantom cell case. Even though the sum of good-put from these two UEs in the macro cell is close to the UE1 in the phantom cell case; however, a larger delay jitter is still seen for these two UEs. To sum up, aforementioned benefits of phantom cell can be simply enabled via adapting dynamic spectrum allocation through implemented SMA.

Cell zooming

The cell zooming concept stems from [218], aiming to adaptively adjust the cell size (i.e., zoom in and zoom out) in order to solve the problem of traffic load imbalance and to reduce the energy consumption in cellular networks. Note that the SMA paves the way for cell zooming by adjusting the corresponding *SMA-policy* (cf. `max_tx_power` in Fig. 6.3) to underlying BSs. This adjustment relies on the latest status from BSs (e.g., traffic load, energy consumption) and/or UEs (e.g., positioning, traffic quality of service, QoS), and also the cell-zooming decision-making algorithm running in SMA. In our experiment, a simple positioning-based cell-zooming mechanism is applied to adjust the transmission power according to the UE distance toward the phantom cell site. Such phantom cell uses the same setting mentioned in Section 6.1.2 at band 7 (2.6 GHz) with 5 MHz bandwidth.

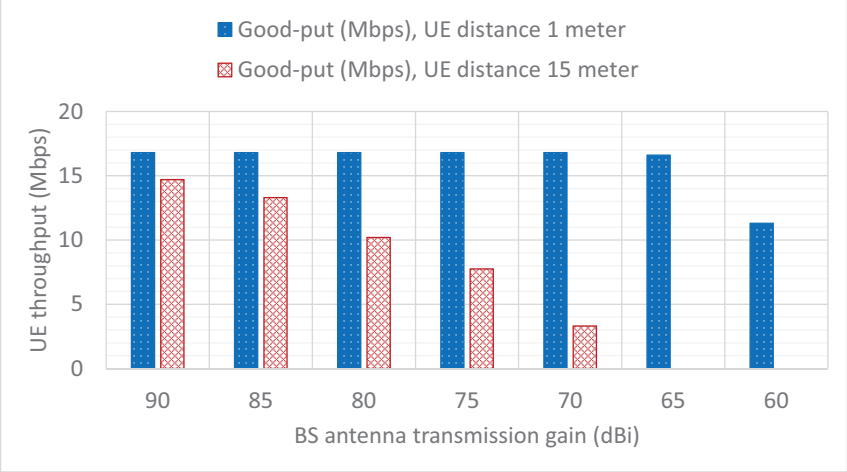

FIGURE 6.9: Cell zooming impacts on different UE distances

In Fig. 6.9, we examine two different UE distances from the cell site with line-of-site environment: (a) 1 meter and (b) 15 meters. Note that the value of eNB transmission antenna gain is adjusted in dBi form, and we inspect the impact on the U-plane performance. Few impacts can be seen on the good-put when UE is close to the cell site (i.e., 1 meter), unless the antenna gain is decreased to 60 dBi. In contrast, distant UEs suffer more drastically and will even lose connection when the antenna gain is reduced to 65 dBi. In summary, SMA is the enabler for cell zooming case via naturally applying its control logics toward underlying eNBs.

Conclusions and summary

We propose the SMA as the open-source tool for spectrum management with high flexibility. Further, we highlight its interactions with the underlay network components (SDK and RAN controller), describe the design details, and examine its functionalities to select the spectrum offers based on applied rules dynamically. Finally, the SMA is implemented on top of OAI and FlexRAN platforms to be applicable in two use cases: (1) phantom cell and (2) cell zooming. In the future, there is a plan to chain SMA with other control applications (e.g., radio resource management, handover) to provide a more sophisticated control logic that can serve the needs of multiple services.

A compact summary of the use of contextual information to improve spectral efficiency is presented in Table 6.1 below.

Ph.D. candidate's publications considering problems discussed in this section	[123], [213]
Context information	The current network administrator's preference; available spectrum bands and their specification and parameters; list of base stations, their location and radio parameters.
Influence on the system	Selection of a frequency band for base stations
Impact on spectrum efficiency	Modification of both the users' bit rate and the width (and carrier frequency) of the currently used band; spectral efficiency improvement possible if it is the actual intention of the operator, otherwise other metrics will be maximized.
Comment	By changing the spectral parameters (SMA), the operator can strive to achieve a certain goal, e.g. maximization user throughput, or lower costs.

Table 6.1: Summary of work presented in chapter 6.1

6.2 Research topic 2: Freemium spectrum sharing and pricing

The pervasive virtualization of communication networks, including wireless networks, and the increasing proliferation of softwarized solutions in wireless communications pave the way for the highly flexible approach to spectrum sharing and pricing. In this section, the popular idea of *freemium* licensing is applied to dynamic spectrum sharing and pricing. The proposed softwarized solution is evaluated through computer simulations, showing the benefits of such elastic solutions. It has been presented in the Ph.D. candidate paper [219].

The spectrum sharing is somehow managed by the database or the spectrum broker, where the policy rules are specified. However, these policies define not only the coexistence rules in terms of power, interference, spectrum masks, etc., but also may specify the pricing for using the spectrum. Moreover, as mentioned at the beginning, currently, the Dynamic Spectrum Access (DSA) may be treated as some sort of software-defined service, and even the spectrum management has been already proposed in form of an application for virtualized wireless networks. In this context, we propose a new spectrum sharing and pricing scheme that takes benefits from all the previously discussed approaches and, at the same time, is in line with modern business trends. Mainly, we follow the *freemium* approach for DSS and call it afterward Freemium Spectrum Sharing (FSS). Freemium, as the term, is the mixture of two words - free and premium. In the freemium-based business model, as shown in Fig. 6.10, the default scheme is to apply free access to resources, and when necessary, the stakeholders may apply for paid premium privileges.

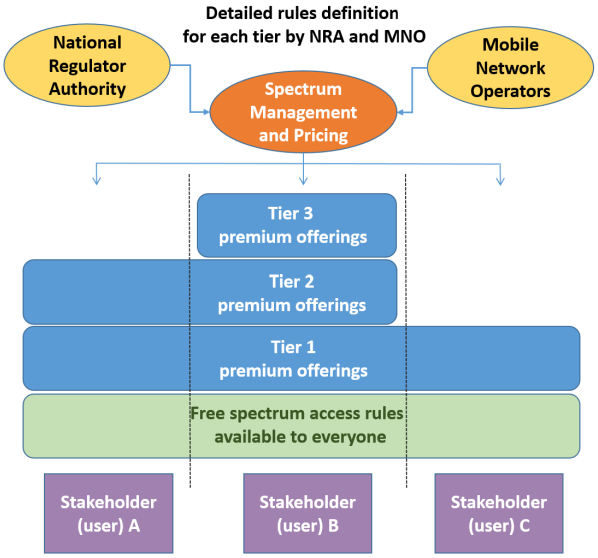

FIGURE 6.10: Freemium spectrum sharing model

6.2.1 Freemium spectrum sharing concept

In the context of DSS, we propose the application of this flexible approach, being the mixture of LSA, CBRS, license-exempt, and PL schemes. In the freemium spectrum sharing and pricing, the default access to frequency resources is free-of-charge so that every interested user may utilize these spectrum resources as in the WLAN case. However, when the specific QoS is necessary, the premium options may be selected by paying some fees to the spectrum regulator (e.g., NRA) or another license holder (like MNO). For example, the premium users may transmit with a higher power (in the same band) or may utilize other spectrum bands, for which access requires some fee. However, please note that in the proposed freemium model, the number of premium options

(denoted as tiers in Fig. 6.10) may be high - more privileges may be guaranteed to the interested stakeholders at the expense of higher fees. The privileges in terms of spectrum sharing and wireless communications may be translated to a set of classes of the QoS rules. The number of tiers, as well as their detailed definition, maybe elastically (in a software way) changed by the NRA and MNO. Moreover, the specification of the privileges associated with each tier may be time- and location-dependent, i.e., some set of rules may be activated only for a specific geographic area or for a specific period. This approach is then in line with the ongoing trend for virtualization and softwarization of radio access and core networks. In the following section, we evaluate the performance of some arbitrarily selected sets of premium privileges and related prices, with the ultimate goal of showing the flexibility of the proposed scheme. As the rationale behind the proposed packages may be justified in some cases, other approaches may be better otherwise. Knowing these limitations, we have arbitrarily selected some package proposals to evaluate the freemium sharing scheme quantitatively.

Brief comparison with other schemes

Finally, let us briefly compare the proposed freemium spectrum sharing and pricing model with the selected existing, mature schemes. First, as in LSA, the two-tier approach is considered (when the Secondary Users (SUs) can transmit data with the support of the LSA repository as long as they do not violate the cooperation rules with Primary Users (PU, incumbents), in the FSS scheme the number of layers is not specified. Moreover, it may be directly applied to both vertical and horizontal spectrum sharing, whereas in LSA the PU-SU scheme is considered. Next, in LSA, the SU may transmit over a dedicated time period as long as this activity is allowed by the LSA repository. In the proposed scheme, the free-of-charge access does not necessarily require any coordination (although it may be applied) as it operates according to the rules applicable in the considered band. For example, LTE users operating in the free-of-charge tier will follow the standardized spectrum access rules, as well as the IEEE 802.11 users will apply the classic WLAN solutions. Non-free-of-charge users will still follow the standardized rules, e.g., have access to a wider set of resources. When comparing with the CBRS approach, similar conclusions as above can be drawn. In particular, CBRS-scheme assumes the presence of a dedicated spectrum access system that is responsible for incumbent protection. Moreover, as this approach can be easily applied in the freemium spectrum sharing and pricing scheme, the latter is not restricted. This dynamic spectrum sharing scheme can also be applied in loosely coordinated scenarios. Finally, the LSA, CBRS (or in general broker-based) solutions are often considered on a relatively long time scale, as at each point of time, the compliance with the other existing PUs/incumbent users has to be guaranteed. As the proposed scheme can be applied both to vertical and horizontal sharing, the time scale may be reduced to very low ranges. Thus, the key features of the proposed freemium spectrum sharing and pricing scheme are to:

- benefit from the opportunities provided by the progressive virtualization of communication networks at the radio access part, i.e., to make the elastic use of spectrum more profitable
- provides the framework for multi-tier resource management from the MNO level to the end-user level
- consider the case when the spectrum sharing is done in a short time scale (e.g., per end-user request)
- extends classic access-privileges or priority classes also to spectrum resources

Experimentation scenario

In the simulations performed, we assumed the existence of a network operating in a 9 km square area, 3.5 GHz carrier frequency and four base stations near the center of the area. Each base station transmits data with transmit power 20 dBm over maximally 40 MHz of bandwidth. There are 50, 200, or 800 users distributed uniformly over the analyzed area. Such a number of users can be named low, medium, and high user density. An example of the network topology is presented in Fig. 6.11.

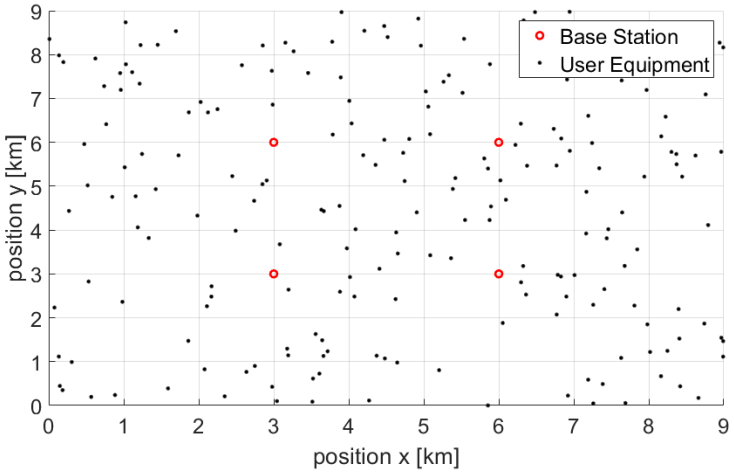

FIGURE 6.11: Example of the network topology with medium user density

In our evaluation, the FSS packages are defined as the set of rules describing the way of accessing available spectrum bands. In particular, without loss of generality, we arbitrarily assume that there are $N_{ch} = 4$ equal-size frequency bands available, as illustrated in Fig. 6.12, mainly:

- B_1 - first band, which interferes with and is interfered with by the second band (B_2), every user can access this band freely; the interference is due to the light requirements put on the out-of-band emission
- B_2 - second band, which interferes with and is interfered with by the first band (B_1); this band is assumed to be occupied less often than the first one, as only premium users have access to it; the first and second band may even overlap
- B_3 - the third band does not interfere with the first and second bands (orthogonal in the frequency domain); this band is protected from interference by the guard band
- B_4 - access to the fourth band is limited to a fixed number of users (10 in our example) and is divided in the time domain

As shown in Fig. 6.12, the phenomenon of adjacent-channel interference is due to the non-ideal in practice transmit and reception filters, i.e., instead of brick-wall-like filter characteristics (transmittance), the density of the transmit power is limited in standards by SEM, showed in Fig. 6.12 by solid lines. Similarly, the performance of the receiver chain is specified by the equivalent reception filter characteristics (marked by a dashed line). The effect of mutual adjacent-channel interference may be minimized in various ways, e.g., by adding some guard bands or by modifying the SEM and reception filter characteristics. In our analysis, we assume that bands B2, B3, and B3 are separated by some dedicated Guard Band (GB), whereas bands B1 and B2 constitute a wider contiguous one.

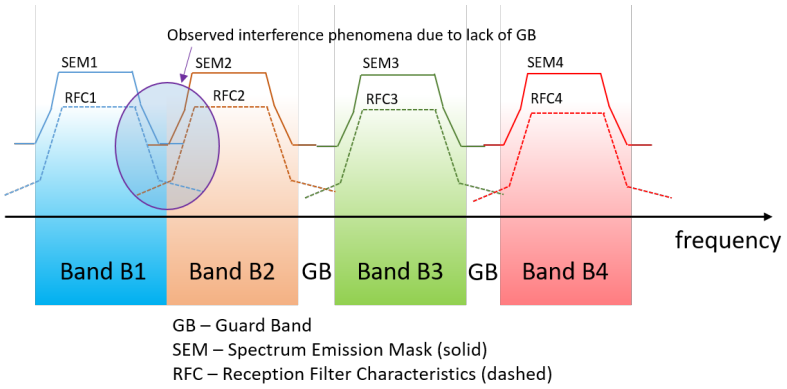

FIGURE 6.12: Considered frequency bands

Once SEM and reception filter characteristics are known, the total interference observed due to the non-ideal transmit and receiver characteristics can be calculated. Typically, these two phenomena are described by two parameters, namely, ACS and ACLR, as discussed in Sec. 3.3. Thus, assuming the transmit power P_j of the wireless node (base station or user) is equally distributed among j-th band (i.e., B_j), the total amount of adjacent-channel interference I^A_m observed by the i-th receiver operating within m-th band (i.e., B_m) could be calculated as:

$$I^A_{i,m} = \sum_{j=1, j\neq m}^{M} \int P_j \xi_{j,i} \cdot \mathrm{SEM}_j(f) \cdot \mathrm{RFC}_i(f) df, \tag{6.1}$$

where f is frequency, $\mathrm{SEM}(f)$ and $\mathrm{RFC}(f)$ are frequency-domain transmittances of the transmitter and receiver, respectively. $\xi_{j,i}$ is the path-loss observed between j-th transmitter and i-th receiver. As the adjacent-channel interference will be significant only in the neighboring frequency bands, the path loss can be approximated as constant and calculated for, e.g., the operating frequency of the i-th node. Besides the adjacent-channel interference, there is a need to consider also co-channel interference originating from the distance transmissions, i.e., the transmission existing between the other base stations and distant users utilizing the same m-th frequency band (B_m) as the i-th user does. Denoting the set of wireless nodes (base stations or users) utilizing the same frequency band as $\mathcal{Q}$, the total co-channel interference observed by i-th user at m-th frequency band, i.e., I^C_m, can be calculated as

$$I^C_{i,m} = \sum_{q\in\mathcal{Q}} \int P_q \xi_{q,i} \mathrm{SEM}_q(f) \cdot \mathrm{RFC}_i(f) df, \tag{6.2}$$

where P_q is the transmit power of the q-th station, and $\xi_{q,i}$ defines the path-loss between q-th transmitter and i-th receiver operating in the m-th band. In the case considered in this work, the co-channel interference defined in (6.2) applies to all bands. Besides, the interference between bands B_1 and B_2, calculated by (6.1), is practically defined in detail by the so-called ACIR, i.e. defined in Sec. 3.3 (see equation 3.5).

In case of $\{B_1, B_2\}$, ACIR is set to 40 dB. Thus, the total interference I_m observed by i-th node for bands B_1 and B_2 equals $I_{i,m} = I^A_{i,m} + I^C_{i,m}$, whereas for bands B_3 and B_4 it is set to $I_{i,m} = I^A_{i,m}$. We assumed that the bandwidth of each frequency band $\{B_1, B_2, B_3, B_4\}$ is equal 10 MHz. Basically the rate T_i achieved by i-th single user is calculated using Shannon formula

$$T_i = B_i \log_2 \left(1 + \frac{Pr_i}{I_i + N_i}\right), \tag{6.3}$$

where Pr_i is the received power by the i-th user (being a function of the transmit power P_i and the observed path-loss $\xi_{i,i}$, modelled here as the free space one), I_i and N_i denote the power of observed total interfering signals and noise in band B_i assigned to the i-th user, respectively.

The thermal noise power observed over band B_i is equal to $N_i = kTB_i$, where T is the temperature in Kelvin, and k refers to Boltzmann constant. Please note that the band occupied by the respective user will be the mixture of above-mentioned bands $\{B_1, B_2, B_3, B_4\}$, depending on the selected FSS package.

In our experiment, we have analyzed the prospective benefits of the considered scenario from two viewpoints, mainly from a user- and operator perspective. In each case, users/operators may select one FSS package denoted as A, B, C, and D. Let us remind that an FSS package is a set of privileges associated with each tier in the freemium model shown in Fig. 6.10.

FSS packages: users perspective

Two prospective scenarios were considered here:

- in the first one, users using package:
  - A - can utilize band: B_1
  - B - can utilize band: B_2
  - C - can utilize band: B_3
  - D - can utilize band: B_4
- in the second one, users using package:
  - A - can utilize band: B_1
  - B - can utilize bands: B_1, and B_2
  - C - can utilize bands: B_1, B_2, and B_3
  - D - can utilize all bands: B_1, B_2, B_3, B_4

FSS packages: operator perspective

An analogous approach has been prepared to present the possible benefits of using our solution from the operator's perspective. Here, as a reference scenario, we treat a situation where each network user can utilize the whole band (40 MHz). This reference scenario will be compared with the case where the following FSS packages are defined:

- A - can utilize band: B_1
- B - can utilize bands: B_1, and B_2
- C - can utilize bands: B_1, B_2, and B_3
- D - can utilize bands: B_1, and B_4

6.2.2 Simulation results

To evaluate the performance of the proposed FSS scheme, extensive computer simulations have been conducted, reflecting the two described perspectives.

Performance of the FSS scheme from the user perspective

In both scenarios within the user perspective, there are 79 % users who use package A, 10 % use package B, 10 % use package C, and 1 % use package D. The simulation results were generated for 1,000 different random network topologies. In Fig. 6.13-6.15 we show the distribution of the rate achieved in the first scenario for each package for three considered user densities. In a nutshell, the user selecting a certain package may access only one band. For comparison, in Fig. 6.16 we show the results for the second scenario, where many bands may be used simultaneously.

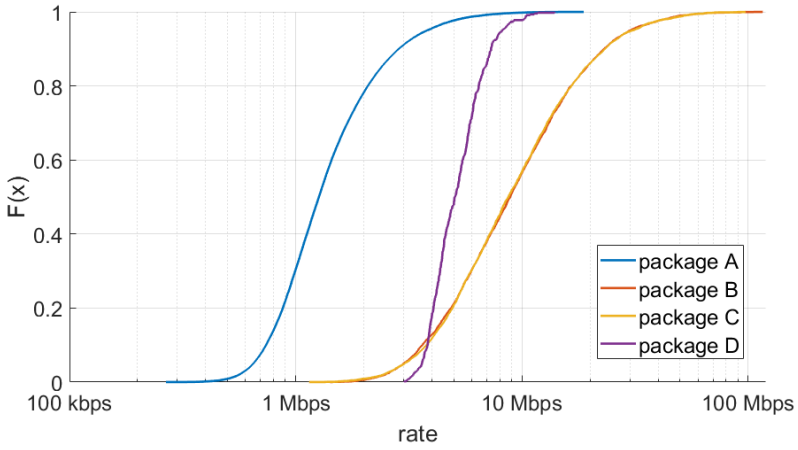

FIGURE 6.13: Distribution of user rate for low user density

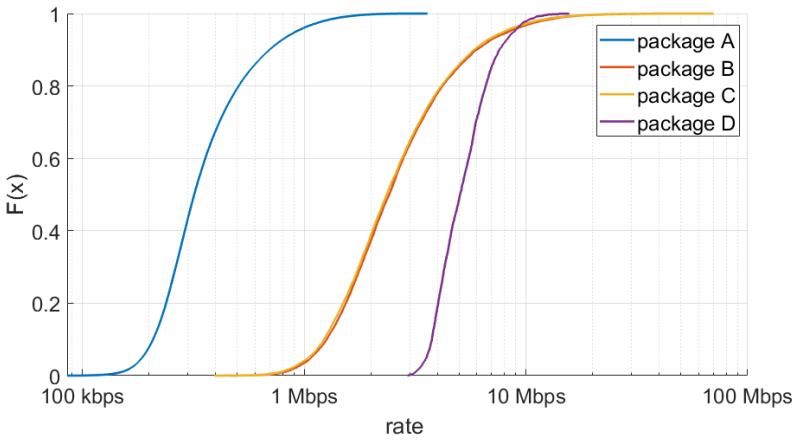

FIGURE 6.14: Distribution of user rate for medium user density

However, to effectively evaluate each of the scenarios from the perspective of a typical consumer, we introduced a dedicated evaluation metric *package score*. Its purpose is to assess the quality of offered services to the user within a given package. This metric is defined as follows:

$$\mathrm{PS}_i = w_{10}\frac{T_{10}}{T_{10}^{\max}} + w_{\mathrm{mean}}\frac{T_{\mathrm{mean}}}{T_{\mathrm{mean}}^{\max}}, \tag{6.4}$$

where PS_i is the "package score" associated with i-th package, T_{10} is the 10th percentile of rate, T_{mean} is the mean rate, $T_{10}^{\max}$ and $T_{\mathrm{mean}}^{\max}$ are the respectively maximum 10th percentile and mean rate achieved by user of any package, w_{10} and w_{mean} are the weights of metric components. For a typical consumer, we assumed the weight values at the following level: $w_{10} = 0.8$ and $w_{\mathrm{mean}} = 0.2$. This is supported by the fact that for a typical user it is more important to ensure the access to the service itself, and only then the average bit rate offered by the service. Obviously, both the weights adopted, the components of the presented metric and its definitions are purely exemplary.

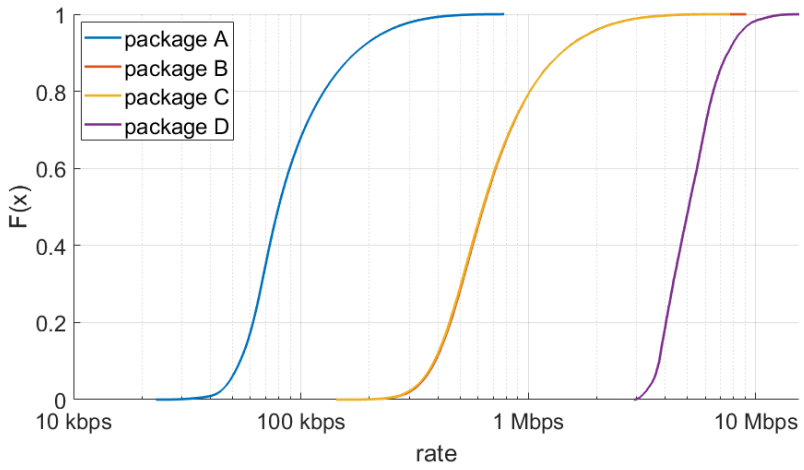

FIGURE 6.15: Distribution of user rate for high user density

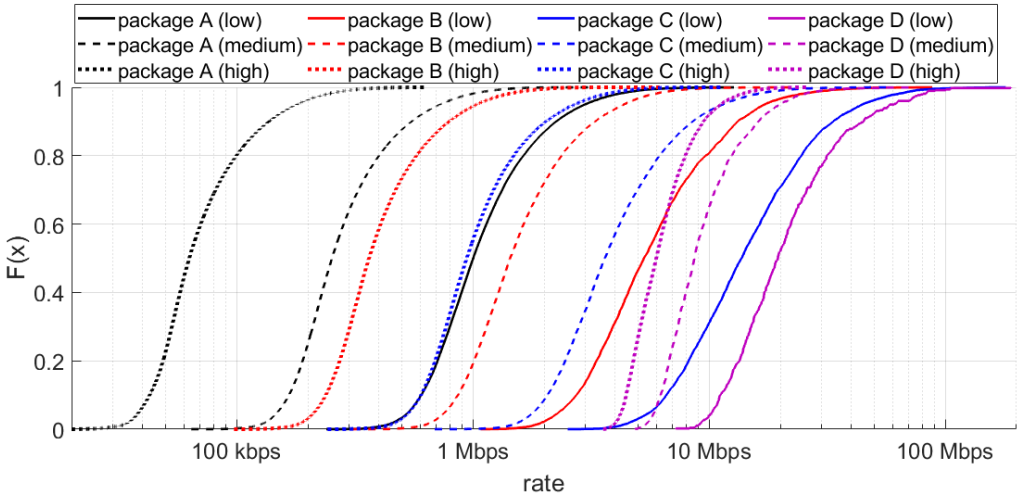

FIGURE 6.16: Distribution of user rate (second scenario)

Its intended to show an idea rather than a specific solution. For the previously presented bit rates achieved in different conditions and in different packages, the values of the "package score" metric presented in Table 6.2 were prepared.

TABLE 6.2: Package Scores

Scenario	**UE density**	**Package**			
		A	***B***	***C***	***D***
first	low	0.18	0.94	1.00	0.89
	medium	0.06	0.38	0.38	1.00
	high	0.02	0.11	0.11	1.00
second	low	0.05	0.26	0.62	1.00
	medium	0.03	0.15	0.36	1.00
	high	0.01	0.06	0.14	1.00

The presented results show that in the first scenario, packages B and C are very close to each other, are always better than package A and, importantly, in the case of a small number of network users, they can be better than package D. However, in the second scenario, there is a simple dependency - where package D is the best, package C is slightly worse, package B is even worse, and package A is the worst.

Performance of the FSS scheme from the operator perspective

In the second analysis, the prospective benefits observed by the network operators are briefly analyzed. There are 49 % users who use package A, 25 % use package B, 25 % use package C, and 1 % use package D. The simulation results were generated for 1,000 different random network topologies and all three users densities: 50 - low, 200 - medium, and 800 - high.

In Fig. 6.17-6.18 we can observe the same dependence - regardless of the density of users. Package A users always achieve bit rates lower than users of the reference scenario. Users of packages C and D always achieve higher throughput than users of the reference scenario - while users of package D have a much better quality of service in the case of a higher density of users. On the other hand, users of the B package have bit rates very similar to those achieved by the users of the reference scenario. The number of users of packages was deliberately selected in such a way as to achieve this effect.

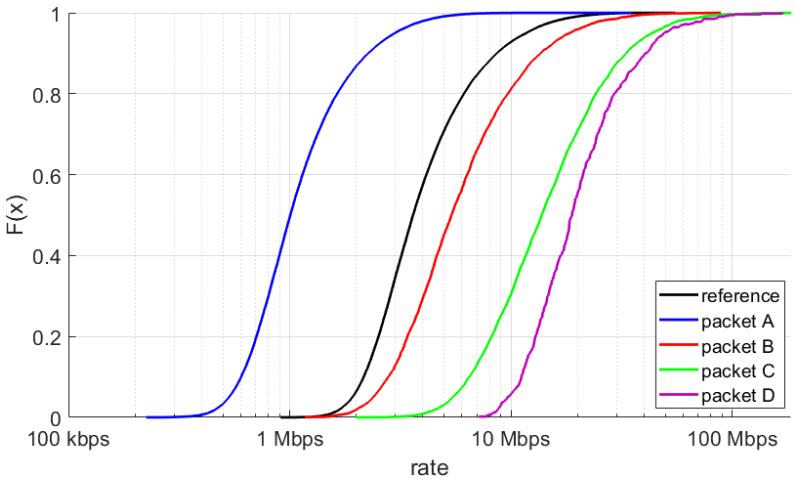

FIGURE 6.17: Distribution of user rate for low user density

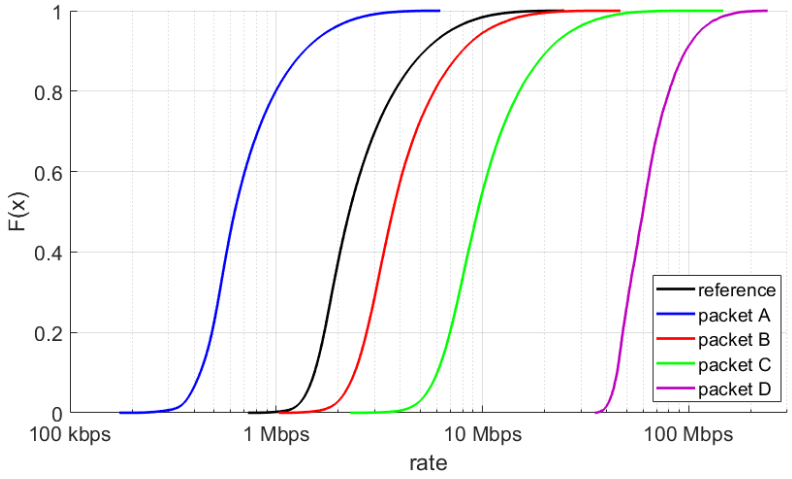

FIGURE 6.18: Distribution of user rate for high user density

Let us assume that the users of the reference scenario pay a fee for using the system in the amount of X cost units. Thus, if there are N users in the network, the approximate profit of the operator is $N \cdot X$ in a certain time unit. Let us assume that package users pay the following fees: package A - it is free; package B - X cost units; package C - $3X$ cost units; package D - $10X$ cost units. Since we obtained similar user throughput from the reference scenario and users of package B - the fee was set at the same value (for a very similar quality of service).

Users of package C always have a better quality of service; therefore, their fee is higher, and users of package D always have the best conditions; thus, their fee is also the highest. In this case, $(0.49 \cdot N \cdot 0) + (0.25 \cdot N \cdot X) + (0.25 \cdot N \cdot 3X) + (0.01 \cdot N \cdot 10X) = 1.1 \cdot N \cdot X$ is the operator's profit in a certain time unit. As can be seen from the presented results, the operator, with very similar profits, has the opportunity to expand the offer for users with more diverse products - which can reach a wider audience.

Conclusions and summary

In this section, we have discussed freemium spectrum sharing and pricing, where the popular concept of freemium access to resources is applied. The simulations showed the potential of this flexible approach toward spectrum sharing, which offers new degrees of freedom for license holders to manage spectrum and prices. First, spectrum resources may be utilized dynamically (what leads to their better utilization). Second, various licensing and pricing packages can be defined, which are tailored to the end-users needs. Moreover, this spectrum sharing access is in line with the ongoing trend for wireless network virtualization, where most of the services are software-defined. Recall that the results have been presented in [219].

A compact summary of the use of contextual information to improve spectral efficiency is presented in Table 6.3 below.

Ph.D. candidate's publications considering problems discussed in this section	[219]
Context information	The current network administrator's preference based on the observation of network parameters (contextual information)
Influence on the system	Selection of a available spectrum access and pricing plans
Impact on spectrum efficiency	Modification of both the users' bit rate and the width (and carrier frequency) of the currently used band; spectral efficiency improvement possible if it is the actual intention of the operator, otherwise other metrics will be maximized.
Comment	By appropriately allocating the bandwidth and matching appropriate plans for users, the operator is able to influence the network efficiency - including if it is the operator's goal - spectral efficiency.

Table 6.3: Summary of work presented in chapter 6.2

6.3 Research topic 3: Open radio network access

The development of cellular wireless systems has entered the phase when 5G networks are being deployed, and the foundations of 6G solutions are being identified. However, in parallel to this, another technological breakthrough is observed, as the concept of open radio access networks is coming into play [220–222]. Advancing network virtualization and programmability may reshape how the functionalities and services related to radio access are designed, leading to modular and flexible implementations. This work overviews the idea of open radio access networks and presents ongoing O-RAN Alliance standardization activities in this context. The whole analysis is supported by a study of the traffic steering use case implemented in a modular way, following the open networking approach. Results of such analysis and traffic steering implementation description were published in the author's paper [223].

Motivation

The current world and national economic development will be significantly driven by the practical and wide-scale deployments of 5G cellular networks. Various use cases have been identified and extensively investigated over the last decade, where 5G solutions should incentivize investors in various vertical industry sectors to strengthen their involvement. At the same time, the scientific community all over the world discusses the requirements and challenges for the next technological leap in the wireless communication domain, i.e., the sixth generation of cellular networks [224,225]. One of the key aspects in this context is the increasing role of artificial intelligence tools, which are considered for 5G and also for future 6G networks [226,227].

In parallel to this development process, another significant transition is happening in the wireless communication domain that is not part of the main 5G ecosystem [220]. As this will affect the functioning of cellular networks from the MNO and infrastructure vendors' perspective, it will have a very limited influence on the end-user. Namely, the architecture of the RAN is rapidly evolving from a solid, black-box approach (also known as a silo) to guaranteeing a high level of openness. In the former case, the hardware manufacturers are typically delivering harmonized and integrated solutions to MNOs, leaving them rather limited possibilities of influencing the internals beyond a typical configuration. In contrast, the so-called Open RAN approach benefits from RAN virtualization and its structural openness [220, 221]. Thus, the underlying hardware can be abstracted, allowing for easy and flexible modification of its software. Please note that this process is one of the consequences of overall network virtualization, of moving various functionalities to the cloud or the edge [228]. Next, the openness of intra-RAN interfaces creates opportunities for flexible software delivery by various telecom vendors. Moreover, the software running on open RAN-supported hardware can be structured in a specific way, where selected algorithms (needed for operating the wireless networks) will be treated as separate applications, managed by a dedicated controller. Following the O-RAN Alliance (here referred to as O-RAN in contrast to Open RAN) specifications, such applications are called xApps or rApps, depending on their time scale of operations [229]. An intelligent controller is often considered a sophisticated entity, equipped with Artificial Intelligence (AI) and Machine Learning (ML) capabilities. Thus, the MNOs, or in a wider scope Service Provider (SP) may modify, update, replace or extend selected functions within the RAN protocol stack whenever it is needed.

Such a programmable and highly modular structure of the RAN architecture will have a significant impact not only on the structure of the future wireless networking market but also on the prospective research and development process in this domain.

The presence of AI/ML-equipped modules, as well as independence from the underlying hardware and the necessity of xApp modularity and flexibility, entails the need to redefine the ways new algorithms are invented [230, 231]. Let us mention that it could be necessary to consider specific kinds of application interfaces (and, consequently, access to specific types of data) between the controller and other applications. Furthermore, a high level of RAN virtualization in the Open RAN concept opens new directions of RAN implementation, which may now be moved to the cloud. This option may be of interest to all MNOs and SPs in the context of deployment of private mobile networks due to the reduction in the time-to-market and installation costs. Finally, Open RAN is brought forward as one of the important elements in the mobile systems evolution towards the 6G era [232, 233]. Seeing the practical realization of the Open RAN concept as a driver in the wireless communication domain, in this work, we overview the recent achievements in this context. We start with the presentation of RAN transformation from the classic, highly centralized manner to the Open RAN idea. Next, we present the current yet selected standardization activities in the O-RAN area, concentrating on the xApp development process. In that spirit, the key contribution of this work is the description of the traffic steering xApp, which has been implemented in a hierarchical and modular manner [234]. The presented results highlight the benefits of such a modular approach by showing how the AI/ML tools may be used for intelligent management of the xApp functioning, and in consequence, for improving system performance.

6.3.1 Open RAN concept

The transformation from the legacy RAN towards the Open RAN can be described in phases. In the first generations of cellular networks, the radio access part was realized in black-box hardware delivered by a single selected vendor. With the evolution of the network architecture, cloud-based approaches have increased their importance. Mainly, the so-called Cloud RAN appeared to be an important element of the 4G network architecture. Evolving further towards Open RAN (and more specifically, O-RAN), the Base Station (BS) has been split into the Centralized Unit (CU), Distributed Unit (DU), and Remote Unit (RU). Different vendors can develop those due to the open interfaces between them, including F1, E1, and Open Fronthaul (see Fig. 6.19). In addition to that, the RAN Intelligent Controller (RIC) is separated from the processing units and allows us to gather Radio Resource Management (RRM) and Self-Organizing Network (SON) functions, which control the radio resources and network. In the O-RAN concept, this is where the intelligence sits, employing AI models for radio network automation.

O-RAN

In O-RAN, all BS parts mentioned above get the "O-" prefix, meaning that they are adapted to the O-RAN Alliance definition and architecture (see Fig. 6.19). Those entities are connected to RIC via the E2-interface and are called "E2 Nodes". Furthermore, RIC is split into "near-Real Time RIC" (near-RT RIC) and "Non-Real Time RIC" (Non-RT RIC). The latter one sits at the Service Management and Orchestration (SMO) system. This split allows a hierarchization of RRM, differentiating algorithm operations on the timescale of operation [229].

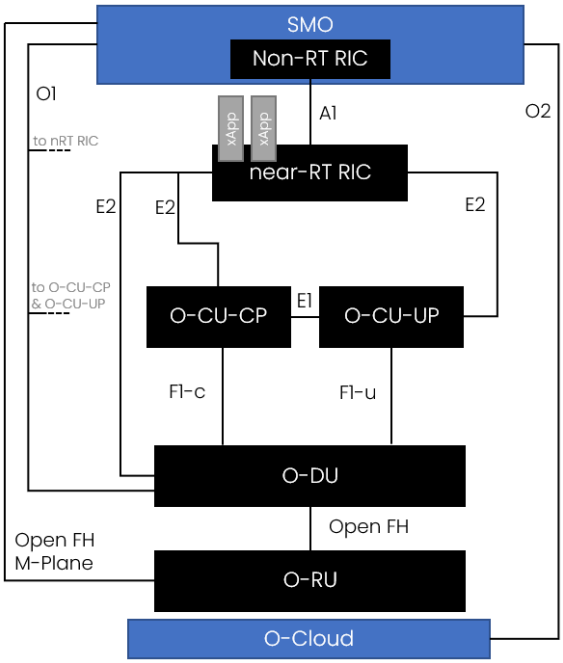

FIGURE 6.19: O-RAN architecture

The key characteristics of the O-RAN concept are:

- disaggregation of BS into granular functions (O-CU/O-DU/O-RU), decoupling of software from hardware, and opening up internal BS interfaces
- the above encourages the development of an open and enlarged telco ecosystem with different vendors, such as O-CU vendors, RIC vendors, algorithm/xApp developers, and system integrators
- intelligent and holistic management enabled by RIC, where the system intelligence is embedded within the O-RAN architecture using AI models and RRM functions, like Traffic Steering (TS), Interference Management (IM), QoS Management, Load Balancing, etc.

RAN Intelligent Controller (RIC)

RIC is one of the key elements in the O-RAN architecture. It is a platform for which, e.g., xApp software vendors can provide RRM/SON algorithms to allow the optimization of radio resource usage for specific applications. The motivation for RIC is to provide controllability to RAN in order to optimize and improve system performance, taking into account the current state of mobile systems. The complexity of those is increased due to network densification, new spectrum bands, multi-radio-access technology, and heterogeneous network scenarios brought on by 5G. Therefore, the task of optimally allocating radio resources, managing handovers or interference, balance the load between multiple cells and carriers is not trivial [234, 235]. With the use of RIC, RRM is decoupled from the RAN stack and enables the implementation of various algorithms collectively utilizing a common set of data. This approach provides holistic control by RRM across all technologies, spectrum bands, cells, and antenna ports. An additional benefit of using this concept is the per-use-case-based management of RAN. According to it, policy-based control allows performance-based decisions adjusted to specific applications.

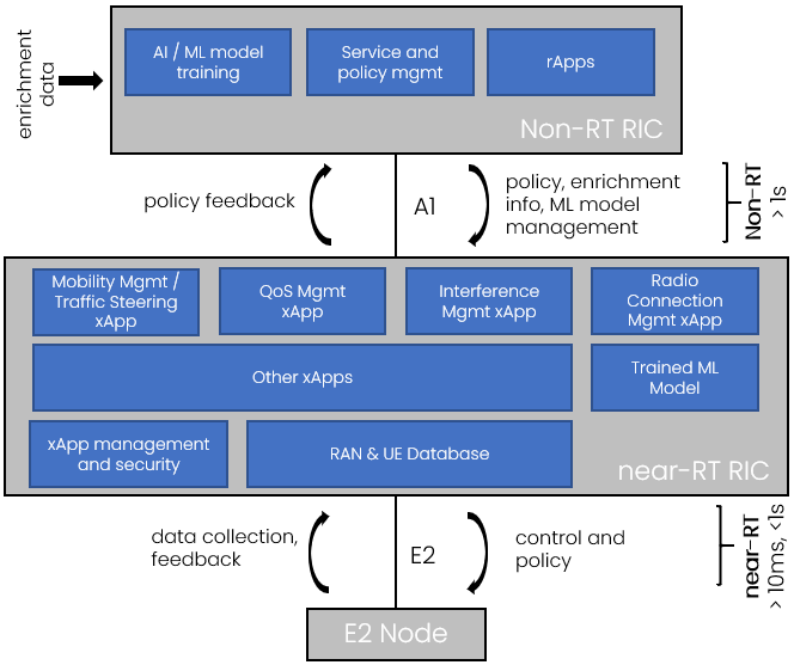

FIGURE 6.20: RAN Intelligent Controller: non-RT RIC and near-RT RIC

Fig. 6.20 shows the details of the RIC split into near-RT RIC and non-RT RIC. The former is responsible for handling the near-RT RRM/SON functions (on a timescale between $>$ 10 ms and $<$1 s), such as Mobility Management, IM, etc. The latter handles the high-level/orchestration functions and provides policies to near-RT RIC over the A1 interface. Note that the Real-Time (RT) RRM is still there, embedded in O-DU (e.g., MAC scheduler). The scheduler can be controlled by near-RT RIC only via general policies. To summarize, there are three control loops, RT ($<$10 ms) handled by O-DU, near RT ($>$10 ms, $<$1 s) handled by near-RT RIC, and non-RT ($>$1 s) handled by non-RT RIC. It is a hierarchical design, which allows for the separation of resource handling concerns [232]. Near-RT RIC, being responsible for RAN control and optimization, incorporates RRM/SON algorithms (through xApps) and bases its operation on UE- and cell-specific metrics.

As per [236], and as shown in Fig. 6.20, near-RT RIC:

- provides a database storing the configurations related to E2 nodes, cells, bearers, flows, UEs, and mappings between them
- provides ML tools that support data pipelining
- provides the messaging infrastructure to support information exchange between xApps and the near-RT RIC framework
- provides logging, tracing, and metrics collection from the near-RT RIC framework and xApps to SMO
- supports the conflict resolution function to resolve the potential overlaps that may be caused by various xApps
- supports A1 interface used to provide policies and ML model management to near-RT RIC and obtain feedback from its operation using those policies and models
- supports E2 interface used to send control/policy messages down to E2 Nodes for resource allocation/prioritization and obtain fine-grained UE/RAN statistics from E2 Nodes

Interface E2 in Open RAN must allow reception of many pieces of information in the network, like receiver power measurement reports, the current state of UEs, serving cells, etc. So, interface E2 is nothing but a source of contextual information for the application.

6.3.2 Traffic steering use case analysis

The O-RAN Alliance specifies the use cases to be addressed by xApps, rApps, and RIC and defines the policies by which the algorithms designed to support the use cases can be controlled. The use cases are prioritized as per MNOs' requirements. One such typical example is TS, the objective of which is to steer the user traffic through a specific cell, taking into account available schemes (such as handover, dual connectivity, carrier aggregation, license-assisted access, HetNet) and resources (such as multi-RAT, licensed and unlicensed carriers, etc.). Optimal traffic steering has been a challenge in wireless networks for many years, and numerous solutions have been proposed in the rich literature, addressing its various aspects [237–240]. As per [241], the challenge to be addressed by use cases is that the typical TS schemes use radio conditions of a cell by treating all users in the same way and are limited to adjusting cell priorities and cell reselection/handover thresholds. The O-RAN Alliance aims to address the TS use case by customizing UE-centric strategies and proactive optimization by predicting network conditions and allowing MNOs to specify different objectives for traffic management depending on the scenario, and flexibly configure optimization policies. In this context, RIC is to control the adaptation of diverse scenarios and objectives and control TS strategies through AI/ML learning from user/network data.

Let us investigate a wireless network with open interfaces through which it is possible to implement network functionality externally. The goal of the conducted simulations and analyses is to show the possibility of applying the concept of Open RAN, where individual elements of RAN are replaced to optimize the operation of the entire network.

Simulation setup

We consider a typical HetNet deployed, consisting of one high-power macro-BS and four small cells. To promote access to small cells, O-RAN Service Provider (OSP) can apply a dedicated power offset (achieving cell range extension). All cells may operate in two separated bands, i.e., a carrier frequency of 800 MHz with 5 MHz channel bandwidth and 2 GHz with 10 MHz bandwidth. Only DL transmission is considered. From the point of view of MNO, there is a cost c associated with the selection of lower and higher frequency bands, which reflect various kinds of loads for MNO, such as energy consumption cost, prices for a license, etc. Over the considered area, two types of users are randomly deployed with uniform distribution. A total of 80% are voice users (whose traffic is characterized by the constant and relatively low bit rate of $\approx$ 250 kbps), and the rest are MBB users (with a constant and high bit rate of 3 Mbps). The user is assumed to be in an outage when its achieved bit rate is below the required one. Let us also mention that our implementation is generic, i.e., we intentionally did not apply any of the existing platforms for RIC simulation. Our goal is to illustrate the benefits of xApp modularity supported by defined interfaces and the independence of the RIC platform. Let us remind that results have been published in [223].

xApp implementation

The key goal is to make the TS functionality modular, changeable, controlled by an AI engine, and accessible by other external applications and by human administrators, as shown in Fig. 6.21.

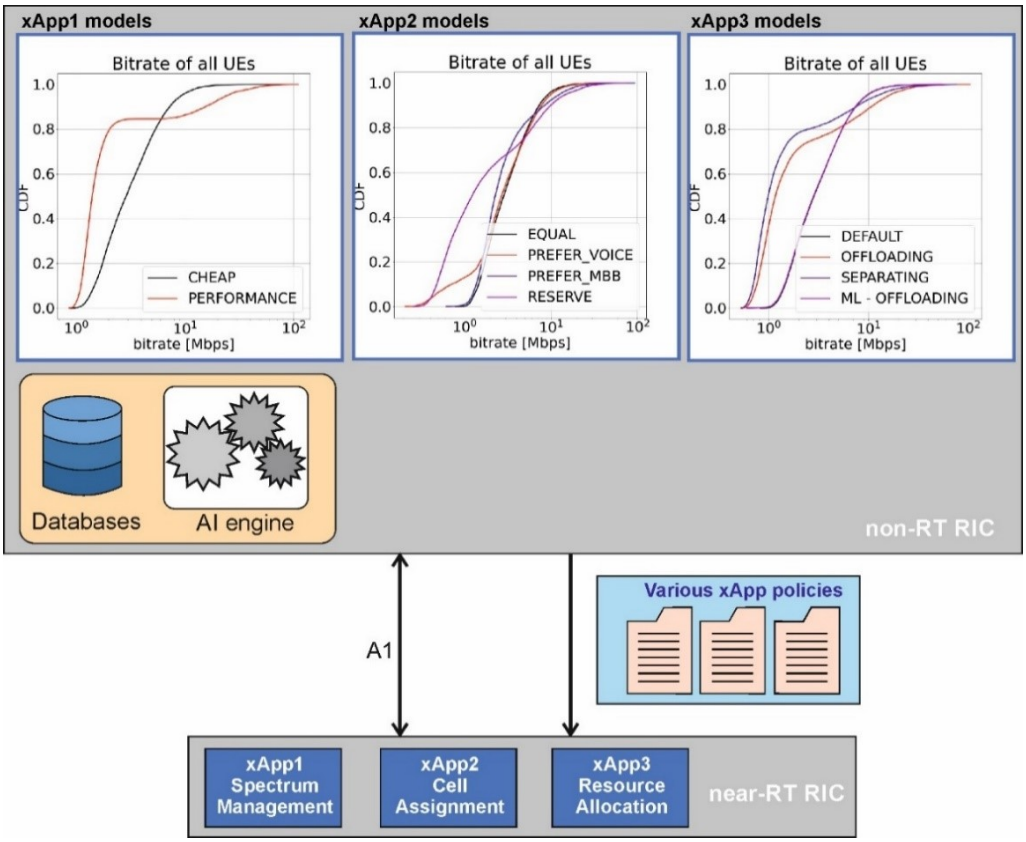

FIGURE 6.21: Mapping of xApps installations to RICs (xApp1—Spectrum Management, xApp2—Cell Assignment, xApp3—Resource Allocation)

We focused on the TS case, where OSP can apply various functioning policies, which are passed to independent xApps and realized in near-RT RIC. First, OSP may specify the rules of how the available two frequency bands should be utilized—this functionality is delivered to OSP in the form of xApp1. Second, OSP may define the preferences of usage of either the macro base station or the small cells (functionality delivered by xApp2). Finally, the priorities between the two types of users may be applied while offering them wireless services (defined within xApp3). Within each xApp, all necessary computations are performed to effectively apply the policies selected by OSP. In addition to that, non-RT RIC is equipped with an ML model to properly adjust policies to achieve certain goals based on non-RT measurements.

xApp1 (Spectrum Management) for Frequency Band Selection

One of the prospective TS schemes is to offload traffic from a congested frequency band to a less occupied one. When moving the operating central frequency from higher bands to lower values, one may talk about the cell-zooming approach [242], also investigated in Sec. 6.1 in the context of SMA. However, in a broader sense, various rules may be specified depending on the currently identified circumstances and needs of OSP. As we want to allow for RT modification of the policies, we define them in the form of specified tuples, which may be stored in the form of simple files, such as JSON or YAML, creating an Application Platform Interfaces (API). Let us note that the policy can specify that, for example, the small cells should "prefer" larger bandwidths over costs

or expected range, and the macro-cell should minimize its range. The word "prefer" should be treated loosely, allowing for various implementations by different applications. In the experiment, two policy options have been defined:

- CHEAP — where each cell should use the band with the lowest cost c
- PERFORMANCE — where macro-cells should prefer a band with a higher range, and small cells should prefer a band with greater bandwidth

xApp2 (Cell Assignment) for User Assignment to BS

Analogously, one may specify the policies for user assignment to BS. The set of rules, in this case, specifies the "preference" of cell classes for different user classes. As an example, the policy can specify that small cells should "prefer" MBB users over voice users, and macro-cells should "prefer" voice users over MBB users. In this work, the following policies were considered:

- DEFAULT — where users are assigned to cells based on strongest received power
- OFFLOADING — where MBB users should be preferred in small cells and voice users should be preferred in macro-cells
- SEPARATING — where MBB users should be assigned only to small cells, and voice users should be assigned only to macro-cells

xApp3 (Resource Allocation) for Resource Scheduling

Finally, the last xApp is responsible for the definition of the prospective resource allocation strategy per BS. The policies in this case specify the "preference" of users of a specific class in terms of resource allocation. As an example, the policy can specify that MBB users will have more bandwidth allocated than voice users. Four policies have been identified:

- EQUAL — where all users have an equal amount of bandwidth allocated
- PREFER_VOICE — where voice users have a larger bandwidth allocated (proportionally)
- PREFER_MBB — where MBB users have a larger bandwidth allocated (proportionally)
- RESERVE — where a specific user class has a reserved portion of bandwidth that can be used only by users of this class

To be able to measure the performance of the system, the default setup of the network has been defined, where the cheapest frequency band is selected, the users are assigned to the cell-based on received signal power, and the radio resources are allocated equally among the users.

System training

Once the applications have been defined and implemented, we verified their functioning in all configurations. Thus, the performance of each xApp has been tested in terms of observed rate and outage probability, averaged over numerous user location deployments. Moreover, various joint configurations have been tested, e.g., simultaneous installation of xApp1 and xApp2. The achieved results have been presented and stored in the form of Cumulative Density Functions (CDF). Selected results are also shown in Fig. 6.21 for illustrative purposes only. By analyzing each particular plot, one can observe that while in some situations it is worth applying a certain

policy, it is not that beneficial in other cases. Thus, to select the most promising policy, either the system administrator should analyze the curves and decide on the best strategy or let AI tools do it based on predefined criteria. In our tests, we have applied a simple ML tool (sitting at the non-RT RIC)—logistic regression, which allows for the selection of the policy that reduces outage in the system. Fig. 6.21 presents the trained models, or more precisely, achieved CDFs, which are available in non-RT RIC and influence the policy choice by near-RT RIC. Having such a system, we have performed experiments proving the benefits of xApp modularity, as discussed in the next section.

6.3.3 Simulation results

In our experiments, we did not concentrate on the performance of an individual xApp, but rather we focused on the modularity and flexibility of the whole O-RAN application. Thus, we specified three experimentation scenarios, for which we showed selected performance metrics (mean bitrate for MBB and Voice users and outage probability) as a function of time for a random but fixed deployment of users. These scenarios have been considered to observe the benefits of temporal installation or de-installation of certain xApps, or at least modification of their operating policies (see Fig. 6.22). Please notice that the reference setup to each scenario is the one where specific TS, spectrum management, and cell assignment algorithm is applied, and it is not subject to any changes.

Scenario 1: We start with the default, reference setup with no active xApp; at the 50 s time stamp, xApp1 is started, with the default CHEAP policy (analogous to the default setup), and thus no changes are observed; at 100 s, the policy changes to PERFORMANCE, leading to some mean bitrate increase (for both MBB and Voice users) but at the expense of some outage degradation; at 150 s, the system returns to the prior setup. As both the policy within xApp1, as well as the xApp1 itself can be modified (or even replaced, uninstalled, etc.), this scenario illustrates the benefits of xApp modularity and flexibility. OSP will have the opportunity to install or modify the selected features of its system even for a short time and observe the achieved results. Such performance measurements can also be analyzed by the AI engine to adjust the software to an instantaneous network change.

Scenario 2: Here, we extend the previous case to the situation where two separate xApps are installed, we observe interactions between them and react accordingly; thus, at 50 s, xApp3 starts preferring MBB users over voice users, thus the bitrate of MBB uses increases, and for Voice users, it decreases, leading at the same time to an improvement of outage probability; at 100 s, xApp1 chooses PERFORMANCE, which in this network state (i.e., location of users, their requests for resources) causes performance degradation; thus, the system selects again the CHEAP strategies at 150 s. This scheme shows the benefits of flexibility available to OSP—it can select the most suitable setup of the installed xApps and react immediately when any performance deterioration is observed. Please note that it is also possible to change or apply new policies within each xApp in order to adjust them to the current OSP needs. Such flexibility may not be easily available in a static, non-O-RAN scheme. This scheme also shows the prospective challenge that OSP has to face, i.e., maintaining the conformance of installed applications. Thus, the application of AI tools may be necessary.

Scenario 3: This is the most complicated scheme in our investigation. We start with all considered xApps running, and xApp1 works in the PERFORMANCE mode. Next, at 50 s, xApp starts preferring MBB users (resulting in MBB bitrate increase at no other cost), and at 100 s xApp2 selects the OFFLOADING policy (which is associated with some additional cost for OSP,

some deterioration of Voice bitrate but significant gain in outage probability), whereas at 150 s, xApp1 returns to the CHEAP mode. One can observe that by testing these variants, at the end, OSP can find the best setup. Such an approach offers OSP the possibility to dynamically adjust the system setup to the changing network state. As the immediate installation and modification of selected features are not easily available in a black-boxed approach, the modularity and flexibility can then be treated as a good performance improvement opportunity.

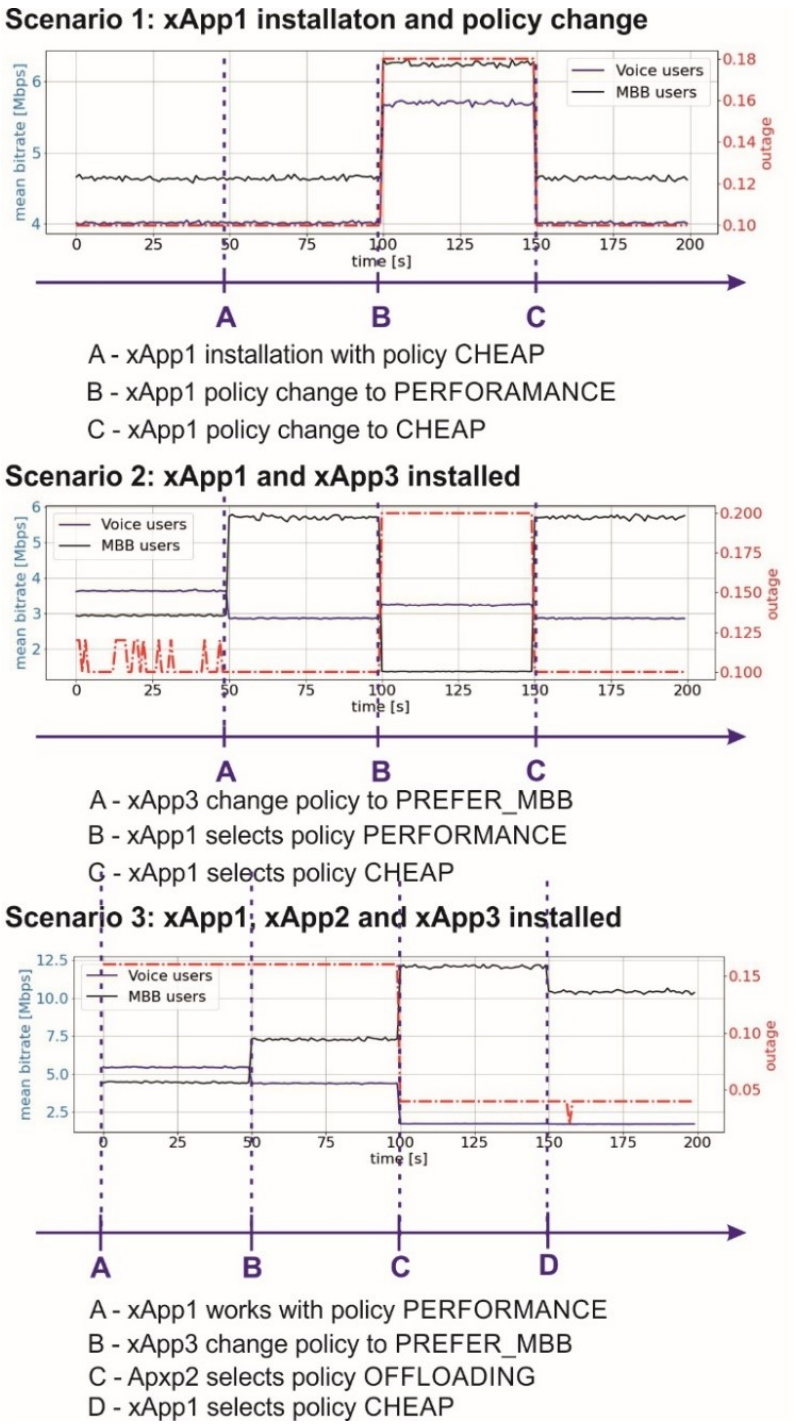

FIGURE 6.22: Achieved results for three considered experimentation schemes

Discussion

We provided an overview of the O-RAN concept with particular emphasis on the RIC platform and RRM algorithm implementation and interaction in the form of xApps, along with ML-equipped modules. Such a programmable and highly modular RAN structure has a significant impact on future wireless network implementation. Using the O-RAN concept offers various benefits, such as:

- adding intelligence to network with external entities (such as xApps or RIC)
- controlling RAN behavior by declarative policies
- combination of various applications to realize certain objectives/strategies
- a hierarchical and modular approach to resource management
- flexibility and modularity of RAN
- defining applications/xApps per use case basis

Looking into the interactions between the example xApps developed in the due time of this work, namely Cell Assignment, Spectrum Management, and Resource Allocation, the following holds:

- this approach increases the flexibility of controlling radio resources within the whole Traffic Steering use case, by playing with the radio resources on three levels
- combining the policies for the different xApps offers a possibility to optimize the usage of radio resources according to the selected strategy
- hierarchization allows for the separation of the concerns and focusing on a specific item
- modularization allows for expanding the framework with new xApps in a plug-and-play manner, which does not change the overall structure

Summarizing the achieved results, one can observe that the possibility of installing/uninstalling the xApp jointly with the tailored method for selecting the best policy creates promising ways for OSP to improve the network performance depending on its (current) needs. The software modularity allows for fast adjustments of network functioning, thus leading to efficiency increase and adaptation to a particular situation or scenario.

Regarding the machine learning application within the Open RAN design, one example is the prediction of latency performed at RIC. Based on the predicted latency, near-RT RIC could, e.g., request O-DU to modify the scheduling priority of an individual user or primary/secondary cell reselection. One such application scenario is ultra-reliable and low latency communications, where keeping low and/or predictive latency is one of the key requirements. In addition to that, management of the network slices is one of the key applications of Open RAN, where dynamic set up, modification, scaling, and deleting of a network slice requires such an approach to virtualized and dynamically managed RAN.

Summary

A compact summary of the use of contextual information to improve spectral efficiency is presented in Table 6.4 below.

Ph.D. candidate's publications considering problems discussed in this section	[222], [223]
Context information	The current network administrator's preference; list of cells with their parameters available through E2 interface, i.e. list of UEs associated with particular cell, radio parameters, and position; list of UEs with thier parameters available through E2 interface, i.e. receiver power reports, QoS reports, channel quality estimation, and bitrate.
Influence on the system	Modification of the association process of UEs to cells; modification of the allocation process of radio resources to UEs; modification of the selection process of the band used by cells.
Impact on spectrum efficiency	Modification of the system operation on many levels; spectral efficiency improvement possible if it is the actual intention of the operator, otherwise other metrics will be maximized.
Comment	By using the presented applications, the administrator can increase the dynamic control over the system and choose the priorities at a given time.

Table 6.4: Summary of work presented in chapter 6.3

Chapter 7

Conclusions

In this dissertation, we discussed the challenges associated with ineffective utilization of radio resources in contemporary and future wireless networks. As described and explained extensively in this thesis, one of the ways to improve spectral efficiency is to use a Dynamic Spectrum Access (DSA) system, the integral and necessary part of which is access to rich contextual information. The method of collecting, storing, and using contextual information is not trivial, requires careful development, and adaptation to a specific situation, i.e., to the designed DSA system. As an example, the process of both collecting and processing data regarding the signal in the TV band was presented. Such context information effectively served as the basis for the DSA systems presented in the following parts of the dissertation. Let us recall the research thesis put forward at the beginning: *With the use of contextual information, it is possible to design a spectrum management algorithm, as a result of which the spectral efficiency of the system is increased.*

The dissertation collects the results of research on various types of context information applied to improve spectral efficiency in various ways. In Table 7.1, we summarized the investigated types of contextual information and compared their impact on the system performance. From among all the studies carried out, we distinguished eight aspects of the system, which may be modified leading to the spectral efficiency improvement of the entire system. These are enabling, among others, access to the spectrum for unlicensed users, modification of the spectrum allocation method, or the method of assigning users to base stations. A similar step was taken for the contextual information collected in all investigations, such as the position of devices, transmission parameters, the quality of service observed, or applied policy. The types of contextual information have been additionally grouped as information specific to the primary, and secondary systems, or others. It is worth noting that in the situations where the spectrum was not shared between two systems, the contextual information was only related to the primary system, which can be seen in Table 7.1.

It can be observed that the possibility of allowing transmissions for an unlicensed user, controlling the transmit power, or selecting the used band is associated with with the necessity to have a large amount of contextual data. As repeatedly mentioned in the thesis, it is understandable, as the mentioned actions significantly impact the radio environment. In particular, they can introduce harmful interference to users of the primary system, which should be protected against such a situation. For this reason, detailed information about the primary system should be available for the DSA system, like a list of protected devices, with their interference requirements, receiver characteristics, QoS reports, occupied frequency range, etc. In Chap. 3, and Chap. 4, it was shown that, with the above assumptions, it is possible to develop a DSA system that allows access to the spectrum for unlicensed users.

TABLE 7.1: Summary of context information influence on the wireless system

Utilized types of context information		Influence on the system by: A) access to spectrum for unlicensed users	B) allowed transmit power selection	C) band selection among transmitters	D) spectrum allocation among users (scheduling)	E) users to cells assignment	F) use of emergency network nodes	G) selection of a spectrum access and pricing plans	H) modification of routes used in the network
Primary system	Position	✓	✓	✓	✓	✓	✓	✓	✓
	Transmit power	✓	✓	✓	✓	✓		✓	
	Received power	✓	✓	✓	✓	✓	✓		✓
	Device type	✓	✓	✓	✓	✓		✓	
	Bitrate	✓	✓		✓	✓			
	QoS reports	✓	✓	✓	✓	✓	✓	✓	✓
	List of devices	✓	✓	✓	✓	✓			
	Allowed interference	✓	✓	✓	✓	✓			
	Transmitter parameters	✓	✓	✓	✓	✓	✓	✓	✓
Secondary system	Position	✓	✓	✓	✓	✓			
	Transmit power	✓	✓	✓	✓	✓			
	Allocated bandwidth	✓	✓	✓	✓	✓			
	Allocated frequency	✓	✓	✓	✓	✓			
	Bitrate	✓	✓		✓	✓			
	MCS allocation	✓	✓		✓	✓			
	List of devices	✓	✓	✓	✓	✓			
	Allowed interference	✓	✓	✓					
	Waveform capabilities	✓	✓	✓					
	Receiver parameters	✓	✓	✓	✓	✓		✓	
	Transmitter parameters	✓	✓	✓	✓	✓			
	Transmission requirements	✓	✓	✓	✓	✓			
Miscellaneous	NRA regulations	✓	✓	✓				✓	
	LSA rules	✓	✓		✓	✓			
	User to cell association		✓				✓		✓
	Setup of CRE	✓	✓		✓	✓			
	Channel quality estimation	✓	✓	✓			✓		✓
	Available spectrum bands	✓	✓	✓				✓	
	Administrator's preferences	✓	✓	✓				✓	
	Emergency detection		✓				✓		✓

An important observation is that it is possible to identify some key contextual information that allows the improvement of spectral efficiency in the network through all the aspects identified in this paper. This includes the position of devices, primary user transmission parameters, received signal power, and QoS reports. Obviously, not all information is needed at once for all DSA systems. It is important to be able to estimate the interference that will be introduced to primary users after the transmission of unlicensed users is allowed. For this purpose, one can use QoS reports, reflecting how much the interference affects the primary users. When we do not have access to this information or want to improve the described mechanism, we can additionally estimate the interference in advance. However, we need to know at least the approximate location and transmission parameters of primary system devices for this.

Not so much contextual information is required to improve spectral efficiency by changing the radio resource allocation method for users (scheduling). There is less risk of introducing excessive interference to other systems in this case, as we distribute radio resources within the already occupied fragment of the spectrum. However, contextual information is needed here more to improve the efficiency of the throughput, or more generally the quality of service, of the users of a given network. Hence, in this process, the knowledge of the historical location, throughput, requests, and quality of the radio channel can be useful in the resource allocation process, as shown, for example, in Chap. 4. Similarly, in simple solutions, emergency network nodes require only a small amount of contest information. The data is needed here primarily to determine the moment of switching on or off an additional device and estimate the emergency device's location, which will most effectively improve the operation of the network. As such a device somehow replaces the transmission of a broken device, the radio environment does not change significantly.

It is worth adding that the presented table contains only simplified information. For most types of contextual information, it is much more beneficial to collect data over time and analyze the history of changes in value data. As opposed to access only the instantaneous value of given contextual information, we can distinguish certain patterns that allow us to make even better decisions. Moreover, it should be noted that in each of the systems under consideration, regardless of the type of contextual information, it is necessary to constantly update the collected data. The frequency and method of updating them obviously depend on a specific case. So in the case of e.g. the TV band, rare updates are sufficient (because the parameters of TV signal transmitters are rarely changed or new transmitters are rarely deployed), but in more dynamic networks, such as 5G or networks using M-MIMO technologies, the updating of data has to be much more detailed and frequent. Let us stress that all of the above conclusions are in line with the key research thesis of this work - we see the opportunities created by the access to rich context information with the purpose of improving spectral efficiency.

To summarize, we also provide a brief conclusion of the work performed within each chapter. Additionally, Table 7.2 presents a list of Ph.D. candidate publications classified according to the way they affect the radio network with the use of contextual information.

Table 7.2: Summary of system aspects modified with context information utilization in author's publications

Influence on the system by		Used in the author's publications
A)	access to spectrum for unlicensed users	[75] [114] [115] [116] [119] [124] [125] [133] [134] [137] [138] [213] [219] [223]
B)	allowed transmit power selection	[75] [114] [116] [119] [123] [124] [125] [133] [134] [178] [180] [189] [190] [191] [194] [197] [209] [210] [223]
C)	band selection among transmitters	[75] [114] [115] [116] [119] [123] [124] [125] [133] [134] [213] [219] [222] [223]
D)	spectrum allocation among users (scheduling)	[133] [134] [137] [138] [145] [223]
E)	users to cells assignment	[133] [134] [137] [138] [145] [222] [223]
F)	use of emergency network nodes	[177] [180] [188] [189] [190] [191] [194] [197] [210]
G)	selection of a spectrum access and pricing plans	[123] [124] [125] [213] [219] [222] [223]
H)	modification of routes used in the network	[177] [178] [180] [188] [189] [190] [191] [194] [197] [209] [210]

The whole Chap. 3 is devoted to context information utilization in DSA systems, deliberately bypassing the limitations of existing networks. In Sec. 3.1 it was shown that, without a doubt, as a result of computer simulation, it is possible to improve spectral efficiency, assuming the presence of a contextual information database and using an appropriate algorithm that takes this contextual information into account when operating in the system. The most important example is the television spectrum access system for unlicensed users - where, according to simulations, in a huge number of cases (potential unlicensed user positions), it is possible to gain access to the spectrum while not disturbing primary users. Then, in Sec. 3.2, the pre-verified theorem was subjected to another trial where the same system, as in Sec. 3.1, was tested with real hardware. As a result, it was possible to carry out video transmissions between unlicensed users who used the television band in laboratory conditions while maintaining the possibility of receiving terrestrial television in the same place. It is worth emphasizing here that enabling transmission is possible in many places (especially inside buildings) due to the low use of the TV band and the often low level of the signal received inside buildings (where an external antenna is necessary for proper TV reception). In Sec. 3.3, rich context information about CBSDs was used in the CBRS-SAS system to develop an algorithm of the joint spectrum and power allocation between CBSDs. Thanks to the use of contextual information, it was possible to maximize the mean bitrate per km^2 of CBSDs, which increases a spectrum efficiency over an area unit. Moreover, in Sec. 3.4, the algorithm of waveform selection of secondary users improves the spectrum efficiency of the system through increased flexibility in spectrum allocation to users, which in turn translates into a greater number of users using the same part of the spectrum. Such an algorithm requires contextual information to work. The research described in this chapter mainly addresses the use of contextual information to improve spectral efficiency, as shown in Table 7.1, by enabling spectrum access for unlicensed users, selecting the band used by the devices, and controlling the transmit power of the devices.

After such two attempts (simulation and experiment in the laboratory), the next step was made to verify the validity of this thesis. We try to face the challenges due to the inclusion of existing networks or applied standards and regulations. In Sec. 4.1, another system of access to the spectrum was designed, which, this time in field tests in the real network, confirmed the possibility of using the spectrum by unlicensed users without a noticeable decrease in the quality of licensed transmission. This experiment, carried out using real equipment and a commercial radio-access network to the Internet, was another confirmation of the validity of the thesis put forward here. Next, in Sec. 4.2, through simulation of the network which serves access for indoor and outdoor users, the algorithm of semi-persistent scheduling was described. By taking advantage of contextual information about the resource allocation history for users, some users get resources allocated for a longer time (than the default). This results in a reduction in the amount of control data sent over the network by reducing the number of scheduler decisions. Moreover, the applied algorithm enables spectrum sharing between users inside the building and that outside. Here again, the algorithm's operation would not be possible without access to rich contextual information about network users. Additionally, in Sec. 4.3, it has been shown by simulation that having contextual information about the history of assigning users to cells, it is possible to improve the current assignment of users to cells. In this section, the main challenge was using the LTE-A standard requirements, limiting the freedom to modify the method of assigning users to cells. However, it is still possible to modify the CRE parameter. In this case, the use of contextual information improves the throughput of all network users, with a low cost of more switches between cells. The research described in this chapter addresses the use of contextual information to improve spectral efficiency (see Table 7.1) by enabling spectrum access for unlicensed users, controlling the transmit power of the devices, scheduling radio resources among users, and assigning of users to cells.

In Chap. 5, the simulation presents several inspirations from the human nervous system that can be used in ultra-dense networks. The most important assumption in this proposal is the use of a very simplified transmission in the network and the addition of network nodes that perform additional functions to improve the system's reliability. In this case, individual network nodes collect, store, and use contextual information about neighboring nodes, which makes it possible to provide more reliable transmission. Reliability of transmission is crucial from the point of view of spectral efficiency because, of course, only a correct and effectively transmitted message is of value in this context. In Sec. 5.1 reliability and availability of the proposed exemplary network were analyzed utilizing RBDs. In Sec. 5.2, in turn, a more general reliability assessment of proposed solutions was presented with the use of stochastic geometry, i.e., percolation theory. The research described in this chapter mainly addresses the use of contextual information to improve spectral efficiency, as shown in Table 7.1, by controlling the transmit power of the devices, using of emergency network nodes, and modifying routes used in the network.

Then, in Chap. 6, the SMA concept is presented along with examples of its development, implementation, and even verification with the use of hardware. This concept is an important part of radio access virtualization, which assumes the implementation of specific functionalities of the RAN network in the form of software. SMA application requires contextual information to operate, thanks to which it can meet the operator's expectations, which are defined in the form of the currently applied policy set. In Sec. 6.1 we showed SMA implementation, which was verified with the usage of real equipment. The results of such an experiment are shown in the real-time possibility of the policy-based spectrum management, realized in the form of an application working within the RAN controller. Context information about available bands, their parameters, and operator preferences was fundamental to system operation. In Sec. 6.2, we show an innovative concept for the design of a SMA, where the operator band is distributed between base stations (and, consequently, users) according to the freemium concept. Inspiration for this work was a quite popular concept in mobile services and applications, which assumes free access to the service for all users, with a limited scope of these services or a wider range of services and improved quality of service for an additional fee. In Sec. 6.3, we show the use of an application (so-called xApp) managing user traffic in an open radio network. By changing the method of assigning bands to base stations, assigning users to cells, or allocating radio resources to users, it is possible to improve the spectral efficiency of the entire system. However, it is worth noting that this must be an objective defined in the policies. The research described in this chapter mainly addresses the use of contextual information to improve spectral efficiency, as shown in Table 7.1, by enabling spectrum access for unlicensed users, controlling the transmit power of the devices, selecting the band used by the devices, and selecting spectrum access and pricing plans.

In this dissertation, it has been shown from many perspectives and in many ways that it is indeed possible to improve the spectral effectiveness of the network by using contextual information, which confirms the thesis put forward in this thesis.

Bibliography

[1] J. Mitola and G. Maguire, "Cognitive radio: making software radios more personal," *IEEE Personal Communications*, vol. 6, no. 4, pp. 13–18, 1999.

[2] M. A. McHenry, P. A. Tenhula, D. McCloskey, D. A. Roberson, and C. S. Hood, "Chicago spectrum occupancy measurements & analysis and a long-term studies proposal," in *Proceedings of the First International Workshop on Technology and Policy for Accessing Spectrum*, TAPAS '06, (New York, NY, USA), p. 1–es, Association for Computing Machinery, 2006.

[3] M. Wellens, J. Riihijärvi, and P. Mähönen, "Empirical time and frequency domain models of spectrum use," *Physical Communication*, vol. 2, no. 1, pp. 10–32, 2009. Cognitive Radio Networks: Algorithms and System Design.

[4] A. Palaios, J. Riihijärvi, P. Mähönen, V. Atanasovski, L. Gavrilovska, P. Van Wesemael, A. Dejonghe, and P. Scheele, "Two days of spectrum use in Europe," in *2012 7th International ICST Conference on Cognitive Radio Oriented Wireless Networks and Communications (CROWNCOM)*, pp. 24–29, 2012.

[5] A. Palaios, J. Riihijärvi, O. Holland, and P. Mähönen, "A week in London: Spectrum usage in metropolitan London," in *2013 IEEE 24th Annual International Symposium on Personal, Indoor, and Mobile Radio Communications (PIMRC)*, pp. 2522–2527, 2013.

[6] M. Lopez-Benitez, F. Casadevall, A. Umbert, J. Perez-Romero, R. Hachemani, J. Palicot, and C. Moy, "Spectral occupation measurements and blind standard recognition sensor for cognitive radio networks," in *2009 4th International Conference on Cognitive Radio Oriented Wireless Networks and Communications*, pp. 1–9, 2009.

[7] T. Yucek and H. Arslan, "A survey of spectrum sensing algorithms for cognitive radio applications," *IEEE Communications Surveys Tutorials*, vol. 11, no. 1, pp. 116–130, 2009.

[8] M. Höyhtyä, A. Mämmelä, M. Eskola, M. Matinmikko, J. Kalliovaara, J. Ojaniemi, J. Suutala, R. Ekman, R. Bacchus, and D. Roberson, "Spectrum occupancy measurements: A survey and use of interference maps," *IEEE Communications Surveys Tutorials*, vol. 18, no. 4, pp. 2386–2414, 2016.

[9] P. Angueira, M. Fadda, J. Morgade, M. Murroni, and V. Popescu, "Field measurements for practical unlicensed communication in the UHF band," *Telecommun. Syst.*, vol. 61, p. 443–449, mar 2016.

[10] V. Popescu, M. Fadda, M. Murroni, J. Morgade, and P. Angueira, "Co-channel and adjacent channel interference and protection issues for DVB-T2 and IEEE 802.22 WRAN operation," *IEEE Transactions on Broadcasting*, vol. 60, no. 4, pp. 693–700, 2014.

[11] M. Fadda, M. Murroni, V. Popescu, P. Angueira, J. Morgade, and M. Sanchez, "Hidden node margin and man-made noise measurements in the UHF broadcasting bands," in *IEEE international Symposium on Broadband Multimedia Systems and Broadcasting*, pp. 1–5, 2012.

[12] S. Contreras, G. Villardi, R. Funada, and H. Harada, "An investigation into the spectrum occupancy in Japan in the context of TV White Space systems," in *2011 6th International ICST*

Conference on Cognitive Radio Oriented Wireless Networks and Communications (CROWNCOM), pp. 341–345, 2011.

[13] M. T. Masonta, A. Kliks, and M. Mzyece, "Unlocking the potential of unoccupied spectrum in developing countries: Southern African development community – case study," *Development Southern Africa*, vol. 34, no. 2, pp. 224–244, 2017.

[14] ECC, "Harmonised technical and regulatory conditions for the use of the band 2300 - 2400 MHz for Mobile/Fixed Communications Networks (MFCN)," Decision 14(02), European Electronic Communications Committee, June 2014.

[15] ETSI, "White Space Devices (WSD); Wireless Access Systems operating in the 470 MHz to 790 MHz TV broadcast band; Harmonized EN covering the essential requirements of article 3.2 of the R&TTE Directive," Tech. Rep. EN 301 598, European Telecommunications Standards Institute, April 2014.

[16] RSPG, "Strategic roadmap towards 5G for Europe; Opinion on spectrum related aspects for next-generation wireless systems (5G)," Tech. Rep. RSPG16-032, Radio Spectrum Policy Group, Nov. 2016.

[17] FCC, "Final Acts of the Regional Radiocommunication Conference for planning of the digital terrestrial broadcasting service in parts of Regions 1 and 3, in the frequency bands 174-230 MHz and 470-862 MHz (RRC-06)," tech. rep., International Telecommunication Union, June 2006.

[18] P. Lamy, "Report on the future use of the UHF band." `http://ec.europa.eu/newsroom/dae/document.cfm?doc_id=6721`, Aug. 2014.

[19] Office of Communications, "Implementing TV White Spaces." `http://stakeholders.ofcom.org.uk/binaries/consultations/white-space-coexistence/statement/tvws-statement.pdf`, Feb. 2015.

[20] Office of Communications, "Licensing manually configurable White Space devices." `http://stakeholders.ofcom.org.uk/binaries/consultations/manually-configurable-wsds/statement/Licensing_manually_configurable_white_space_devices.pdf`, Sept. 2015.

[21] ETSI, "Reconfigurable Radio Systems (RRS); System requirements for operation of Mobile Broadband Systems in the 2300 MHz - 2400 MHz band under Licensed Shared Access (LSA)," Tech. Rep. TS 103 154 V1.1.1, European Telecommunications Standards Institute, Oct. 2014.

[22] FCC, "Order on reconsideration and second report and order in the matter of amendment of the commissions rules with regard to commercial operations in the 3550-3650 MHz band," Tech. Rep. 16-55, Federal Communications Commission, May 2016.

[23] ITU, "Minimum requirements related to technical performance for IMT 2020 radio interface(s)," tech. rep., International Telecommunication Union, Nov. 2017.

[24] K. King, "5G in the wild: Verizon and Nokia mark two industry firsts over 3GPP New Radio technology." `https://www.verizon.com/about/news/5g-wild-verizon-and-nokia-mark-two-industry-firsts-over-3gpp-new-radio-technology`, 2018.

[25] M. Latva-aho, and K. Lappanen, "Key drivers and research challenges for 6G ubiquitous wireless intelligence." `http://jultika.oulu.fi/files/isbn9789526223544.pdf`, 2019.

[26] H. Tataria, M. Shafi, A. F. Molisch, M. Dohler, H. Sjöland, and F. Tufvesson, "6G wireless systems: Vision, requirements, challenges, insights, and opportunities," *Proceedings of the IEEE*, vol. 109, no. 7, pp. 1166–1199, 2021.

[27] T. Irnich, J. Kronander, Y. Selén, and G. Li, "Spectrum sharing scenarios and resulting technical requirements for 5G systems," in *2013 IEEE 24th International Symposium on Personal, Indoor and Mobile Radio Communications (PIMRC Workshops)*, pp. 127–132, 2013.

[28] J. G. Andrews, S. Buzzi, W. Choi, S. V. Hanly, A. Lozano, A. C. K. Soong, and J. C. Zhang, "What Will 5G Be?," *IEEE Journal on Selected Areas in Communications*, vol. 32, no. 6, pp. 1065–1082, 2014.

[29] R. H. Tehrani, S. Vahid, D. Triantafyllopoulou, H. Lee, and K. Moessner, "Licensed spectrum sharing schemes for mobile operators: A survey and outlook," *IEEE Communications Surveys Tutorials*, vol. 18, no. 4, pp. 2591–2623, 2016.

[30] Y. R. Ramadan, H. Minn, and Y. Dai, "A new paradigm for spectrum sharing between cellular wireless communications and radio astronomy systems," *IEEE Transactions on Communications*, vol. 65, no. 9, pp. 3985–3999, 2017.

[31] C. Galiotto, G. K. Papageorgiou, K. Voulgaris, M. M. Butt, N. Marchetti, and C. B. Papadias, "Unlocking the deployment of spectrum sharing with a policy enforcement framework," *IEEE Access*, vol. 6, pp. 11793–11803, 2018.

[32] J. Van De Beek, T. Cai, S. Grimoud, B. Sayrac, P. Mahonen, J. Nasreddine, and J. Riihijarvi, "How a layered REM architecture brings cognition to today's mobile networks," *IEEE Wireless Communications*, vol. 19, no. 4, pp. 17–24, 2012.

[33] C. Suarez-Rodriguez, Y. He, and E. Dutkiewicz, "Theoretical analysis of REM-based handover algorithm for heterogeneous networks," *IEEE Access*, vol. 7, pp. 96719–96731, 2019.

[34] M. Yao, M. Sohul, V. Marojevic, and J. H. Reed, "Artificial intelligence defined 5G radio access networks," *IEEE Communications Magazine*, vol. 57, no. 3, pp. 14–20, 2019.

[35] T. Yucek and H. Arslan, "A survey of spectrum sensing algorithms for cognitive radio applications," *IEEE Communications Surveys Tutorials*, vol. 11, pp. 116–130, First 2009.

[36] M. Höyhtyä, A. Mämmelä, M. Eskola, M. Matinmikko, J. Kalliovaara, J. Ojaniemi, J. Suutala, R. Ekman, R. Bacchus, and D. Roberson, "Spectrum occupancy measurements: A survey and use of interference maps," *IEEE Communications Surveys Tutorials*, vol. 18, pp. 2386–2414, Fourthquarter 2016.

[37] FCC, "Unlicensed Operation in the TV Broadcast Bands/Additional Spectrum for Unlicensed Devices Below 900 MHz and in the 3 GHz Band," Tech. Rep. 12-36, Federal Communications Commission, Apr. 2012.

[38] FCC, "FCC establishes rules for unlicensed operations in the TV and the 600 MHz bands," Tech. Rep. 15-99, Federal Communications Commission, Aug. 2015.

[39] ECC, "ECC Report 159, Technical and operational requirements for the possible operation of cognitive radio systems in the White Spaces of the frequency band 470-790 MHz," tech. rep., Electronic Communications Committee, Jan. 2011.

[40] ECC, "ECC Report 185, Complementary Report to ECC Report 159 Further definition of technical and operational requirements for the operation of White Space devices in the band 470-790 MHz," tech. rep., Electronic Communications Committee, Jan. 2013.

[41] ECC, "ECC Report 186, Technical and operational requirements for the operation of White Space devices under geo-location approach," tech. rep., Electronic Communications Committee, Jan. 2013.

[42] K. B. Letaief and W. Zhang, "Cooperative communications for cognitive radio networks," *Proceedings of the IEEE*, vol. 97, no. 5, pp. 878–893, 2009.

[43] K. Cichoń, A. Kliks, and H. Bogucka, "Energy-efficient cooperative spectrum sensing: A survey," *IEEE Communications Surveys Tutorials*, vol. 18, no. 3, pp. 1861–1886, 2016.

[44] H. B. Yilmaz, T. Tugcu, F. Alagöz, and S. Bayhan, "Radio Environment Map as enabler for practical cognitive radio networks," *IEEE Communications Magazine*, vol. 51, no. 12, pp. 162–169, 2013.

[45] L. M. Gavrilovska and V. M. Atanasovski, "Dynamic REM towards flexible spectrum management," in *2013 11th International Conference on Telecommunications in Modern Satellite, Cable and Broadcasting Services (TELSIKS)*, vol. 01, pp. 287–296, 2013.

[46] J. Perez-Romero, A. Zalonis, L. Boukhatem, A. Kliks, K. Koutlia, N. Dimitriou, and R. Kurda, "On the use of Radio Environment Maps for interference management in heterogeneous networks," *IEEE Communications Magazine*, vol. 53, no. 8, pp. 184–191, 2015.

[47] ECC, "ECC Report 236, Guidance for national implementation of a regulatory framework for TV WSD using geo-location databases," tech. rep., Electronic Communications Committee, May 2015.

[48] A. B. MacKenzie, J. H. Reed, P. Athanas, C. W. Bostian, R. M. Buehrer, L. A. DaSilva, S. W. Ellingson, Y. T. Hou, M. Hsiao, J.-M. Park, C. Patterson, S. Raman, and C. R. C. M. da Silva, "Cognitive radio and networking research at virginia tech," *Proceedings of the IEEE*, vol. 97, no. 4, pp. 660–688, 2009.

[49] J. Zander, L. K. Rasmussen, K. W. Sung, P. Mahonen, M. Petrova, R. Jantti, and J. Kronander, "On the scalability of cognitive radio: assessing the commercial viability of secondary spectrum access," *IEEE Wireless Communications*, vol. 20, no. 2, pp. 28–36, 2013.

[50] J. Xiao, R. Q. Hu, Y. Qian, L. Gong, and B. Wang, "Expanding lte network spectrum with cognitive radios: From concept to implementation," *IEEE Wireless Communications*, vol. 20, no. 2, pp. 12–19, 2013.

[51] T. Dudda and T. Irnich, "Capacity of cellular networks deployed in TV White Space," in *2012 IEEE International Symposium on Dynamic Spectrum Access Networks*, pp. 254–265, 2012.

[52] A. Achtzehn, M. Petrova, and P. Mähönen, "On the performance of cellular network deployments in TV whitespaces," *2012 IEEE International Conference on Communications (ICC)*, pp. 1789–1794, 2012.

[53] A. K. Dey, G. D. Abowd, and D. Salber, "A conceptual framework and a toolkit for supporting the rapid prototyping of context-aware applications," *Hum.-Comput. Interact.*, vol. 16, p. 97–166, dec 2001.

[54] Q. Tang, O. Ermis, C. D. Nguyen, A. D. Oliveira, and A. Hirtzig, "A systematic analysis of 5G networks with a focus on 5G core security," *IEEE Access*, vol. 10, pp. 18298–18319, 2022.

[55] B. Schilit, D. Hilbert, and J. Trevor, "Context-aware communication," *IEEE Wireless Communications*, vol. 9, no. 5, pp. 46–54, 2002.

[56] A. L'Heureux, K. Grolinger, H. F. Elyamany, and M. A. M. Capretz, "Machine Learning with Big Data: Challenges and approaches," *IEEE Access*, vol. 5, pp. 7776–7797, 2017.

[57] M. Lee and D. Han, "Voronoi tessellation based interpolation method for wi-fi radio map construction," *IEEE Communications Letters*, vol. 16, no. 3, pp. 404–407, 2012.

[58] C. M. Wen, "The distance power inverse method of weight constraint and its application in three-dimensional modeling," in *2018 3rd International Conference on Smart City and Systems Engineering (ICSCSE)*, pp. 509–512, 2018.

[59] A. Konak, "Estimating path loss in wireless local area networks using ordinary kriging," in *Proceedings of the 2010 Winter Simulation Conference*, pp. 2888–2896, 2010.

[60] D. Denkovski, V. Rakovic, M. Pavloski, K. Chomu, V. Atanasovski, and L. Gavrilovska, "Integration of heterogeneous spectrum sensing devices towards accurate REM construction," in *2012 IEEE Wireless Communications and Networking Conference (WCNC)*, pp. 798–802, 2012.

[61] A. Chowdhery, R. Chandra, P. Garnett, and P. Mitchell, "Characterizing spectrum goodness for dynamic spectrum access," in *2012 50th Annual Allerton Conference on Communication, Control, and Computing (Allerton)*, pp. 1360–1367, 2012.

[62] M. M. Kassem and M. K. Marina, "Future wireless spectrum below 6 GHz: A UK perspective," in *2015 IEEE International Symposium on Dynamic Spectrum Access Networks (DySPAN)*, pp. 59–70, 2015.

[63] N. Wang, Y. Gao, and B. Evans, "Database-augmented spectrum sensing algorithm for cognitive radio," in *2015 IEEE International Conference on Communications (ICC)*, pp. 7468–7473, 2015.

[64] P. Tengkvist, G. P. Koudouridis, C. Qvarfordt, M. Dryjański, and M. Cellier, "Multi-dimensional radio service maps for position-based self-organized networks," in *2017 IEEE 22nd International Workshop on Computer Aided Modeling and Design of Communication Links and Networks (CAMAD)*, pp. 1–6, 2017.

[65] Z. Zhou, X. Chen, E. Li, L. Zeng, K. Luo, and J. Zhang, "Edge intelligence: Paving the last mile of artificial intelligence with edge computing," *Proceedings of the IEEE*, vol. 107, no. 8, pp. 1738–1762, 2019.

[66] I. Dagres, A. Polydoros, J. Riihijärvi, J. Nasreddine, P. Mähönen, L. Gavrilovska, V. Atanasovski, J. van de Beek, B. Sayrac, S. Grimoud, and et al., *Radio Environmental Maps: information models and reference model. Document number D4.1.* Apr 2011.

[67] IEEE Communications Society, "IEEE standard for definitions and concepts for dynamic spectrum access: Terminology relating to emerging wireless networks, system functionality, and spectrum management," *IEEE Std 1900.1-2019 (Revision of IEEE Std 1900.1-2008)*, pp. 1–78, 2019.

[68] IEEE Communications Society, "IEEE recommended practice for the analysis of in-band and adjacent band interference and coexistence between radio systems," *IEEE Std 1900.2-2008*, pp. 1–94, 2008.

[69] IEEE Communications Society, "IEEE standard for architectural building blocks enabling network-device distributed decision making for optimized radio resource usage in heterogeneous wireless access networks," *IEEE Std 1900.4-2009*, pp. 1–130, 2009.

[70] IEEE Communications Society, "IEEE standard for policy language for dynamic spectrum access systems," *1900.5.1-2020*, pp. 1–204, 2021.

[71] IEEE Communications Society, "IEEE standard for spectrum sensing interfaces and data structures for dynamic spectrum access and other advanced radio communication systems.," *IEEE Std 1900.6-2011*, pp. 1–168, 2011.

[72] IEEE Communications Society, "IEEE standard for radio interface for White Space Dynamic spectrum access radio systems supporting fixed and mobile operation," *IEEE Std 1900.7-2015*, pp. 1–67, 2016.

[73] Y. Ye, D. Wu, Z. Shu, and Y. Qian, "Overview of LTE Spectrum Sharing Technologies," *IEEE Access*, vol. 4, pp. 8105–8115, 2016.

[74] S. Haykin, "Cognitive radio: brain-empowered wireless communications," *IEEE Journal on Selected Areas in Communications*, vol. 23, pp. 201–220, Feb 2005.

[75] A. Kliks, P. Kryszkiewicz, A. Umbert, J. Perez-Romero, F. Casadevall, and Ł. Kułacz, "Application of Radio Environment Maps for dynamic broadband access in TV bands in urban areas," *IEEE Access*, vol. 5, pp. 19842–19863, 2017.

[76] A. Kliks, L. Goratti, and T. Chen, "REM: Revisiting a cognitive tool for virtualized 5G networks," in *2016 23rd International Conference on Telecommunications (ICT)*, pp. 1–5, May 2016.

[77] ECC, "Licensed Shared Access (LSA)," Report 205, European Electronic Communications Committee, Feb. 2014.

[78] FCC, "Part 96 — Citizens Broadband Radio Service," tech. rep., Federal Communications Commission, 2015. https://www.ecfr.gov/current/title-47/chapter-I/subchapter-D/part-96.

[79] M. T. Masonta, M. Mzyece, and N. Ntlatlapa, "Spectrum Decision in Cognitive Radio Networks: A Survey," *IEEE Communications Surveys Tutorials*, vol. 15, pp. 1088–1107, Third 2013.

[80] E. Z. Tragos, S. Zeadally, A. G. Fragkiadakis, and V. A. Siris, "Spectrum Assignment in Cognitive Radio Networks: A Comprehensive Survey," *IEEE Communications Surveys Tutorials*, vol. 15, pp. 1108–1135, Third 2013.

[81] E. Ahmed, A. Gani, S. Abolfazli, L. J. Yao, and S. U. Khan, "Channel Assignment Algorithms in Cognitive Radio Networks: Taxonomy, Open Issues, and Challenges," *IEEE Communications Surveys Tutorials*, vol. 18, pp. 795–823, Firstquarter 2016.

[82] R. H. Tehrani, S. Vahid, D. Triantafyllopoulou, H. Lee, and K. Moessner, "Licensed Spectrum Sharing Schemes for Mobile Operators: A Survey and Outlook," *IEEE Communications Surveys Tutorials*, vol. 18, pp. 2591–2623, Fourthquarter 2016.

[83] F. Paisana, N. Marchetti, and L. A. DaSilva, "Radar, TV and Cellular Bands: Which Spectrum Access Techniques for Which Bands?," *IEEE Communications Surveys Tutorials*, vol. 16, pp. 1193–1220, Third 2014.

[84] RSPG, "Report on Collective Use of Spectrum (CUS) and other spectrum sharing approaches, RSPG 11-392," tech. rep., Radio Spectrum Policy Group, 2011.

[85] M. Matinmikko, M. Mustonen, D. Roberson, J. Paavola, M. Höyhtyä, S. Yrjölä, and J. Röning, "Overview and comparison of recent spectrum sharing approaches in regulation and research: From opportunistic unlicensed access towards Licensed Shared Access," in *2014 IEEE International Symposium on Dynamic Spectrum Access Networks (DYSPAN)*, pp. 92–102, April 2014.

[86] M. Mustonen, M. Matinmikko, D. Roberson, and S. Yrjölä, "Evaluation of recent spectrum sharing models from the regulatory point of view," in *1st International Conference on 5G for Ubiquitous Connectivity*, pp. 11–16, Nov 2014.

[87] J. Kalliovaara, T. Jokela, H. Kokkinen, and J. Paavola, "Licensed Shared Access Evolution to Provide Exclusive and Dynamic Shared Spectrum Access for Novel 5G Use Cases," in *Cognitive Radio in 4G/5G Wireless Communication Systems* (S. S. Moghaddam, ed.), ch. 3, Rijeka: IntechOpen, 2018.

[88] T. Jokela, H. Kokkinen, J. Kalliovaara, J. Ojaniemi, A. Kivinen, T. Lakner, J. Hallio, and J. Paavola, "Trial of Spectrum Sharing in 2.3GHz Band for Two Types of PMSE Equipment and Mobile Network," in *2018 IEEE International Symposium on Broadband Multimedia Systems and Broadcasting (BMSB)*, pp. 1–5, June 2018.

[89] President's Council of Advisors on Science and Technology (PCAST), "Realizing the Full Potential of Government-Held Spectrum to Spur Economic Growth." https://www.whitehouse.gov/sites/default/files/microsites/ostp/pcast_spectrum_report_final_july_20_2012.pdf, 2012.

[90] M. M. Sohul, M. Yao, T. Yang, and J. H. Reed, "Spectrum access system for the Citizen Broadband Radio Service," *IEEE Communications Magazine*, vol. 53, pp. 18–25, July 2015.

[91] CBRS Alliance, "CBRS Network Service Technical Specification." https://www.cbrsalliance.org/specifications/, 2018.

[92] Ł. Kułacz, P. Kryszkiewicz, A. Kliks, H. Bogucka, J. Ojaniemi, J. Paavola, J. Kalliovaara, and H. Kokkinen, "Coordinated spectrum allocation and coexistence management in CBRS-SAS wireless networks," *IEEE Access*, vol. 7, pp. 139294–139316, 2019.

[93] FCC, "Shared Commercial Operations in the 3550–3650 MHz Band; 47 CFR Parts 0, 1, 2, 90, 95, and 96." `https://www.law.cornell.edu/rio/citation/80_FR_36222`, 2015.

[94] FCC, "Part 96—Citizens Broadband Radio Service." `https://www.ecfr.gov`, 2019.

[95] A. Sahoo, "Fair resource allocation in the Citizens Bbroadband Radio Service band," in *2017 IEEE International Symposium on Dynamic Spectrum Access Networks (DySPAN)*, pp. 1–2, March 2017.

[96] Wireless Innovation Forum, "Operations for Citizens Broadband Radio Service (CBSD); GAA Spectrum Coordination (GSC) Technical Report - Approach 1; WINNF-TR-2003, v.1.0.0, April 2019," tech. rep., 2019.

[97] Wireless Innovation Forum, "Operations for Citizens Broadband Radio Service (CBSD); GAA Spectrum Coordination (GSC) Technical Report - Approach 1; WINNF-TR-2004, v.1.0.0, May 2019," tech. rep., 2019.

[98] Wireless Innovation Forum, "Operations for Citizens Broadband Radio Service (CBSD); GAA Spectrum Coordination (GSC) Technical Report - Approach 1; WINNF-TR-3; WINNF-TR-2005, v.1.0.0, May 2019," tech. rep., 2019.

[99] Z. Youssef, E. Majeed, M. D. Mueck, I. Karls, C. Drewes, G. Bruck, and P. Jung, "Concept Design of Medium Access Control for Spectrum Access Systems in 3.5 GHz," in *2018 International Conference on Wireless Communications, Signal Processing and Networking (WiSPNET)*, pp. 1–8, March 2018.

[100] Z. Youssef, E. Majeed, M. D. Mueck, I. Karls, C. Drewes, G. Bruck, and P. Jung, "Performance Enhancement of the CSMA/CA MAC Mechanisms Using a Reject Request to Send (RRTS) Message for 3.5 GHz Shared Spectrum Systems," in *2018 International Conference on Wireless Communications, Signal Processing and Networking (WiSPNET)*, pp. 1–8, March 2018.

[101] X. Ying, M. M. Buddhikot, and S. Roy, "Coexistence-aware dynamic channel allocation for 3.5 GHz shared spectrum systems," in *2017 IEEE International Symposium on Dynamic Spectrum Access Networks (DySPAN)*, pp. 1–2, March 2017.

[102] X. Ying, M. M. Buddhikot, and S. Roy, "SAS-Assisted Coexistence-Aware Dynamic Channel Assignment in CBRS Band," *IEEE Transactions on Wireless Communications*, vol. 17, pp. 6307–6320, Sep. 2018.

[103] I. Belikaidis, A. Georgakopoulos, E. Kosmatos, V. Frascolla, and P. Demestichas, "Management of 3.5-GHz Spectrum in 5G Dense Networks: A Hierarchical Radio Resource Management Scheme," *IEEE Vehicular Technology Magazine*, vol. 13, pp. 57–64, June 2018.

[104] N. N. Krishnan, N. Mandayam, I. Seskar, and S. Kompella, "Experiment: Investigating Feasibility of Coexistence of LTE-U with a Rotating Radar in CBRS Bands," in *2018 IEEE 5G World Forum (5GWF)*, pp. 65–70, July 2018.

[105] M. Palola, M. Höyhtyä, P. Aho, M. Mustonen, T. Kippola, M. Heikkilä, S. Yrjölä, V. Hartikainen, L. Tudose, A. Kivinen, R. Ekman, J. Hallio, J. Paavola, M. Mäkeläinen, and T. Hänninen, "Field trial of the 3.5 GHz Citizens Broadband Radio Service governed by a Spectrum Access System (SAS)," in *2017 IEEE International Symposium on Dynamic Spectrum Access Networks (DySPAN)*, pp. 1–9, March 2017.

[106] A. Kliks, P. Kryszkiewicz, Ł. Kułacz, K. Kowalik, M. Kołodziejski, H. Kokkinen, J. Ojaniemi, and A. Kivinen, "Application of the CBRS model for wireless systems coexistence in 3.6–3.8 GHz band," in *Cognitive Radio Oriented Wireless Networks* (P. Marques, A. Radwan, S. Mumtaz, D. Noguet, J. Rodriguez, and M. Gundlach, eds.), (Cham), pp. 100–111, Springer International Publishing, 2018.

[107] R. Caromi, M. Souryal, and W. Yang, "Detection of Incumbent Radar in the 3.5 GHz CBRS Band," in *2018 IEEE Global Conference on Signal and Information Processing (GlobalSIP)*, pp. 241–245, Nov 2018.

[108] A. Kliks, P. Kryszkiewicz, J. Perez-Romero, A. Umbert, and F. Casadevall, "Spectrum occupancy in big cities - comparative study - measurement campaigns in Barcelona and Poznan," in *ISWCS 2013; The Tenth International Symposium on Wireless Communication Systems*, pp. 1–5, 2013.

[109] A. Kliks, P. Kryszkiewicz, K. Cichoń, A. Umbert, J. Perez-Romero, and F. Casadevall, "DVB-T channels power measurements in indoor/outdoor cases," in *IEICE Information and Communication Technology Forum*, pp. 1–6, May 2014.

[110] A. Umbert, J. Perez-Romero, F. Casadevall, A. Kliks, and P. Kryszkiewicz, "On the use of indoor Radio Environment Maps for HetNets deployment," in *9th International Conference on Cognitive Radio Oriented Wireless Networks and Communications (CROWNCOM)*, pp. 448–453, June 2014.

[111] A. Kliks, P. Kryszkiewicz, K. Cichoń, A. Umbert, J. Perez-Romero, and F. Casadevall, "DVB-T channels measurements for the deployment of outdoor REM databases," *Journal of telecommunications and information technology*, vol. 2014, no. 3, pp. 42–52, 2014.

[112] A. Kliks, P. Kryszkiewicz, A. Umbert, J. Perez-Romero, and F. Casadevall, "TVWS indoor measurements for HetNets," in *IEEE Wireless Communications and Networking Conference Workshops (WCNCW)*, pp. 76–81, April 2014.

[113] J. Ojaniemi, J. Kalliovaara, A. Alam, J. Poikonen, and R. Wichman, "Optimal field measurement design for Radio Environment Mapping," in *2013 47th Annual Conference on Information Sciences and Systems (CISS)*, pp. 1–6, March 2013.

[114] Ł. Kułacz, A. Kliks, and P. Kryszkiewicz, "Wykorzystanie baz danych środowiska radiowego REM do zarządzania przydziałem zasobów widmowych," *Przegląd Telekomunikacyjny + Wiadomosci Telekomunikacyjne*, vol. nr 6, pp. 462–465, CD, 2017.

[115] A. Kliks, P. Kryszkiewicz, and Ł. Kułacz, "Measurement-based coverage maps for indoor REMs operating in TV band," in *2017 IEEE International Symposium on Broadband Multimedia Systems and Broadcasting (BMSB)*, pp. 1–7, 2017.

[116] A. Kliks and Ł. Kułacz, "System dynamicznego dostępu do widma wykorzystujący mapy środowiska radiowego," *Przegląd Telekomunikacyjny + Wiadomosci Telekomunikacyjne*, vol. nr 6, pp. 216–219, CD, 2018.

[117] Ł. Kułacz, "Dynamic Spectrum Management System Based on the Radio Environment Maps," Master's thesis, Poznan University of Technology, Poland, 2018.

[118] M. Barbiroli, C. Carciofi, A. Guidotti, and D. Guiducci, "Evaluation and analysis of the hidden node margin for cognitive radio system operation in a real scenario," in *Proceedings of the 5th European Conference on Antennas and Propagation (EUCAP)*, pp. 1309–1313, 2011.

[119] A. Kliks and Ł. Kułacz, "REM-based indoor wireless network deployment - an experimental study," in *Cognitive Radio Oriented Wireless Networks. 12th International Conference, CROWNCOM 2017, Lisbon, Portugal, September 20-21, 2017, Proceedings*, Mar 2018.

[120] "Big Buck Bunny." `https://peach.blender.org/`, 2022.

[121] A. Kliks and P. Kryszkiewicz, "Multichannel simultaneous uplink and downlink transmission scheme for flexible duplexing," *EURASIP Journal on Wireless Communications and Networking*, vol. 2017, p. 111, Jun 2017.

[122] Wireless Innovation Forum, "Requirements for Commercial Operation in the U.S. 3550-3700 MHz Citizens Broadband Radio Service Band. Working Document WINNF-TS-0112 version v1.4.1," tech. rep., 2018.

[123] Ł. Kułacz, A. Kliks, and S. N. Khan, "Network graphs reflecting transmission policies," in *2018 Baltic URSI Symposium (URSI)*, pp. 85–86, May 2018.

[124] Ł. Kułacz, P. Kryszkiewicz, A. Kliks, and J. Perez-Romero, "Waveform flexibility in database-oriented cognitive wireless systems," in *2018 Global Information Infrastructure and Networking Symposium (GIIS)*, pp. 1–4, 2018.

[125] Ł. Kułacz, P. Kryszkiewicz, and A. Kliks, "Waveform flexibility for network slicing," *Wireless Communications and Mobile Computing*, vol. 2019, pp. 1–15, Mar. 2019.

[126] B. Farhang-Boroujeny, "OFDM versus filter bank multicarrier," *IEEE Signal Processing Magazine*, vol. 28, no. 3, pp. 92–112, 2011.

[127] H. Bogucka, P. Kryszkiewicz, and A. Kliks, "Dynamic spectrum aggregation for future 5G communications," *IEEE Communications Magazine*, vol. 53, no. 5, pp. 35–43, 2015.

[128] H. Bogucka, A. Kliks, and P. Kryszkiewicz, *Multicarrier Technologies for Flexible Spectrum Usage*, pp. 219–245. 2016.

[129] P. Kryszkiewicz, A. Kliks, and H. Bogucka, "Small-Scale Spectrum Aggregation and Sharing," *IEEE Journal on Selected Areas in Communications (JSAC)*, vol. 34, no. 10, pp. 2630–2641, 2016.

[130] ETSI, *LTE; Evolved Universal Terrestrial Radio Access (E-UTRA); Base Station (BS) radio transmission and reception (3GPP TS 36.104 version 11.3.1 Release 11)*, Feb. 2013.

[131] P. Kryszkiewicz and A. Kliks, "TVWS Indoor Propagation Model," *WSA 2016, 20th International ITG Workshop on Smart Antennas*, 2016.

[132] A. Umbert, J. Perez-Romero, F. Casadevall, A. Kliks, and P. Kryszkiewicz, "On the Use of Indoor Radio Environment Maps for HetNets Deployment," *2014 9th International Conference on Cognitive Radio Oriented Wireless Networks and Communications (CROWNCOM)*, pp. 448–453, 2014.

[133] A. Kliks, P. Kryszkiewicz, Ł. Kułacz, K. Kowalik, M. Kołodziejski, H. Kokkinen, J. Ojaniemi, and A. Kivinen, "Spectrum Management Application for virtualized wireless vehicular networks: A step toward programmable spectrum management in future wireless networks," *IEEE Vehicular Technology Magazine*, vol. 13, no. 4, pp. 94–105, 2018.

[134] A. Kliks, P. Kryszkiewicz, Ł. Kułacz, K. Kowalik, J. Ojaniemi, H. Kokkinen, and H. Bogucka, "Database supported flexible spectrum access - field trials in commercial networks," in *2019 IEEE International Conference on Communications Workshops (ICC Workshops)*, pp. 1–6, 2019.

[135] Wireless Innovation Forum, "Spectrum Access System (SAS) - Citizens Broadband Radio Service Device (CBSD) Interface Technical Specification; WINNF-16-S-0016, v2.0.0, June 2017," tech. rep., 2017.

[136] V. Abhayawardhana, I. Wassell, D. Crosby, M. Sellars, and M. Brown, "Comparison of empirical propagation path loss models for fixed wireless access systems," in *2005 IEEE 61st Vehicular Technology Conference*, vol. 1, pp. 73–77 Vol. 1, 2005.

[137] A. Kliks, Ł. Kułacz, P. Kryszkiewicz, H. Bogucka, M. Dryjański, M. Isaksson, G. P. Koudouridis, and P. Tengkvist, "Beyond 5G: Big data processing for better spectrum utilization," *IEEE Vehicular Technology Magazine*, vol. 15, no. 3, pp. 40–50, 2020.

[138] P. Kryszkiewicz, A. Kliks, Ł. Kułacz, H. Bogucka, G. P. Koudouridis, and M. Dryjański, "Context-based spectrum sharing in 5G wireless networks based on Radio Environment Maps," *Wireless Communications and Mobile Computing*, vol. 2018, pp. 1–15, Nov. 2018.

[139] P. Kyösti, J. Meinilä, L. Hentila, X. Zhao, T. Jämsä, C. Schneider, M. Narandzic, M. Milojević, A. Hong, J. Ylitalo, V.-M. Holappa, M. Alatossava, R. Bultitude, Y. Jong, and T. Rautiainen, "WINNER II channel models," *IST-4-027756 WINNER II D1.1.2 V1.2*, 02 2008.

[140] H. Song, R. Kwan, and J. Zhang, "On statistical characterization of EESM Effective SNR over frequency selective channels," *IEEE Transactions on Wireless Communications*, vol. 8, pp. 3955–3960, 08 2009.

[141] R. Kwan, C. Leung, and J. Zhang, "Proportional Fair multiuser scheduling in LTE," *IEEE Signal Processing Letters*, vol. 16, no. 6, pp. 461–464, 2009.

[142] F. Capozzi, G. Piro, L. Grieco, G. Boggia, and P. Camarda, "Downlink packet scheduling in lte cellular networks: Key design issues and a survey," *IEEE Communications Surveys Tutorials*, vol. 15, no. 2, pp. 678–700, 2013.

[143] K. Walch, "The seven patterns of AI." `https://www.forbes.com/sites/cognitiveworld/2019/09/17/the-seven-patterns-of-ai/`, 2019.

[144] D. Xin, W. Yingkang, G. Xinyu, L. Xin, and Z. Lin, "Analysis of cell range extension and a bias configuration strategy in dense small cell networks," in *2014 4th IEEE International Conference on Network Infrastructure and Digital Content*, pp. 425–429, 2014.

[145] Ł. Kułacz, P. Sroka, A. Kliks, and G. P. Koudouridis, "Cell range extension adaptation in coordinated LTE-A network," in *2020 Baltic URSI Symposium (URSI)*, pp. 134–137, 2020.

[146] 3GPP, "Evolved Universal Terrestrial Radio Access (E-UTRA); Radio Resource Control (RRC); Protocol specification," Technical Specification (TS) 36.331, 3rd Generation Partnership Project (3GPP), 01 2020. Version 14.13.0.

[147] T.-T. Tran, Y. Shin, and O.-S. Shin, "Overview of enabling technologies for 3GPP LTE-advanced," *EURASIP Journal on Wireless Communications and Networking*, vol. 2012, Feb. 2012.

[148] M. M. Hasan, S. Kwon, and J.-H. Na, "Adaptive mobility load balancing algorithm for lte small-cell networks," *IEEE Transactions on Wireless Communications*, vol. 17, no. 4, pp. 2205–2217, 2018.

[149] X. Gu, W. Li, and L. Zhang, "Adaptive cell range control in heterogeneous network," in *2013 International Conference on Wireless Communications and Signal Processing*, pp. 1–5, 2013.

[150] M. Jaber, M. Imran, R. Tafazolli, and A. Tukmanov, "An adaptive backhaul-aware cell range extension approach," in *2015 IEEE International Conference on Communication Workshop (ICCW)*, pp. 74–79, 2015.

[151] P. Agyapong, "Mobile and wireless communications Enablers for the Twenty-twenty Information Society (METIS); Deliverable D6.1, Simulation guidelines." `https://cordis.europa.eu/docs/projects/cnect/9/317669/080/deliverables/001-METISD61v1pdf.pdf`, 2013.

[152] 3GPP, "LTE; Evolved Universal Terrestrial Radio Access (E-UTRA); Physical channels and modulation," Technical Specification (TS) 36.211, 3rd Generation Partnership Project (3GPP), 04 2017. Version 14.2.0.

[153] Qamcom, "Qamcom/QCM." `https://github.com/qamcom/QCM`, 2022.

[154] 5GPPP, "KPIs." `https://5g-ppp.eu/kpis/`, 2019.

[155] NGMN Alliance, "Recommendations for NGMN KPIs and requirements for 5G." `https://www.ngmn.org/publications/recommendations-for-ngmn-kpis-and-requirements-for-5g.html`, 2016.

[156] A. Damnjanovic, J. Montojo, Y. Wei, T. Ji, T. Luo, M. Vajapeyam, T. Yoo, O. Song, and D. Malladi, "A survey on 3gpp heterogeneous networks," *IEEE Wireless Communications*, vol. 18, no. 3, pp. 10–21, 2011.

[157] M. Agiwal, A. Roy, and N. Saxena, "Next generation 5G wireless networks: A comprehensive survey," *IEEE Communications Surveys Tutorials*, vol. 18, no. 3, pp. 1617–1655, 2016.

[158] J. G. Andrews, X. Zhang, G. D. Durgin, and A. K. Gupta, "Are we approaching the fundamental limits of wireless network densification?," *IEEE Communications Magazine*, vol. 54, no. 10, pp. 184–190, 2016.

[159] N. Bhushan, J. Li, D. Malladi, R. Gilmore, D. Brenner, A. Damnjanovic, R. T. Sukhavasi, C. Patel, and S. Geirhofer, "Network densification: the dominant theme for wireless evolution into 5G," *IEEE Communications Magazine*, vol. 52, no. 2, pp. 82–89, 2014.

[160] F. A. Khan, H. He, J. Xue, and T. Ratnarajah, "Performance analysis of cloud radio access networks with distributed multiple antenna remote radio heads," *IEEE Transactions on Signal Processing*, vol. 63, no. 18, pp. 4784–4799, 2015.

[161] A. Asadi, V. Sciancalepore, and V. Mancuso, "On the efficient utilization of radio resources in extremely dense wireless networks," *IEEE Communications Magazine*, vol. 53, no. 1, pp. 126–132, 2015.

[162] M. Kamel, W. Hamouda, and A. Youssef, "Ultra-dense networks: A survey," *IEEE Communications Surveys Tutorials*, vol. 18, no. 4, pp. 2522–2545, 2016.

[163] M. Li, P. Chen, and S. Gao, "Cooperative game-based energy efficiency management over ultra-dense wireless cellular networks," *Sensors*, vol. 16, no. 9, 2016.

[164] W. Lei, Y. Ye, and M. Xiao, "Deep reinforcement learning-based spectrum allocation in integrated access and backhaul networks," *IEEE Transactions on Cognitive Communications and Networking*, vol. 6, no. 3, pp. 970–979, 2020.

[165] 6G Flagship, "Key drivers and research challenges for 6G ubiquitous wireless intelligence." `http://jultika.oulu.fi/files/isbn9789526223544.pdf`, 2019.

[166] M. K. Naeem, R. Abozariba, M. Asaduzzaman, and M. Patwary, "Towards the mobility issues of 5G-NOMA through user dissociation and re-association control," in *2020 IEEE 21st International Symposium on "A World of Wireless, Mobile and Multimedia Networks" (WoWMoM)*, pp. 427–432, 2020.

[167] S. Okasaka, R. J. Weiler, W. Keusgen, A. Pudeyev, A. Maltsev, I. Karls, and K. Sakaguchi, "Proof-of-concept of a millimeter-wave integrated heterogeneous network for 5G cellular," *Sensors*, vol. 16, no. 9, 2016.

[168] N. Primeau, R. Falcon, R. Abielmona, and E. M. Petriu, "A review of computational intelligence techniques in wireless sensor and actuator networks," *IEEE Communications Surveys Tutorials*, vol. 20, no. 4, pp. 2822–2854, 2018.

[169] F. Oldewurtel and P. Mahonen, "Neural wireless sensor networks," in *2006 International Conference on Systems and Networks Communications (ICSNC'06)*, pp. 28–28, 2006.

[170] D. Goyal and M. R. Tripathy, "Routing protocols in wireless sensor networks: A survey," in *2012 Second International Conference on Advanced Computing Communication Technologies*, pp. 474–480, 2012.

[171] A. Nazi, M. Raj, M. Di Francesco, P. Ghosh, and S. K. Das, "Efficient communications in wireless sensor networks based on biological robustness," in *2016 International Conference on Distributed Computing in Sensor Systems (DCOSS)*, pp. 161–168, 2016.

[172] F. Dressler and O. B. Akan, "Bio-inspired networking: from theory to practice," *IEEE Communications Magazine*, vol. 48, no. 11, pp. 176–183, 2010.

[173] M. Bélanger, I. Allaman, and P. Magistretti, "Brain energy metabolism: Focus on astrocyte-neuron metabolic cooperation," *Cell Metabolism*, vol. 14, no. 6, pp. 724–738, 2011.

[174] T. Nakano, "Biologically inspired network systems: A review and future prospects," *IEEE Transactions on Systems, Man, and Cybernetics, Part C (Applications and Reviews)*, vol. 41, no. 5, pp. 630–643, 2011.

[175] P. Cong Vinh, *Nature-Inspired Networking*. CRC Press, Feb. 2018.

[176] J. Bullock, *Physiology*. Philadelphia: Lippincott Williams & Wilkins, 2001.

[177] Ł. Kułacz and A. Kliks, "Neuroplasticity and microglia functions applied in dense wireless networks," *Journal of Telecommunications and Information Technology*, vol. 1, pp. 39–46, Mar. 2019.

[178] Ł. Kułacz and A. Kliks, "Brain-inspired communications in dense wireless networks," in *2018 14th International Conference on Mobile Ad-Hoc and Sensor Networks (MSN)*, pp. 140–145, 2018.

[179] A. London, M. Cohen, and M. Schwartz, "Microglia and monocyte-derived macrophages: functionally distinct populations that act in concert in CNS plasticity and repair," *Frontiers in Cellular Neuroscience*, vol. 7, 2013.

[180] Ł. Kułacz and A. Kliks, "Simplified and reliable wireless data transmission in ultra dense networks," in *2020 International Conference on Software, Telecommunications and Computer Networks (SoftCOM)*, pp. 1–6, 2020.

[181] B. Gissler and P. Shrivastava, "A system for design decisions based on reliability block diagrams," in *2015 Annual Reliability and Maintainability Symposium (RAMS)*, pp. 1–6, 2015.

[182] HBM Prenscia, "ReliaWiki." `http://reliawiki.org/index.php/Main_Page`, 2020.

[183] S. Distefano and A. Puliafito, "Dependability evaluation with dynamic reliability block diagrams and dynamic fault trees," *IEEE Transactions on Dependable and Secure Computing*, vol. 6, no. 1, pp. 4–17, 2009.

[184] A. E. Zonouz, L. Xing, V. M. Vokkarane, and Y. L. Sun, "A time-dependent link failure model for wireless sensor networks," in *2014 Reliability and Maintainability Symposium*, pp. 1–7, 2014.

[185] R. Hekmat and P. Van Mieghem, "Degree distribution and hopcount in wireless ad-hoc networks," in *The 11th IEEE International Conference on Networks, 2003. ICON2003.*, pp. 603–609, 2003.

[186] HBM Prenscia, "ReliaSoft — BlockSim." `https://www.reliasoft.com/products/reliability-analysis/blocksim`, 2020.

[187] M. Rausand, *System reliability theory: models, statistical methods, and applications*. Hoboken, NJ: Wiley-Interscience, 2004.

[188] A. Kliks and Ł. Kułacz, "Brain inspirations for dense wireless networks: Microglia functionality," in *2018 IEEE 29th Annual International Symposium on Personal, Indoor and Mobile Radio Communications (PIMRC)*, pp. 578–579, 2018.

[189] Ł. Kułacz and A. Kliks, "Gęsta sieć bezprzewodowa inspirowana układem nerwowym," *Przegląd Telekomunikacyjny + Wiadomosci Telekomunikacyjne*, vol. nr 6, pp. 487–492, CD, 2019.

[190] Ł. Kułacz and A. Kliks, "Dense wireless network inspired by the nervous system," *International Journal of Electronics and Telecommunications*, vol. vol. 66, no. No 1, pp. 93–98, 2020.

[191] Ł. Kułacz and A. Kliks, "Brain-inspired data transmission in dense wireless network," *Sensors*, vol. 21, no. 2, 2021.

[192] D.-T. Do, T.-T. T. Nguyen, C.-B. Le, and J. W. Lee, "Two-way transmission for low-latency and high-reliability 5G cellular V2X communications," *Sensors*, vol. 20, no. 2, 2020.

[193] X. Wei, H. Guo, X. Wang, X. Wang, C. Wang, M. Guizani, and X. Du, "A co-design-based reliable low-latency and energy-efficient transmission protocol for uwsns," *Sensors*, vol. 20, no. 21, 2020.

[194] Ł. Kułacz and A. Kliks, "Reliability of bio-inspired ultra-dense networks," in *2020 Baltic URSI Symposium (URSI)*, pp. 15–18, 2020.

[195] Y. Song, W. Yang, Z. Xiang, B. Wang, and Y. Cai, "On the performance of random cognitive mmwave sensor networks," *Sensors*, vol. 19, no. 14, 2019.

[196] M. Haenggi, J. G. Andrews, F. Baccelli, O. Dousse, and M. Franceschetti, "Stochastic geometry and random graphs for the analysis and design of wireless networks," *IEEE Journal on Selected Areas in Communications*, vol. 27, no. 7, pp. 1029–1046, 2009.

[197] Ł. Kułacz and A. Kliks, "Reliability assessment of bio-inspired ultra-dense networks using percolation theory," in *2020 IEEE 21st International Symposium on "A World of Wireless, Mobile and Multimedia Networks" (WoWMoM)*, pp. 173–175, 2020.

[198] J. V. V. Sobral, J. J. P. C. Rodrigues, R. A. L. Rabêlo, K. Saleem, and V. Furtado, "Loadng-iot: An enhanced routing protocol for internet of things applications over low power networks," *Sensors*, vol. 19, no. 1, 2019.

[199] Y. del Valle, G. K. Venayagamoorthy, S. Mohagheghi, J.-C. Hernandez, and R. G. Harley, "Particle swarm optimization: Basic concepts, variants and applications in power systems," *IEEE Transactions on Evolutionary Computation*, vol. 12, no. 2, pp. 171–195, 2008.

[200] K. M. Sim and W. H. Sun, "Ant colony optimization for routing and load-balancing: survey and new directions," *IEEE Transactions on Systems, Man, and Cybernetics - Part A: Systems and Humans*, vol. 33, no. 5, pp. 560–572, 2003.

[201] Z. Zhang, K. Long, J. Wang, and F. Dressler, "On swarm intelligence inspired self-organized networking: Its bionic mechanisms, designing principles and optimization approaches," *IEEE Communications Surveys Tutorials*, vol. 16, no. 1, pp. 513–537, 2014.

[202] R. Xu and D. Wunsch, "Survey of clustering algorithms," *IEEE Transactions on Neural Networks*, vol. 16, no. 3, pp. 645–678, 2005.

[203] F. J. Ordóñez and D. Roggen, "Deep convolutional and lstm recurrent neural networks for multimodal wearable activity recognition," *Sensors*, vol. 16, no. 1, 2016.

[204] T. Fukuda and T. Shibata, "Theory and applications of neural networks for industrial control systems," *IEEE Transactions on Industrial Electronics*, vol. 39, no. 6, pp. 472–489, 1992.

[205] M. Lee, J. Zheng, Y.-B. Ko, and D. Shrestha, "Emerging standards for wireless mesh technology," *IEEE Wireless Communications*, vol. 13, no. 2, pp. 56–63, 2006.

[206] P. C. Pinto, A. Giorgetti, M. Z. Win, and M. Chiani, "A stochastic geometry approach to coexistence in heterogeneous wireless networks," *IEEE Journal on Selected Areas in Communications*, vol. 27, no. 7, pp. 1268–1282, 2009.

[207] D. Li, Q. Zhang, E. Zio, S. Havlin, and R. Kang, "Network reliability analysis based on percolation theory," *Reliability Engineering & System Safety*, vol. 142, pp. 556–562, 2015.

[208] M. Z. Win, P. C. Pinto, and L. A. Shepp, "A mathematical theory of network interference and its applications," *Proceedings of the IEEE*, vol. 97, pp. 205–230, Feb. 2009.

[209] Ł. Kułacz, A. Kliks, P. Kryszkiewicz, and B. Bossy, "Dynamic transmit profile selection in dense wireless networks," *Sensors*, vol. 21, no. 1, 2021.

[210] Ł. Kułacz, A. Kliks, B. Bossy, and P. Kryszkiewicz, "Adaptacyjny wybór profilu transmisyjnego w gęstych sieciach bezprzewodowych," *Przegląd Telekomunikacyjny + Wiadomosci Telekomunikacyjne*, vol. nr 7-8, pp. 212–215, CD, 2020.

[211] N. Nikaein, C.-Y. Chang, and K. Alexandris, "Mosaic5G: Agile and flexible service platforms for 5G research," *ACM SIGCOMM Comp. Com. Rev.*, vol. 47, July 2018.

[212] N. Nikaein, M. K. Marina, S. Manickam, A. Dawson, R. Knopp, and C. Bonnet, "OpenAirInterface: A flexible platform for 5G research," *ACM SIGCOMM Comp. Com. Rev.*, vol. 44, pp. 33–38, Oct. 2014.

[213] C.-Y. Chang, Ł. Kułacz, R. Schmidt, A. Kliks, and N. Nikaein, "Spectrum Management Application - a tool for flexible and efficient resource utilization," in *2018 IEEE Global Communications Conference (GLOBECOM)*, pp. 1–7, 2018.

[214] A. Kliks, B. Bossy, S. N. Khan, R. Riggio, and L. Goratti, "An architecture for spectrum management and coordinated control in 5G heterogeneous networks," in *2016 International Symposium on Wireless Communication Systems (ISWCS)*, pp. 648–652, 2016.

[215] G. Ding, J. Wang, Q. Wu, Y.-D. Yao, R. Li, H. Zhang, and Y. Zou, "On the limits of predictability in real-world radio spectrum state dynamics: from entropy theory to 5G spectrum sharing," *IEEE Commun. Mag.*, vol. 53, pp. 178–183, July 2015.

[216] S. Bhattarai, J.-M. J. Park, B. Gao, K. Bian, and W. Lehr, "An overview of dynamic spectrum sharing: Ongoing initiatives, challenges, and a roadmap for future research," *IEEE Trans. Cogn. Commun. Netw.*, vol. 2, pp. 110–128, June 2016.

[217] H. Ishii, Y. Kishiyama, and H. Takahashi, "A novel architecture for LTE-B: C-plane/U-plane split and phantom cell concept," in *2012 IEEE Globecom Workshops*, pp. 624–630, 2012.

[218] Z. Niu, Y. Wu, J. Gong, and Z. Yang, "Cell zooming for cost-efficient green cellular networks," *IEEE Commun. Mag.*, vol. 48, pp. 74–79, Nov. 2010.

[219] Ł. Kułacz and A. Kliks, "Freemium spectrum sharing and pricing," in *2021 International Conference on Software, Telecommunications and Computer Networks (SoftCOM)*, pp. 1–6s, 2021.

[220] S. K. Singh, R. Singh, and B. Kumbhani, "The evolution of radio access network towards open-ran: Challenges and opportunities," in *2020 IEEE Wireless Communications and Networking Conference Workshops (WCNCW)*, pp. 1–6, 2020.

[221] L. Gavrilovska, V. Rakovic, and D. Denkovski, "From cloud RAN to open RAN," *Wireless Personal Communications*, vol. 113, pp. 1523–1539, Mar. 2020.

[222] Ł. Kułacz and A. Kliks, "Dynamic spectrum allocation using multi-source context information in OpenRAN networks," *Sensors*, vol. 22, no. 9, 2022.

[223] M. Dryjański, Ł. Kułacz, and A. Kliks, "Toward modular and flexible Open RAN implementations in 6G networks: Traffic steering use case and O-RAN xApps," *Sensors*, vol. 21, no. 24, 2021.

[224] M. Giordani, M. Polese, M. Mezzavilla, S. Rangan, and M. Zorzi, "Toward 6G networks: Use cases and technologies," *IEEE Communications Magazine*, vol. 58, pp. 55–61, Mar. 2020.

[225] Z. Zhang, Y. Xiao, Z. Ma, M. Xiao, Z. Ding, X. Lei, G. K. Karagiannidis, and P. Fan, "6G wireless networks: Vision, requirements, architecture, and key technologies," *IEEE Vehicular Technology Magazine*, vol. 14, no. 3, pp. 28–41, 2019.

[226] V. P. Rekkas, S. Sotiroudis, P. Sarigiannidis, S. Wan, G. K. Karagiannidis, and S. K. Goudos, "Machine Learning in beyond 5G/6G networks—state-of-the-art and future trends," *Electronics*, vol. 10, p. 2786, Nov. 2021.

[227] M. Wasilewska, A. Kliks, H. Bogucka, K. Cichoń, J. Ruseckas, G. Molis, A. Mackute-Varoneckiene, and T. Krilavicius, "Artificial intelligence for radio communication context-awareness," *IEEE Access*, vol. 9, pp. 144820–144856, 2021.

[228] L. Ruiz, R. Durán, I. de Miguel, P. Khodashenas, J.-J. Pedreño-Manresa, N. Merayo, J. Aguado, P. Pavón-Marino, S. Siddiqui, J. Mata, P. Fernández, R. Lorenzo, and E. Abril, "A genetic algorithm for VNF provisioning in NFV-enabled cloud/MEC RAN architectures," *Applied Sciences*, vol. 8, p. 2614, Dec. 2018.

[229] O-RAN Alliance, "O-RAN specifications." `https://www.o-ran.org/specifications`, 2021.

[230] H. Lee, J. Cha, D. Kwon, M. Jeong, and I. Park, "Hosting AI/ML workflows on O-RAN RIC platform," in *2020 IEEE Globecom Workshops*, pp. 1–6, 2020.

[231] H. Kumar, V. Sapru, and S. K. Jaisawal, "O-RAN based proactive ANR optimization," in *2020 IEEE Globecom Workshops*, pp. 1–4, 2020.

[232] S. Niknam, A. Roy, H. S. Dhillon, S. Singh, R. Banerji, J. H. Reed, N. Saxena, and S. Yoon, "Intelligent O-RAN for beyond 5G and 6G wireless networks," 2020.

[233] K. Koufos, K. E. Haloui, M. Dianati, M. Higgins, J. Elmirghani, M. A. Imran, and R. Tafazolli, "Trends in intelligent communication systems: Review of standards, major research projects, and identification of research gaps," *Journal of Sensor and Actuator Networks*, vol. 10, p. 60, Oct. 2021.

[234] M. Dryjański and A. Kliks, "A hierarchical and modular radio resource management architecture for 5G and beyond," *IEEE Communications Magazine*, vol. 58, pp. 28–34, July 2020.

[235] M. Dryjański and M. Szydełko, "A unified traffic steering framework for LTE radio access network coordination," *IEEE Communications Magazine*, vol. 54, pp. 84–92, July 2016.

[236] O-RAN Alliance, "Near-Real-Time RAN Intelligent Controller (near-RT RIC) architecture." `https://www.o-ran.org/specifications`, 2020.

[237] N. Zhang, S. Zhang, S. Wu, J. Ren, J. W. Mark, and X. Shen, "Beyond coexistence: Traffic steering in LTE networks with unlicensed bands," *IEEE Wireless Communications*, vol. 23, pp. 40–46, Dec. 2016.

[238] S. Zhang, N. Zhang, S. Zhou, J. Gong, Z. Niu, and X. Shen, "Energy-sustainable traffic steering for 5G mobile networks," *IEEE Communications Magazine*, vol. 55, pp. 54–60, Nov. 2017.

[239] Y. il Choi and J. H. Kim, "Reliable data transmission in 5G network using access traffic steering method," in *2020 International Conference on Information and Communication Technology Convergence (ICTC)*, IEEE, Oct. 2020.

[240] M. R. Anwar, S. Wang, M. F. Akram, S. Raza, and S. Mahmood, "5G-enabled MEC: A distributed traffic steering for seamless service migration of internet of vehicles," *IEEE Internet of Things Journal*, vol. 9, pp. 648–661, Jan. 2022.

[241] O-RAN Alliance, "Non-RT RIC & A1 interface: Use cases and requirements." `https://www.o-ran.org/specifications`, 2021.

[242] X. Xu, C. Yuan, W. Chen, X. Tao, and Y. Sun, "Adaptive cell zooming and sleeping for green heterogeneous ultradense networks," *IEEE Transactions on Vehicular Technology*, vol. 67, pp. 1612–1621, Feb. 2018.

[243] M. Wasilewska and Ł. Kułacz, "Machine Learning-based small cell location selection process," *Journal of Telecommunications and Information Technology*, vol. 2, pp. 120–126, Mar. 2021.

[244] P. Kryszkiewicz, A. Kliks, Ł. Kułacz, and B. Bossy, "Power consumption variation for a single technology wireless transceivers," in *2020 IEEE 21st International Symposium on "A World of Wireless, Mobile and Multimedia Networks" (WoWMoM)*, pp. 179–181, 2020.

[245] P. Kryszkiewicz, A. Kliks, Ł. Kułacz, and B. Bossy, "Stochastic power consumption model of wireless transceivers," *Sensors*, vol. 20, no. 17, 2020.

[246] Ł. Kułacz, A. Kliks, B. Bossy, and P. Kryszkiewicz, "Transmission profile selection in dense wireless networks," in *2020 Baltic URSI Symposium (URSI)*, pp. 130–133, 2020.

Appendix A

Author's publications

This appendix lists the 34 publications that describe the author's research and obtained results. A short description of the author's involvement and contribution in joint works has been added to each publication.

1) A. Kliks, P. Kryszkiewicz, A. Umbert, J. Perez-Romero, F. Casadevall, and Ł. Kułacz, "Application of Radio Environment Maps for dynamic broadband access in TV bands in urban areas," *IEEE Access*, vol. 5, pp. 19842–19863, 2017. (cited as [75])
Author's contribution: *measurements, software, simulations, validation, visualization.*

2) Ł. Kułacz, P. Kryszkiewicz, A. Kliks, H. Bogucka, J. Ojaniemi, J. Paavola, J. Kalliovaara, and H. Kokkinen, "Coordinated spectrum allocation and coexistence management in CBRS-SAS wireless networks," *IEEE Access*, vol. 7, pp. 139294–139316, 2019. (cited as [92])
Author's contribution: *software, hardware implementation, validation, visualization.*

3) A. Kliks, P. Kryszkiewicz, Ł. Kułacz, K. Kowalik, M. Kołodziejski, H. Kokkinen, J. Ojaniemi, and A. Kivinen, "Application of the CBRS model for wireless systems coexistence in 3.6–3.8 GHz band," in *Cognitive Radio Oriented Wireless Networks* (P. Marques, A. Radwan, S. Mumtaz, D. Noguet, J. Rodriguez, and M. Gundlach, eds.), (Cham), pp. 100–111, Springer International Publishing, 2018. (cited as [106])
Author's contribution: *software, simulations, hardware implementation, validation, visualization.*

4) Ł. Kułacz, A. Kliks, and P. Kryszkiewicz, "Wykorzystanie baz danych środowiska radiowego REM do zarządzania przydziałem zasobów widmowych," *Przegląd Telekomunikacyjny + Wiadomosci Telekomunikacyjne*, vol. nr 6, pp. 462–465, CD, 2017. (cited as [114])
Author's contribution: *measurements, software, simulations, validation, visualization.*

5) A. Kliks, P. Kryszkiewicz, and Ł. Kułacz, "Measurement-based coverage maps for indoor REMs operating in TV band," in *2017 IEEE International Symposium on Broadband Multimedia Systems and Broadcasting (BMSB)*, pp. 1–7, 2017. (cited as [115])
Author's contribution: *measurements, software, simulations, validation, visualization.*

6) A. Kliks and Ł. Kułacz, "System dynamicznego dostępu do widma wykorzystujący mapy środowiska radiowego," *Przegląd Telekomunikacyjny + Wiadomosci Telekomunikacyjne*, vol. nr 6, pp. 216–219, CD, 2018. (cited as [116])
Author's contribution: *measurements, software, simulations, validation, writing original draft, visualization.*

7) A. Kliks and Ł. Kułacz, "REM-based indoor wireless network deployment - an experimental study," in *Cognitive Radio Oriented Wireless Networks. 12th International Conference,*

CROWNCOM 2017, Lisbon, Portugal, September 20-21, 2017, Proceedings, Mar 2018. (cited as [119])
Author's contribution: *software, simulations, hardware implementation, validation, visualization*.

8) Ł. Kułacz, A. Kliks, and S. N. Khan, "Network graphs reflecting transmission policies," in *2018 Baltic URSI Symposium (URSI)*, pp. 85–86, May 2018. (cited as [123])
Author's contribution: *conceptualization, writing original draft*.

9) Ł. Kułacz, P. Kryszkiewicz, A. Kliks, and J. Perez-Romero, "Waveform flexibility in database-oriented cognitive wireless systems," in *2018 Global Information Infrastructure and Networking Symposium (GIIS)*, pp. 1–4, 2018. (cited as [124])
Author's contribution: *software, simulations, validation, writing original draft, visualization*.

10) Ł. Kułacz, P. Kryszkiewicz, and A. Kliks, "Waveform flexibility for network slicing," *Wireless Communications and Mobile Computing*, vol. 2019, pp. 1–15, Mar. 2019. (cited as [125])
Author's contribution: *software, simulations, validation, writing original draft, visualization*.

11) A. Kliks, P. Kryszkiewicz, Ł. Kułacz, K. Kowalik, M. Kołodziejski, H. Kokkinen, J. Ojaniemi, and A. Kivinen, "Spectrum Management Application for virtualized wireless vehicular networks: A step toward programmable spectrum management in future wireless networks," *IEEE Vehicular Technology Magazine*, vol. 13, no. 4, pp. 94–105, 2018. (cited as [133])
Author's contribution: *software, simulations, hardware implementation, validation, visualization*.

12) A. Kliks, P. Kryszkiewicz, Ł. Kułacz, K. Kowalik, J. Ojaniemi, H. Kokkinen, and H. Bogucka, "Database supported flexible spectrum access - field trials in commercial networks," in *2019 IEEE International Conference on Communications Workshops (ICC Workshops)*, pp. 1–6, 2019. (cited as [134])
Author's contribution: *software, hardware implementation, validation, visualization*.

13) A. Kliks, Ł. Kułacz, P. Kryszkiewicz, H. Bogucka, M. Dryjański, M. Isaksson, G. P. Koudouridis, and P. Tengkvist, "Beyond 5G: Big data processing for better spectrum utilization," *IEEE Vehicular Technology Magazine*, vol. 15, no. 3, pp. 40–50, 2020. (cited as [137])
Author's contribution: *software, simulations, validation, writing original draft, visualization*.

14) P. Kryszkiewicz, A. Kliks, Ł. Kułacz, H. Bogucka, G. P. Koudouridis, and M. Dryjański, "Context-based spectrum sharing in 5G wireless networks based on Radio Environment Maps," *Wireless Communications and Mobile Computing*, vol. 2018, pp. 1–15, Nov. 2018. (cited as [138])
Author's contribution: *software, simulations, validation, visualization*.

15) Ł. Kułacz, P. Sroka, A. Kliks, and G. P. Koudouridis, "Cell range extension adaptation in coordinated LTE-A network," in *2020 Baltic URSI Symposium (URSI)*, pp. 134–137, 2020. (cited as [145])
Author's contribution: *conceptualization, methodology, software, simulations, validation, writing original draft, visualization*.

16) Ł. Kułacz and A. Kliks, "Neuroplasticity and microglia functions applied in dense wireless networks," *Journal of Telecommunications and Information Technology*, vol. 1, pp. 39–46, Mar. 2019. (cited as [177])
Author's contribution: *conceptualization, methodology, software, simulations, validation, writing original draft, visualization*.

17) Ł. Kułacz and A. Kliks, "Brain-inspired communications in dense wireless networks," in *2018 14th International Conference on Mobile Ad-Hoc and Sensor Networks (MSN)*, pp. 140–145, 2018. (cited as [178])

Author's contribution: *conceptualization, methodology, software, simulations, validation, writing original draft, visualization.*

18) Ł. Kułacz and A. Kliks, "Simplified and reliable wireless data transmission in ultra dense networks," in *2020 International Conference on Software, Telecommunications and Computer Networks (SoftCOM)*, pp. 1–6, 2020. (cited as [180])
Author's contribution: *conceptualization, methodology, software, simulations, validation, writing original draft, visualization.*

19) A. Kliks and Ł. Kułacz, "Brain inspirations for dense wireless networks: Microglia functionality," in *2018 IEEE 29th Annual International Symposium on Personal, Indoor and Mobile Radio Communications (PIMRC)*, pp. 578–579, 2018. (cited as [188])
Author's contribution: *conceptualization, methodology, software, simulations, validation, writing original draft, visualization.*

20) Ł. Kułacz and A. Kliks, "Gęsta sieć bezprzewodowa inspirowana układem nerwowym," *Przegląd Telekomunikacyjny + Wiadomosci Telekomunikacyjne*, vol. nr 6, pp. 487–492, CD, 2019. (cited as [189])
Author's contribution: *conceptualization, methodology, software, simulations, validation, writing original draft, visualization.*

21) Ł. Kułacz and A. Kliks, "Dense wireless network inspired by the nervous system," *International Journal of Electronics and Telecommunications*, vol. vol. 66, no. No 1, pp. 93–98, 2020. (cited as [190])
Author's contribution: *conceptualization, methodology, software, simulations, validation, writing original draft, visualization.*

22) Ł. Kułacz and A. Kliks, "Brain-inspired data transmission in dense wireless network," *Sensors*, vol. 21, no. 2, 2021. (cited as [191])
Author's contribution: *methodology, software, validation, writing original draft, and visualization.*

23) Ł. Kułacz and A. Kliks, "Reliability of bio-inspired ultra-dense networks," in *2020 Baltic URSI Symposium (URSI)*, pp. 15–18, 2020. (cited as [194])
Author's contribution: *methodology, software, simulations, validation, writing original draft, visualization.*

24) Ł. Kułacz and A. Kliks, "Reliability assessment of bio-inspired ultra-dense networks using percolation theory," in *2020 IEEE 21st International Symposium on "A World of Wireless, Mobile and Multimedia Networks" (WoWMoM)*, pp. 173–175, 2020. (cited as [197])
Author's contribution: *methodology, software, simulations, validation, writing original draft, visualization.*

25) Ł. Kułacz, A. Kliks, P. Kryszkiewicz, and B. Bossy, "Dynamic transmit profile selection in dense wireless networks," *Sensors*, vol. 21, no. 1, 2021. (cited as [209])
Author's contribution: *conceptualization, methodology, software, simulations, validation, writing original draft, visualization.*

26) Ł. Kułacz, A. Kliks, B. Bossy, and P. Kryszkiewicz, "Adaptacyjny wybór profilu transmisyjnego w gęstych sieciach bezprzewodowych," *Przegląd Telekomunikacyjny + Wiadomosci Telekomunikacyjne*, vol. nr 7-8, pp. 212–215, CD, 2020. (cited as [210])
Author's contribution: *measurements, software, simulations, validation, writing original draft, visualization.*

27) C.-Y. Chang, Ł. Kułacz, R. Schmidt, A. Kliks, and N. Nikaein, "Spectrum Management Application - a tool for flexible and efficient resource utilization," in *2018 IEEE Global Communications Conference (GLOBECOM)*, pp. 1–7, 2018. (cited as [213])
Author's contribution: *conceptualization, methodology, software, simulations, hardware implementation, validation, visualization*.

28) Ł. Kułacz and A. Kliks, "Freemium spectrum sharing and pricing," in *2021 International Conference on Software, Telecommunications and Computer Networks (SoftCOM)*, pp. 1–6s, 2021. (cited as [219])
Author's contribution: *conceptualization, methodology, software, simulations, validation, writing original draft, visualization*.

29) Ł. Kułacz and A. Kliks, "Dynamic spectrum allocation using multi-source context information in OpenRAN networks," *Sensors*, vol. 22, no. 9, 2022. (cited as [222])
Author's contribution: *conceptualization, methodology, software, simulations, validation, writing original draft, visualization*.

30) M. Dryjański, Ł. Kułacz, and A. Kliks, "Toward modular and flexible Open RAN implementations in 6G networks: Traffic steering use case and O-RAN xApps," *Sensors*, vol. 21, no. 24, 2021. (cited as [223])
Author's contribution: *software, simulations, validation, writing original draft, visualization*.

31) M. Wasilewska and Ł. Kułacz, "Machine Learning-based small cell location selection process," *Journal of Telecommunications and Information Technology*, vol. 2, pp. 120–126, Mar. 2021. (cited as [243])
Author's contribution: *methodology, channel generation, writing original draft, visualization*.

32) P. Kryszkiewicz, A. Kliks, Ł. Kułacz, and B. Bossy, "Power consumption variation for a single technology wireless transceivers," in *2020 IEEE 21st International Symposium on "A World of Wireless, Mobile and Multimedia Networks" (WoWMoM)*, pp. 179–181, 2020. (cited as [244])
Author's contribution: *software, simulations, validation, writing original draft, visualization*.

33) P. Kryszkiewicz, A. Kliks, Ł. Kułacz, and B. Bossy, "Stochastic power consumption model of wireless transceivers," *Sensors*, vol. 20, no. 17, 2020. (cited as [245])
Author's contribution: *measurements, software, simulations, validation, writing original draft, visualization*.

34) Ł. Kułacz, A. Kliks, B. Bossy, and P. Kryszkiewicz, "Transmission profile selection in dense wireless networks," in *2020 Baltic URSI Symposium (URSI)*, pp. 130–133, 2020. (cited as [246])
Author's contribution: *measurements, software, simulations, validation, writing original draft, visualization*.